CANMET

Canada Centre for Mineral and Energy Technology

Centre canadien de la technologie des minéraux et de l'énergie

Energy Research Laboratories

Laboratoires de recherche sur l'énergie

Energy, Mines and Resources Canada

Énergie, Mines et Ressources Canada

Canada

THE ENERGY OF OUR RESOURCES • THE POWER OF OUR IDEAS

L'ENERGIE DE NOS RESSOURCES • NOTRE FORCE CREATRICE

FLUID FLOW PHENOMENA IN HETEROGENEOUS SYSTEMS

VOLUME 2

MONITORING OF FLUID SATURATIONS

AND CONING CONTROL

FINAL REPORT

by:

Apostolos Kantzas

Daniel F. Marentette

Les Stehmeier

Grant Ferris

Part of Energy Mines and Resources
Cost-shared Energy Conversion Program
and Part of the Program of the Federal Panel
on Energy R&D [PERD]
June 30, 1991

MICROMEDIA

NOVA HUSKY Research Corporation
2928 - 16St. N.E.
Calgary AB T2E 7K7

Work on this project was conducted under the auspices of the Canada Centre for Mineral and Energy Technology, Energy, Mines and Resources Canada.

DSS File No: 006SQ.23440-9-9258
DSS Contract Serial No: 23440-9-9258/01-SQ
CANMET Scientific Authority: Dr. Kamal Jha

© 1991 NOVA HUSKY RESEARCH CORPORATION

92-06655/

DISTRIBUTION LIST

	No. of Copies
Energy Mines and Resources Canada	5
Husky Oil Ltd:	
I. Adamache	1
V. Cheung	1
F. McIntyre	1
J. Peggs	1
M. Pow	1
NOVA HUSKY Research Corporation:	
G. Ferris	1
T. Jack	1
A. Kantzas	1
D. Marentette	1
B. Nikakhtar	1
L. Stehmeier	1
Husky Oil Library	2
NHRC Library	1
Files	1
TOTAL	**20**

© 1991 NOVA HUSKY RESEARCH CORPORATION

TABLE OF CONTENTS

Page no.

LIST OF FIGURES iv

EXECUTIVE SUMMARY viii

1.0 OBJECTIVES 1

2.0 LITERATURE SURVEY 1
- a. Computer Assisted Tomography 1
- b. Bacteriological Mineral Plugging 4

3.0 EXPERIMENTAL 7
- a. Computer Assisted Tomography 7
- b. Bacteriological Mineral Plugging 11

4.0 DISCUSSION 13
- a. Computer Assisted Tomography 13
- b. Bacteriological Mineral Plugging 15

5.0 CONCLUSIONS 15

6.0 ACKNOWLEDGEMENTS 16

7.0 REFERENCES 16

FIGURES

© 1991 NOVA HUSKY RESEARCH CORPORATION

LIST OF FIGURES

Figure 1: Photographs of 7070 scanner gantry.
Figure 2: Photographs of 7070 scanner holder.
Figure 3: Photographs of 7070 scanner control system and console.
Figure 4: Photographs of the 5005 scanner and console.
Figure 5: CT number color code for sandpack column SP10x100.
Figure 6: Vuggy sandpack SP10x100 CT images of slices 1 to 20 (arrangement by rows).
Figure 7: Vuggy sandpack SP10x100 CT images of slices 21 to 40 (arrangement by rows).
Figure 8: Vuggy sandpack SP10x100 CT images of slices 41 to 60 (arrangement by rows).
Figure 9: Vuggy sandpack SP10x100 CT images of slices 61 to 80 (arrangement by rows).
Figure 10: Vuggy sandpack SP10x100 CT images of slices 81 to 92 (arrangement by rows).
Figure 11: Colorcode for saturation images.
Figure 12: MPH1: Oil saturation during oilflood @ 8 cm from inlet (time in minutes).
Figure 13: MPH1: Water saturation during oilflood @ 8 cm from inlet (time in minutes).
Figure 14: MPH1: Oil saturation during oilflood @ 16 cm from inlet (time in minutes).
Figure 15: MPH1: Water saturation during oilflood @ 16 cm from inlet (time in minutes).
Figure 16: MPH1: Oil saturation during oilflood @ 24 cm from inlet (time in minutes).
Figure 17: MPH1: Water saturation during oilflood @ 24 cm from inlet (time in minutes).
Figure 18: MPH1: Oil saturation after oilflood; slices 1-30.
Figure 19: MPH1: Oil saturation after oilflood; slices 31-61.
Figure 20: MPH1: Water saturation after oilflood; slices 1-30.
Figure 21: MPH1: Water saturation after oilflood; slices 31-61.
Figure 22: MPH1: Oil saturation during waterflood @ 8 cm from inlet (time in minutes).
Figure 23: MPH1: Water saturation during waterflood @ 8 cm from inlet (time in minutes).
Figure 24: MPH1: Oil saturation during waterflood @ 16 cm from inlet (time in minutes).
Figure 25: MPH1: Water saturation during waterflood @ 16 cm from inlet (time in minutes).
Figure 26: MPH1: Oil saturation during waterflood @ 24 cm from inlet (time in minutes).
Figure 27: MPH1: Water saturation during waterflood @ 24 cm from inlet (time in minutes).
Figure 28: *In situ* oil saturation plots of a uniform sandpack (MPH1) during oilflood (drainage).
Figure 29: *In situ* oil saturation plots of a uniform sandpack (MPH1) during waterflood (imbibition).
Figure 30: Cumulative oil production during oilflood in MPH1.
Figure 31: Oil production during oilflood in MPH1.
Figure 32: Cumulative water production during oilflood in MPH1.
Figure 33: Water production during oilflood in MPH1.
Figure 34: Oil water ratio during oilfoood in MPH1.

© 1991 NOVA HUSKY RESEARCH CORPORATION

Figure 35: Cumulative oil production during waterflood in MPH1.
Figure 36: Oil production during waterflood in MPH1.
Figure 37: Cumulative water production during waterflood in MPH1.
Figure 38: Water production during waterflood in MPH1.
Figure 39: Water oil ratio during waterflood in MPH1.
Figure 40: Cumulative oil production during gasflood in MPH1.
Figure 41: Oil production during gasflood in MPH1.
Figure 42: Cumulative water production during gasflood in MPH1.
Figure 43: Water production during gasflood in MPH1.
Figure 44: Cumulative gas production during gasflood in MPH1.
Figure 45: Gas production during gasflood in MPH1.
Figure 46: Water oil ratio during gasflood in MPH1 (cumulative).
Figure 47: Gas water ratio during gasflood in MPH1 (cumulative).
Figure 48: Gas oil ratio during the gasflood in MPH1 (cumulative).
Figure 49: *In situ* concentration profile during miscible displacement in Berea sandstone.
Figure 50: Average CT number versus water saturation at high energy for experiment MPH3.
Figure 51: Average CT number versus oil saturation at high energy for experiment MPH3.
Figure 52: Average CT number versus water saturation at low energy for experiment MPH3.
Figure 53: Saturation color code for experiment MPH3.
Figure 54: Water saturation profile during oilflood at 5 cm from inlet (MPH3).
Figure 55: Oil saturation profile during oilflood at 5 cm from inlet (MPH3).
Figure 56: Water saturation profile of core after oilflood (MPH3).
Figure 57: Oil saturation profile of core after oilflood (MPH3).
Figure 58: Water saturation profile during waterflood at 5 cm from inlet (MPH3).
Figure 59: Oil saturation profile during waterflood at 5 cm from inlet (MPH3).
Figure 60: Water saturation profile of core after waterflood (MPH3).
Figure 61: Oil saturation profile of core after waterflood (MPH3).
Figure 62: Water saturation profile of core after gasflood (MPH3).
Figure 63: Oil saturation profile of core after gasflood (MPH3).
Figure 64: Gas saturation profile of core after gasflood (MPH3).
Figure 65: CT number mean and standard deviation for Berea and Rainbow Lake dolomite at 140 kVp.
Figure 66: Frequency distributions of a relatively homogeneous medium (Berea).
Figure 67: Frequency distributions of a heterogeneous medium (Rainbow dolomite).
Figure 68: Bulk density images for slices 1 to 22 prior to plugging, column A.
Figure 69: Bulk density images for slices 23 to 44 prior to plugging, column A.

© 1991 NOVA HUSKY RESEARCH CORPORATION

Figure 70: Bulk density images for slices 45 to 70 prior to plugging, column A.
Figure 71: Bulk density images for slices 71 to 95 prior to plugging, column A.
Figure 72: Bulk density images for slices 1 to 22 after plugging, column A.
Figure 73: Bulk density images for slices 23 to 44 after plugging, column A.
Figure 74: Bulk density images for slices 1 to 22 prior to plugging, column B.
Figure 75: Bulk density images for slices 23 to 44 prior to plugging, column B.
Figure 76: Bulk density images for slices 45 to 70 prior to plugging, column B.
Figure 77: Bulk density images for slices 71 to 95 prior to plugging, column B.
Figure 78: Bulk density images for slices 1 to 22 after plugging, column B.
Figure 79: Bulk density images for slices 23 to 44 after plugging, column B.
Figure 80: Bulk density images for slices 1 to 22 prior to plugging, column C.
Figure 81: Bulk density images for slices 23 to 44 prior to plugging, column C.
Figure 82: Bulk density images for slices 45 to 70 prior to plugging, column C.
Figure 83: Bulk density images for slices 71 to 95 prior to plugging, column C.
Figure 84: Bulk density images for slices 1 to 22 after plugging, column C.
Figure 85: Bulk density images for slices 23 to 44 after plugging, column C.
Figure 86: Bulk density images for slices 1 to 22 prior to plugging, column D.
Figure 87: Bulk density images for slices 23 to 44 prior to plugging, column D.
Figure 88: Bulk density images for slices 45 to 70 prior to plugging, column D.
Figure 89: Bulk density images for slices 71 to 95 prior to plugging, column D.
Figure 90: Bulk density images for slices 1 to 22 after plugging, column D.
Figure 91: Bulk density images for slices 23 to 44 after plugging, column D.
Figure 92: Porosity images for slices 1 to 22 prior to plugging, column A.
Figure 93: Porosity images for slices 23 to 44 prior to plugging, column A.
Figure 94: Porosity images for slices 45 to 70 prior to plugging, column A.
Figure 95: Porosity images for slices 71 to 95 prior to plugging, column A.
Figure 96: Porosity images for slices 1 to 22 after plugging, column A.
Figure 97: Porosity images for slices 23 to 44 after plugging, column A.
Figure 98: Porosity images for slices 1 to 22 prior to plugging, column B.
Figure 99: Porosity images for slices 23 to 44 prior to plugging, column B.
Figure 100: Porosity images for slices 45 to 70 prior to plugging, column B.
Figure 101: Porosity images for slices 71 to 95 prior to plugging, column B.
Figure 102: Porosity images for slices 1 to 22 after plugging, column B.
Figure 103: Porosity images for slices 23 to 44 after plugging, column B.
Figure 104: Porosity images for slices 1 to 22 prior to plugging, column C.
Figure 105: Porosity images for slices 23 to 44 prior to plugging, column C.

© 1991 NOVA HUSKY RESEARCH CORPORATION

Figure 106: Porosity images for slices 45 to 70 prior to plugging, column C.
Figure 107: Porosity images for slices 71 to 95 prior to plugging, column C.
Figure 108: Porosity images for slices 1 to 22 after plugging, column C.
Figure 109: Porosity images for slices 23 to 44 after plugging, column C.
Figure 110: Porosity images for slices 1 to 22 prior to plugging, column D.
Figure 111: Porosity images for slices 23 to 44 prior to plugging, column D.
Figure 112: Porosity images for slices 45 to 70 prior to plugging, column D.
Figure 113: Porosity images for slices 71 to 95 prior to plugging, column D.
Figure 114: Porosity images for slices 1 to 22 after plugging, column D.
Figure 115: Porosity images for slices 23 to 44 after plugging, column D.
Figure 116: Average slice bulk density prior to and after plugging, Column A.
Figure 117: Average slice bulk density prior to and after plugging, Column B.
Figure 118: Average slice bulk density prior to and after plugging, Column C.
Figure 119: Average slice bulk density prior to and after plugging, Column D.
Figure 120: Average slice porosity prior to and after plugging, Column A.
Figure 121: Average slice porosity prior to and after plugging, Column B.
Figure 122: Average slice porosity prior to and after plugging, Column C.
Figure 123: Average slice porosity prior to and after plugging, Column D.
Figure 124: Photographs of the first section (0 - 6 cm) of column A after completion of the experiment. The small solidified section is shown at the left end.
Figure 125: Photographs of the second section (6 - 18 cm) of column A after completion of the experiment. The solidified sections can be shown.
Figure 126: Photographs of the first section (0 - 6 cm) of column B after completion of the experiment. There is no solidified section.
Figure 127: Photographs of the second section (6 - 20 cm) of column B after completion of the experiment. Two solidified sections can be seen.
Figure 128: Photograph of the remaining sections of columns A and B where no plugging has taken place.
Figure 129: Bacterial Poplulation distributions along the length of the different columns.
Figure 130: Schematic of the bacterial mineral plugging apparatus.

© 1991 NOVA HUSKY RESEARCH CORPORATION

RÉSUMÉ

Ce volume aborde deux sujets: la mesure des saturations en fluide dans le cadre d'une expérience d'écoulement multiphasé in situ et l'évaluation additionnelle du bouchage par des minéraux d'origine bactérienne. Une série d'expériences a été accomplie afin de répondre aux objectifs posés pour les deux sujets:

La détermination de la saturation multiphasée in situ a été entreprise dans une série d'essais où une carotte à été saturée de solution hypersaline, injectée d'huile jusqu'aux conditions d'eau de constitution, injectée d'eau jusqu'aux conditions d'huile résiduelle et ensuite horizontalement injectée d'air. Des algorithmes de détermination à deux phases et à trois phases ont été utilisés pour le calcul des saturations individuelles ainsi qu'un assortiment d'additifs fluides. Il a été trouvé que la détermination quantitative de la saturation peut être obtenue en présence de deux fluides et lorsque les calibrages sont ajustées aux expériences spécifiques. Lorsque trois phases sont présentes, les résultats sont seulement qualitatifs. La phase qui souffre le plus des diverses erreurs est celle qui est calculée indirectement (en faisant la différence).

Une série d'essais a aussi été accomplie afin de reproduire et de démontrer les capacités du bouchage par des minéraux d'origine bactérienne ici proposé et présentement sur le point d'être breveté. Il a été trouvé que les résultats rapportés plus tôt peuvent être reproduits. La population bactérienne in situ, la perméabilité du milieu et la quantité d'éléments nutritifs injectés ont été identifiés comme paramètres ayant une influence sur la performance de la méthode proposée.

© 1991 NOVA HUSKY RESEARCH CORPORATION

EXECUTIVE SUMMARY

This volume addresses two areas: The measurement of fluid saturations in a multiphase flow experiment *in situ* and the further evaluation of bacteriological mineral plugging. A series of experiments were performed to meet the objectives in both areas:

In situ multiphase saturation determination was attempted in a series of tests where a core was saturated with brine, oilflooded to connate water, waterflooded to residual oil and then flooded by air horizontally. Two phase and three phase determination algorithms were used for the calculation of individual saturations along with an assortment of fluid dopants. It was found that quantitative saturation determination can be achieved when two fluid saturations are present and when calibrations are made which are tailored to the specific experiment. When three phases are present, the results are only qualitative. The phase that suffers the most from the various errors is the phase which is calculated indirectly (by difference).

A series of tests was also performed to duplicate and demonstrate the capabilities of the proposed bacteriological mineral pluggings which is currently being patented. It was found that the results reported earlier are reproducible. The *in situ* bacterial populations, the permeability of the medium and the amount of nutrients injected were identified as parameters that affect the performance of the proposed method.

© 1991 NOVA HUSKY RESEARCH CORPORATION

1.0 OBJECTIVES

The objectives of this work are:

i) To determine methods for the in-situ multi-phase saturation measurements using Computer Assisted Tomography (CAT) scanning.
ii) To determine saturation profiles during Gravity Assisted Immiscible Gas Injection (GAIGI).
iii) To study the possibility of coning control using bacteriogenic mineral plugging.

2.0 LITERATURE SURVEY

a. Computer Assisted Tomography

Computer Assisted Tomography has become a standard tool in enhanced oil recovery research. A large number of applications in reservoir characterization and fluid flow visualization has been published. A detailed literature survey on the earlier work in Computer Assisted Tomography has been presented in Kantzas (1990). The most recent publications focus on the application of x-ray CAT scanning for fluid flow studies. One notable exception is the work by Gilliland and Coles (1990) who used the CAT scanner as a tool for the investigation of damage to unconsolidated cores. Their findings are consistent with the results obtained from scanning heavy oil cores from Alberta and Saskatchewan (Kantzas *et al.*, 1989; Kantzas, 1991a). Also, Auzerais *et al.* (1990) used CAT scanning to calculate densities and effective atomic numbers (called photoelectric factors in the original paper) for a number of anisotropic rocks, as part of a larger core characterization project. They found that permeability variations are due to variations in grain size and packing. Moss *et al.* (1990) presented an algorithm for the direct measurement of the constituent porosities in a dual porosity matrix. The method is based on saturating a core with a dopant and use an image subtraction technique while scanning at different times. The algorithm is very similar to the algorithm presented by Withjack *et al.* (1990) which is going to be discussed later. Moss *et al.* (1990) suggest that by following the time sequence of the penetration process one can separate the easily accessible fracture porosity from the matrix porosity. They have studied this approach in coal and shales. They also found that statistically accurate porosity distributions can be obtained from the porosity images. They concluded that the width of the porosity distribution is a good indicator of porosity heterogeneity.

In a more recent study, Chatzis and Berry (1991) used the CAT scanner technology for the determination of vug size distributions in vuggy carbonates. They prepared calibration data using drilled cylinders of

© 1991 NOVA HUSKY RESEARCH CORPORATION

various sizes and back calculated vug size distributions of cores from Fenn-Big Valley core. Their analysis however assumes that total porosity equals vuggy porosity. If a considerable percentage of matrix porosity is present, the porosity predictions of this method will be underestimating the true porosity values.

Honarpour *et al.* (1990) used the CAT scanner as an aid in evaluating the effects of pore geometry and pore size distribution on capillary pressure and wettability index. CT images showed that different fluid distributions resulted for rocks of different pore throat size and pore volume characteristics at similar capillary pressures. These fluid distributions were non-uniform except at high capillary pressures.

The CAT scanner was used by Mohanty and Miller (1988) to assess various factors that influence unsteady relative permeability of mixed-wet rocks. Their work revealed a number of regimes for the cross sectional average saturation profile during low rate waterfloods. These regimes are frontal movement (up to 0.15 PV injected), a non uniform saturation increase (up to 0.6 PV injected) and a uniform saturation increase. CT determined cross-sectional average saturation close to the outlet face indicated that the JBN assumed saturations are incorrect at early times (up to 1 PV throughput). A method for determining porosity profiles from steady-state x-ray saturation data was described in Potter and Groves (1989) for several sandstones and carbonates. The presented apparatus was part of an automated steady-state permeameter. Burchfield and Chung (1989) used CT to examine oil and water saturation profiles in sandpack during CO_2 and N_2 floods.

MacAllister *et al.* (1990) applied CAT scanning techniques to determine gas-water relative permeabilities. They concluded that two phase saturation measurements using the CAT scanner can be accurate, since one phase is measured directly and the other is obtained by difference. Three phase calculations are questionable since the saturation of one phase (in this case the residual oil phase) was estimated independently (the authors did not use the dual scanning approach). This affected mainly the phase obtained by difference. Again, the authors were able to visualize non uniform saturation distributions along the cores tested (which is consistent with the findings of Mohanty and Miller, 1988).

Hicks *et al.* (1990a) measured the porosity and the distribution of residual oil in heterogeneous carbonate cores from Fenn-Big Valley in Alberta and Taylor-Link Field in Texas. A fourth generation CAT scanner was used with the gantry rotated 90° to provide a horizontal scan plane. They also calculated semivariograms and porosity distributions in an effort to quantify rock heterogeneities. Hicks *et al.* (1990b) studied vertical miscible displacements in the same heterogeneous cores and observed the displacement fronts using the vertical scanner. They have also observed that three dimensional CT data

© 1991 NOVA HUSKY RESEARCH CORPORATION

can be used to visualize and to some extent quantify the magnitude of connectivity of the vug pore system.

Withjack *et al.* (1990) also studied miscible displacement and heterogeneities using the CAT scanner. They focused more on heterogeneities due to permeability variations on a sub bedding plane scale. The impressive contribution of this work is that, for the first time, a method for the prediction of core permeability using the CAT scanner is presented. The method is based on a bundle of tubes type model, and the permeability is calculated using the results of a miscible displacement test. The method assumes linear pressure drop along the core which is a good assumption for layered sandstones, but not satisfactory for vuggy and fractured systems. Nonetheless, the method provided very good correlations between porosity and permeability for the cases studied.

Peters and Hardham (1990) performed a number of miscible and immiscible tests in sandpacks in order to visualize fluid displacements. They proposed that CT imaging of stable miscible displacements can provide the means for the determination of the longitudinal dispersion coefficient of a porous medium. The authors also suggested that one can use the saturation data obtained by CAT scanning for the calibration of numerical models.

A method for the calculation of diffusion coefficients using CAT scanners was presented by Hara and Christman (1990). The method was developed to test a hypothesis related to modelling of immiscible CO_2 displacements. It was found that diffusion coefficients can be calculated from looking at the differential images using doped solutions. Successful matching between simulation and CT measurements was achieved.

CAT scanning images were used to compare fluid displacement patterns in Berea cores with patterns obtained by a network flow simulator coupled to an anisotropic multifractal generator (Lenormand *et al.*, 1990). The agreement was good.

Linear saturation models were used by Alvestad *et al.* (1991) to monitor fluid saturations in Berea cores during surfactant floods. They have observed that a marked increase in the oil saturation before the surfactant front. Very small oil production after the oil bank was observed. Although qualitative agreement between simulation and CAT scanner data is observed, there is no mention about the agreement of CT saturation and mass balance.

Two very interesting applications of in-situ measurements of fluid and rock properties are presented in Jasti *et al.* (1990) and in Jasti and Fogler (1990). In the first paper a micro scanner is presented with a

© 1991 NOVA HUSKY RESEARCH CORPORATION

resolution of up to 10 microns. This scanner can be used in the same fashion as the regular CAT scanner but with a lot smaller pieces. Drilling bits could be used for the quantitative characterization of rock and fluid properties. In the second application, a method is presented which takes advantage of the shifts in gamma spectra to determine the location and velocity of a tracer. The method can have potential applications in well tracer tests. In Tores *et al.* (1990), CAT scanning was used as a tool for the understanding of flow phenomena in tuff from the Nevada Test Site. The migration of fluids (predominantly water) was addressed by performing drainage and imbibition tests with water and air at ambient conditions. A radioactive imaging technique for determination of the effects of capillary heterogeneities on local saturation development in long core floods has been presented by Graue (1990). Sprunt *et al.* (1991) were able to monitor saturation non-uniformities in electrical resistivity measurements using CAT scanning and were able to come up with correct interpretation of the saturation exponent. In Barroux *et al.* (1991) an alternate dual energy gamma-ray attenuation technique was presented as a cheaper alternative to x-ray CAT scanning. O'Meara and Vinegar (1990) have patented an algorithm which uses CAT scanning in plugs to monitor fluid saturations and then use the data for the calculation of capillary pressures and relative permeabilities. Finally, CAT scanner algorithms were used to study natural soil macropores (Anderson *et al.*, 1990; Cruvinel *et al.*, 1990) and fracture processes in materials (Antolovich *et al.*, 1990).

All the cited references show the number of applications of CAT scanning in Petroleum Engineering. The qualitative input of the CAT scanner in any core analysis type of test is beyond any doubt. However, when the results need to be quantified, a number of questions rise. These questions predominantly deal with the error associated with these measurements, especially when fluid saturations are measured. Also none of the previous works have, to the best of our knowledge, provided a sensitivity analysis of the data obtained by a CAT scanner. These issues are addressed in this work. Some simple miscible and immiscible displacement tests are presented and the algorithms for the determination of fluid saturations are discussed. Then, a statistical analysis of CAT scanner data is presented which aims in the definition of the limits of reproducibility of the CAT scanner measurements. This is expressed in error with respect to means and standard deviations over a number of measurements. It must be noted that the presented results are dependent on the type of scanner used, and they should be considered as guides only for different scanner models.

b. Bacteriological Mineral Plugging

Microbial Enhanced Oil Recovery (MEOR) is still considered an emerging technology, but it is certainly not new. Both micro-organisms and microbially derived products have been used for over 40 years to recover reservoir oil or provide well bore cleanout (Nelson and Launt, 1991). Microbs are blamed with a

© 1991 NOVA HUSKY RESEARCH CORPORATION

lot of problems related to creation of biofilm that plugs reservoir pores, creation of ferrous sulfide which is often responsible for plugged and fouled production lines and degradation of chemicals used in EOR processes. However, micro-organisms have also been credited for a wide range of metabolic by-products that are helpful to oil recovery. Also some anaerobic micro-organisms produce hydrocarbon gases, and some aerobic organisms produce CO_2 gas.

A variety of MEOR approaches have been used including:

Stimulation of the indigenous (existing) microbial populations.

Injection of nutrients, biocatalysts, and selected micro-organisms with a proven ability to perform *in situ*.

The above ground production of microbial products, such as biosurfactants, biopolymers, fermentation alcohols and ketones which are injected like traditional EOR chemicals (Jack, 1990; Nelson and Launt 1991).

The effects of the presence of bacteria on the permeability of Berea sandstone were investigated by Kalish *et al.* (1964). They injected dead bacteria under a variety of conditions and found that the factors that affect permeability during injection of bacterial suspensions are: (1) concentration of bacteria, (2) core permeability and median pore size, (3) species of bacteria, mode of aggregation and relative size, (4) injection rate or pressure differential, (5) mean pressure and (6) depth of penetration of bacteria. Core permeability was never reduced to zero. Permeability restoration was achieved by acidization in combination with reverse flow. Since the bacteria used in most of the experiments were dead, use of biocides would not be useful. The bacterial effect in oil wells is only a skin effect.

Nutrients such as glucose, ammonia nitrogen and phosphate were found that they can be transported through sandstone in concentrations sufficient to support microbial growth and metabolism for EOR processes (Jenneman *et al.* 1984). Protein in the form of Bacto-Peptone was strongly retained in both brine saturated and oil /brine-saturated cores. Therefore, proteins were not considered as likely to be good sources of carbon or nitrogen for MEOR. Viable cells have been transported through sandstone at a permeability as low as 196 mD. Less than 1% of the injected cells were recovered in the effluent.

Early work in MEOR has been summarized in Proceedings of MEOR workshops (King and Stevens, 1987). NIPER has spent considerable effort in MEOR addressing insitu microbial growth and metabolism, effective plugging by microorganisms, polymer producing bacteria and biosurfactants (McInerney *et al.*, 1983; Knapp *et al.*, 1987).

© 1991 NOVA HUSKY RESEARCH CORPORATION

In some cases the injected bacteria are too large to penetrate the pore space in long distances. The concept of using starved bacteria was introduced (Lappin-Scott *et al.* 1988; Mac Leod *et al.* 1988) under which the bacteria are reduced in size through carbon deprivation, injected into a formation and then let to grow through the injection of nutrients. Permeability reduction for tighter formations can be achieved in such a way.

Micro-organisms and molasses nutrient recovered an average of 32% more of a light crude oil from Berea sandstone cores than after a laboratory simulated waterflood (Bryant and Douglas, 1988). It was also found that micro-organisms that form spores averaged higher recovery efficiencies, but the variation among their recovery efficiencies is greater then the recovery efficiencies in non-spore-forming bacteria. Micro-organisms and molasses nutrient recovered an average 19% more heavy crude oil over that of a waterflood. Strictly aerobic crude-oil-consuming bacteria were not found to be effective in microbial oil recovery. Bryant and Douglas (1988) also found that microbial oil recovery efficiencies in Berea sandstone correlated well with the ability of microbial species to mobilize oil in etched-glass micromodels.

A number of field tests have been performed in the past few years aiming at the implementation of various MEOR schemes in oil reservoirs (Jack 1990, 1991). They included:

1) Application of the NHRC microbial plugging system in Standard Hill (Jack and Stehmeier, 1988; Stehmeier at al., 1990).
2) Augmented Waterflooding tests for conventional oil recovery in Australia, Russia, Romania and Oklahoma.
3) MEOR for carbonate reservoirs in East Germany.

Use of anaerobic bacteria has been proposed by Nelson and Launt (1991) as a method for the utilization of hydrocarbons and the production of biogas (methane or ethane) rather than CO_2. Advances in this method include tolerance of anaerobic bacteria to extremes of temperature, pH, salinity and solvent contamination,elimination of the need for the injection of large volumes of carbohydrate nutrients, etc.

The technology of hydrocarbon oxidizing using bacteria which also generate methane was reported by Belayaev *et al.* (1991). The bacteria release CO_2, fatty acids, aliphatic alcohols and surfactants through a first stage of activation which involves aeration of water pumped into a formation with mineral nitrogen and phosphorus salts added. A second stage follows which involves the activation of methanogens followed by production of supplementary amounts of CO_2 and CH_4. They reported increase in oil production of 20% to 100% and water content decrease of 20% -to 30%.

© 1991 NOVA HUSKY RESEARCH CORPORATION

Premuzic and Lin (1991) have presented studies that dealt with the effects of thermophilic, temperature adapted, acidophilic and chemotrophic micro-organisms on the chemical and physical properties of selected types of crude oils over a wide range of temperatures, pressures and salt concentrations. They found that the micro-organisms used managed to reduce the total sulphur content, decreased the concentration of thianaphthalene organic compounds, decrease the portion of the c20 to c30 alkanes, increase the <C20 type alkanes and form lighter hydrocarbons.

With respect to modelling there are two distinct efforts published in the literature. In the effort initiated in NHRC, microbial transport and growth is modelled (Islam, 1990; Islam and Gianetto, 1990; Jack *et al.*, 1991) by emulating transport of fine particles, as described by Gruesbeck and Collins (1982). In an independent approach NIPER (Bryant *et al.* 1990) developed a mathematical model for the propagation and distribution of nutrients and micro-organisms in a one-dimensional core. Then they incorporated the transport equations for micro-organisms and microbial nutrients into the BOAST simulator.

A fresh approach in the way of bacterial action for MEOR is given in Ferris *et al.* (1990). They invented the first (to our knowledge) inducible bacterial plugging system which does not rely on organic matter to be the plugging agent. It gives thermally stable durable plugs which are capable of withstanding very significant pressure drops. The whole technology is based on the precipitation of carbonate minerals which is induced by the pH change created by microbial activity. The process is similar to the chemical carbonate precipitation reported elsewhere for CO_2 floods (Puon *et al.*, 1988) but can extend to a variety of conditions.

This work is the extension of the work by Ferris *et al.* (1990). Computer Assisted Tomography was used in an effort to provide a critical assessment of the extent of biomineralization under a variety of conditions.

3.0 EXPERIMENTAL

a. Computer Assisted Tomography

The Computer Assisted Tomography laboratory is a unique facility. A second scanner (denoted 7070 as opposed to the old scanner which is denoted 5005) was bought and installed. The gantry has been modified so that vertical columns can be scanned. Scanner 7070 is a fourth generation EMI scanner which can scan a cross section in 3 s and process it in less than 20 s. Figure 1 shows the modified gantry in the horizontal position. In Figure 2 the new holder mechanism is shown. The mechanism was

© 1991 NOVA HUSKY RESEARCH CORPORATION

designed and built to allow precision of 1/100 mm for the positioning of the sample. Figure 3 shows the control console of the new scanner. The new scanner is located in the same laboratory as the old scanner. Both machines can operate in parallel. At the time of the completion of this report the scanner was under testing and calibrations prior to the first core experiment. The presented results are based on experiments on the old scanner 5005, which is shown in Figure 4.

The first set of scans is the scanning of one of the long sandpack columns used in Volume 1 of this report. Figure 5 shows one slice of the column where a vug can be clearly shown. The vugs were made by opening holes in plastic spheres and cylinders and then wrapping them in a fine mesh screen. The color code for the images is also shown. Each color corresponds to a range of 50 CT numbers. The complete set of 92 scans of the column is given in Figures 6 to 10. The location of the vugs and fractures can be easily identified. What is also apparent from the scans is that the sandpack itself is not homogeneous. The heterogeneities in the sand pack itself have a detrimental effect in the process. Of particular importance is the "gap" between the column wall and the sandpack. Although care was taken to eliminate this effect, still the wall effect acts as a fracture and allows fast propagation of the gas phase.

The second set of images depicts one of our first efforts to monitor fluid saturations using the CAT scanner. A sandpack was prepared and mounted in the 5005 scanner (horizontal position). The scanner was saturated with brine which was doped with NaI. The core was flooded with oil to residual water. The column was scanned at three different locations during the flood. The time of each scan was recorded. The two phase saturation algorithm was used to calculate saturations from the CAT scanner images. After the completion of the oilflood the core was scanned from one end to the other. Then a waterflood started and the same scanning protocol was followed. Unfortunately, the core was not scanned after waterflooding. At the end of the waterflood, gas was injected horizontally in an effort to generate three phase saturation data. Air broke through immediately. The core was taken out of the scanner gantry and shut in. The incremental oil recovery was monitored and it will be recovered in this section. However, no more scans were taken. In the following the results of this first multiphase test will be coded as test MPH1.

Figure 11 shows the color code for each of the saturation images. Each color corresponds to a saturation range of 10%. Figure 12 shows the change in oil saturation at a position 0.08 m from the core inlet. The numbers under each slice refer to the scanning times in minutes after the initiation of the oilflood. The images suggest a parabolic type of displacement with a high saturation from the centre to the perimeter. Figure 13 is the water saturation map for the same series of scans as in the previous figure. Similarly, Figures 14 and 15 show the oil and water saturation at a section 0.24 m from the inlet, while Figures 16 and 17 show the corresponding oil and water saturations at a section 0.16 m from the

© 1991 NOVA HUSKY RESEARCH CORPORATION

inlet. The numbers under each image correspond to the scanning time in minutes. Figures 18 and 19 show the oil saturation images of the whole sandpack. The numbers indicate position in the column. Figures 20 and 21 show the corresponding water saturations. The end effects at the production end are very clear. The image sequences for oil and water at 0.08 m 0.16 m and 0.24 m from the injection end are shown in Figures 22/23, 24/25 and 26/27 respectively. Note that the waterflood pattern is a lot different than the oilflood pattern in the same locations. It also happens a lot faster. Waterflooding is an imbibition type process in this test.

This first set of tests was the immiscible displacement of water by oil (drainage) and oil by water (imbibition) in a sandpack. A core holder made from Plexiglass was used to mount a core of dimensions of 0.10 m in diameter and 0.31 m in length. The sandpack was mounted under 140 kPa overburden pressure. The core was saturated with a 2% wt NaCl, 2% wt NaI brine. The brine was displaced by a mineral oil (viscosity 16 mPa.s, density 820 kg/m^3) at a rate of 3.3 10^{-8} m^3/s. The oil saturation at the end of the drainage test was found to be 89% by mass balance. The core was scanned at three locations (0.08, 0.16 and 0.24 m from the inlet face) at different times during the oilflood. The CAT scanner data were transformed into saturations using the equations described in Kantzas (1990) which are mathematically equivalent to the equations presented by Vinegar and Wellington (1987). The physical difference is that the equations in Kantzas (1990) require as input the CT numbers of the fluids only as opposed to the equations by Vinegar and Wellington (1987) which require the input of the data of the core saturated 100% with each one of the fluid phases. The former analysis therefore requires less effort for data collection. Since the time that each scan was taken was recorded, we were able to monitor the change of the saturation as a function of time for the selected locations.

At the three locations where the progress of the oilflood was monitored, a parabolic type of displacement was observed with the high oil saturation appearing first in the center of the core and then spreading to the perimeter. The average slice saturation in each of the three locations as a function of time is given in Figure 28. Note that all the saturation curves level off at approximately 82% saturation which is in close agreement with 89% measured by mass balance.

After the completion of the oilflood, a waterflood was commenced at a rate of 3.3 10^{-8} m^3/s. The core was scanned at the same three locations and the evolution of the saturation was monitored. The change of saturations was completely different in the waterflood than in the oilflood. The saturation contract was a lot less profound. The slice average saturation profiles for the three locations are shown in Figure 29. It can be seen that the saturation profiles are a different, with a lot longer tails, in the case of the waterflood than in the oilflood. The residual oil saturation in the three slices is approximately 20% which

© 1991 NOVA HUSKY RESEARCH CORPORATION

is considerably lower than the value of 38% calculated by mass balance. All the production data are presented in Figures 30 - 48 for reference purposes.

In a second set of experiments a Berea core plug of dimensions 0.038 m in diameter and 0.115 m in length was used. The plug was scanned at two energies (i.e. 140 kV and 85 kV) while dry and then it was saturated with the same mineral oil used in the previous test. Then the oil was displaced by the same oil doped with 7% by volume iododecane. The change in concentration was monitored as a function of time in one location approximately half way through the core length. The slice average concentration of the injected oil (doped) as a function of the pore volumes injected is plotted in Figure 49. A typical profile is observed. Note that the small bumps in the concentration curve could be due to the CT number standard deviation effect which will be discussed in detail in the next section.

After the completion of the miscible test, the core was scanned from end to end at the two energies, dried and it was then saturated with a brine containing 0.5% wt NaCl and 2% wt $Pb(NO_3)_2$. The core was scanned at the two energies from end to end. At this point an oilflood started at a rate of 7.2 10^{-9} m^3/s. The oilflood was followed by a waterflood at a rate of 3.6 10^{-9} m^3/s. The waterflood was followed by a nitrogen immiscible flood at a constant pressure drop of 10 kPa. The core was scanned at the two energies at the end of each flood. The overall saturations calculated either using the method in Vinegar and Wellington (1987) or in Kantzas (1990) were compared with the mass balance results. The agreement was very poor with either method for the oilflood. The agreement of the Vinegar and Wellington approach was good in the waterflooding results. The estimates from the scanner data were 12.6% oil saturation and 87.4% water saturation. The respective saturations from mass balance were 14.3% and 85.7%. The comparison of the three phase results was not as good. The estimates were 2.9% oil saturation, 61.6% water saturation and 35.5% gas saturation. The respective saturations from mass balance were 11.6%, 40.8% and 47.6%. The predictions from the approach of Kantzas (1990) were not good. The discrepancy can be attributed to two factors. First, the mathematical equivalency of the two approaches may not have the equivalent physical analog. The presence of the dopants shifts the x-ray absorption non linearly from the case of the pure fluid measurement to the case of the fluid measurement while in the pore space. The second reason is the fact that when a CT number is analyzed, its standard deviation should be taken into account. This is the topic of the following section.

In a third set of experiments only the brine was doped with 5 % wt NaI. The core used was a Berea plug so that any possible inaccuracies due to sand movement could be eliminated. The core was placed in horizontal position, saturated by each of the phases separately and scanned at 140 and 85 kVp. The flooding procedure was oilflood followed by waterflood followed by immiscible gasflood. The average water saturation after oilflood was 23 %, after waterflood 65 % and after gasflood 34 %. Only traces of oil

© 1991 NOVA HUSKY RESEARCH CORPORATION

were produced after gas injection. The two phase saturation algorithm gave poor results. At this point it was decided to re-evaluate our strategy for the saturation determination. The average saturations, as determined from mass balance were plotted against the average CT numbers at each step. The results are shown in Figure 50 for water at 140 kVp, Figure 51 for oil at 140 kVp and Figure 52 for water at 85 kVp. Looking at Figure 51 one can easily notice that although the water saturations for fully and partially saturated core in the two phase experiments fall within the same straight line, the oil saturated number seriously deviates from this line. At this point it was decided to arbitrarily correct the oil saturation in a way that would bring the oil saturated core in the same line with the rest of the points. This was done at a pixel level by adding a constant at each pixel CT number. After this adjustment the saturation were recalculated. It was found that the agreement at the end of the oilflood improved significantly (32 % estimated water saturation) and it was excellent for the waterflood (65 % estimated water saturation). All the saturation maps which were produced from this analysis are shown in Figures 54 - 61. The three phase calculation were performed using the linear rule and the results were 44 % water, 44 % oil and 12 % gas. Gas was the phase calculated by difference and it was the most seriously affected by the errors in the other two phases. It must be also noted that looking at Figure 50, the water saturation vs CT plot is a higher order model. Parameter estimation techniques could be used to calculate the appropriate model from the average CT data and the mass balance data. This type of algorithm would be custom made and could provide us with more realistic results. Such an approach was attempted by fitting the data for the water phase in a parabolic model. The water saturation number improved but the oil and gas saturation numbers were not accurate. A lot more work is needed in this direction before accurate predictions can become available. The saturation maps as predicted by the linear model are shown in Figures 62 - 64. Form the performed experiments one can conclude that a possible better method than dual scanning might be a method of dual property measurement (i.e sonic and CT, or microwave and CT). If two independent physical properties are to be measured separately but simultaneously, interaction effects could be minimized. This approach is beyond the scope of the present work.

b. Bacteriological Mineral Plugging

As described in Ferris *et al.* (1990) Bacillus pasteurii NRS-673 could be used to promote carbonate precipitation and reduce permeability and porosity in unconsolidated systems. In the current work it was attempted to reproduce the results by Ferris *et al.* (1990) and at the same time try and provide some additional answers with respect to the parameters that play a role in the bacterial mineral plugging process. Four cores, 0.032 m in diameter and 0.50 m in length were prepared and mounted simultaneously in the CAT scanner gantry. They were identified as columns A - D. The columns were all flooded with the same bacterial solution for over 16 hours, and were flooded with the same nutrients. Different rates were used. The columns were scanned before and after the bacterial action took place.

© 1991 NOVA HUSKY RESEARCH CORPORATION

Preliminary tests had already shown that the exposure of the bacteria to x-rays did not seem to have any apparent effect on the bacterial action. A schematic of the experimental apparatus is shown in Figure 130. Bacteria were grown to a concentration of 5.6×10^{-7} /cm^3 in four liters of medium D, which consists of 40g urea, 10g NH_4NO_3, 2 g dehydrated skim milk, 20 g molasses, adjusted pH 8, per liter of water. They were introduced into the columns by gravity feed running the bacteria in and then back through the cores for two complete cycles (constant head assembly). The flood was done from both ends to ensure uniform distribution of bacteria throughout the core. Each column was scanned every 0.005 m starting at 0.005 m from the inlet phase. A total of 95 slices were taken. The data were analyzed using software developed in house (Kantzas, 1990, 1991) for bulk density and porosity. The results are presented in form of the bulk density and porosity images for each column as well as in plots of average slice properties as functions of core length.

Column A was filled with 60 - 100 mesh glass beads. The nutrients were pumped into the system at a rate of 1 cm^3/min until a total of 7,563 cm^3 of nutrient were pumped through the system. The experiment was performed in order to test whether the high permeability glass bead system would be adequate for plugging to take place. It was also used to see whether bacteria could stick onto smooth clay free surfaces such as the glass beads. There was an attempt to measure the permeability reduction by putting pressure gauges at the core inlet. However, the gauges used were not sensitive enough for any permeability reduction calculations. Therefore, simple Carman Kozeny type formulas were used to provide estimates of the permeability reduction due to bacterial mineral plugging. The bulk density images for column A are given in Figures 68 to 73. Figures 68 - 71 show the images of the slices before the bacterial action took place, while Figures 72 and 73 contain the images of the first 44 slices after bacterial action took place. There was no bacterial action observed beyond this point. Figures 92 - 97 show the corresponding porosity images.

Column B was packed with sand (quartz #2, 55D permeability, % sieve analysis #30/0.0, #35/2.3, #40/26.9, #50/61.1, #60/8.2, #70/0.8, Pan/0.7) and flooded at the same rate as in column A for a total pumped volume of 6215 cm^3. This was a lower porosity, lower permeability system. Bacterial plugging was observed. The bulk density images are shown in Figures 74 to 79 in the same order as in the case of column A. The porosity images are shown in Figures 98 to 103.

Column C was packed with the same sand as column B but it was flooded at a lot lower rates, 0.1 cm^3/min. There was no apparent plugging effect seen by the CAT scanner. At the end of the test period, the rate was increased to 2.6 cm^3/min for 3 hours, 1.9 cm^3/min for 40 min and 8 cm^3/min for 65 min. A total volume of 4155 cm^3 was pumped through the system. Some bacterial plugging was observed. The

© 1991 NOVA HUSKY RESEARCH CORPORATION

bulk density images are shown in Figures 80 to 85, while the porosity images are shown in Figures 104 to 109.

Finally, column D was flooded at a rate of 0.5 cm^3/min. A total volume of 905 cm^3 was pumped through the system. It was observed that there was carbonate precipitation along the inlet lines. This was attributed to bacteria travelling back to the injection lines but it was not observed in any other column. The formation of carbonate in the line led in facial plugging. The bulk density images as shown in Figures 86 to 91 while the porosity images are shown in Figures 110 to 115.

Figures 116 to 119 show the average slice density profiles for each one of the columns. Figures 120 to 123 show the average slice porosity profiles for each one of the columns. When all the experiments were completed, the columns were taken apart for visual inspection. Photographs of various sections were taken. Figure 124 shows a section of column A which represents the first six cm of the core. There is only a small piece which is consolidated at the end of the section (consistent with the CAT scanner data). In Figure 125 the second section of column A (6 - 18 cm) is shown were the mineral plugging process occurred. Figures 126 and 127 show the corresponding pieces for column B. Finally, Figure 128 shows the remaining of the two columns were no bacterial plugging took place. Bacterial counts for different sections of the reservoir are shown in Figure 129.

4.0 DISCUSSION

a. Computer Assisted Tomography

It was mentioned earlier that the standard deviation of the CT measurements has to be taken into account when quantitative interpretations of the CT data are attempted. This is of particular interest in the mapping of porosity and fluid saturations. Also with respect to the plots of Figures 28 and 29, one can ask the question of what is the error bar associated with the correlation of conventional core analysis and CAT scanner core analysis. In order to answer these questions, a set of experiments was performed. A full diameter piece of Berea core and a full diameter piece of Rainbow Keg River dolomite core were mounted in the scanner gantry. They were scanned at the same location repeatedly at 140 kV and 85 kV energies. Each core was scanned five consecutive times at each energy level. Four such groups of measurements were taken in a period of two days. The average slice CT numbers were recorded. Several voxels were picked at random and their CT numbers were recorded. Means and standard deviations were calculated for both the slice averages and the individual voxels.

© 1991 NOVA HUSKY RESEARCH CORPORATION

The slice averages for Berea sandstone over the twenty scans had a standard deviation of 2 CT numbers for the high energy (140 kV) and 7 CT numbers for the low energy (85 kV). The dolomite had a standard deviation of 2 CT numbers for the high energy and 5 CT numbers for the low energy. Looking only at the high energy scans one then can easily conclude that on a slice average basis the reproducibility in bulk density has a standard deviation of 3.3 kg/m^3. In other words a good calibration line will provide excellent density predictions. Also observe the fact that at the low energy the standard deviation increases more than twice.

At the voxel level things are not as smooth. Figure 98 shows the distribution of standard deviations for the high energy readings at a voxel level and for a number of randomly selected voxels. It can be seen that for Berea the standard deviation varies between 8 and 15 CT numbers, while for the dolomite the standard deviation varies between 20 and 40 CT numbers. Since 10 CT numbers correspond to density change of 13.6 kg/m^3 the limits of bulk density reproducibility can be easily defined for each type of rock. This sensitivity of the CT number readings is due to the statistical and non-monochromatic nature of the x-rays and it must be machine dependent.

In order to reduce the statistical error in the CT number measurement, averaging is required. As mentioned already, slice averages give highly reproducible results. The standard deviation in Berea drops to 5 CT numbers if averaging of nine voxels is done (Figure 98). Proper averaging can increase the reproducibility of the results to within an acceptable standard deviation. However, care must be taken so that averaging does not smooth heterogeneities. As an example let us illustrate this argument using the frequency distributions for the Berea and the dolomite slices. Figure 99 shows the frequency distributions of the five scans of the Berea slice overlayed. Figure 99A shows the CT number frequency distribution at the high energy, Figure 99B shows the CT number frequency distribution at the low energy, Figure 99C shows the bulk density frequency distribution and Figure 99D shows the porosity frequency distribution. The corresponding frequency plots for the dolomite are given in Figure 100A-D. Note that the scales for the x-axis in each plot were kept the same to enhance the effect of the heterogeneity. Looking at the CT numbers one can observe that the high energy distributions are considerably narrower than the low energy distributions (less statistical error). Also the overlay is almost invisible in Berea and a lot more visible for the dolomite. One would expect that averaging over more voxels should be attempted for the dolomite. However, since the dolomite is the most heterogeneous, the least possible averaging should be attempted to avoid hiding any heterogeneities. Looking at the porosity frequency distributions, Berea is very uniform, but the dolomite has a number of peaks which could be interpreted as overlaying frequency distributions. This is consistent with Moss *et al.* (1990). Averaging can hide this effect. In conclusion, although averaging can increase the precision of the measurements it should be done in a way that does not erase useful information from the data under study.

© 1991 NOVA HUSKY RESEARCH CORPORATION

Looking now at concentration or saturation measurements, one can easily realize that the determination of concentrations or saturations as functions of time and location could be of great importance for reservoir simulation. These functions can be obtained at a voxel level or any other volumetric average of voxels. In order for the saturation measurements to be precise, the contrast between phases has to be at least one order of magnitude larger than the standard deviation. Of course, the larger the averaging the less the effect of the standard deviation. The choice of fluid pairs and method of analysis of the results is dictated by the attainable contrast.

b. Bacteriological Mineral Plugging

The presented experimental results validate the work done earlier on by Ferris *et al.* (1990). Again, bacterial action has promoted mineral plugging in unconsolidated cores and consolidation of unconsolidated material occurred. Porosity and permeability were reduced, although there was no complete plugging of any of the cores. With the exception of column D, where facial plugging was observed, the density and porosity changes occurred in a distance of 8 to 15 cm in length starting from 3 to 6 cm from the face. The fact that the glass bead column was plugged indicates that there is no need for particles, such as clays to exist in order to have bacterial mineral plugging. The results also indicate that the amount of plugging is roughly proportional to the amount of nutrient passed through the core. The permeability and porosity reductions are more profound in column B, followed by columns A, C, D. The lack of considerable plugging in column C also shows that there is a critical rate below which mineral plugging is not really occurring. The position and shape of the porosity profiles after mineral plugging indicates that the bacterial distribution may not be uniform through the core. This, however, is not supported by the bacterial counts performed in sections of all the columns. It was also evident that if the bacteria are allowed to migrate in the core because of low flow rates, facial plugging, the characteristic of all other bacterial processes will occur. It is also evident (Figure 129) that population peaks inside the porous medium are also sites for mineral plugging. The fact that both glass beads and sand pack were plugged and that in both cases consolidation (cementation) occurred should not go without notice. A series of applications related to sand consolidation could spring out of this work. This and other issues will be addressed in future work.

5.0 CONCLUSIONS

Computer Assisted Tomography of x-rays has a great potential for the nondestructive characterization of reservoir rock. Monitoring of multiphase flow experiments can be done using this method. However, the

© 1991 NOVA HUSKY RESEARCH CORPORATION

results are affected by the lack of contrast between the faces. The errors in measurements are predominantly associated with the statistical nature of the x-rays and the accuracy of the calibration process.

Custom made models could increase the accuracy of two phase saturation algorithms to acceptable levels. In the case of three phase saturations there is need for a lot more work before the semi qualitative results which were presented in this report could be quantified any further. A combination of independent property measurements could be more accurate than dual energy scanning.

Bacteriogenic mineral plugging occurs in glass bead as well as in sand packs. There seems to be a critical nutrient injection rate below which bacterial plugging is not practical. Bacterial mineral plugging efficiency is affected by the porous media properties, the number of bacteria present and the total volume of nutrients injected.

6.0 ACKNOWLEDGEMENTS

The authors would like to thank Energy, Mines and Resources Canada for partial funding of this project through the CANMET contract 23440-9-9258 named "Fluid Flow Phenomena in Heterogeneous Systems" and especially the Scientific Authority, Dr. Kamal Jha.

The authors would also like to thank the following people for helping, in one way or another, with the completion of this project: T. Jack, K. Ikeda-Cameron, R. Glover, K. Allsop (NHRC), J. Peggs, I. Adamache, M. Pow, V. Cheung, (Husky Oil).

7.0 REFERENCES

a. Computer Assisted Tomography

Alvestad, J., Gilje, E., Hove, A.O., Langeland, O., Maldal, T. and Schilling, B.E.R.,
"Coreflood Experiments with Surfactant Systems for IOR: Computer Tomography Studies and Numerical Modelling",
Proc. V1B2, p.789, presented at the 6th European IOR Symposium in Stavanger, Norway, May 21-23, 1991.

© 1991 NOVA HUSKY RESEARCH CORPORATION

Anderson, S.H., Peyton, R.L. and Gantzer, C.J.,
"Evaluation of Constructed and Natural Soil Macropores Using X-Ray Computed Tomography",
Geoderma, 46, p.13, 1990.

Antolovich, S.D., Gokhale, A.M. and Bathias, C.,
"Applications of Quantitative Fractography and Computed Tomography to Fracture Processes in Materials",
in Quantitative Methods in Fractography, ASTM STP 1085, B.M. Strauss and S.K. Putatunda, Eds, American Society for Testing and Materials, Philadelphia, p.3, 1990.

Auzerais, F.M., Ellis, D.V., Luthi, S.M., Dussan, E.B.V and Pinoteau, B.J., "Laboratory Characterization of Anisotropic Rocks",
SPE 20602 presented at the 65th Annual Technical Conference and Exhibition of the Society of Petroleum Engineers held in New Orleans, LA, September 23-26, 1990.

Barroux, C., Bouvier, L., Maquignon, P. and Thiebot, B.,
"Alternate Dual-Energy Gamma-Ray Attenuation Technique: A New Tool for Three-Fluid Saturation Measurements in IOR Flood Experiments",
Proc. V1B1, p.193, presented at the 6th European IOR Symposium in Stavanger, Norway, May 21-23, 1991.

Burchfield, T.E. and Chung, F.T.H.,
"Development of Improved Immiscible Gas Displacement Methodology",
NIPER progress report, 1988.

Chatzis, I., Kantzas, A. and Dullien, F.A.L., "On the Investigation of Gravity Assisted Inert Gas Injection Using Micromodels, Long Berea Cores and Computer Assisted Tomography",
SPE 182840 presented at the 63rd Annual Technical Conference and Exhibition of the Society of Petroleum Engineers held in Houston, TX, October 2-5, 1988.

Chatzis, I. and Berry, J.,
"Vug Size Distributions in Vuggy Carbonates Determined Non-Destructively by x-Ray CT",
CIM/AOSTRA 91-74, presented at the 1991 Technical Conference jointly hosted by the Petroleum Society of CIM and Alberta Oil Sands Technology and Research Authority in Banff, Alberta on April 21 to 24, 1991.

Cruvinel, P.E., Cesareo, R., Crestana, S. and Mascarenhas, S.,
"X- and g- Rays Computerized Minitomograph Scanner for Soil Science",
IEEE Trans Instrum Measur, 39(5), p.745, 1990.

Gilliland R.E. and Coles, M.E., "Use of CT Scanning in the Investigation of Damage to Unconsolidated Cores",
SPE 19408, presented at the SPE Formation Damage Control Symposium held in Lafayette, Louisiana, February 22-23, 1990.

Graue, A.,
"Imaging the Effects of Capillary Heterogeneities on Local Saturation Development in Long Core Floods",
SPE 21101, presented at the SPE Latin American Petroleum Engineering Conference held in Rio de Janeiro, October 14-19, 1990.

© 1991 NOVA HUSKY RESEARCH CORPORATION

Hara, S.K. and Christman, P.G.,
"Investigation of a Cyclic Countercurrent Light-Oil/CO_2 Immiscible Process",
SPE/DOE 20207 presented at the SPE/DOE Seventh Symposium on Enhanced Oil Recovery held in Tulsa Oklahoma, April 22-25, 1990.

Hicks, P.J.Jr., Deans, H.A. and Narayanan, K., "Experimental Measurement of the Distribution of Residual Oil Saturations in Heterogeneous Carbonate Cores Using X-Ray Computerized Tomography",
CIM/SPE 90-68, SPE 21574 presented at the International Technical Meeting Jointly hosted by the Petroleum Society of CIM and the Society of Petroleum Engineers in Calgary, June 10-13, 1990.

Hicks, P.J.Jr., Narayanan, R. and Deans, H.A., "An Experimental Study of Miscible Displacements in Heterogeneous Carbonate Cores Using X-Ray CT",
SPE 20492, presented at the 65th Annual Technical Conference and Exhibition of the Society of Petroleum Engineers held in New Orleans, LA, September 23-26, 1990.

Honarpour, M., Maloney, D., Suzuki, S. and Tomutsa, L., "Investigation of Cycle Dependent Centrifuge Capillary Pressure and Wettability Index Behavior for Water-wet High Permeability Sandstones",
Paper 9006, presented at the Fourth Annual Technical Conference of the Society of Core Analysts, held in Dallas, TX, August 15-16, 1990.

Jasti, J. and Fogler, H.S.,
"Determination of Flow Profiles in Porous Media Using Shifts in Gama Spectra",
AIChE J, 36(6), p.827, 1990.

Jasti, J., Jesion, G. and Feldkamp, L.,
"Microscopic Imaging of Porous Media Using X-Ray Computer Tomography",
SPE 20495, presented at the 65th Annual Technical; Conference and Exhibition of the Society of Petroleum Engineers held in New Orleans, LA, September 23-26, 1990.

Kantzas, A., Marentette, D.F., Erno, B. and Harding, S., "Characterization of a Heavy Oil Reservoir Using Computer Assisted Tomography of Core Material",
Paper No 16, presented at the Third Petroleum Conference of the South Saskatchewan Section of the Petroleum Society of CIM held in Regina, Sask., Sept. 25-27, 1989.

Kantzas, A., Marentette, D.F. and Skalinski, M., "Computer Assisted Tomography as a Complementary Tool to Well Logging",
Paper P, presented at the Twelfth Formation Evaluation Symposium of the Canadian Well Logging Society held in Calgary, Alberta, Sept. 26-28, 1989.

Kantzas, A., "Investigation of Physical Properties of Porous Rocks and Fluid Flow Phenomena in Porous Media Using Computer Assisted Tomography",
In Situ, 14(1), p.77, 1990.

Kantzas, A., "Applications of Computer Assisted Tomography in the Quantitative Characterization of Reservoir Rocks",
J Can Pet Tech, submitted for publication, 1991.

© 1991 NOVA HUSKY RESEARCH CORPORATION

Kantzas, A., "Determination of Sulphur Saturation in Dolomitic Sour Gas Reservoir Using Computer Assisted Tomography",
In Situ, submitted for publication, 1991.

Lenormand, R., Kalaydjian, F., Bieber, M-T. and Lombard, J-M., "Use of Multifractal Approach for Multiphase Flow in Heterogeneous Porous Media: Comparison with CT-Scanning Experiment",
SPE 20475, presented at the 65th Annual Technical Conference and Exhibition of the Society of Petroleum Engineers held in New Orleans, LA, September 23-26, 1990.

MacAllister, D.J., Miller, K.C., Graham, S.K. and Yang, C.T.,
"Application of X-Ray CT Scanning to the Determination of Gas-Water Relative Permeabilities",
SPE 20494, presented at the 65th Annual Technical Conference and Exhibition of the Society of Petroleum Engineers held in New Orleans, LA, September 23-26, 1990.

Mohanty, K.K. and Miller, A.E., "Factors Influencing Unsteady Relative Permeability of a Mixed-Wet Reservoir Rock",
SPE 18292, presented at the 63rd Annual Technical Conference and Exhibition of the Society of Petroleum Engineers held in Houston, TX, October 2-5, 1988.

Moss, R.M., Pepin, G.P. and Davis, L.A., "Direct Measurement of the Constituent Porosities in a Dual Porosity Matrix",
Paper 9003, presented at the Fourth Annual Technical Conference of the Society of Core Analysts, held in Dallas, TX August 15-16, 1990.

O'Meara, D.J. and Vinegar, H.J.,
"Method for determining Capillary Pressure and Relative Permeability by Imaging",
U.S. Patent 4,893,504, 1990.

Poter, G.F. and Groves, D.R.,
"Displacements, Saturations, and Porosity Profiles from Steady-State Permeability Measurements",
SPE 19679, presented at the 64th Annual Technical Conference and Exhibition of the Society of Petroleum Engineers held in San Antonio, TX, October 8-11, 1989.

Peters, E.J.and Hardham, W.D., "Visualization of Fluid Displacements in Porous Media Using Computed Tomography Imaging",
J Pet Sci Eng, 4, p.155, 1990.

Sprunt, E.S., Desai, K.P., Coles, M.E., Davis, E.M. and Muegge, E.L.,
"CT-Scan-Monitored Electrical Resistivity Show Problems Achieving Homogeneous Saturation",
SPERE, 6(2), p.134, 1991.

Torres, G., Tester, V.J. and Sharer, J.,
"Computerized Tomography as a Geoscience Tool",
in Rock Mechanics Contributions and Challenges, Hustrulid and Johnson editors, Balkema, Rotterdam, p.637, 1990.

Vinegar, H.J. and Wellington, S.L., "Tomographic Imaging of Three-phase Flow Experiments",
Rev. Sci. Instrum., 58(1), p.96, 1987.

© 1991 NOVA HUSKY RESEARCH CORPORATION

Withjack, E.M., Graham., S.K. and Yang, C-T., "Determination of Heterogeneities and Miscible Displacement Characteristics in Corefloods by CT Scanning",
SPE 20490, presented at the 65th Annual Technical Conference and Exhibition of the Society of Petroleum Engineers held in New Orleans, LA, September 23-26, 1990.

b. Bacteriological Mineral Plugging

Belyaev, S.S., Ivanov, M.V., Matz, A.A. and Borisov, A.Y.,
"Pilot tests of Biotechnology Applied to Enhance Oil Recovery"
Proceedings V2B1, p.243, presented at the 6th European IOR Symposium in Stavanger, Norway, May 21-23, 1991.

Berner, R.A.,
"Early Diagenesis A Theoretical Approach",
Princeton University Press, 1980.

Bryant, R.S. and Douglas, J.,
"Evaluation of Microbial Systems in Porous Media for EOR",
SPERE, 3(2), p.489, 1988.

Bryant, R.S., Chung, F.T.H., Chang, M.M. and Burchfield, T.E.,
"Development of an MEOR Process Simulator for Laboratory and Porous Media Studies",
Status Report, NIPER 490 October 1990.

Ferris, F.G., Stehmeier, L. and Islam, R.,
"Microbial Selective Plugging for Reservoir Conformance Correction to Enhance Heavy Oil Recovery",
NHRC report No. 525, 1990.

Gruesbeck, G. and Collins, R.E.,
"Entrainment and Deposition of Fine Particles in Porous Media",
Soc Pet Eng J, 22(12), p.847, 1982.

Islam, M.R. and Gianetto, A.,
"Mathematical Modelling and Scaling Up of Microbial Enhanced Oil Recovery",
CIM/SPE 90-131, presented at the International Technical Meeting Jointly Hosted by the Petroleum Society of CIM and the Society of Petroleum Engineers in Calgary, June 10 to 13, 1990.

Islam, M.R.,
"Mathematical Modeling of Microbial Enhanced Oil Recovery",
SPE 20480, presented at the 65th Annual Technical Conference and Exhibition of the Society of Petroleum Engineers held in New Orleans, LA, September 23-26, 1990.

Jack, T.R. and Stehmeier, L.G.,
"Selective Plugging in Watered-out Oil Wells",
Proceedings of the Symposium on Application of Microorganisms to Petroleum Technology, Bartlesville, Oklahoma, August 12-13, 1987 W. Linville, editor, U.S. Department of Energy, Bartlesville, OK, 1988.

© 1991 NOVA HUSKY RESEARCH CORPORATION

Jack, T.R.,
"International Workshop on Microbially Enhanced Oil Recovery",
NHRC memorandum, 90/06/06.

Jack, T.R.,
"Microbial Enhancement of Oil Recovery",
Current Opinion in Biotechnology, 1991.

Jack, T.R., Stehmeier, L.G., Islam, M.R. and Ferris, F.G.,
"Microbial Selective Plugging to Control Water Channelling",
In Microbial Enhancement of Oil Recovery - Recent Advances, E.C. Donaldson, Editor, CH.F-6, p.433, 1991.

Jenneman, G.E., Knapp, R.M., McInerey, M.J., Menzie, D.E. and Revus, D.E.,
"Experimental Studies of In-situ Microbial Enhanced Oil Recovery",
Soc Pet Eng J, 24(2), p.33, 1984.

Kalish, P.J., Stewart, J.A., Rogers, W.F. and Bennett, E.O.,
"The Effect of Bacteria on Sandstone Permeability",
J Pet Tech, 6, p.805, July 1964.

King, J.W. and Stevens, D.A.,
Editors, "Proceedings of the First International MEOR Workshop, April 1-3, 1986",
DOE/BC/10852-1, January 1987.

Knapp, R.M., McInerney, M.J. and Menzie, D.E.
"Microbial Strains and Products for Mobility Control and Oil Displacement. Final Report for the Period July 1, 1980 - February 28, 1986",
DOE/BC/10300-45, December 1987.

Lappin-Scott, H.M., Cusack, F. and Costerton, J.W.,
"Nutrient Resuscitation and Growth of Starved Cells in Sandstone Cores: a Novel Approach to Enhanced Oil Recovery",
Appl Envir Microbiol, 54(6), p.1373, 1988.

MacLeod, F.A., Lappin-Scott, H.M. and Costerton, J.W.,
"Plugging of a Model Rock System by Using Starved Bacteria",
Appl Envir Microbiol, 54(6), p.1365, 1988.

McInerney, M.J., Menzie, D.E., Jenneman, G.E. and Knapp, R.M.,
"The Use of Microorganisms in Enhanced Oil Recovery. First Annual Report, Oct. 1, 1980 - Sept. 30 , 1982",
DOE/BC/10300-34, September 1983.

Nelson, S.J. and Launt, P.D.,
"Stripper Well Production Increased with MEOR Treatment",
Oil and Gas Journal, p.114, March 18, 1991.

© 1991 NOVA HUSKY RESEARCH CORPORATION

Premuzic, E.T. and Lin, M.,
"Prospects for Thermophilic Microorganisms in Microbial Enhanced Oil Recovery (MEOR)",
SPE 21015, presented at the SPE International Symposium on Oilfield Chemistry held in Anaheim, California, February 20-22, 1991.

Puon, R.S., Ameri, S., Aminian, K., Durham, D.L., Wasson, J.A. and Watts, R.J.,
"CO_2 Mobility Control Carbonate Precipitation: Experimental Study",
SPE 18529 presented at the SPE Eastern Regional Meeting in Charleston, WV, November 1-4, 1988.

Stehmeier, L.G., Jack, T.R., Blakely, B.A. and Cambell, J.M.,
"Field Test of a Microbial Plugging System at Standard Hill, Saskatchewan to Inhibit Oilfield Water Encroachment",
Biohydrometallurgy, Proceedings of the International Symposium, Jackson Hole, Wyoming, J. Salley, R.G.L. McCready, P.L. Wichlacz, editors, p.699, 1990.

© 1991 NOVA HUSKY RESEARCH CORPORATION

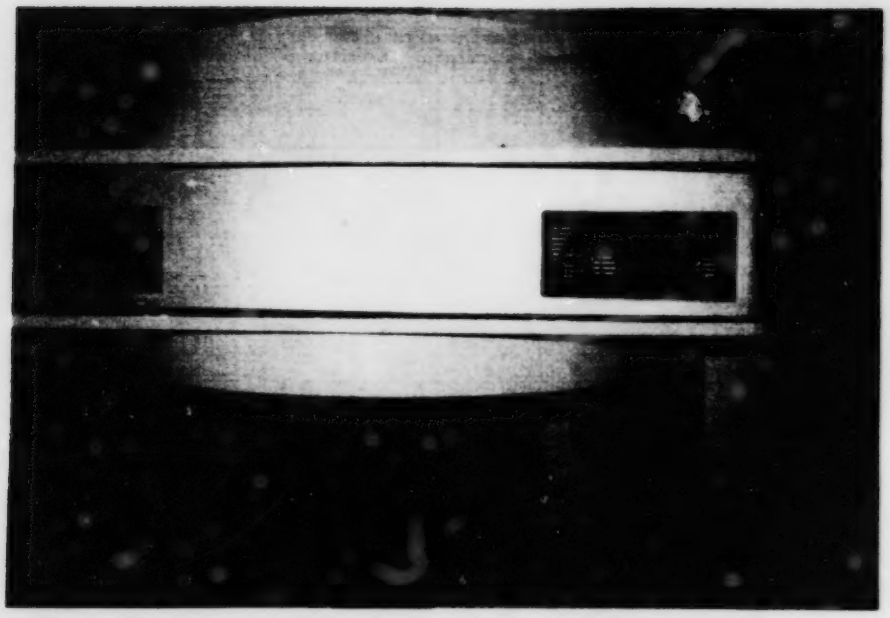

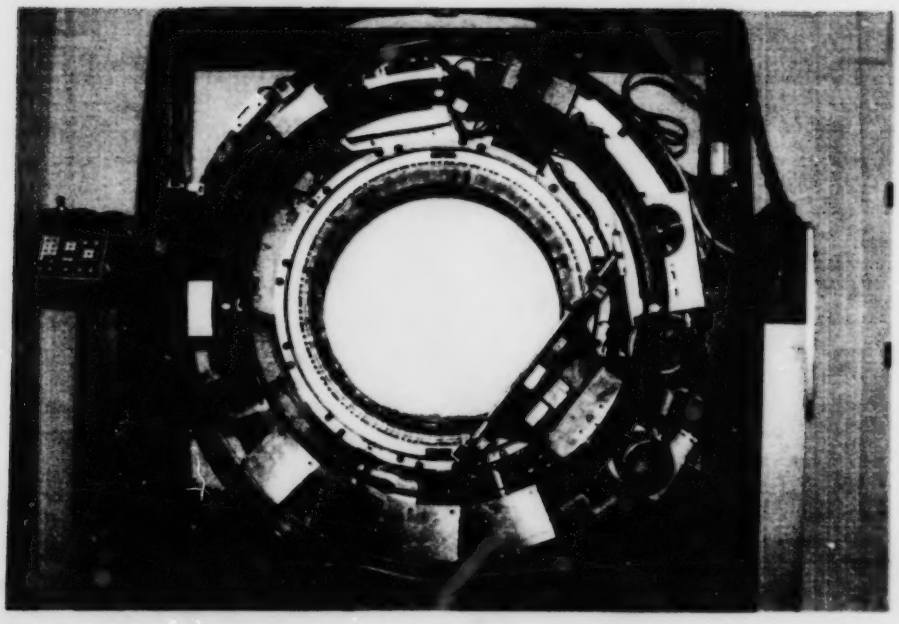

Figure 1: Photographs of 7070 scanner gantry.

© 1991 NOVA HUSKY RESEARCH CORPORATION

Figure 2: Photographs of 7070 scanner holder.

© 1991 NOVA HUSKY RESEARCH CORPORATION

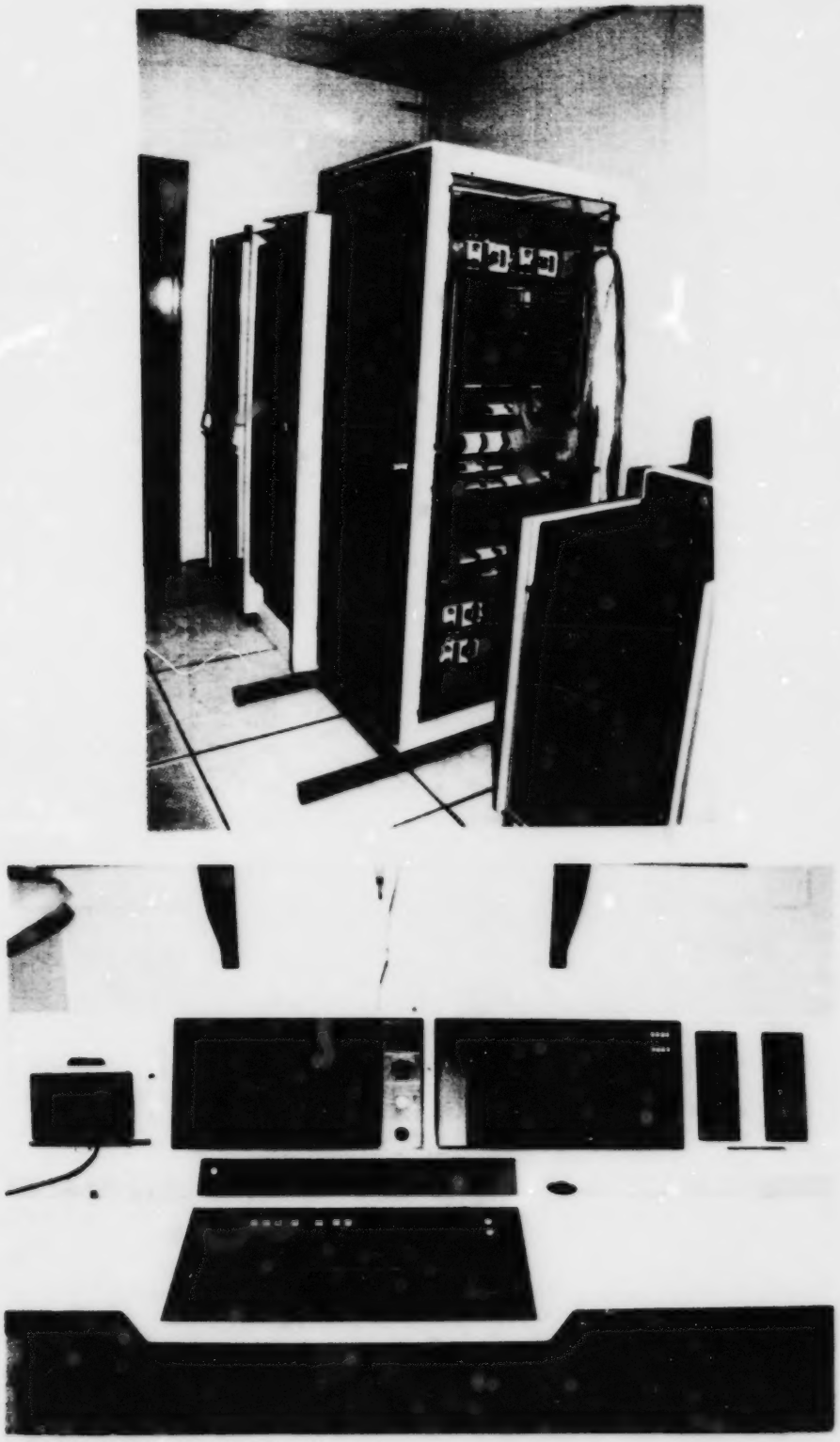

Figure 3: **Photographs of 7070 scanner control system and console.**

© 1991 NOVA HUSKY RESEARCH CORPORATION

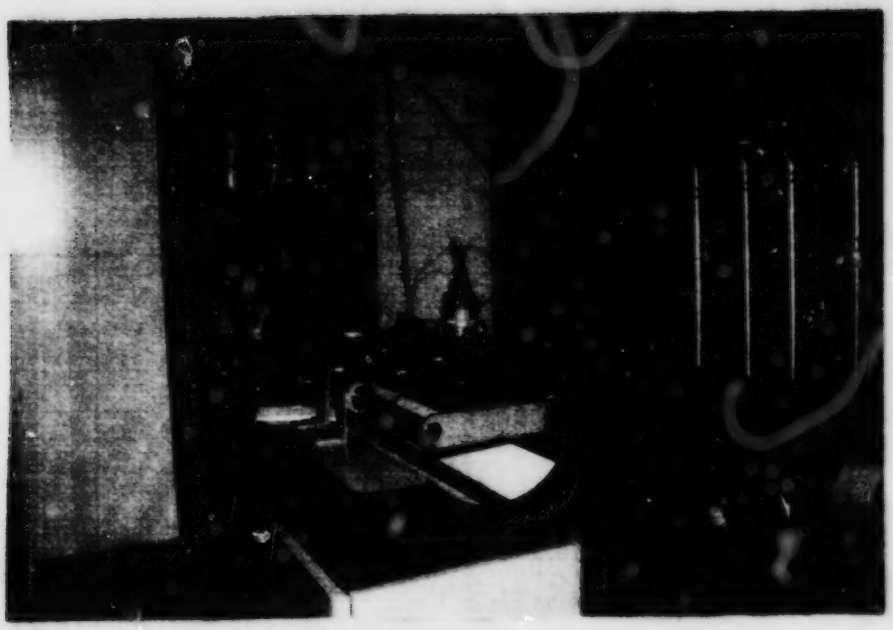

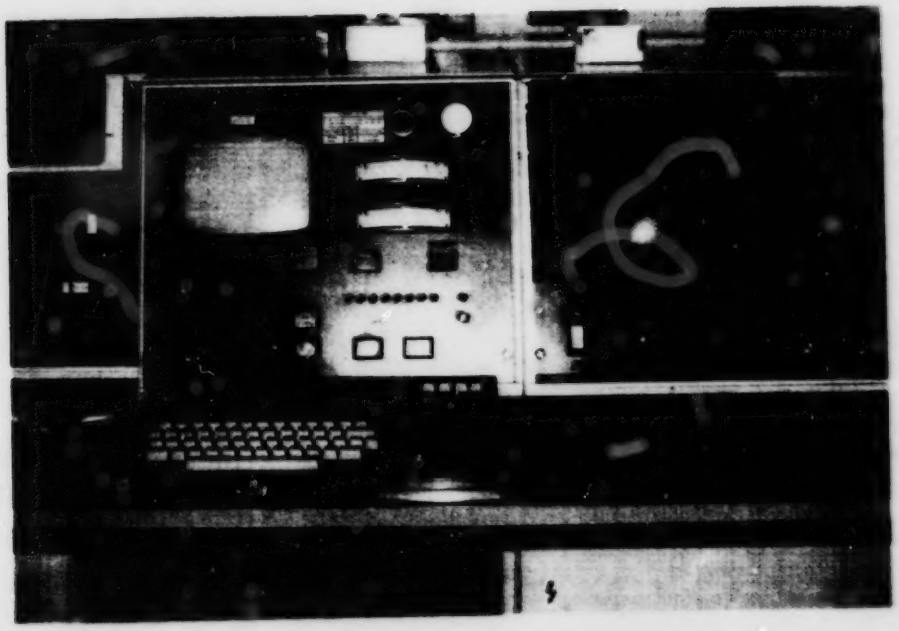

Figure 4: **Photographs of the 5005 scanner and console.**

© 1991 NOVA HUSKY RESEARCH CORPORATION

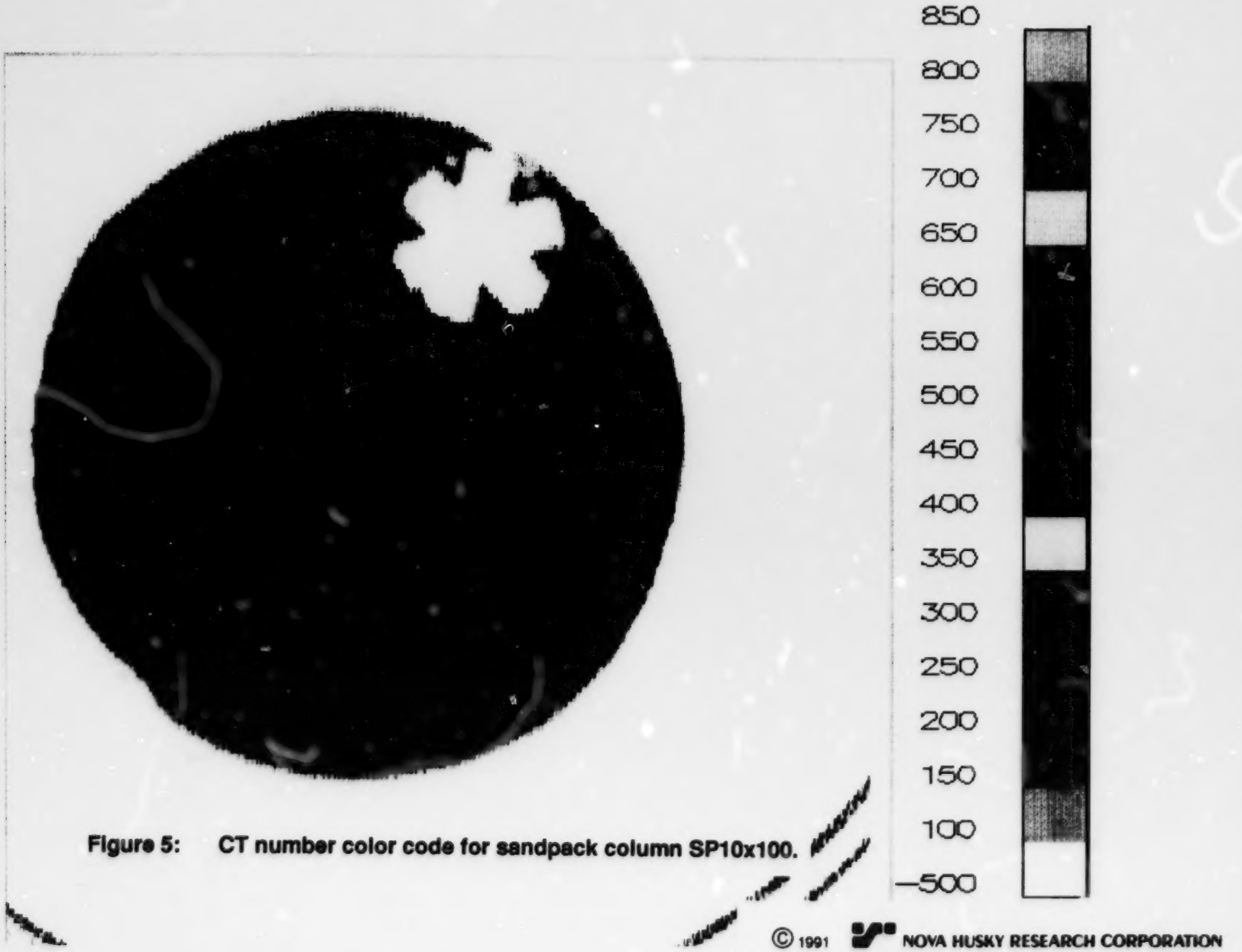

Figure 5: CT number color code for sandpack column SP10x100.

© 1991 NOVA HUSKY RESEARCH CORPORATION

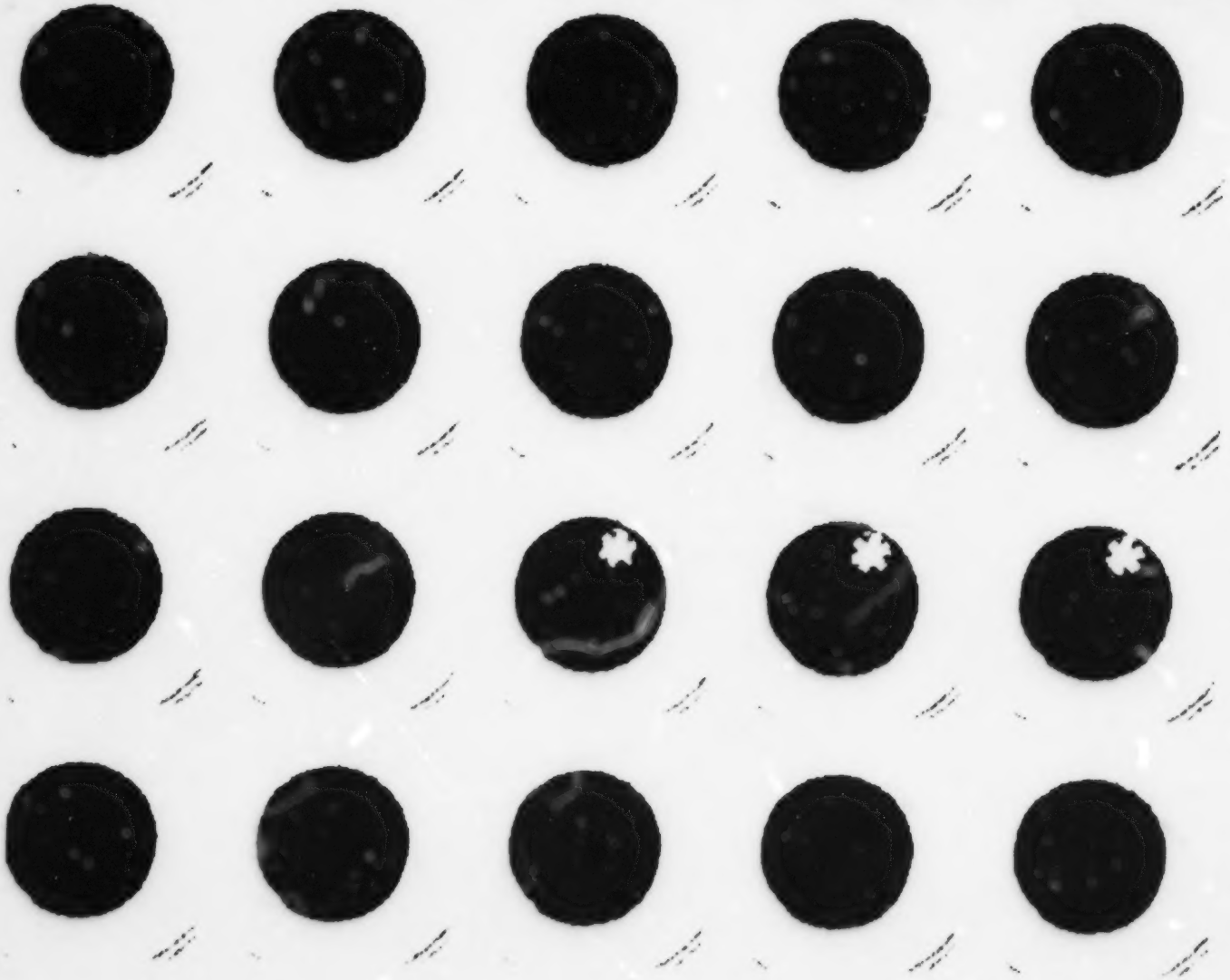

Figure 6: **Vuggy sandpack SP10x100 CT images of slices 1 to 20 (arrangement by rows).**

© 1991 NOVA HUSKY RESEARCH CORPORATION

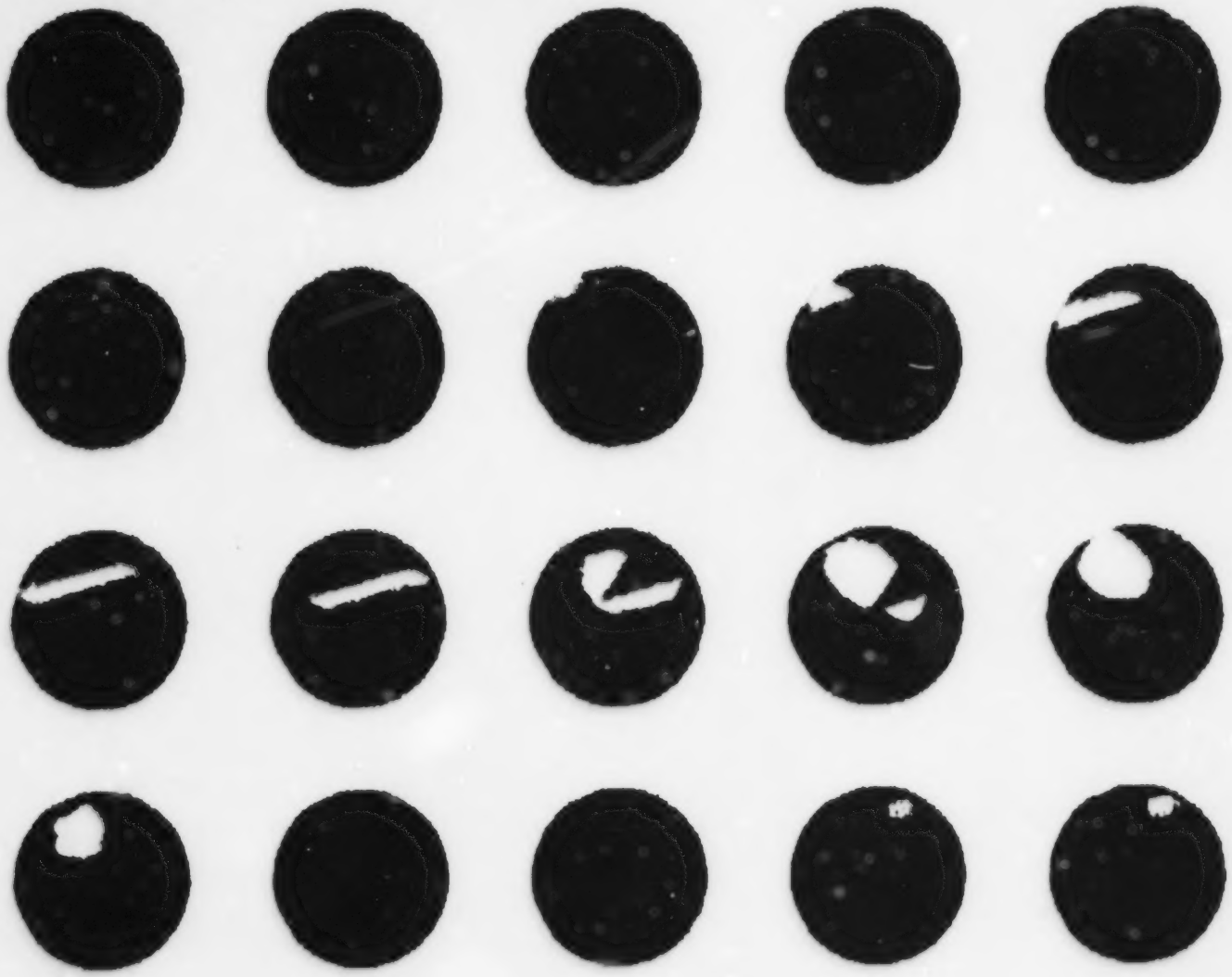

Figure 7: Vuggy sandpack SP10x100 CT images of slices 21 to 40 (arrangement by rows).

© 1991 NOVA HUSKY RESEARCH CORPORATION

Figure 8: Vuggy sandpack SP10x100 CT images of slices 41 to 60 (arrangement by rows).

© 1991 NOVA HUSKY RESEARCH CORPORATION

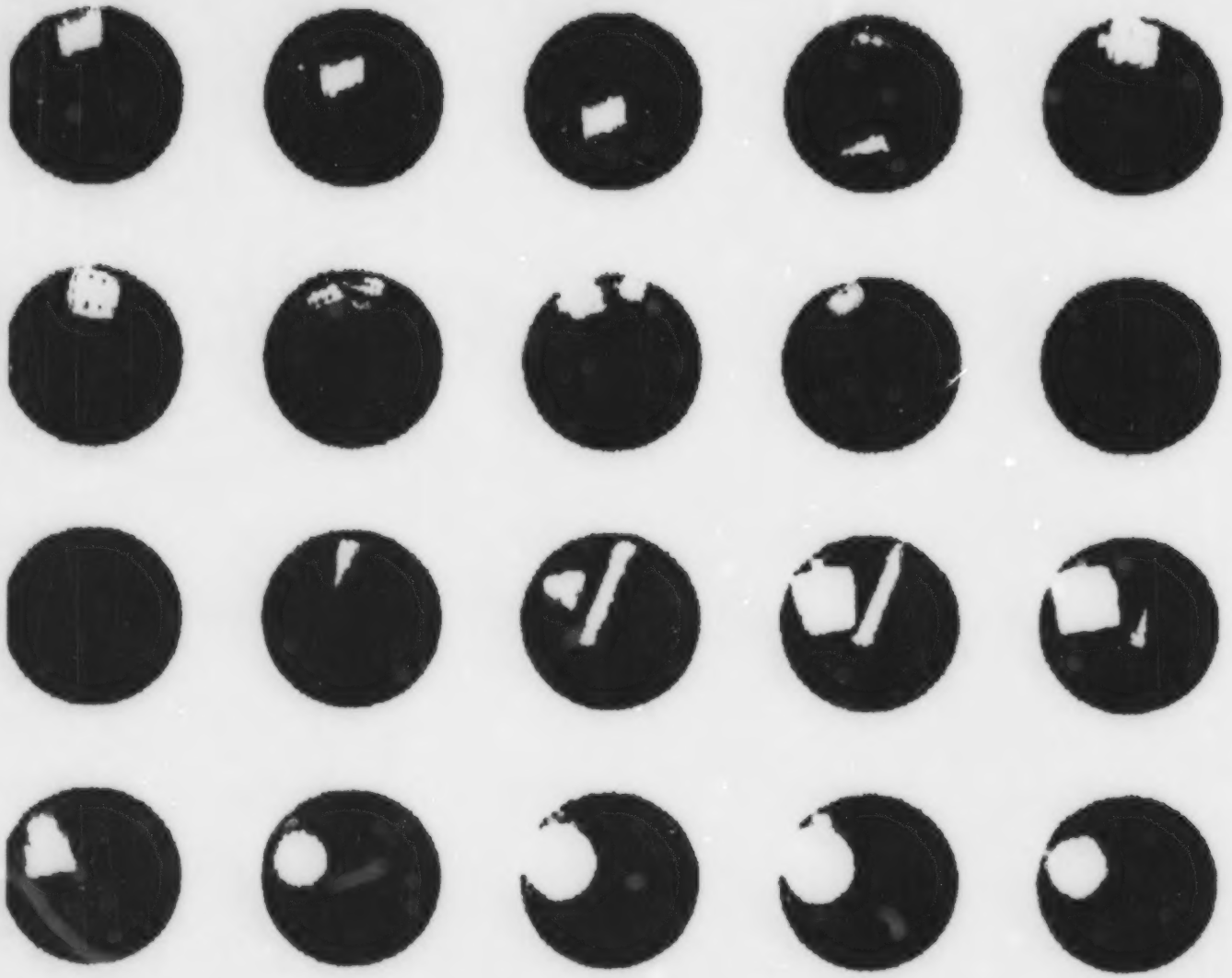

Figure 9: Vuggy sandpack SP10x100 CT images of slices 61 to 80 (arrangement by rows).

© 1991 NOVA HUSKY RESEARCH CORPORATION

Figure 10: Vuggy sandpack SP10x100 CT images of slices 81 to 92 (arrangement by rows).

© 1991 NOVA HUSKY RESEARCH CORPORATION

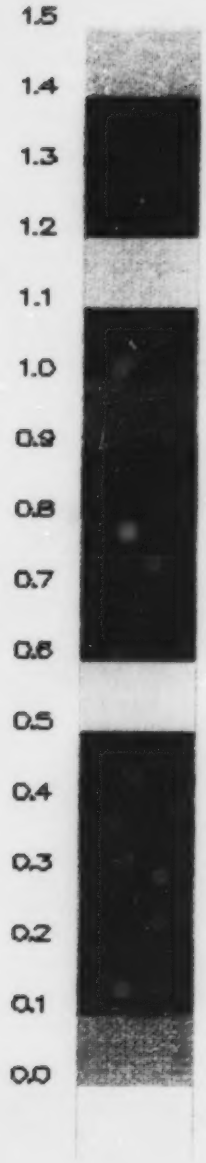

Figure 11: Colorcode for saturation images.

© 1991 NOVA HUSKY RESEARCH CORPORATION

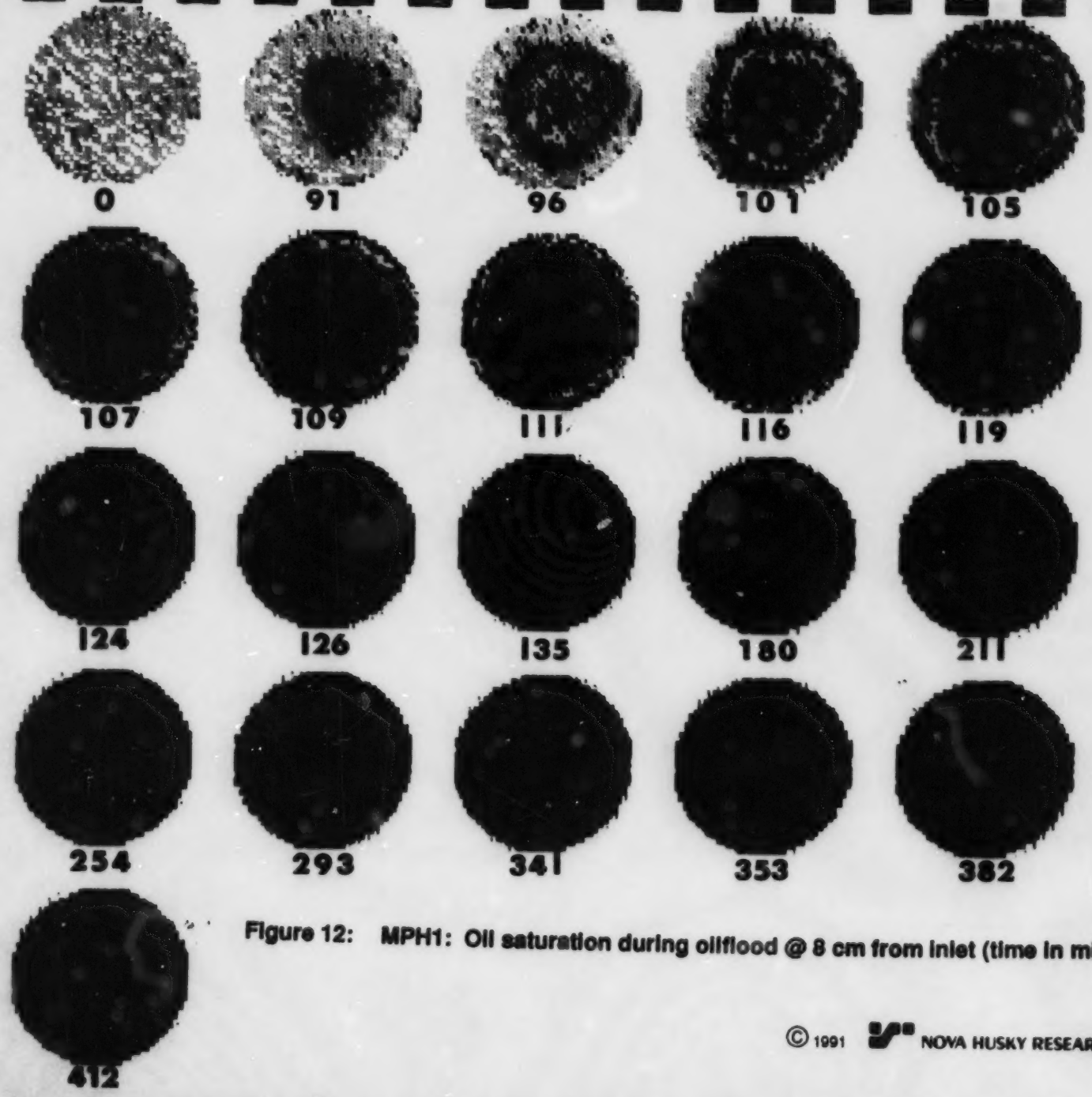

Figure 12: MPH1: Oil saturation during oilflood @ 8 cm from inlet (time in minutes).

© 1991 NOVA HUSKY RESEARCH CORPORATION

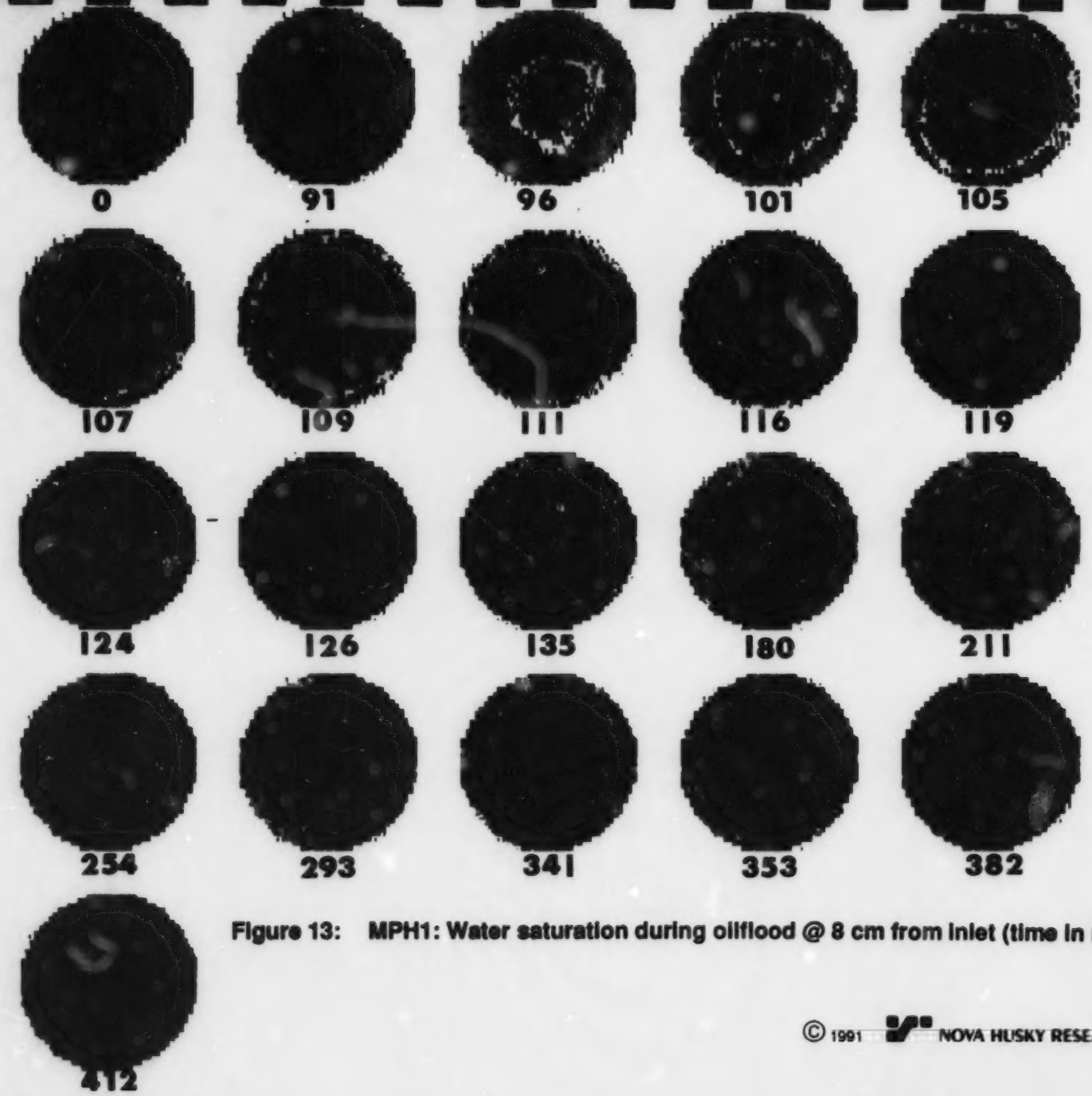

Figure 13: MPH1: Water saturation during oilflood @ 8 cm from inlet (time in minutes).

© 1991 NOVA HUSKY RESEARCH CORPORATION

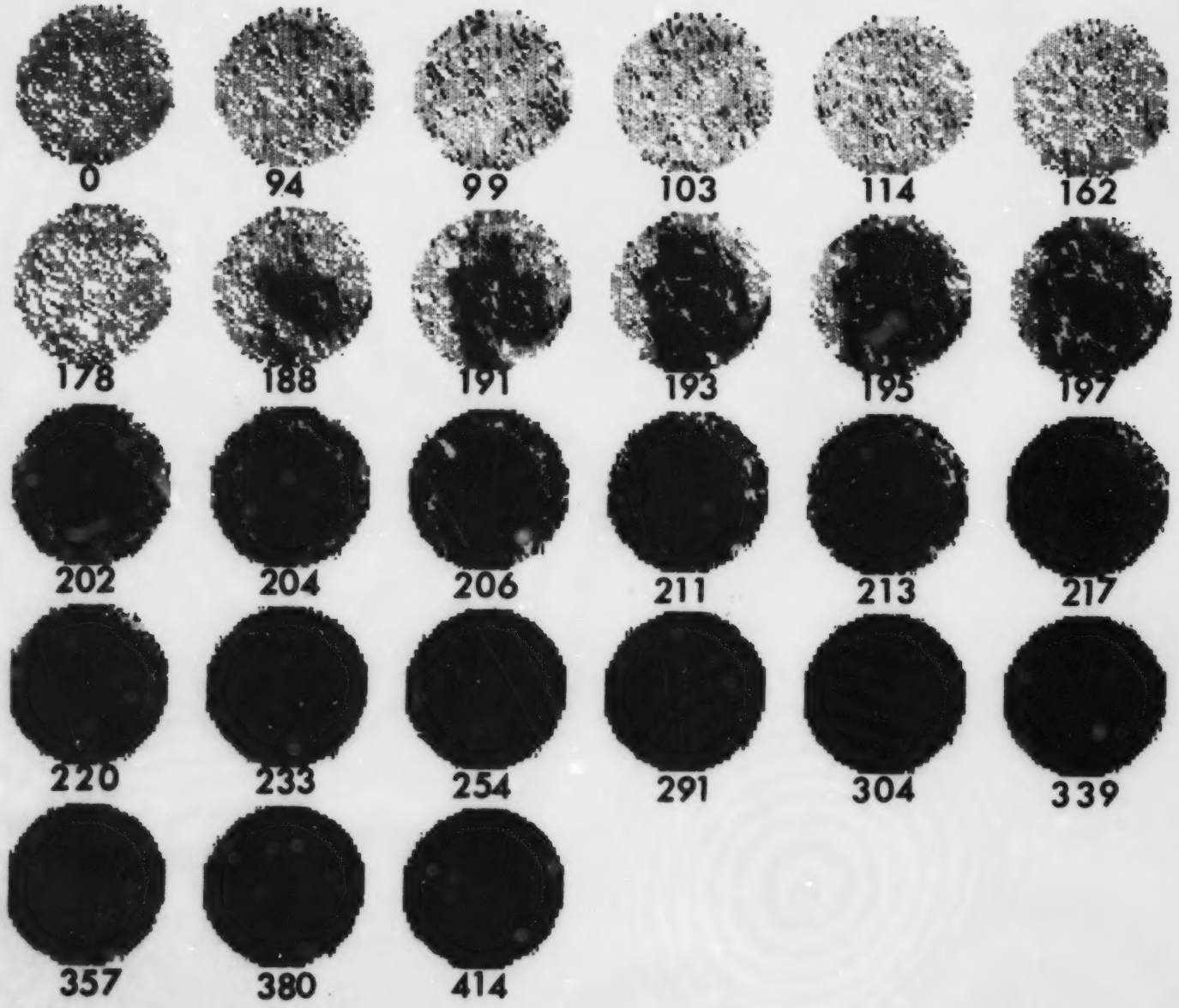

Figure 14: MPH1: Oil saturation during oilflood @ 16 cm from inlet (time in minutes).

© 1991 NOVA HUSKY RESEARCH CORPORATION

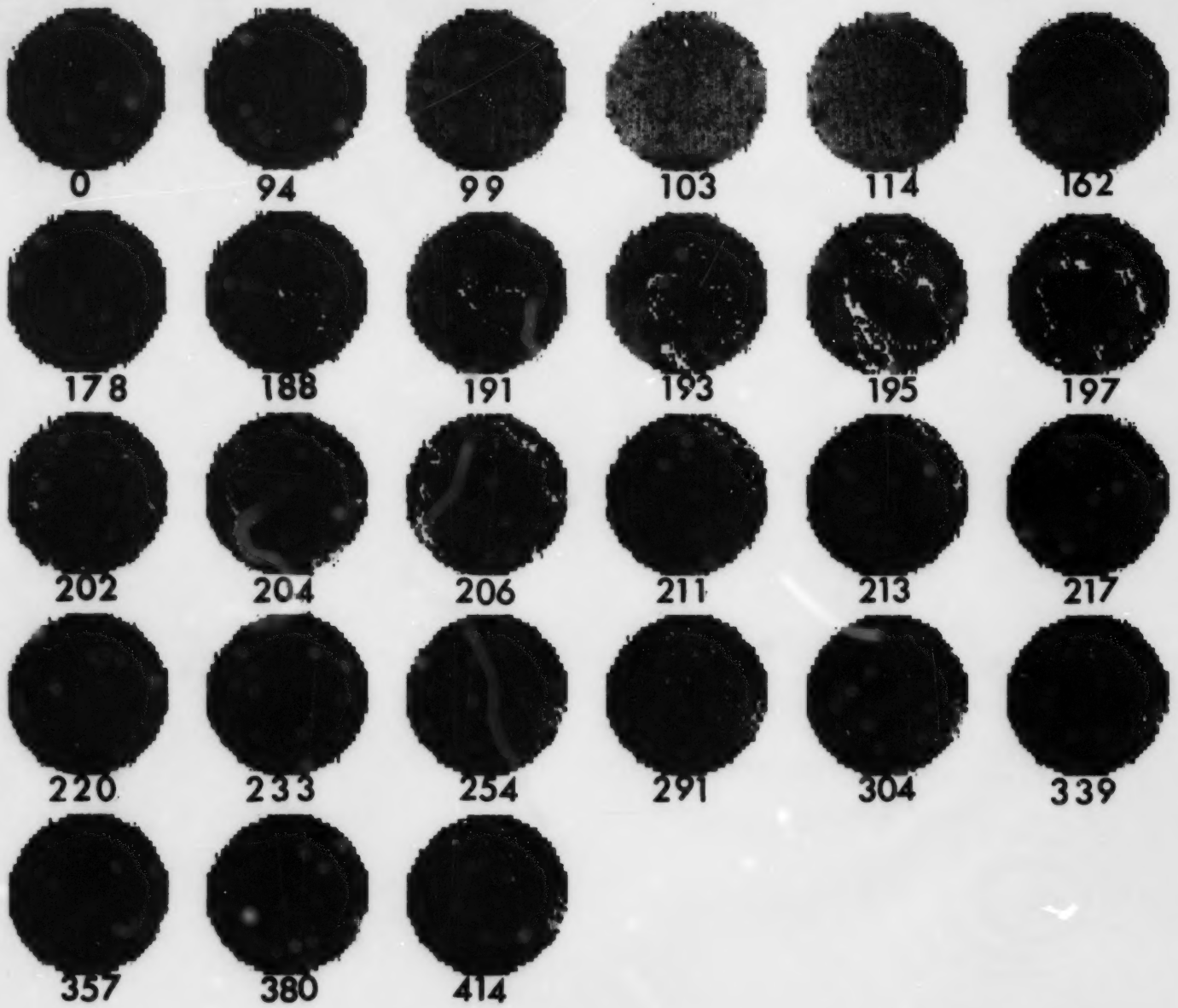

Figure 15: MPH1: Water saturation during oilflood @ 16 cm from inlet (time in minutes).

© 1991 NOVA HUSKY RESEARCH CORPORATION

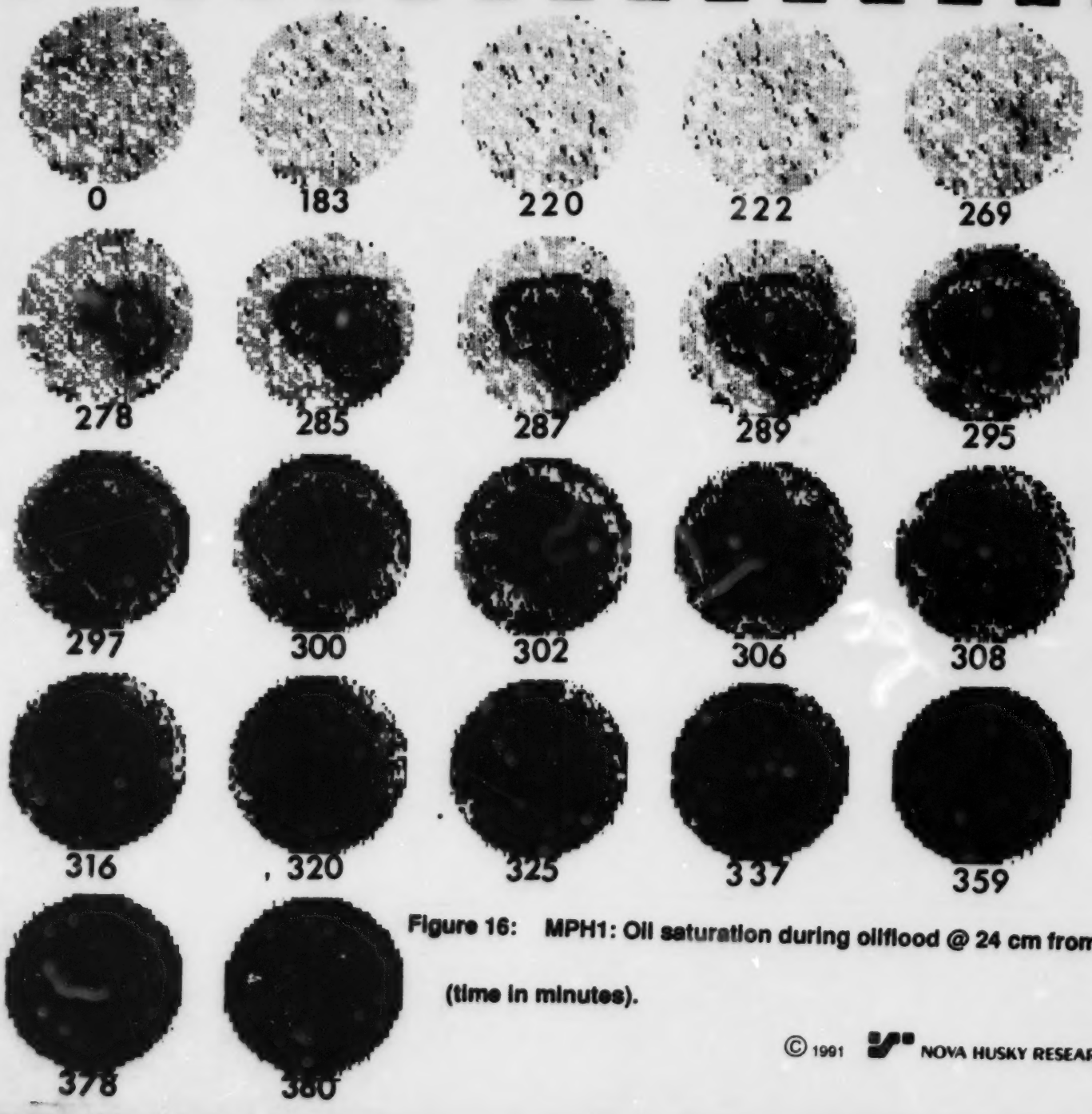

Figure 16: MPH1: Oil saturation during oilflood @ 24 cm from inlet (time in minutes).

© 1991 NOVA HUSKY RESEARCH CORPORATION

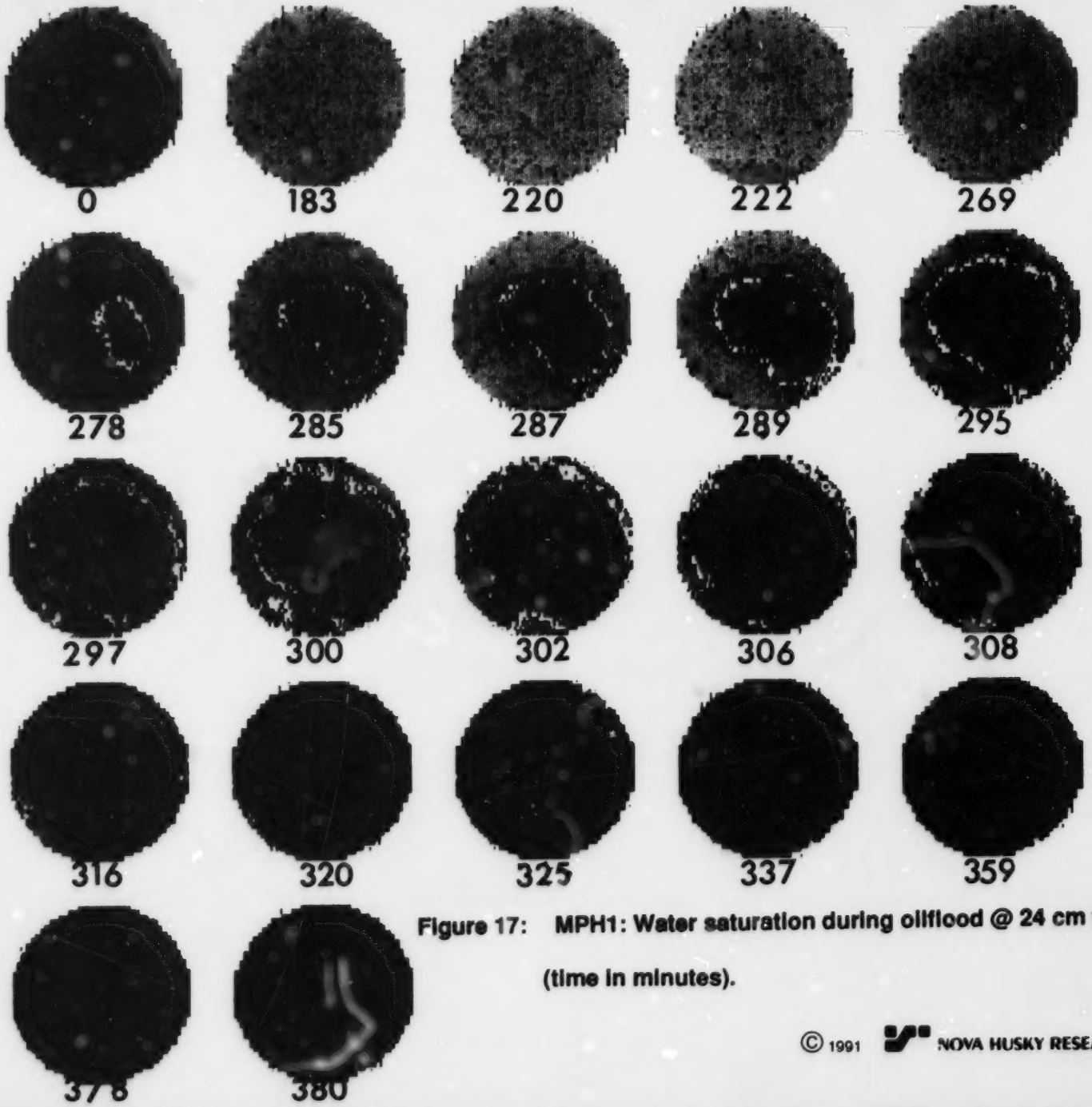

Figure 17: MPH1: Water saturation during oilflood @ 24 cm from inlet (time in minutes).

© 1991 NOVA HUSKY RESEARCH CORPORATION

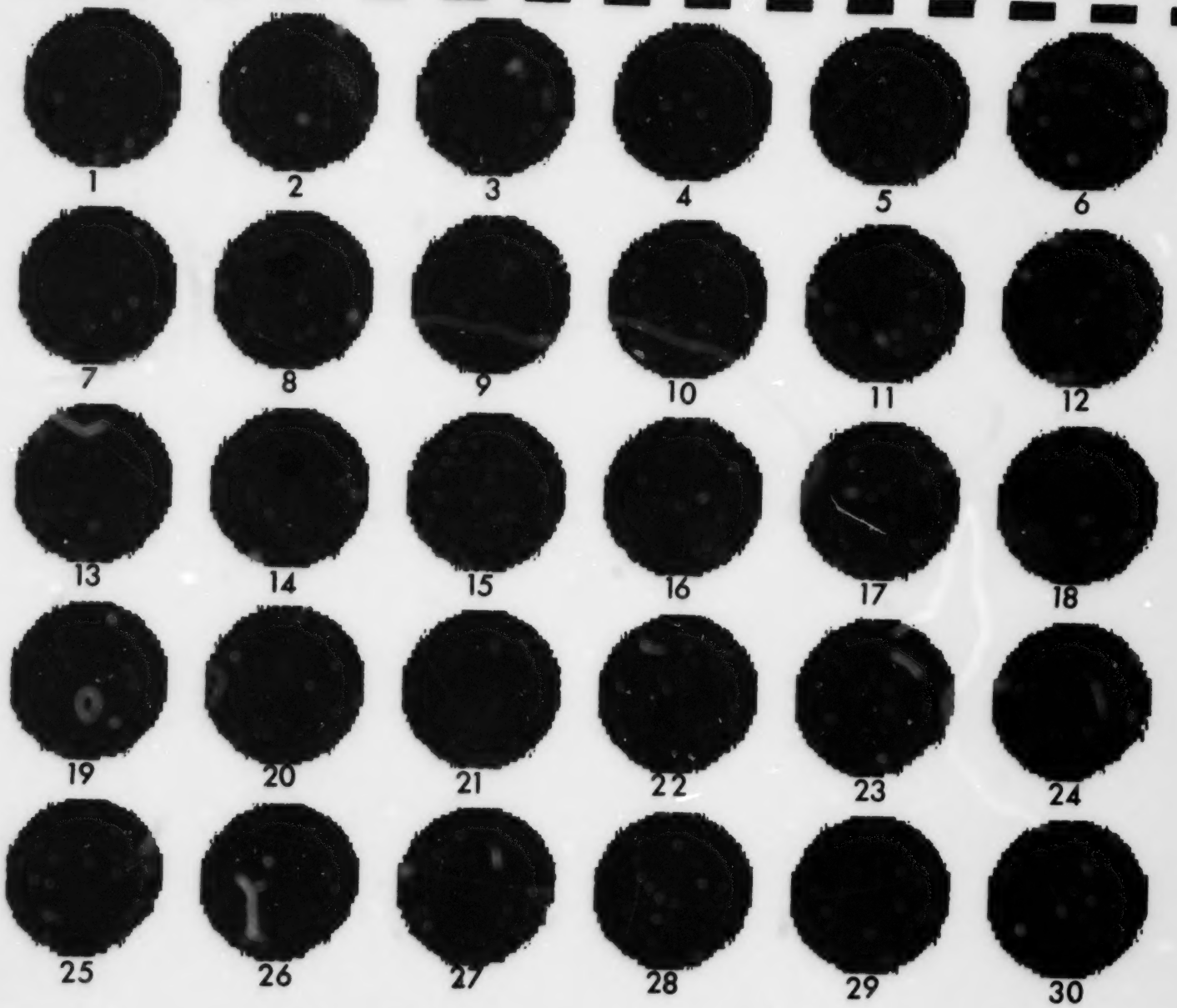

Figure 18: MPH1: Oil saturation after oilflood; slices 1-30.

© 1991 NOVA HUSKY RESEARCH CORPORATION

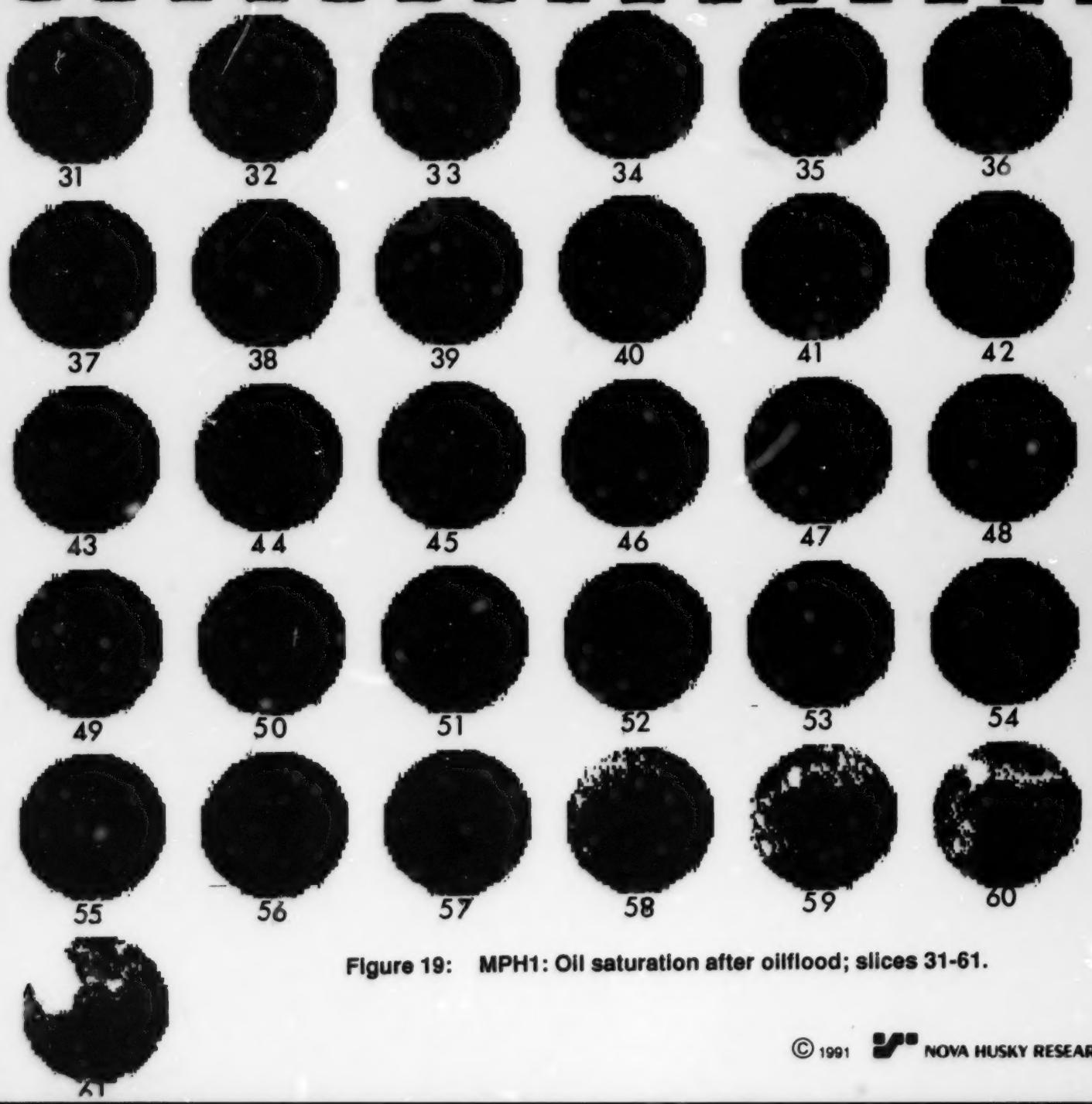

Figure 19: MPH1: Oil saturation after oilflood; slices 31-61.

© 1991 NOVA HUSKY RESEARCH CORPORATION

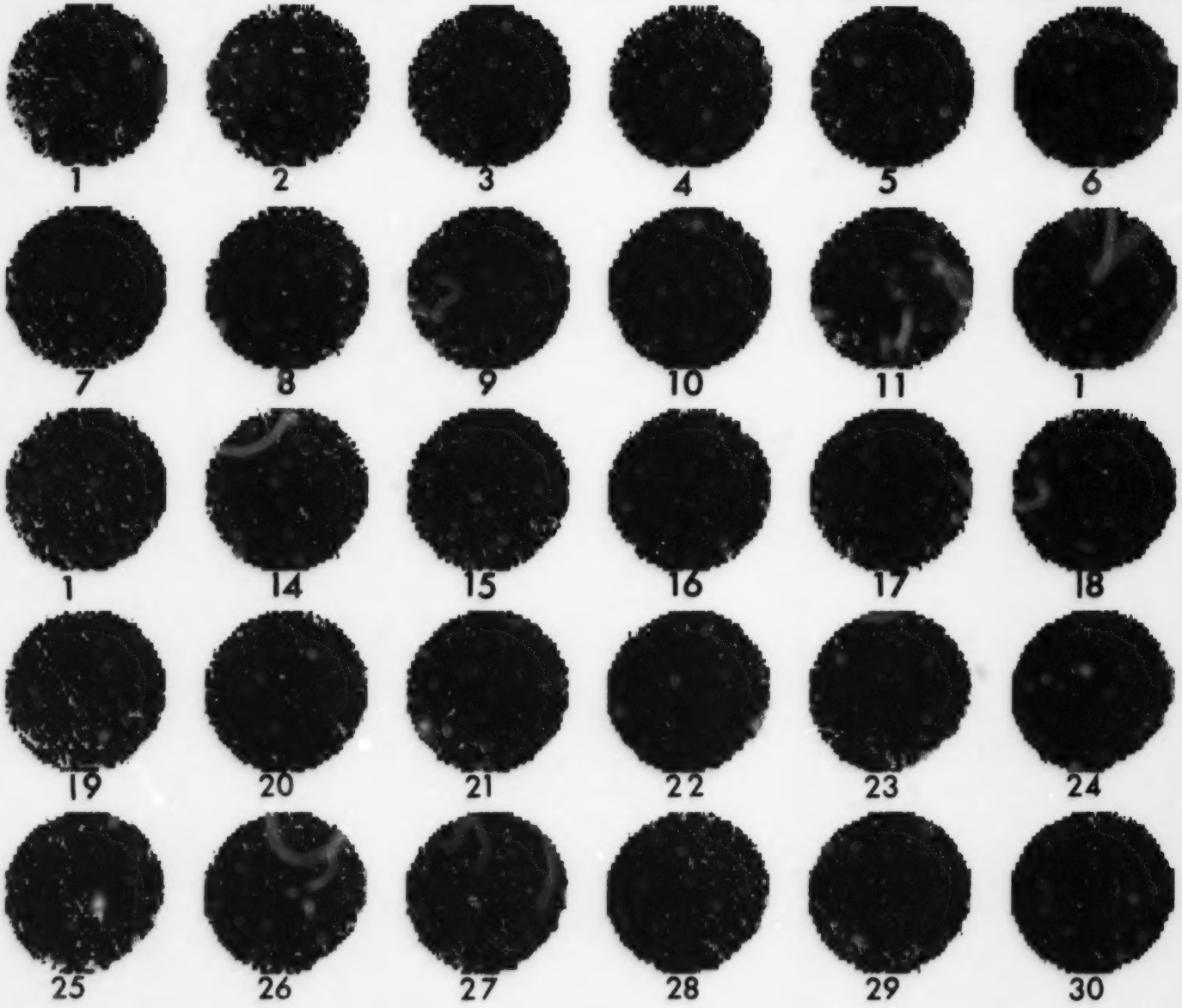

Figure 20: MPH1: Water saturation after oilflood; slices 1-30.

© 1991 NOVA HUSKY RESEARCH CORPORATION

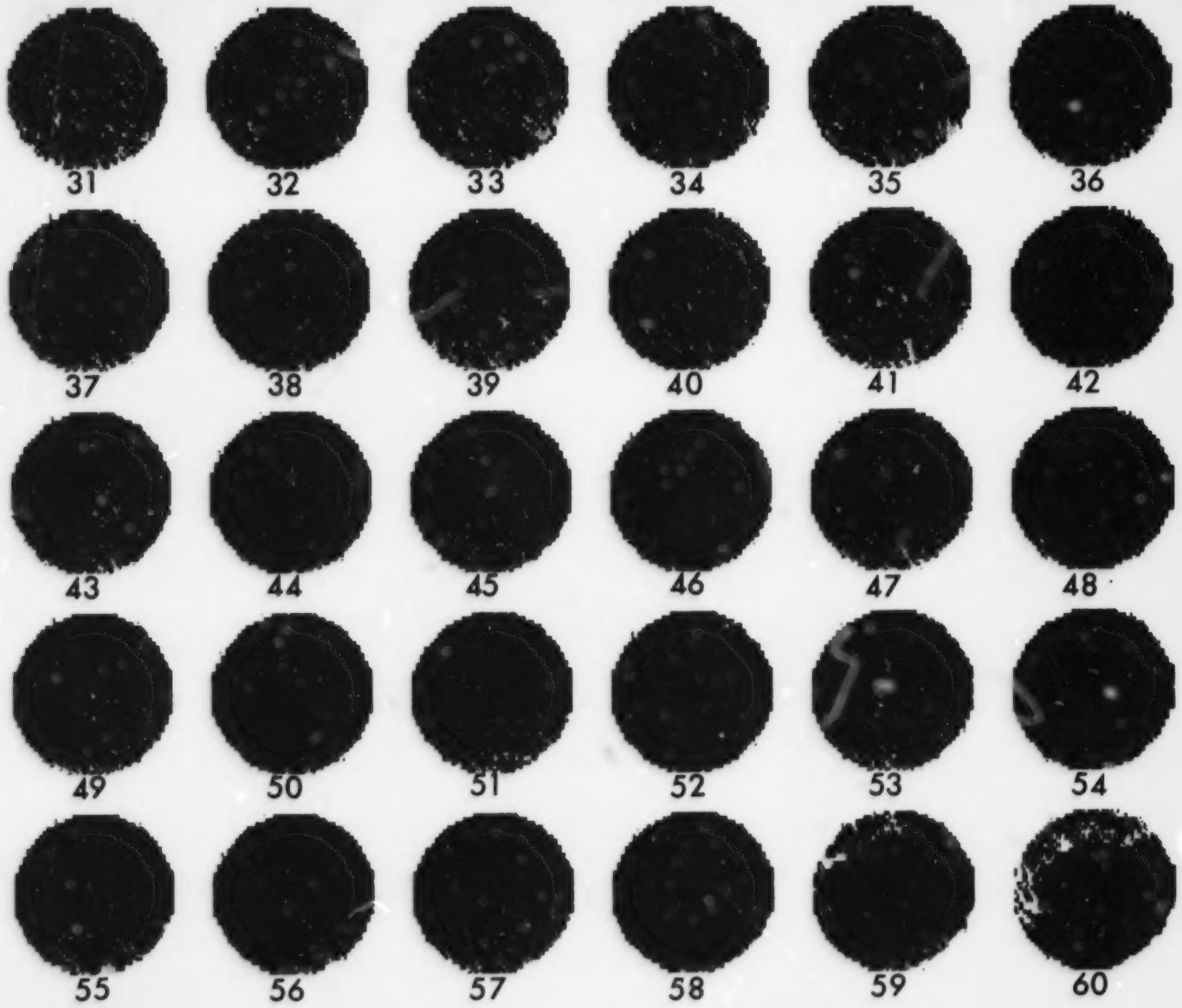

Figure 21: MPH1: Water saturation after oilflood; slices 31-61.

© 1991 NOVA HUSKY RESEARCH CORPORATION

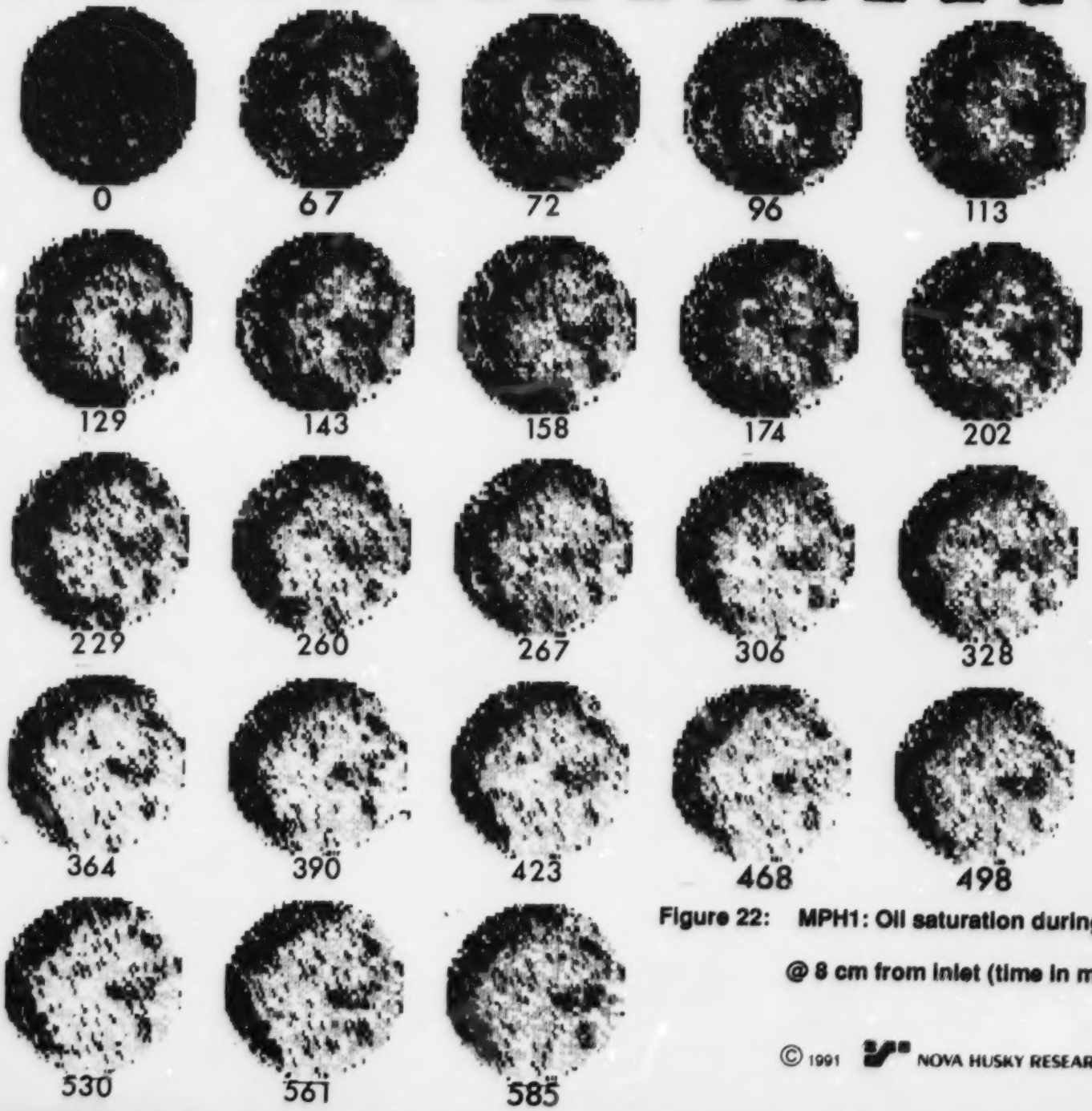

Figure 22: MPH1: Oil saturation during waterflood @ 8 cm from inlet (time in minutes).

© 1991 NOVA HUSKY RESEARCH CORPORATION

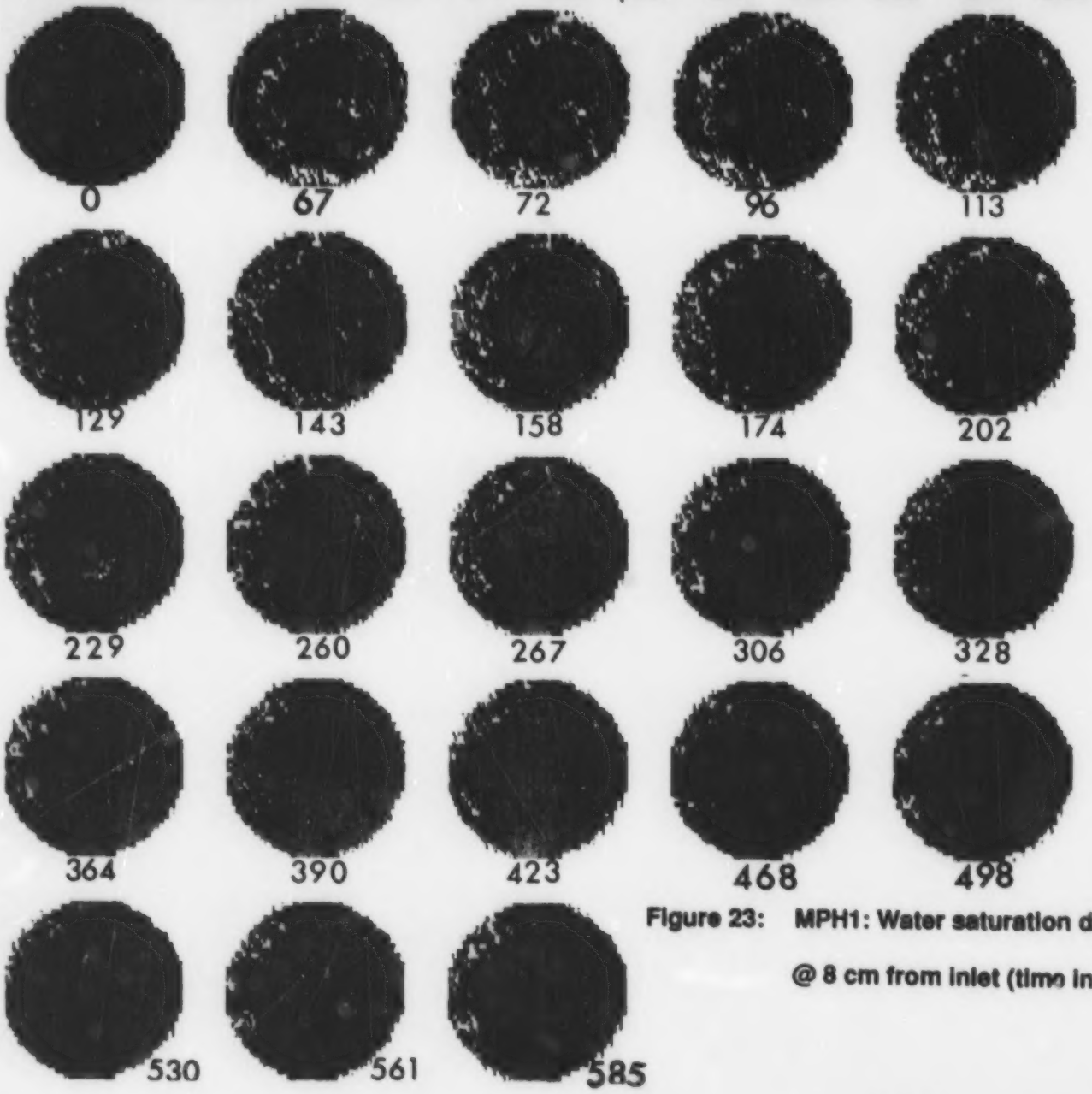

Figure 23: MPH1: Water saturation during waterflood @ 8 cm from inlet (time in minutes).

© 1991 NOVA HUSKY RESEARCH CORPORATION

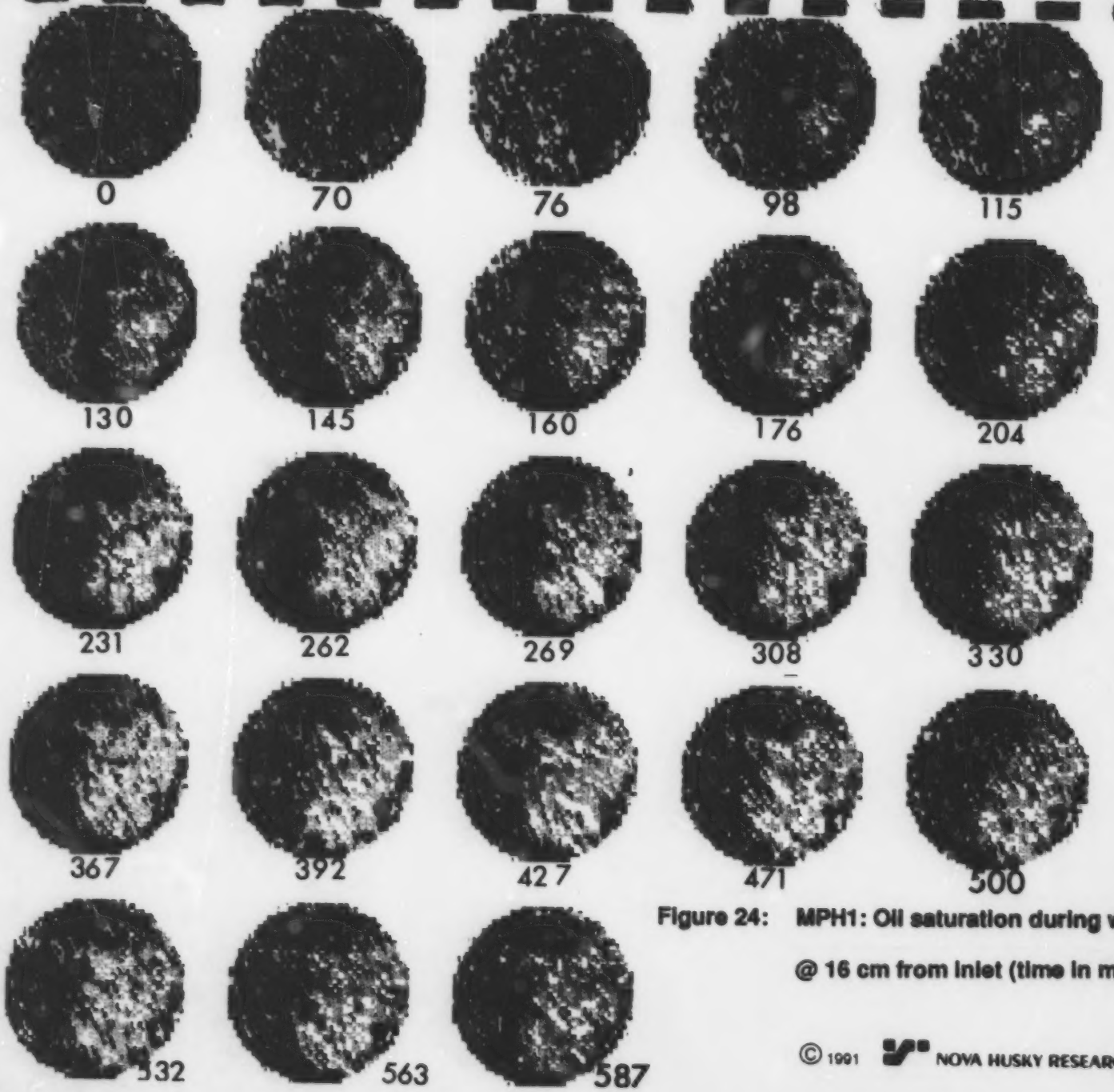

Figure 24: MPH1: Oil saturation during waterflood @ 16 cm from inlet (time in minutes).

© 1991 NOVA HUSKY RESEARCH CORPORATION

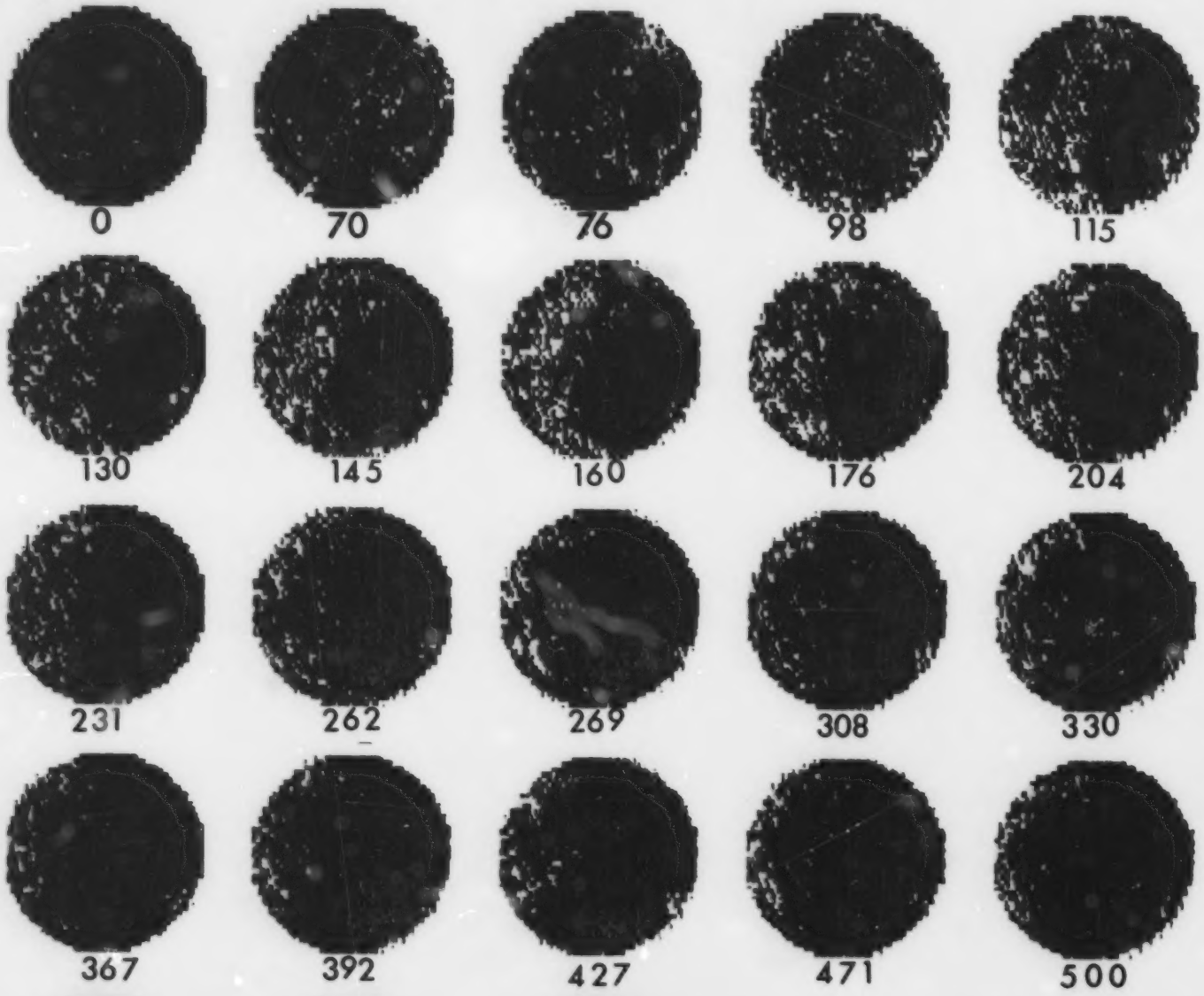

Figure 25: MPH1: Water saturation during waterflood @ 16 cm from inlet (time in minutes).

© 1991 NOVA HUSKY RESEARCH CORPORATION

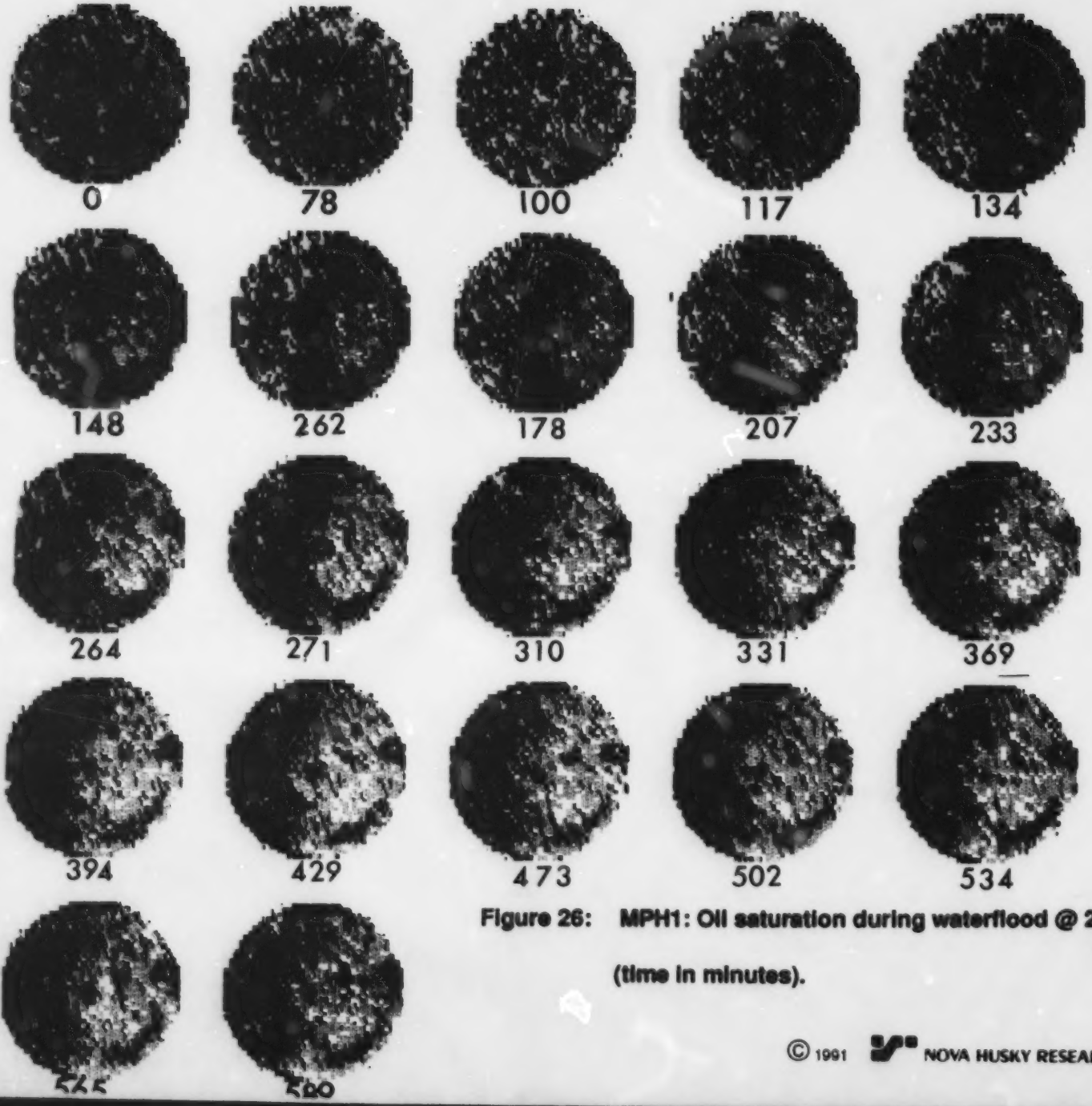

Figure 26: MPH1: Oil saturation during waterflood @ 24 cm from inlet (time in minutes).

© 1991 NOVA HUSKY RESEARCH CORPORATION

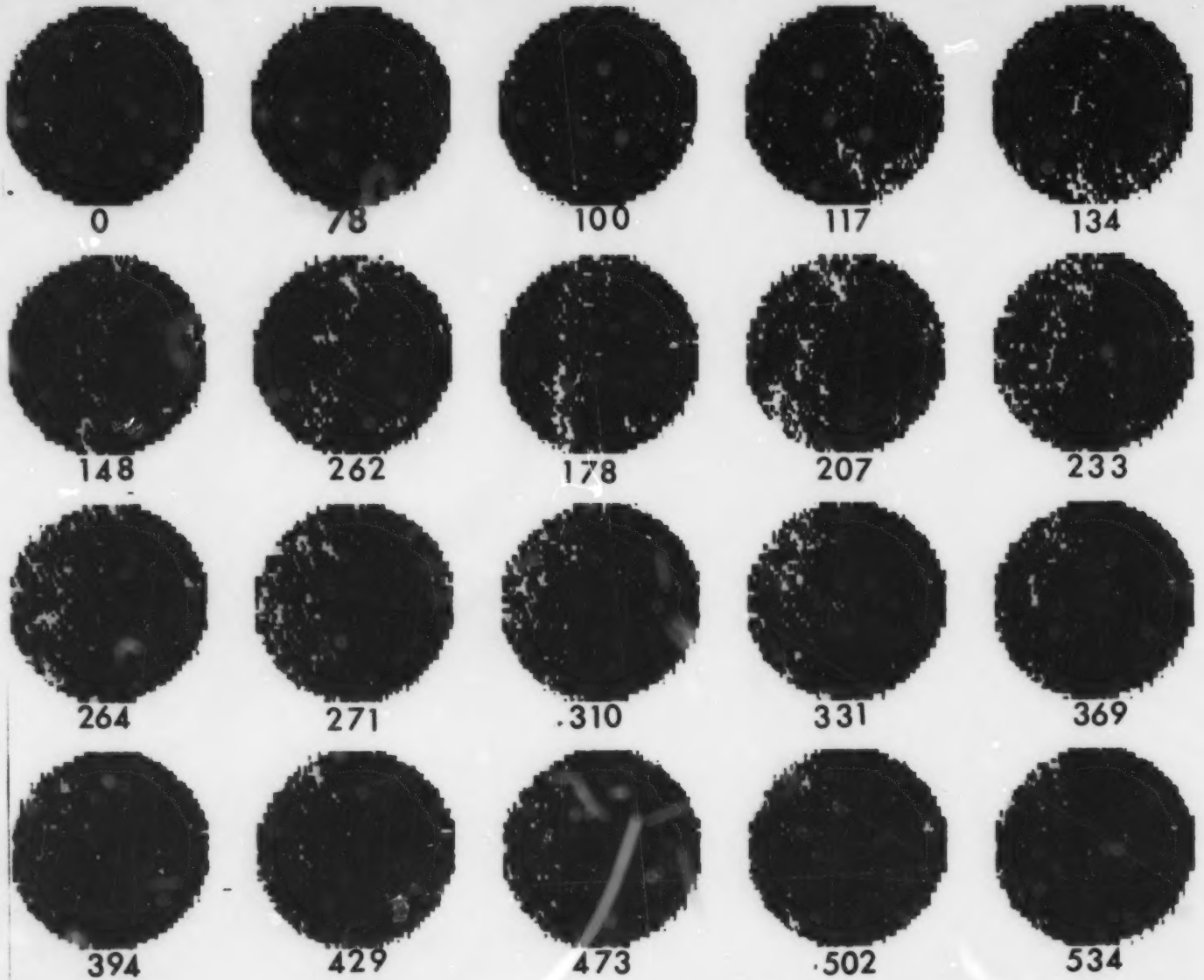

Figure 27: MPH1: Water saturation during waterflood @ 24 cm from inlet (time in minutes).

© 1991 NOVA HUSKY RESEARCH CORPORATION

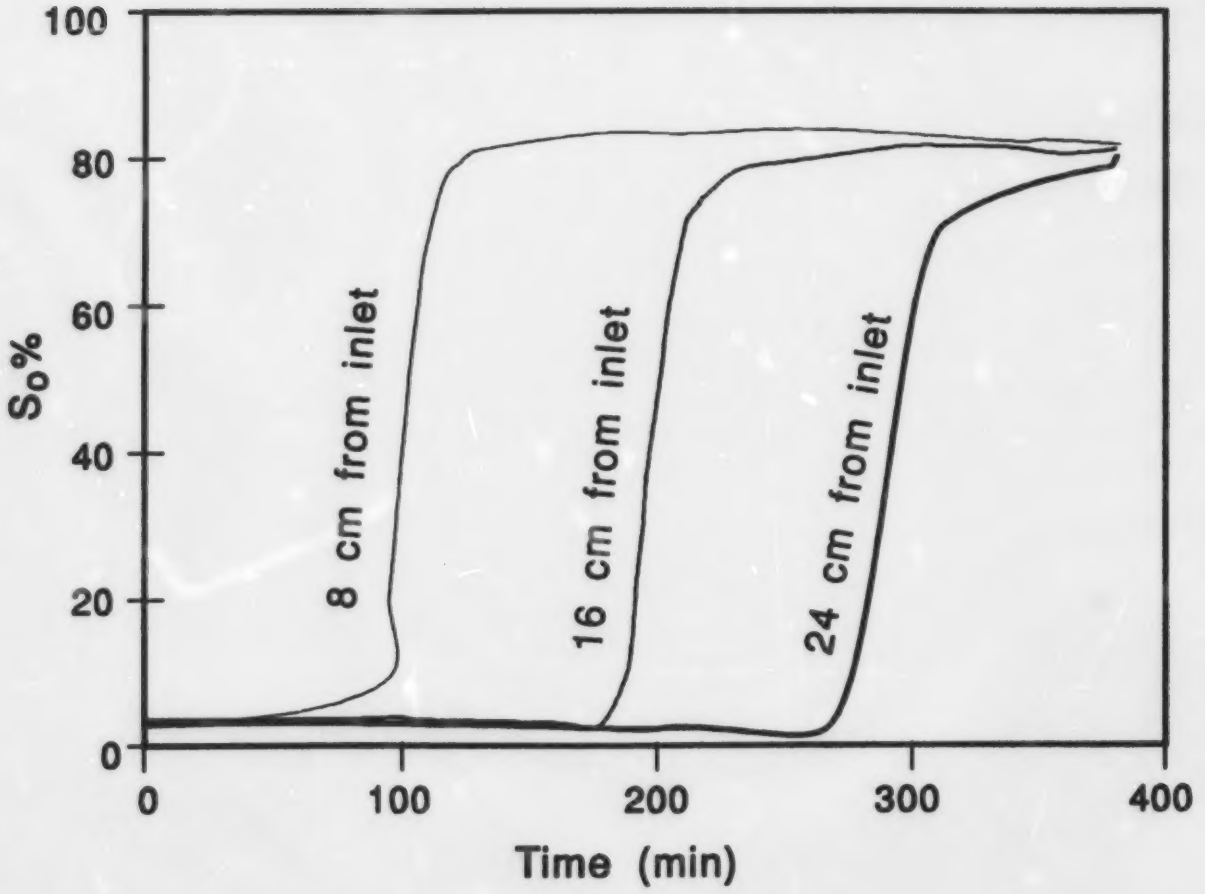

Figure 28: ***In situ*** **oil saturation plots of a uniform sandpack (MPH1) during oilflood (drainage).**

© 1991 NOVA HUSKY RESEARCH CORPORATION

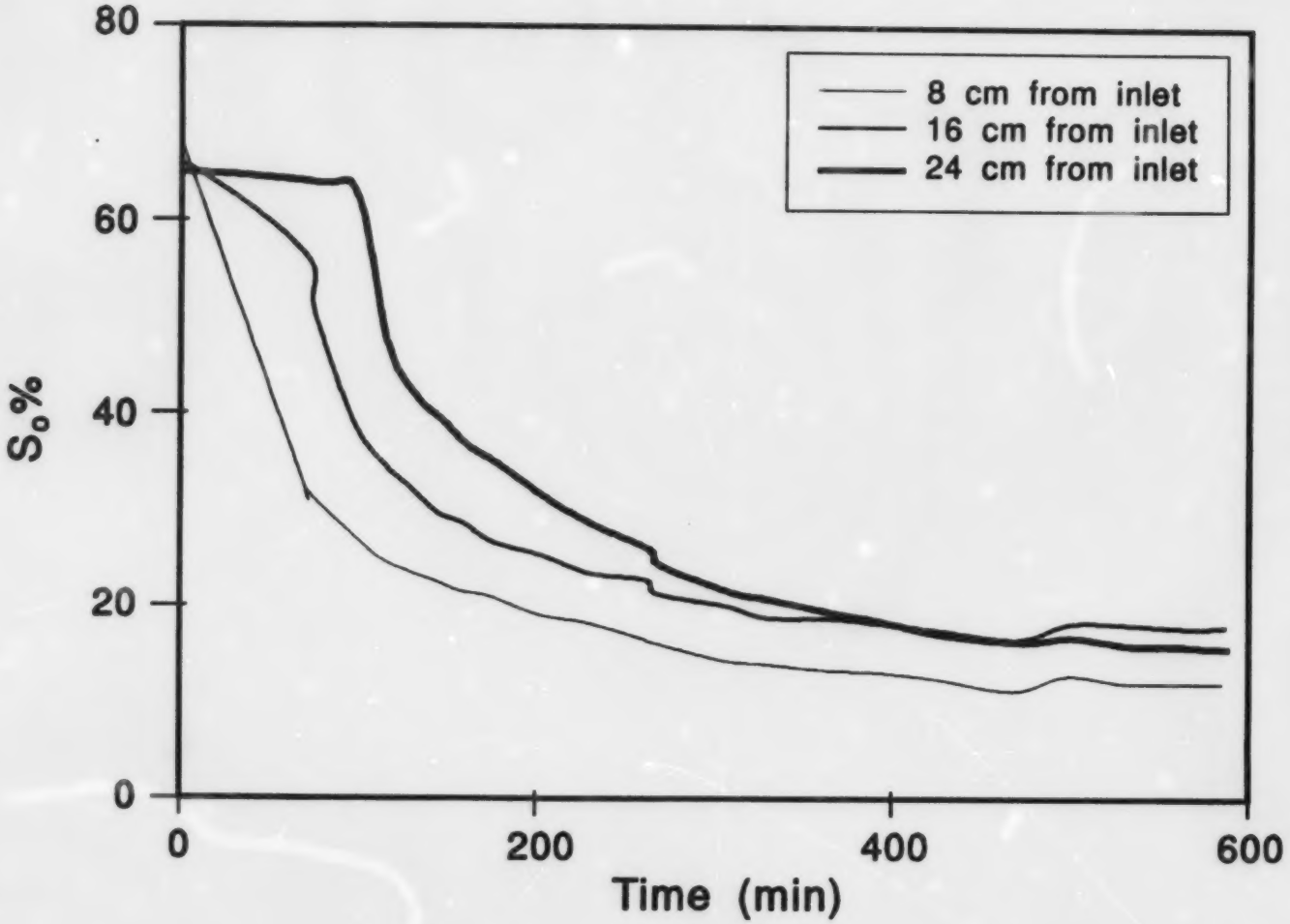

Figure 29: ***In situ*** **oil saturation plots of a uniform sandpack (MPH1) during waterflood (imbibition).**

© 1991 NOVA HUSKY RESEARCH CORPORATION

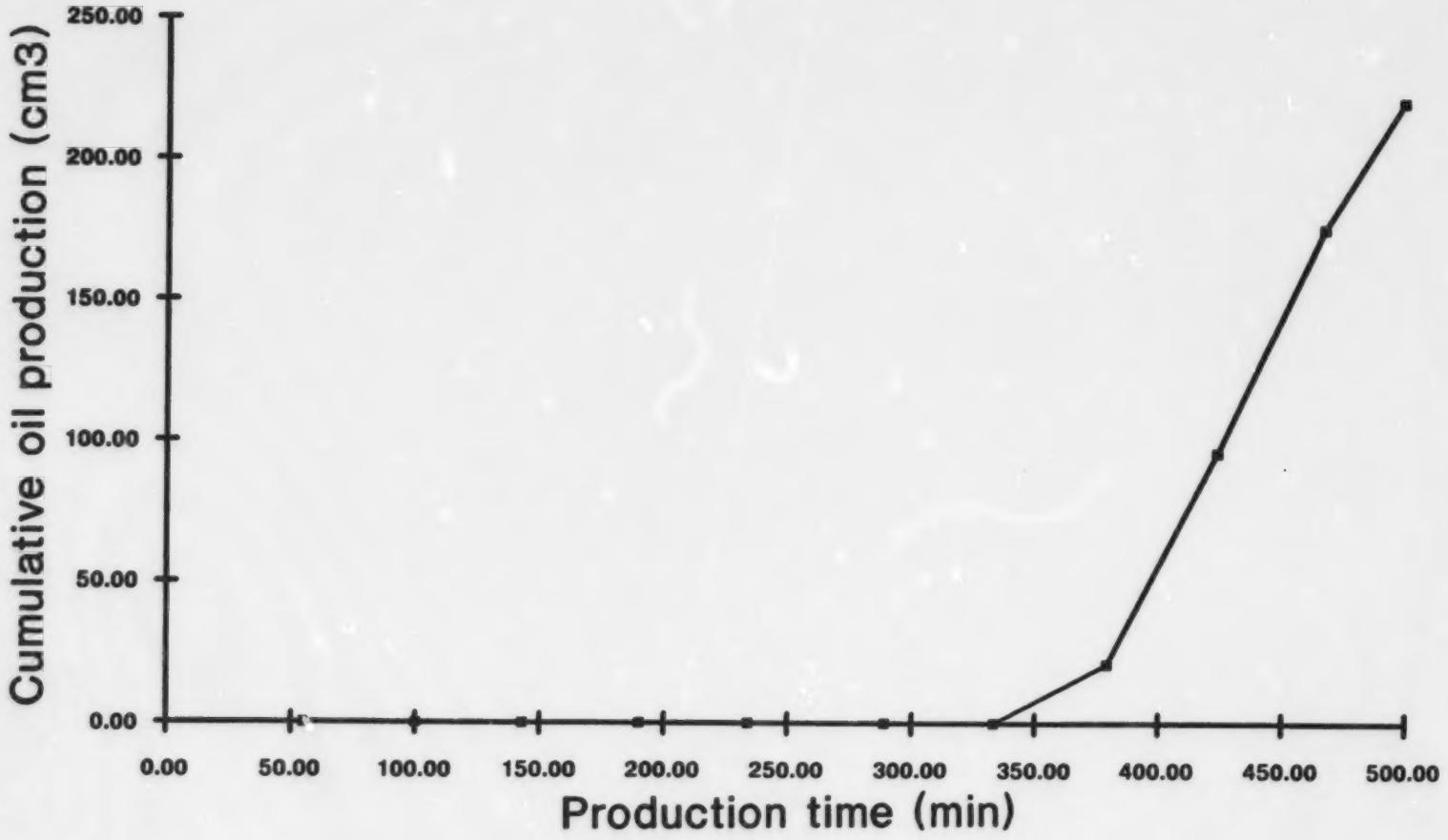

Figure 30: Cumulative oil production during oilflood in MPH1.

© 1991 NOVA HUSKY RESEARCH CORPORATION

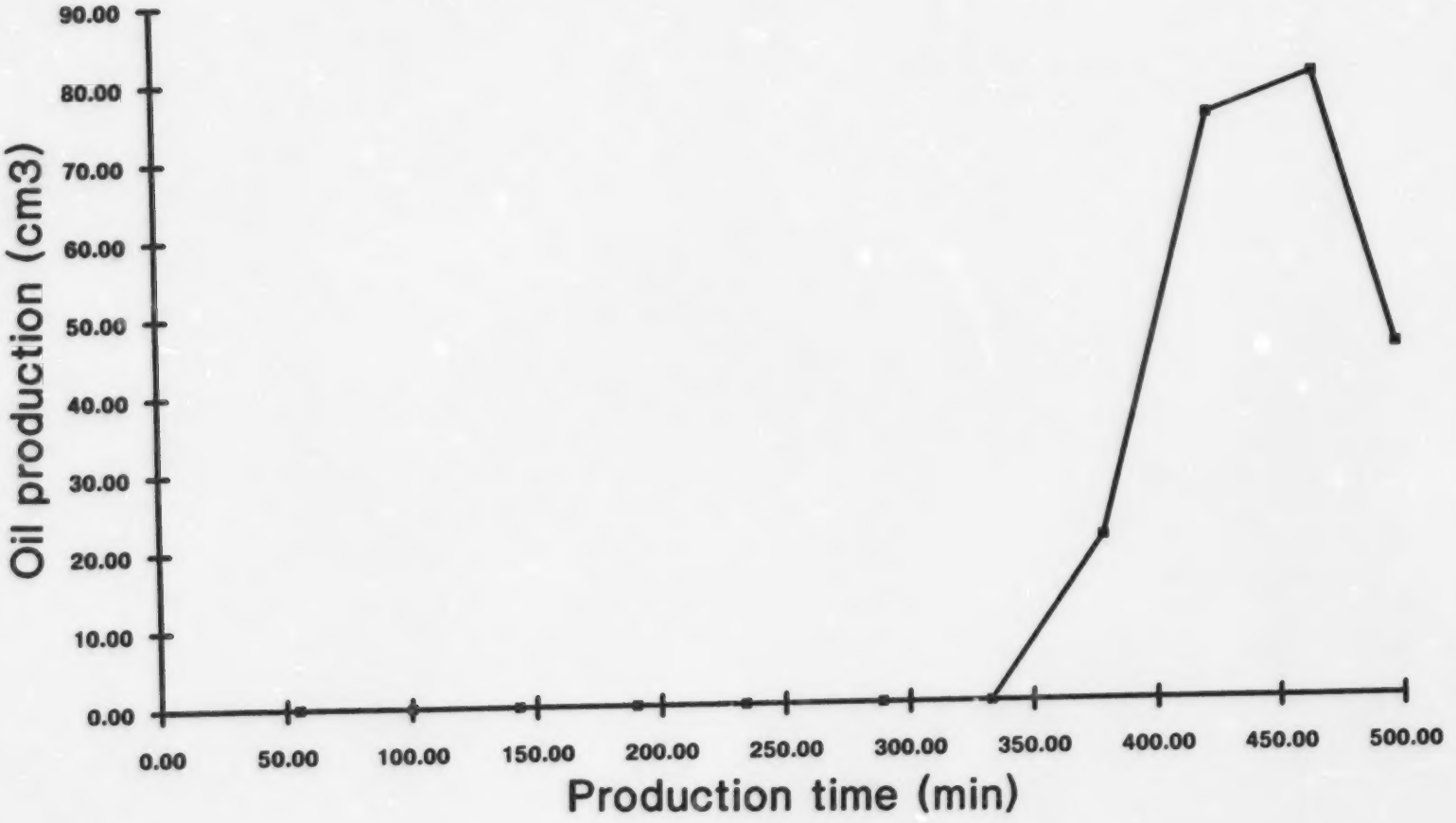

Figure 31: Oil production during oilflood in MPH1.

© 1991 NOVA HUSKY RESEARCH CORPORATION

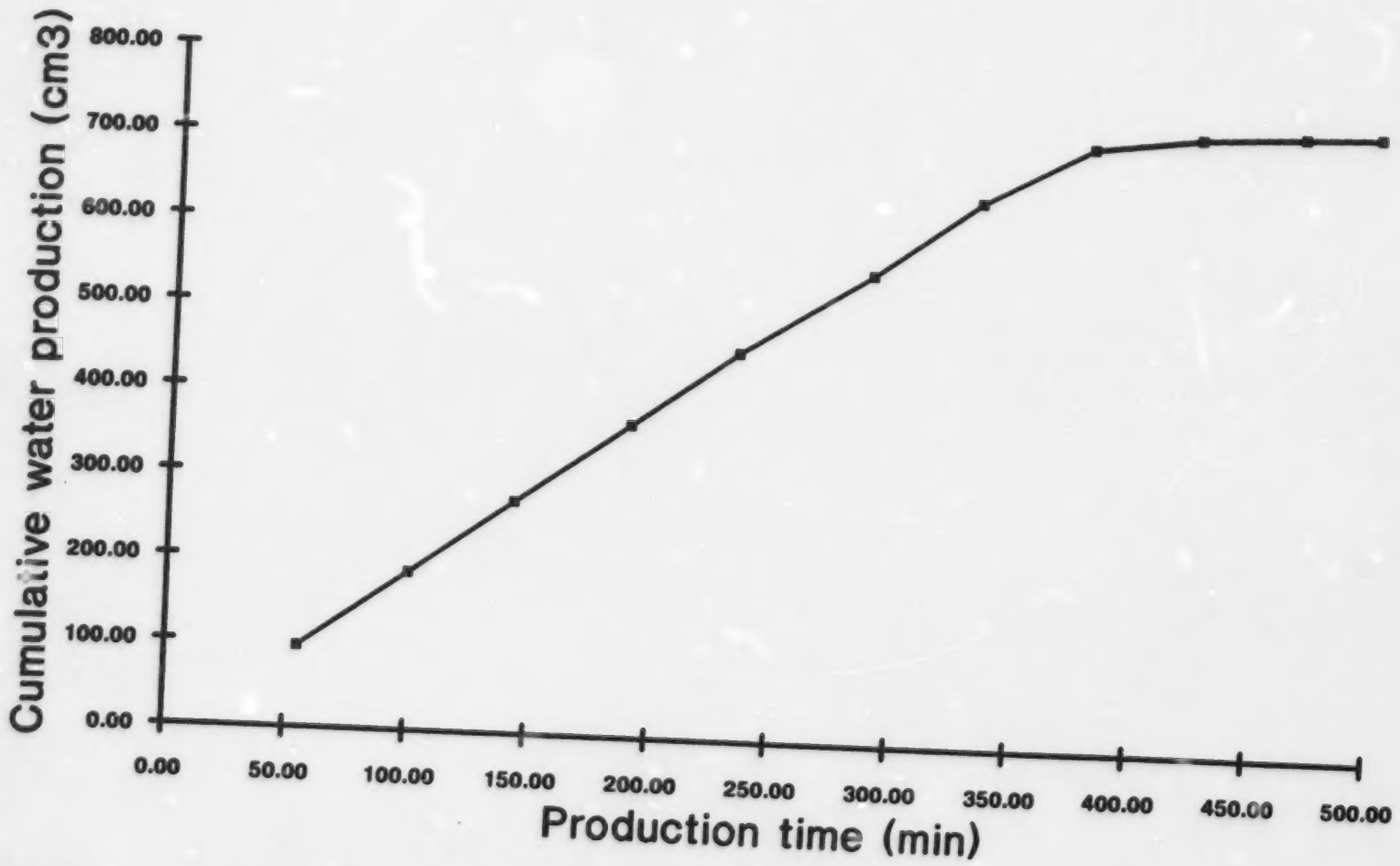

Figure 32: Cumulative water production during oilflood in MPH1.

© 1991 NOVA HUSKY RESEARCH CORPORATION

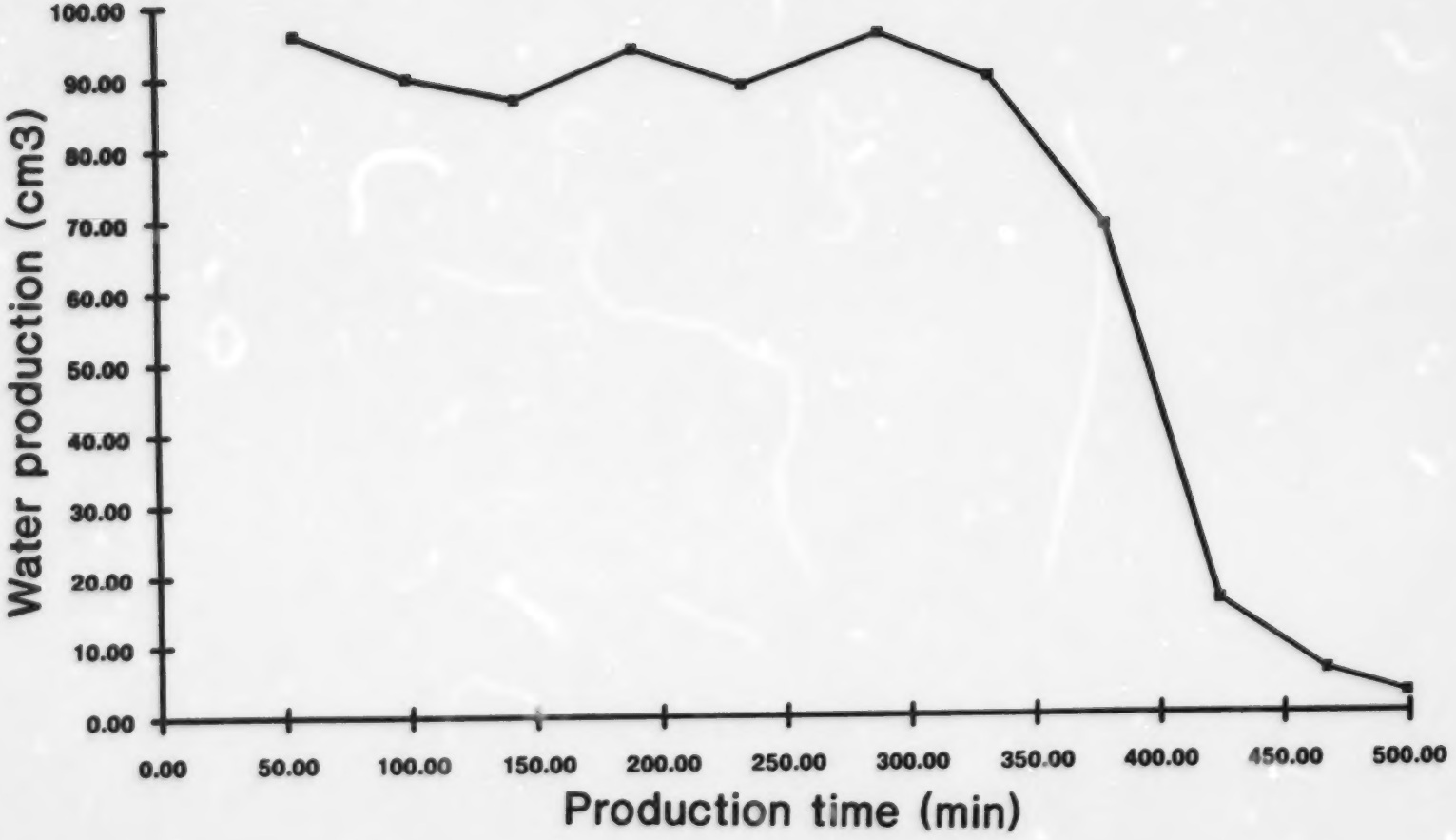

Figure 33: Water production during oilflood in MPH1.

© 1991 NOVA HUSKY RESEARCH CORPORATION

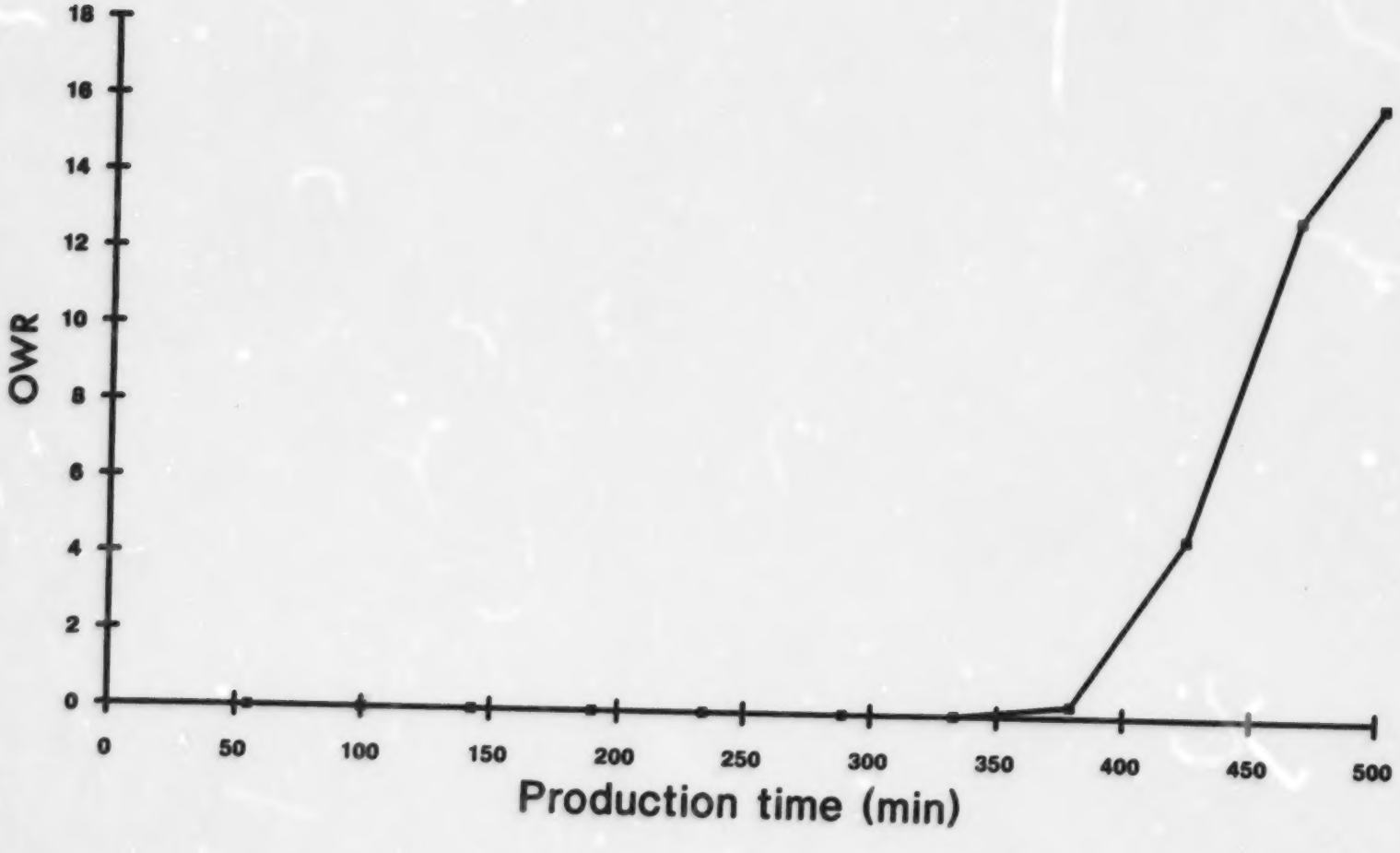

Figure 34: Oil water ratio during oilfoood in MPH1.

© 1991 NOVA HUSKY RESEARCH CORPORATION

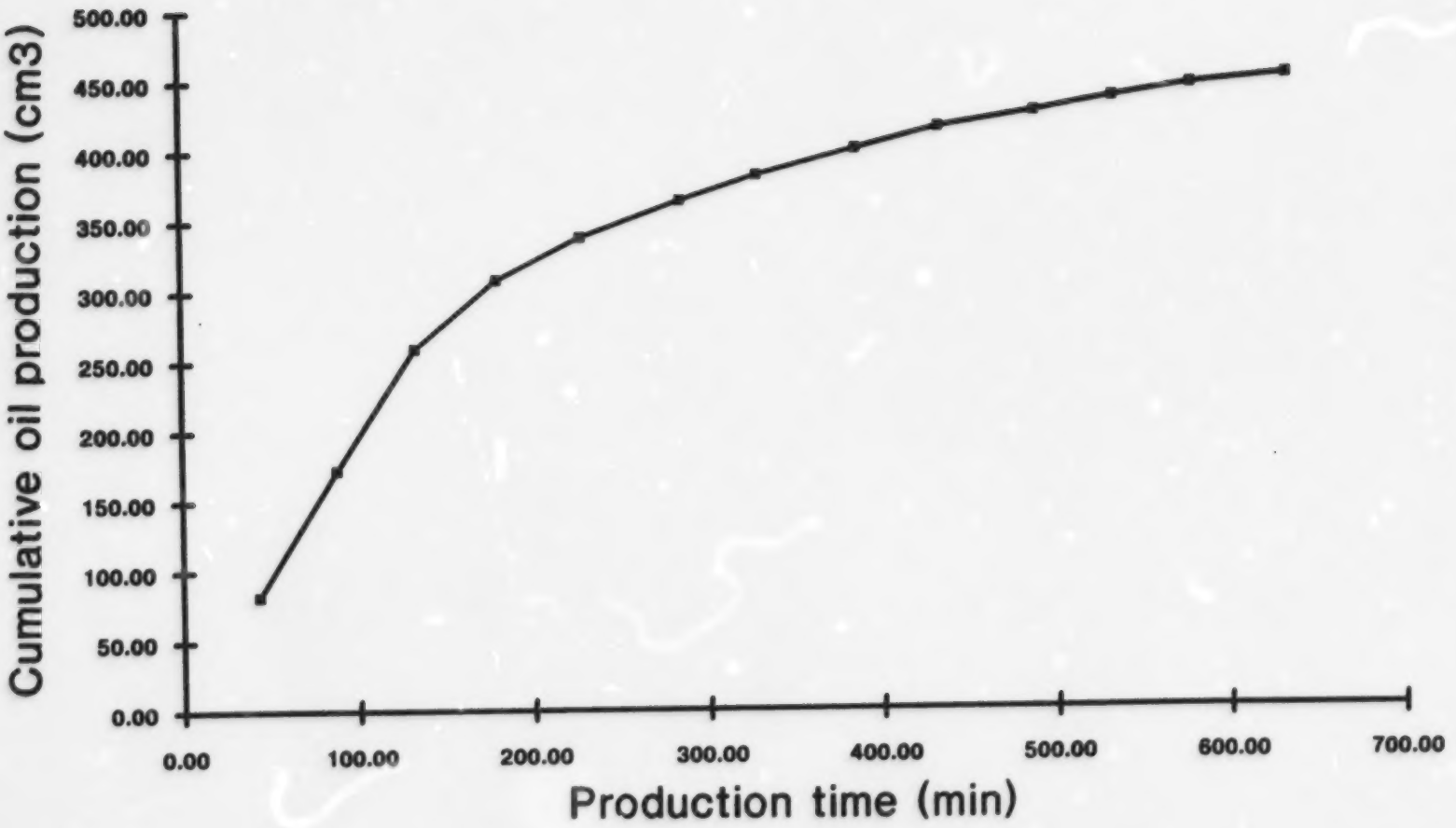

Figure 35: Cumulative oil production during waterflood in MPH1.

© 1991 NOVA HUSKY RESEARCH CORPORATION

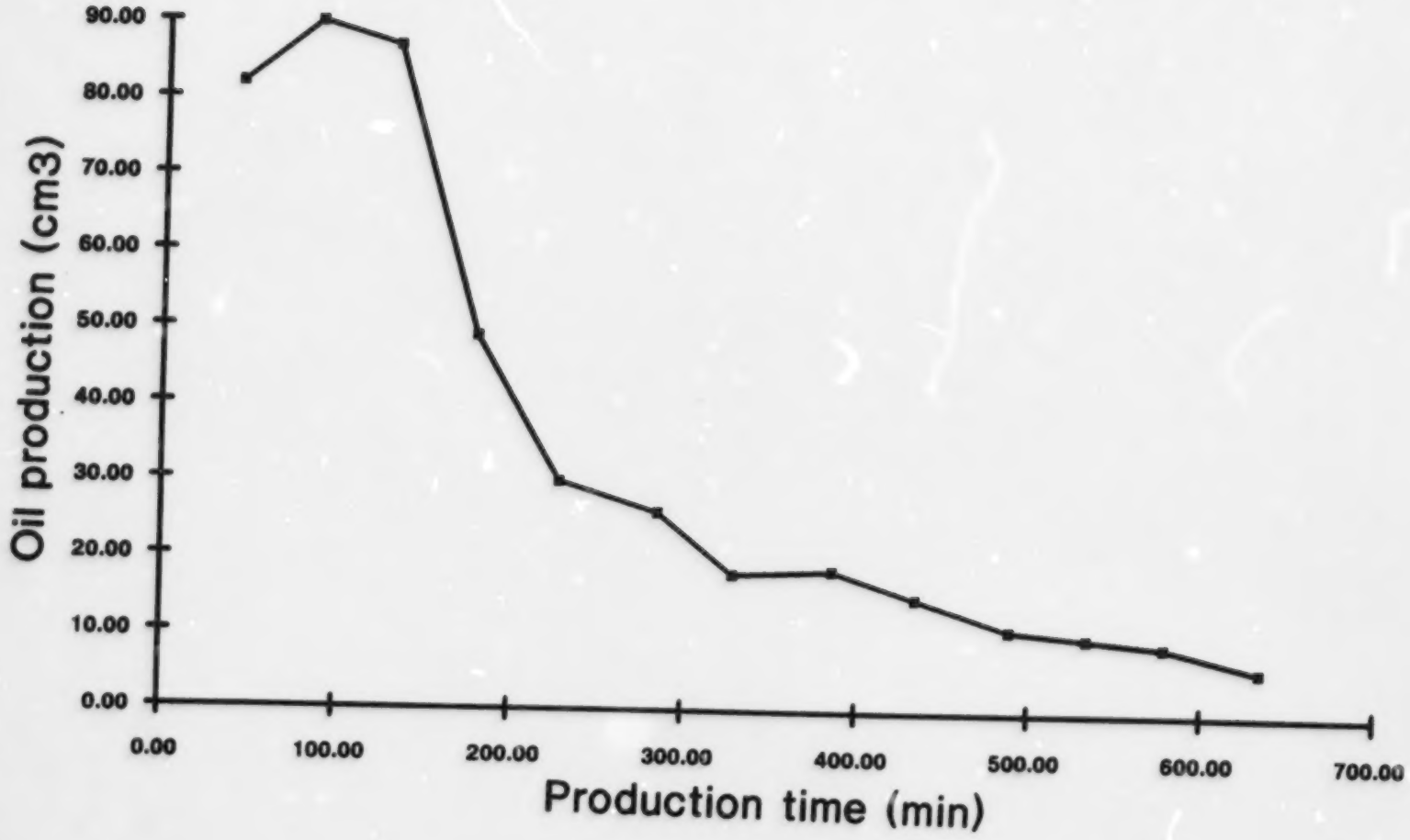

Figure 36: Oil production during waterflood in MPH1.

© 1991 NOVA HUSKY RESEARCH CORPORATION

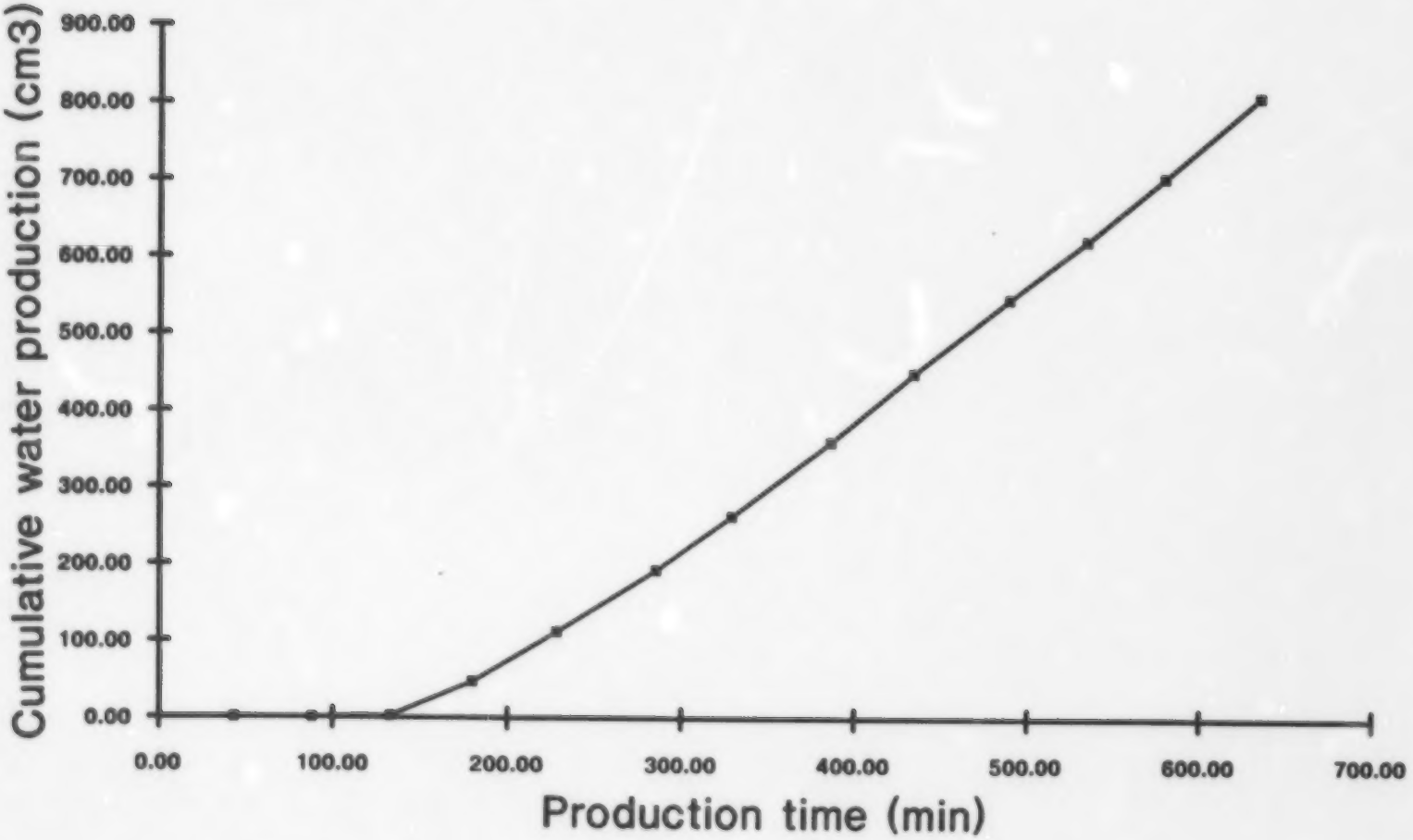

Figure 37: Cumulative water production during waterflood in MPH1.

© 1991 NOVA HUSKY RESEARCH CORPORATION

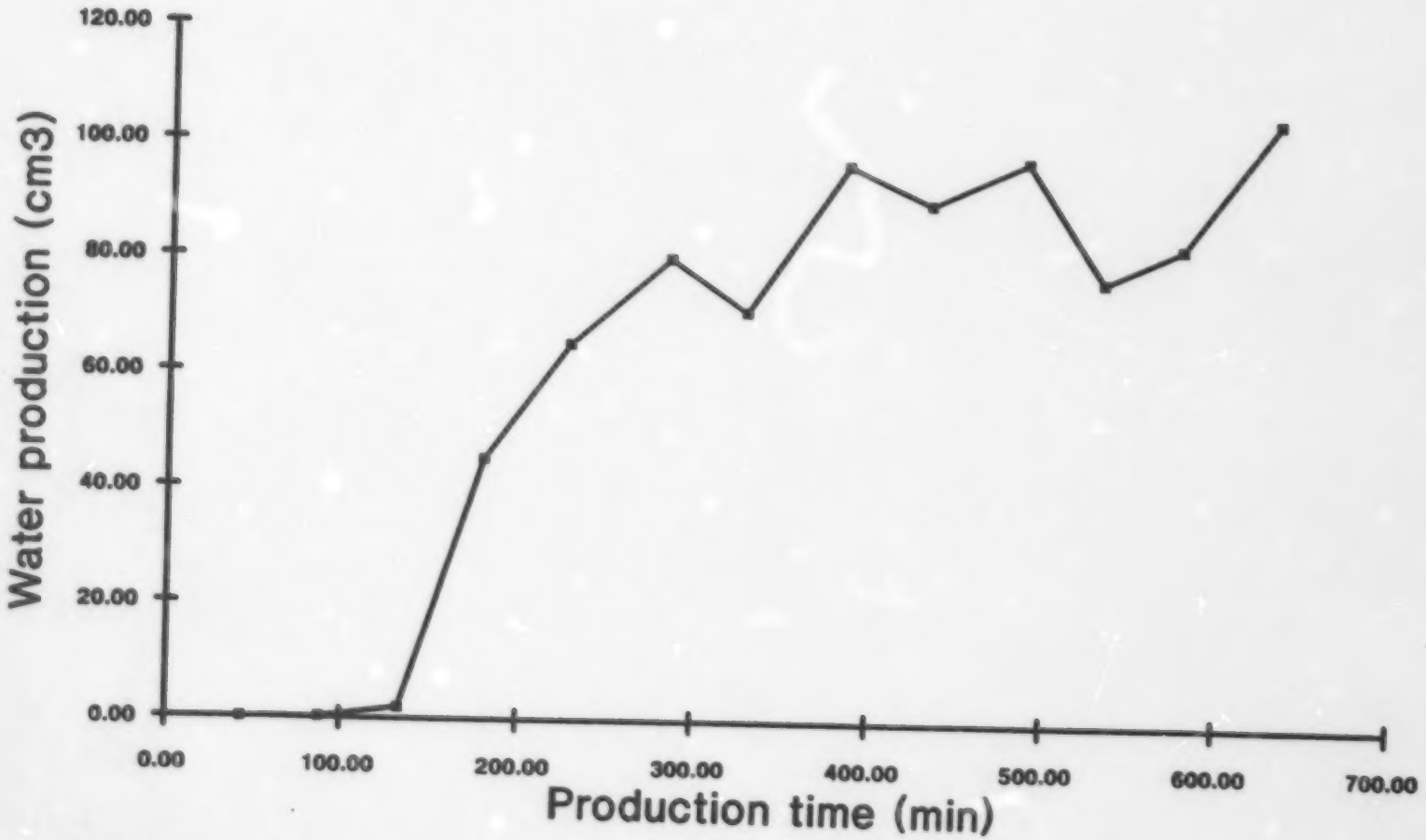

Figure 38: Water production during waterflood in MPH1.

© 1991 NOVA HUSKY RESEARCH CORPORATION

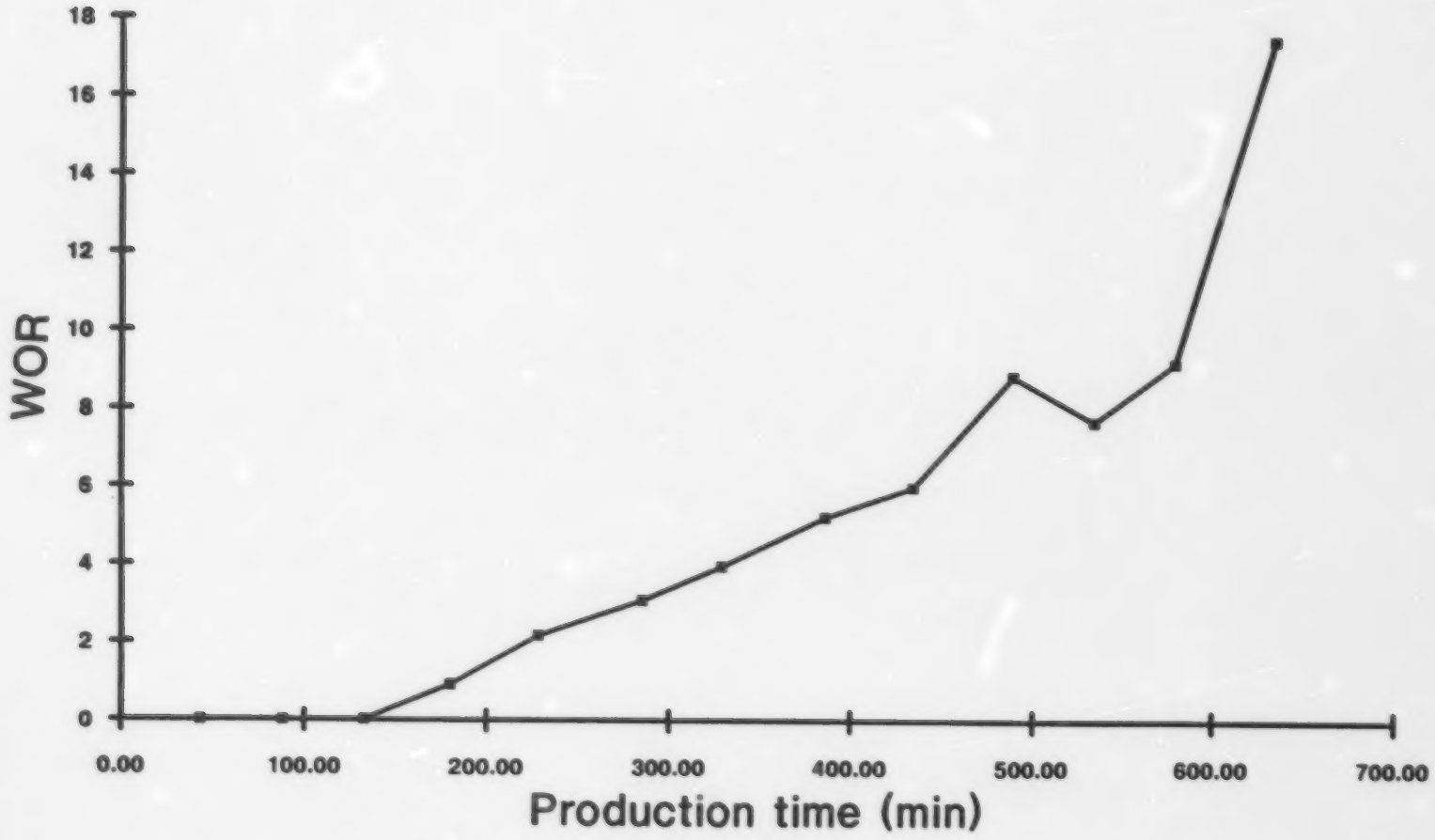

Figure 39: Water oil ratio during waterflood in MPH1.

© 1991 NOVA HUSKY RESEARCH CORPORATION

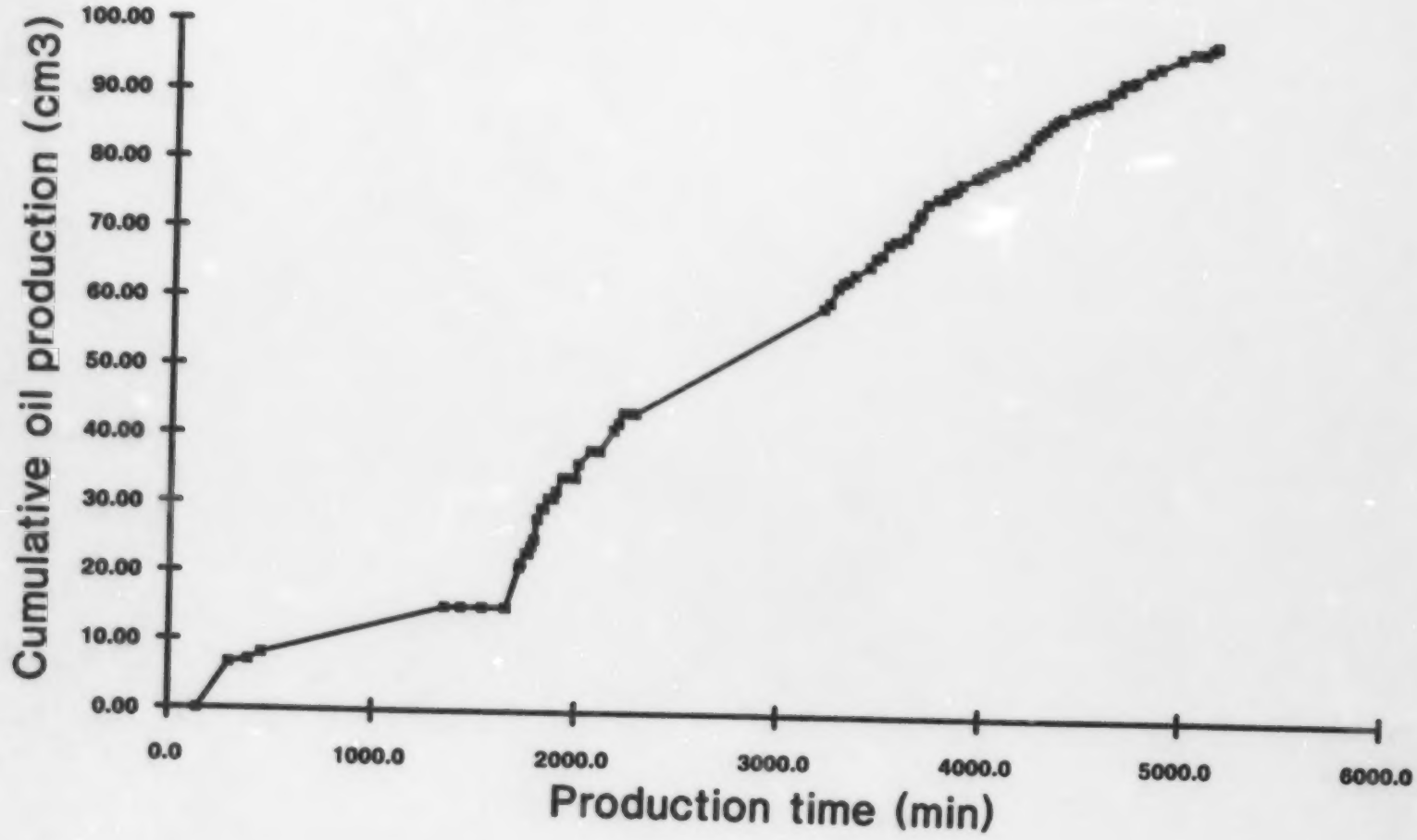

Figure 40: Cumulative oil production during gasflood in MPH1.

© 1991 NOVA HUSKY RESEARCH CORPORATION

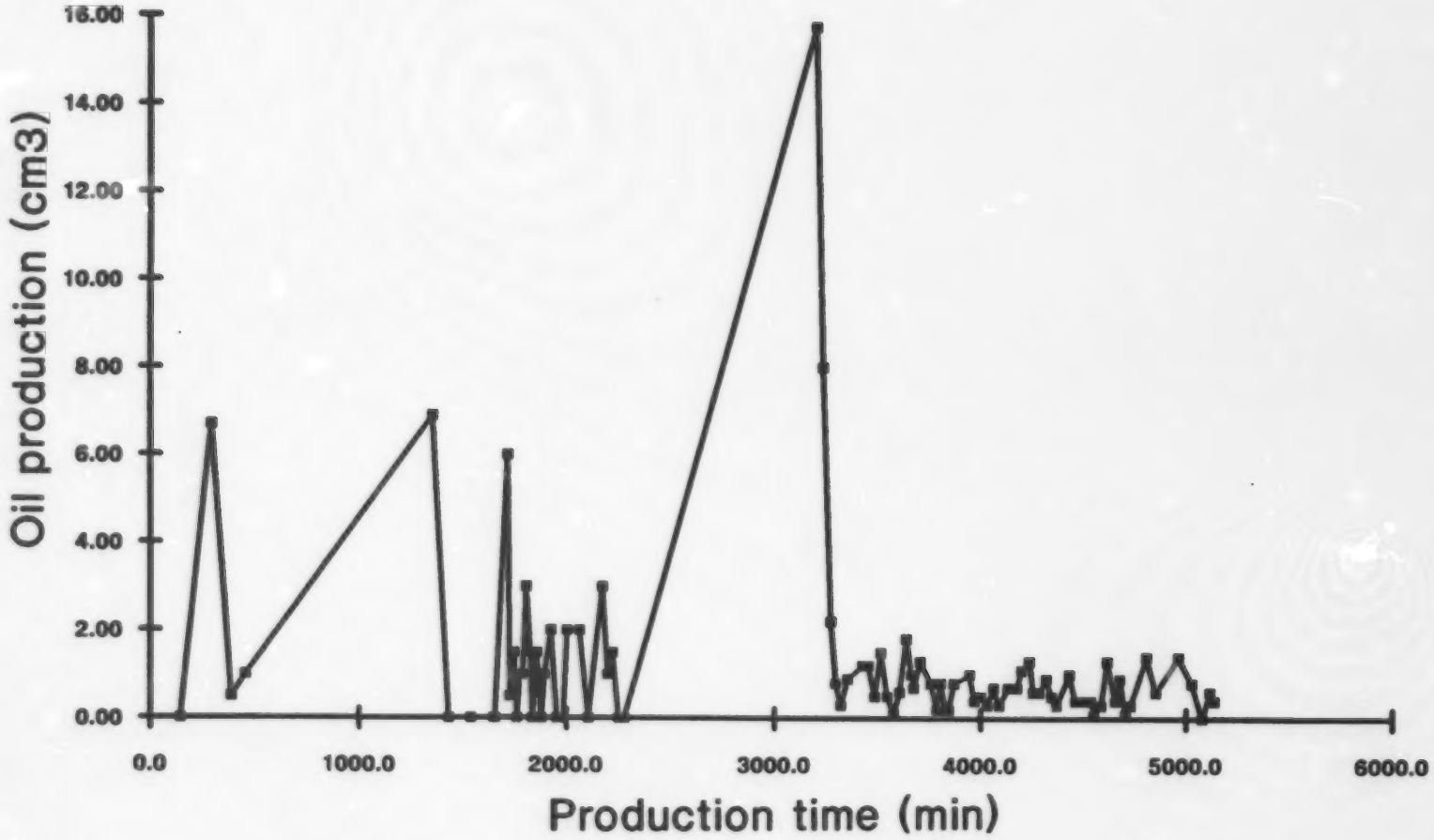

Figure 41: Oil production during gasflood in MPH1.

© 1991 NOVA HUSKY RESEARCH CORPORATION

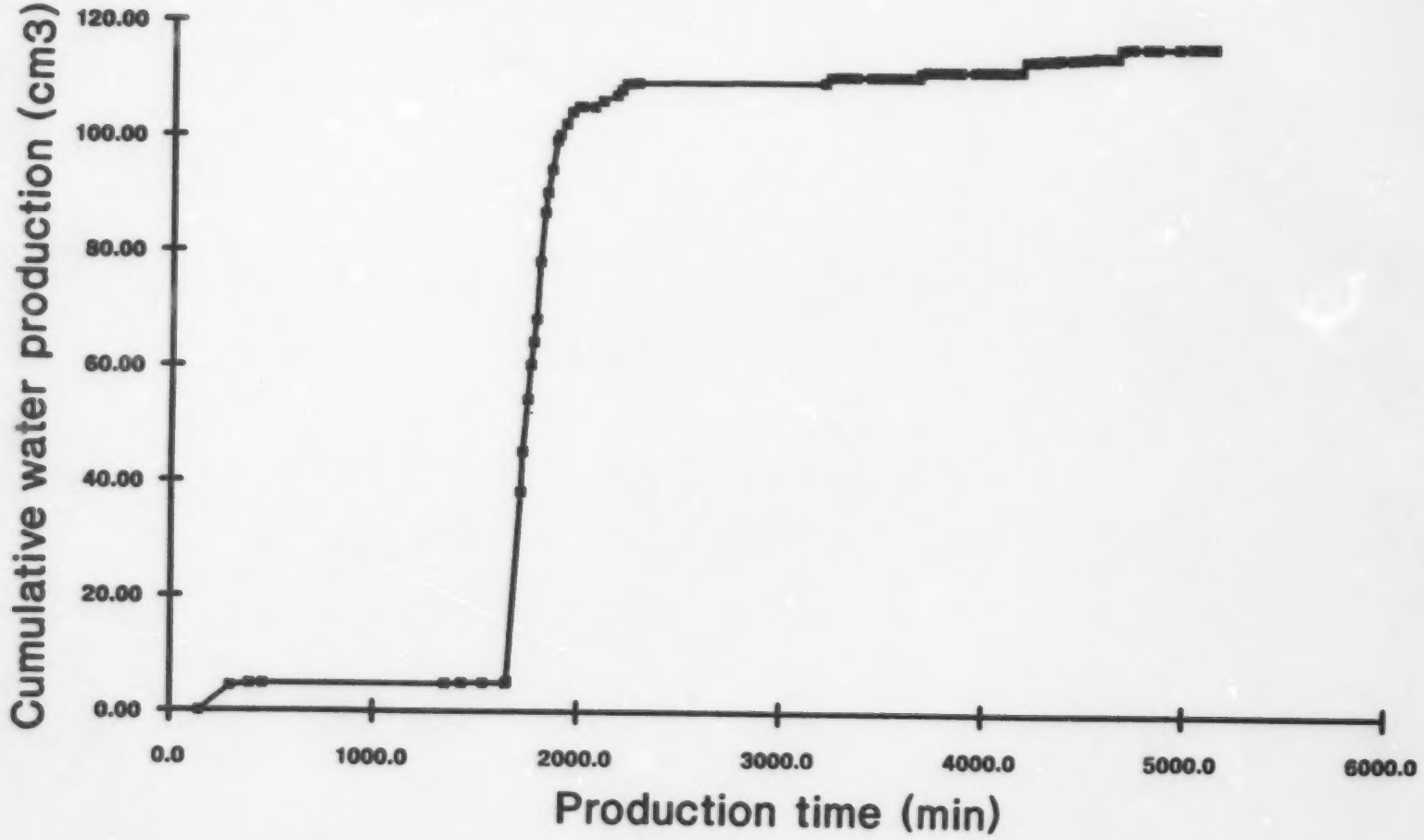

Figure 42: Cumulative water production during gasflood in MPH1.

© 1991 NOVA HUSKY RESEARCH CORPORATION

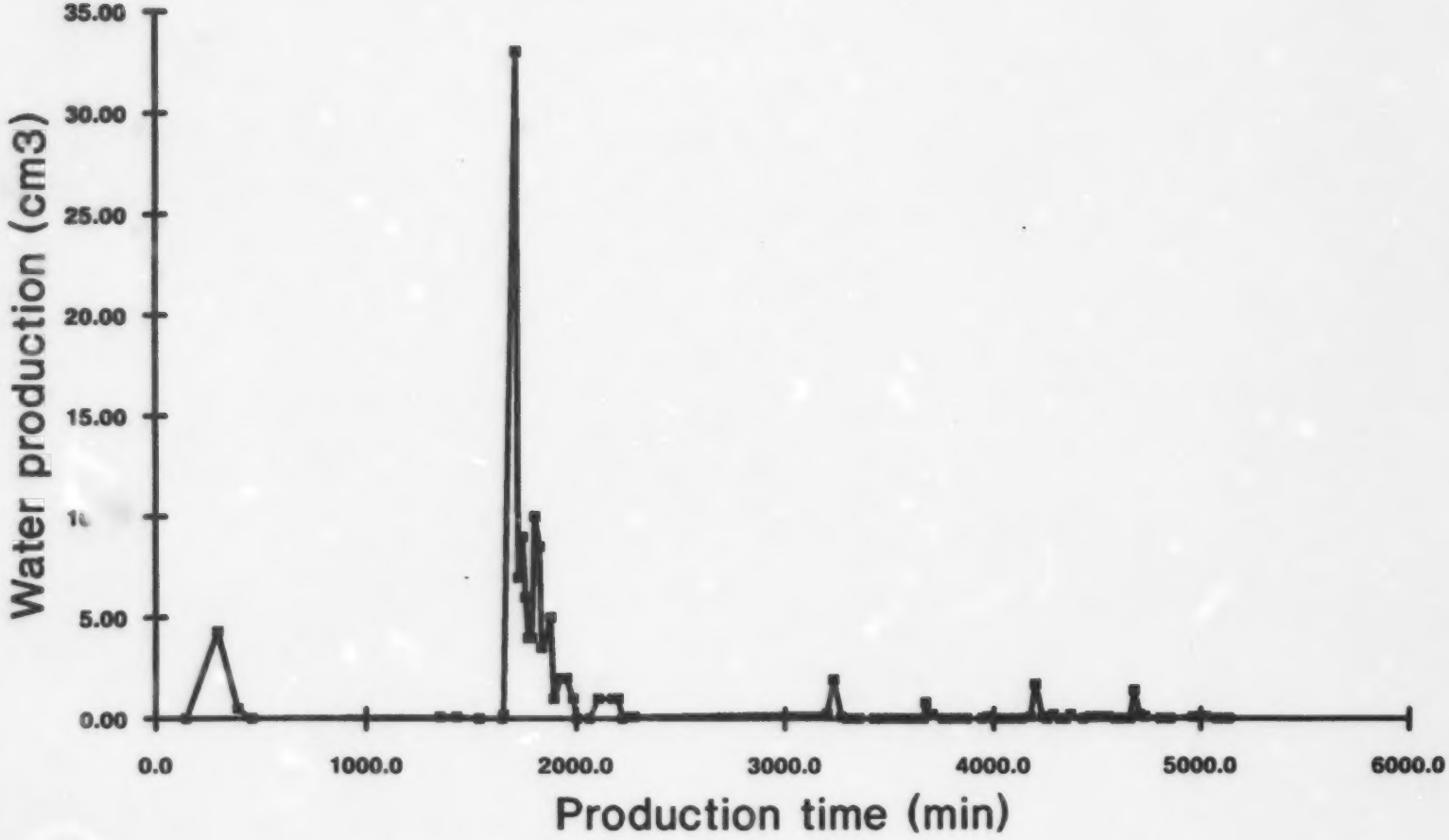

Figure 43: Water production during gasflood in MPH1.

© 1991 NOVA HUSKY RESEARCH CORPORATION

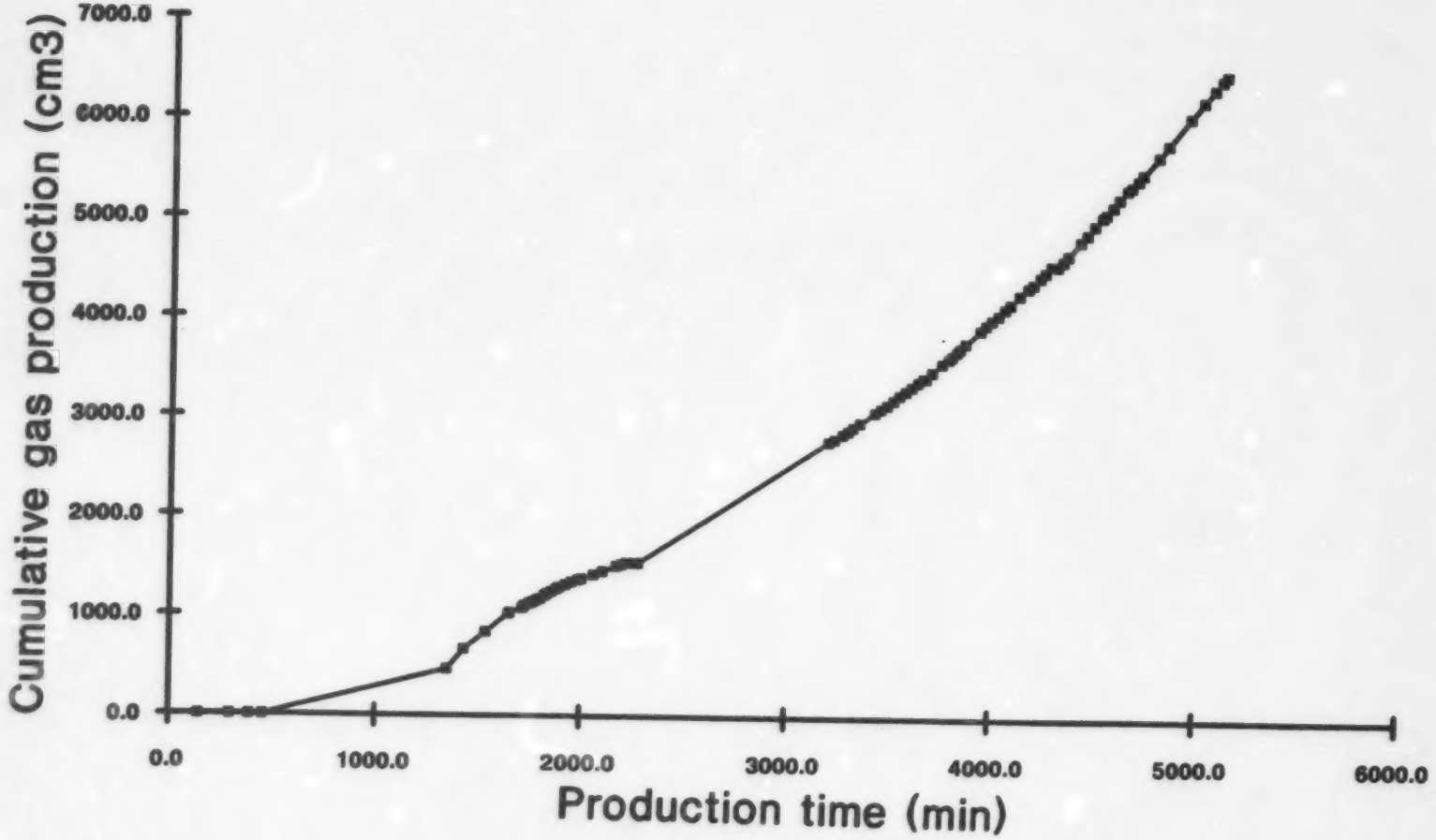

Figure 44: Cumulative gas production during gasflood in MPH1.

© 1991 NOVA HUSKY RESEARCH CORPORATION

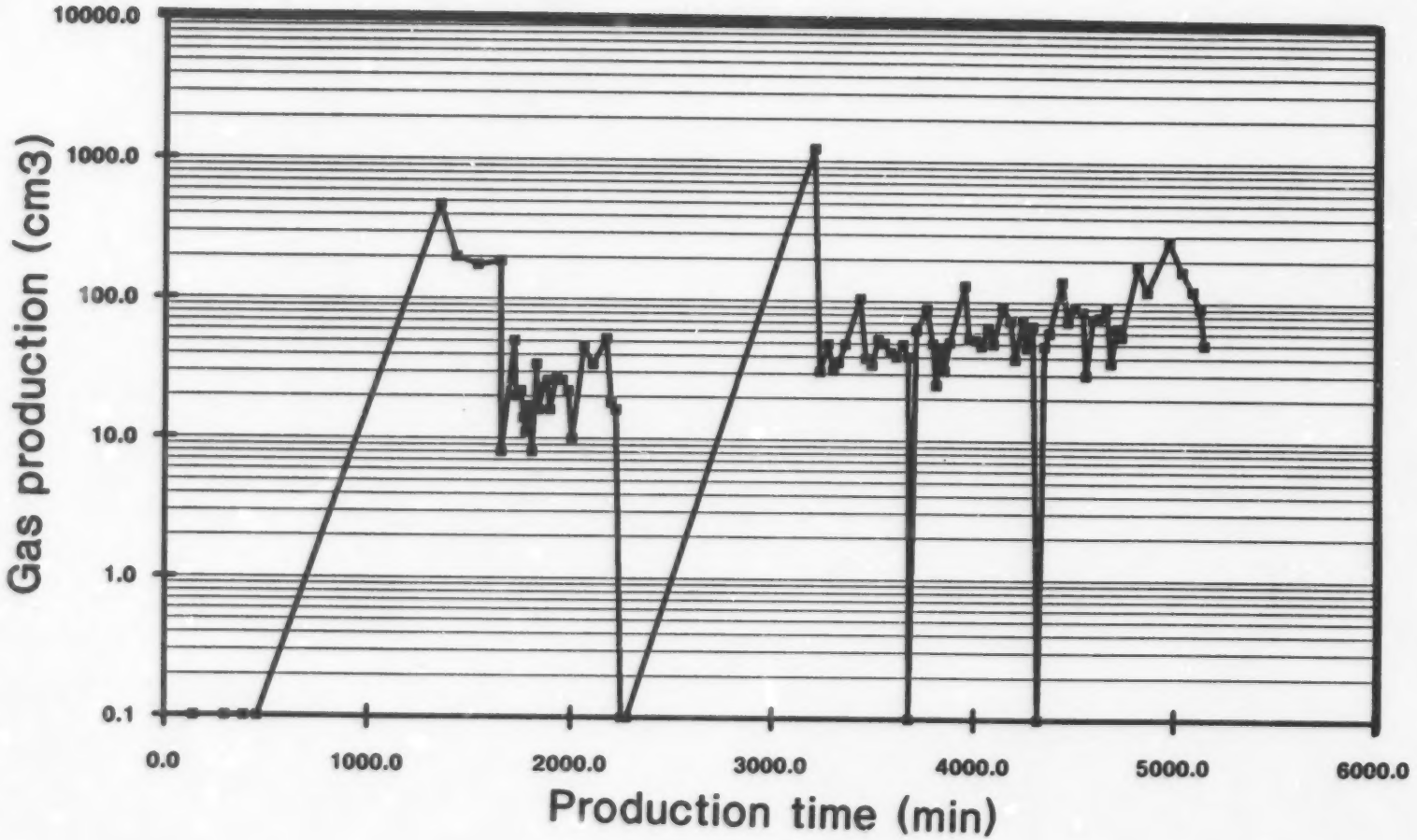

Figure 45: Gas production during gasflood in MPH1.

© 1991 NOVA HUSKY RESEARCH CORPORATION

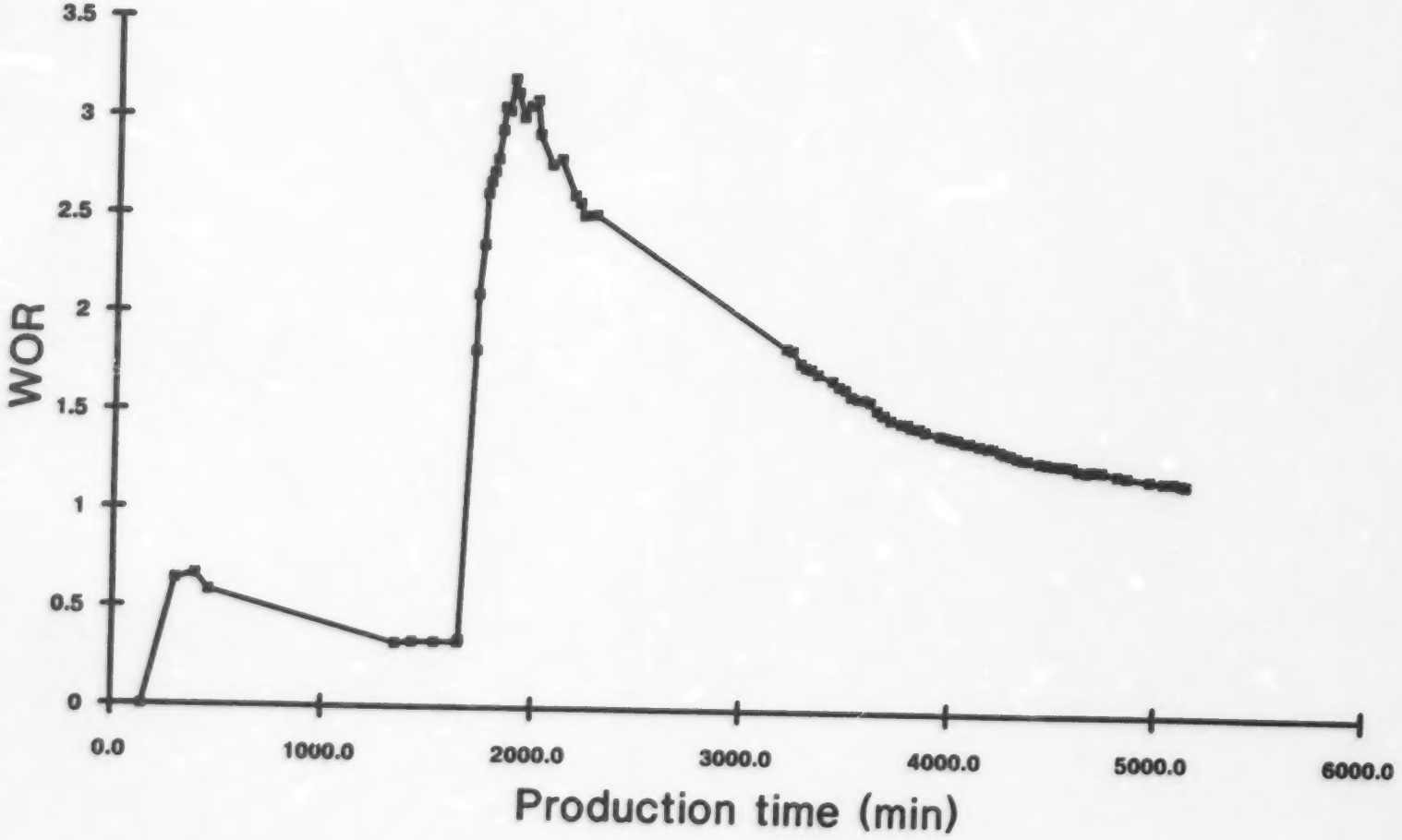

Figure 46: Water oil ratio during gasflood in MPH1 (cumulative).

© 1991 NOVA HUSKY RESEARCH CORPORATION

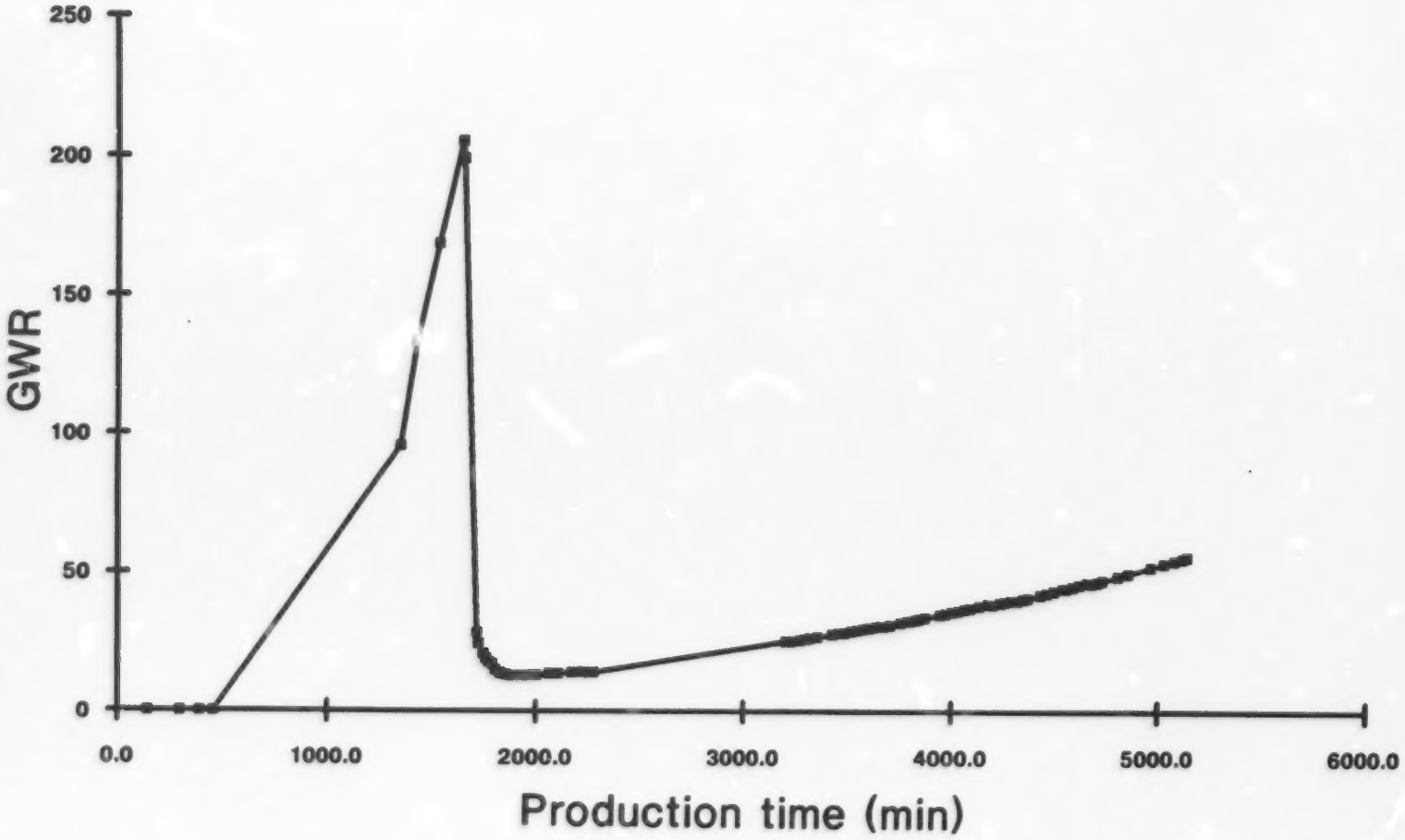

Figure 47: Gas water ratio during gasflood in MPH1 (cumulative).

© 1991 NOVA HUSKY RESEARCH CORPORATION

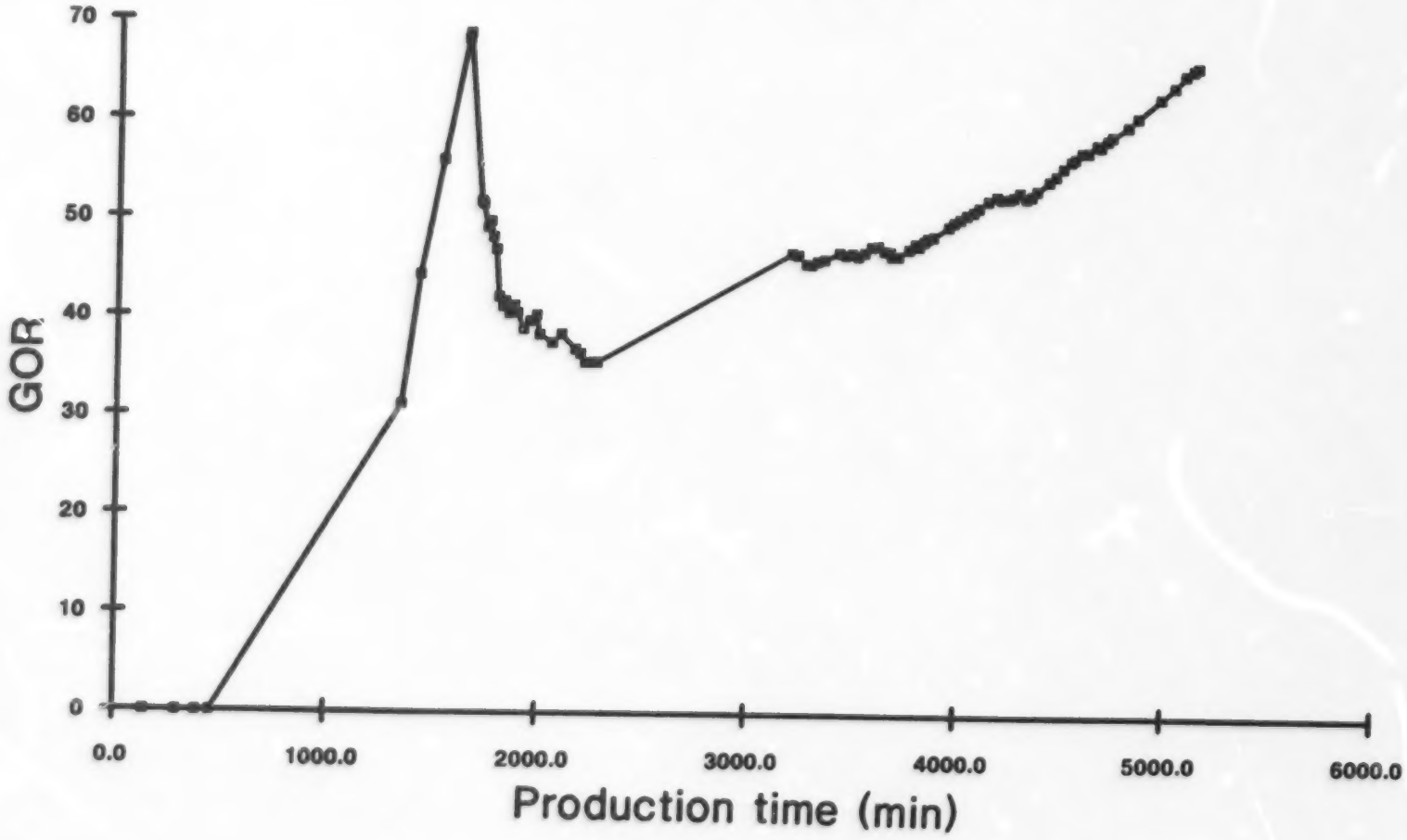

Figure 48: Gas oil ratio during the gasflood in MPH1 (cumulative).

© 1991 NOVA HUSKY RESEARCH CORPORATION

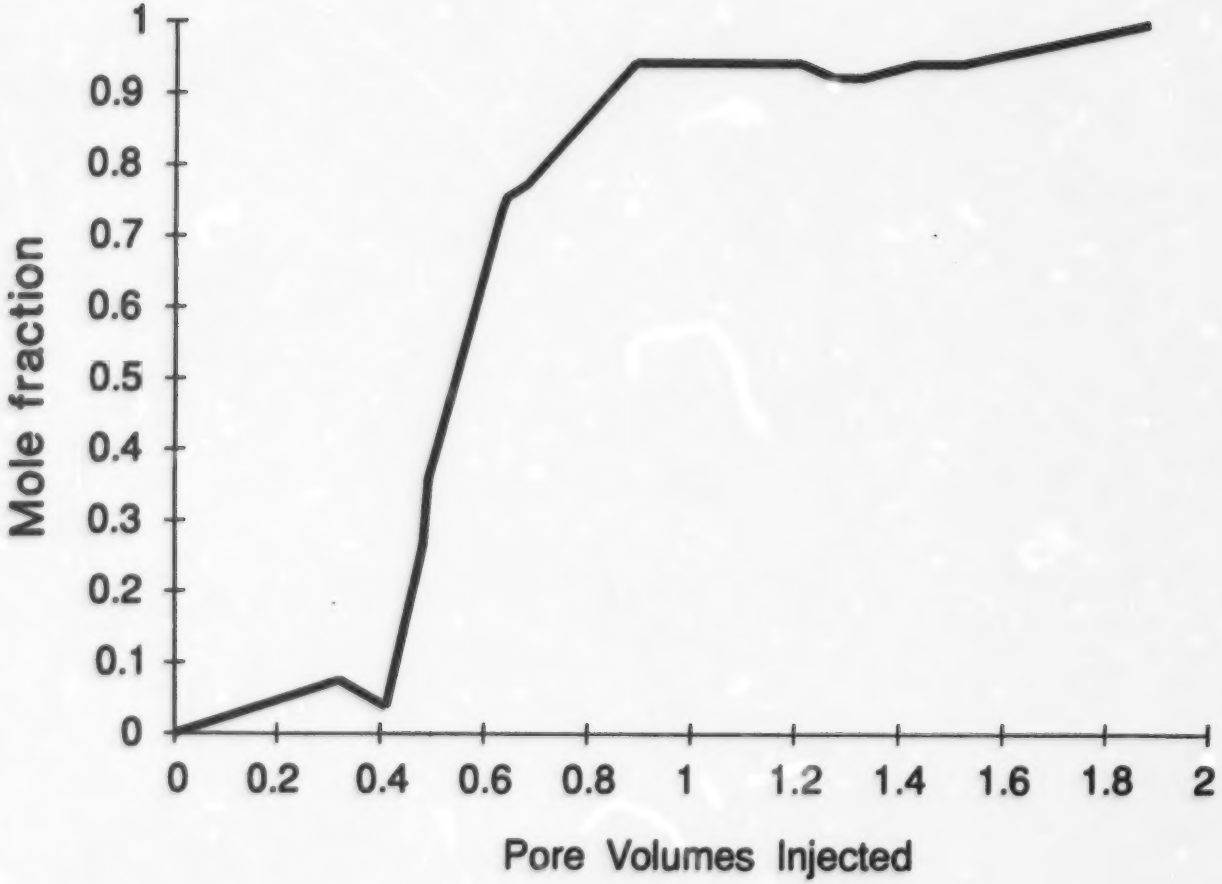

Figure 49: ***In situ*** **concentration profile during miscible displacement in Berea sandstone.**

© 1991 NOVA HUSKY RESEARCH CORPORATION

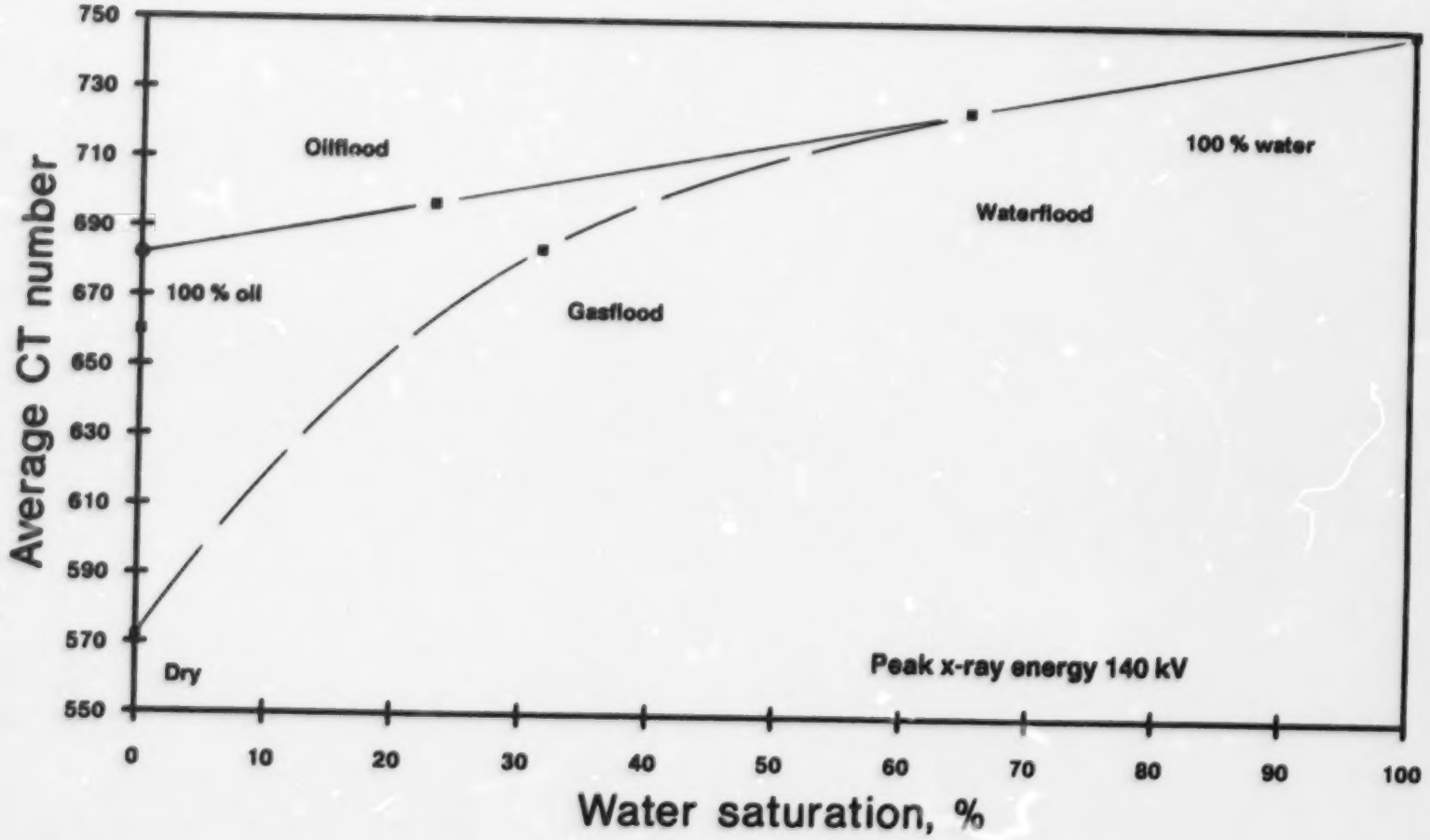

Figure 50: Average CT number versus water saturation at high energy for experiment MPH3.

© 1991 NOVA HUSKY RESEARCH CORPORATION

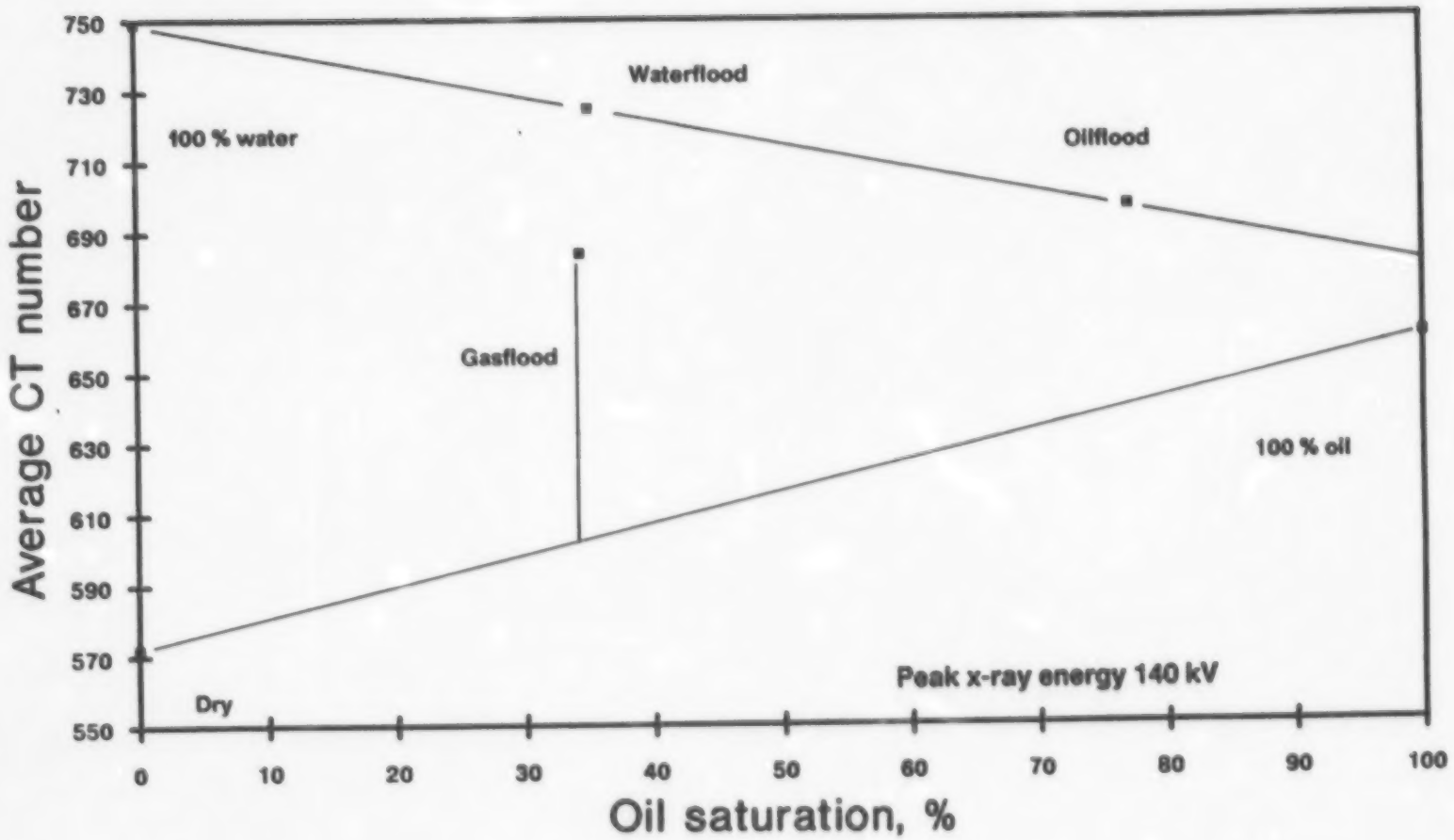

Figure 51: Average CT number versus oil saturation at high energy for experiment MPH3.

© 1991 NOVA HUSKY RESEARCH CORPORATION

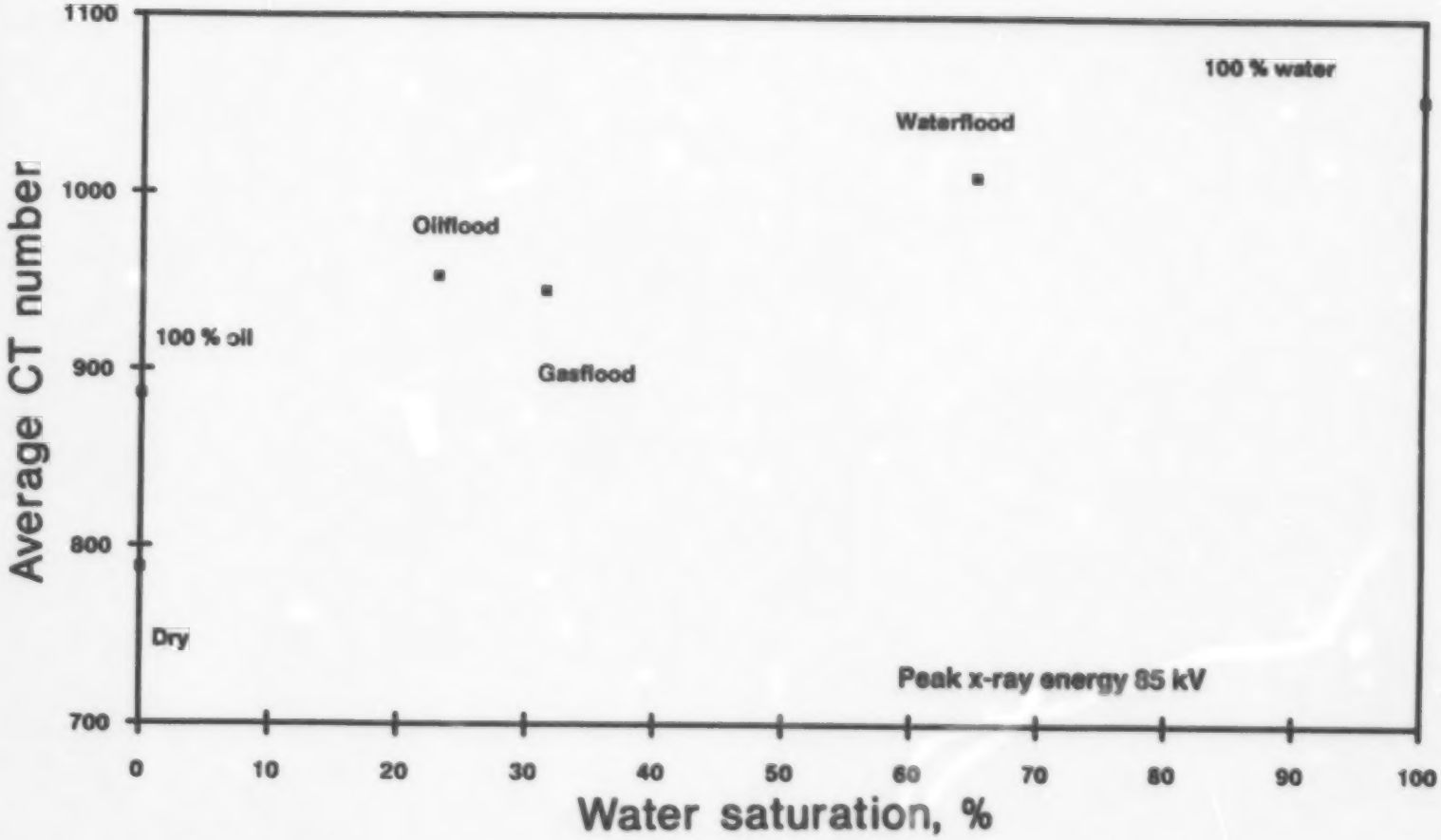

Figure 52: Average CT number versus water saturation at low energy for experiment MPH3.

© 1991 NOVA HUSKY RESEARCH CORPORATION

Figure 53: Saturation color code for experiment MPH3.

© 1991 NOVA HUSKY RESEARCH CORPORATION

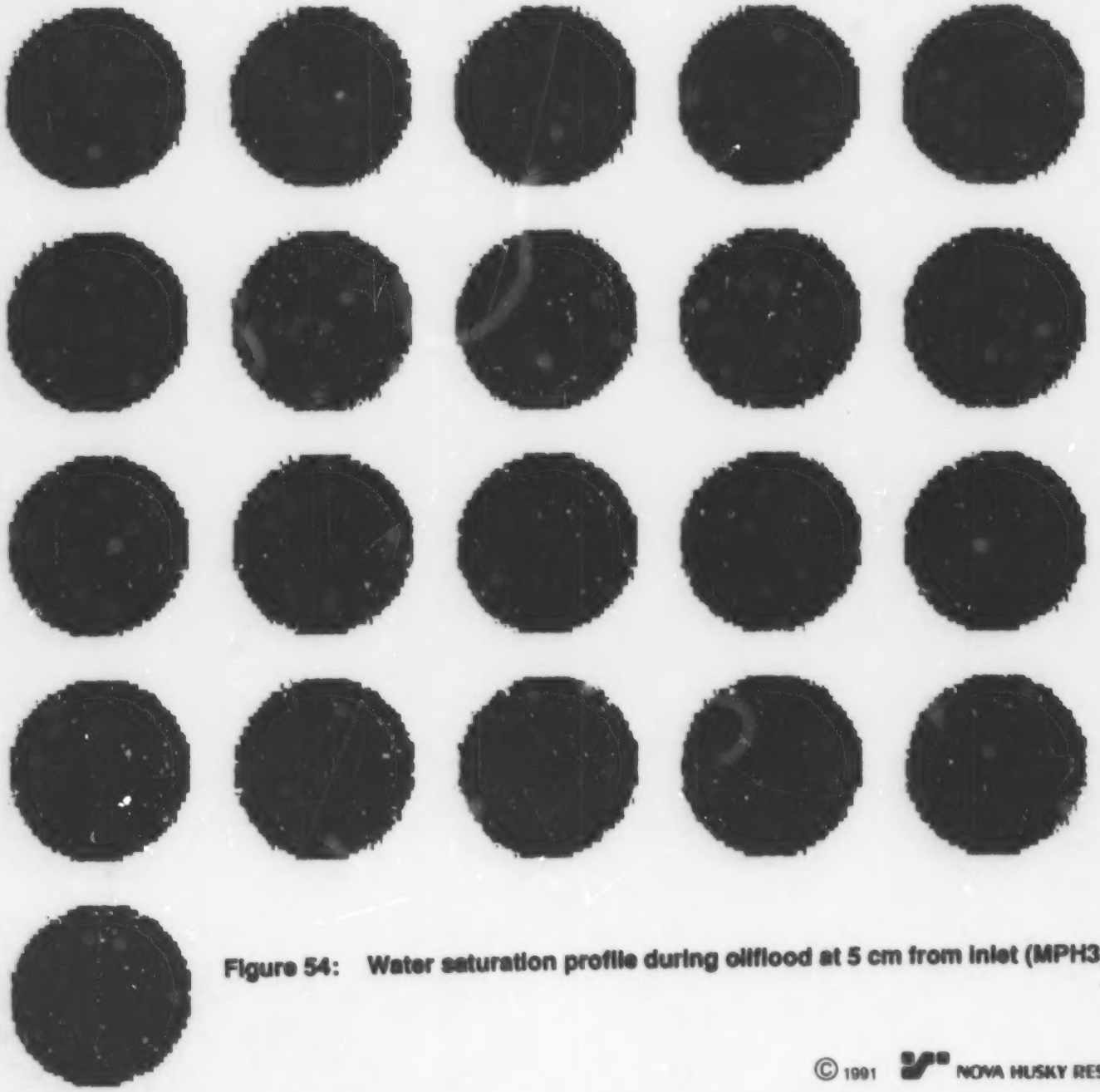

Figure 54: Water saturation profile during oilflood at 5 cm from inlet (MPH3).

© 1991 NOVA HUSKY RESEARCH CORPORATION

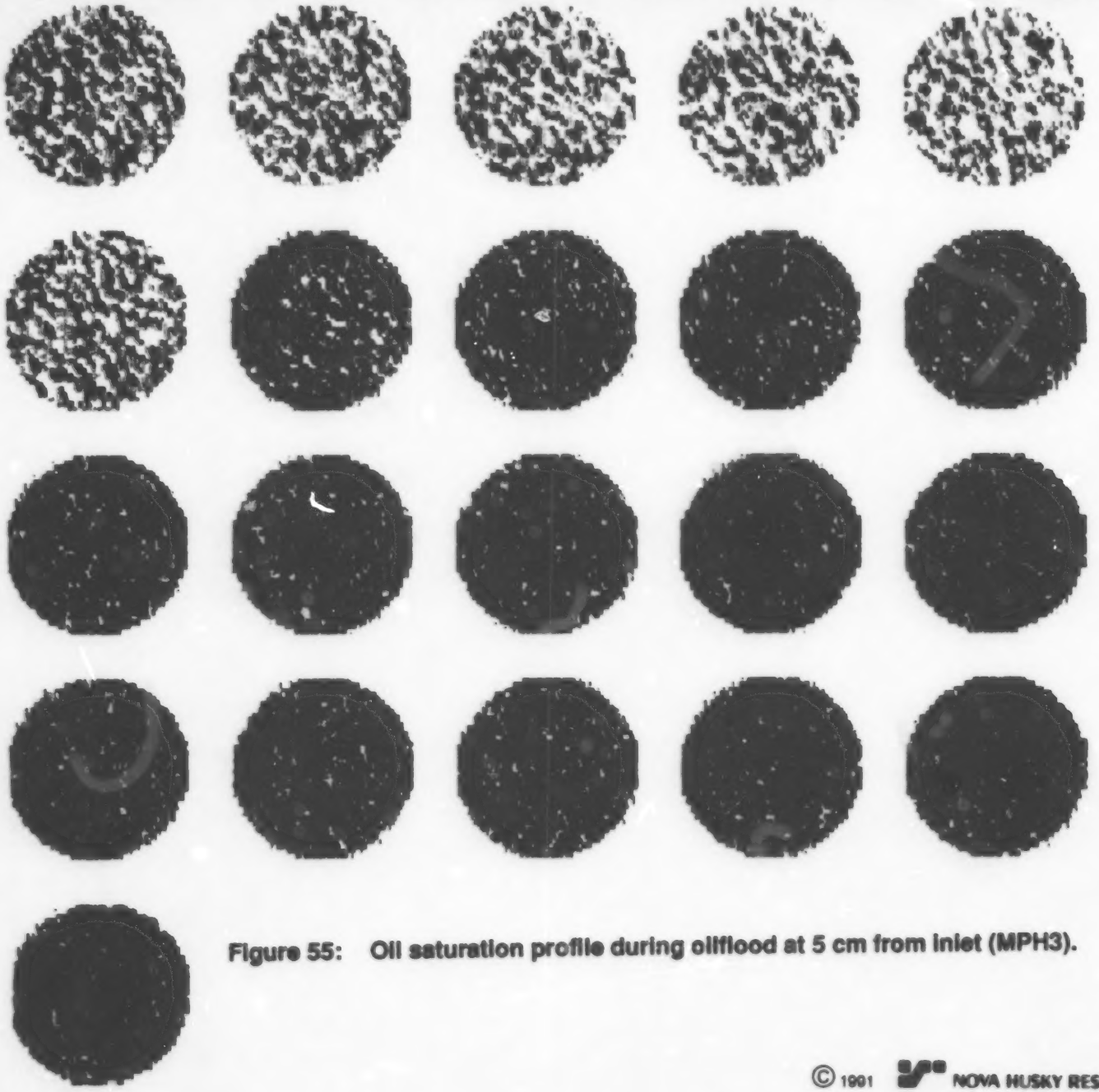

Figure 55: Oil saturation profile during oilflood at 5 cm from inlet (MPH3).

© 1991 NOVA HUSKY RESEARCH CORPORATION

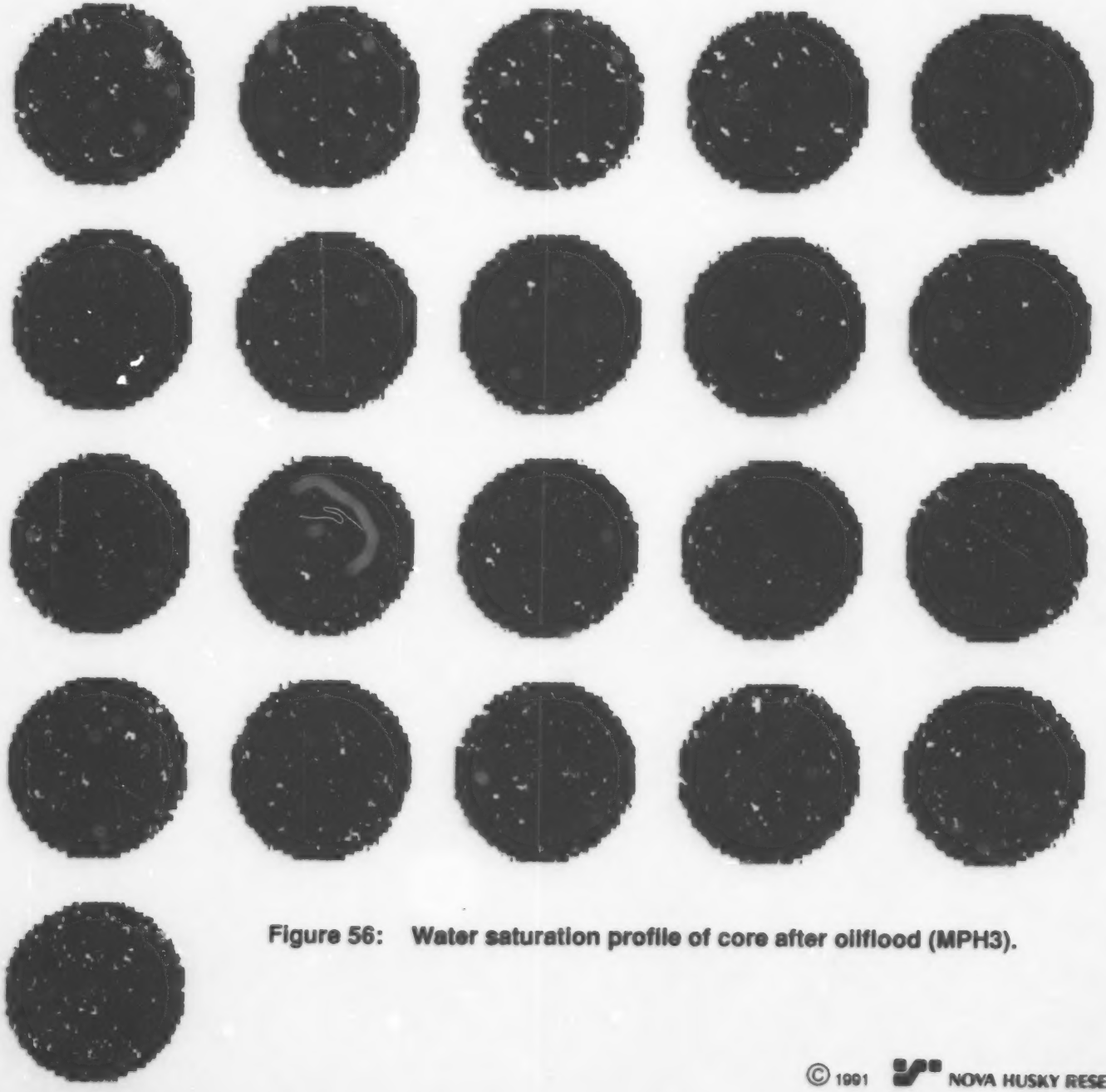

Figure 56: Water saturation profile of core after oilflood (MPH3).

© 1991 NOVA HUSKY RESEARCH CORPORATION

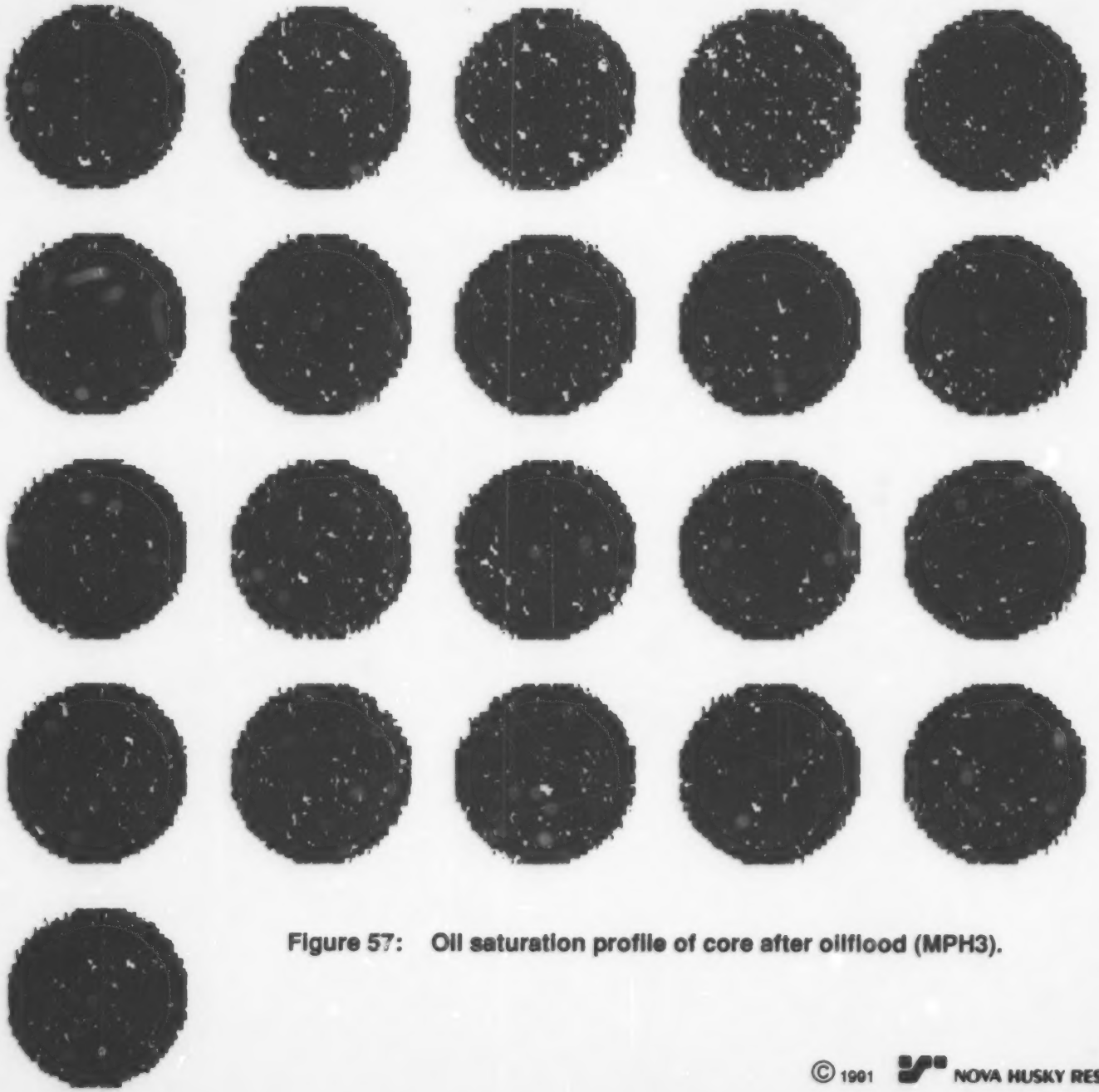

Figure 57: Oil saturation profile of core after oilflood (MPH3).

© 1991 NOVA HUSKY RESEARCH CORPORATION

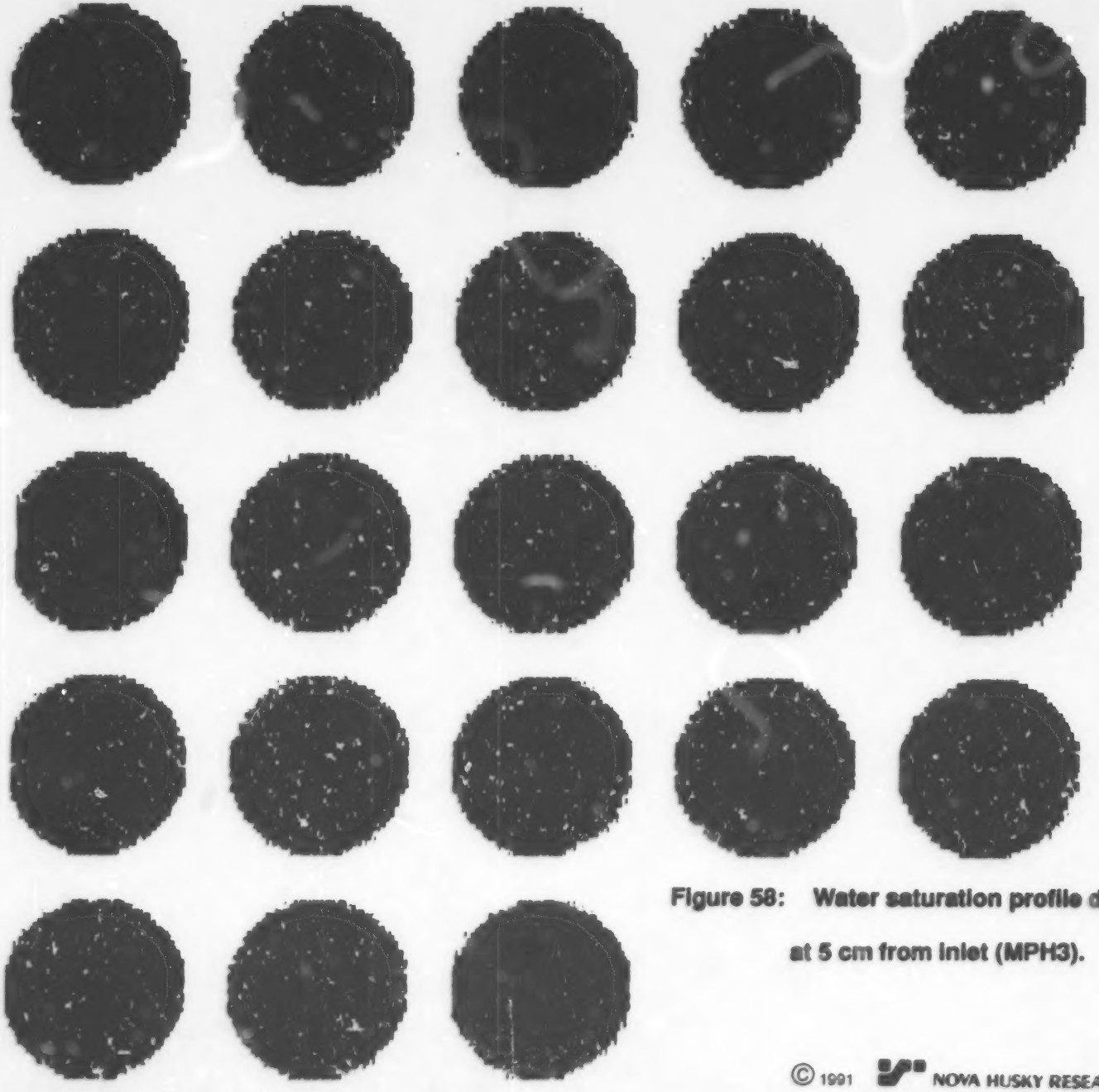

Figure 58: Water saturation profile during waterflood at 5 cm from inlet (MPH3).

© 1991 NOVA HUSKY RESEARCH CORPORATION

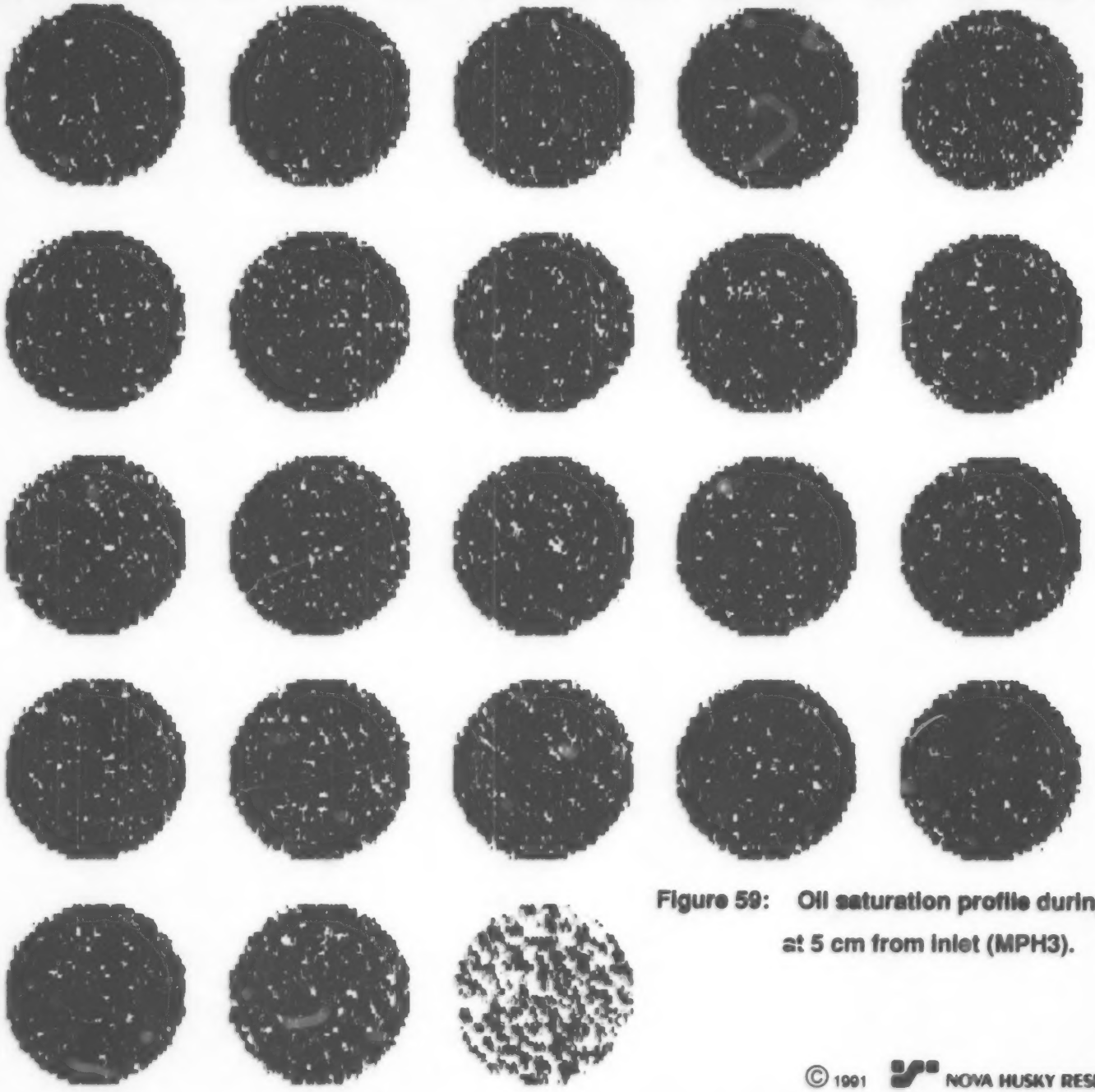

Figure 59: Oil saturation profile during waterflood at 5 cm from inlet (MPH3).

© 1991 NOVA HUSKY RESEARCH CORPORATION

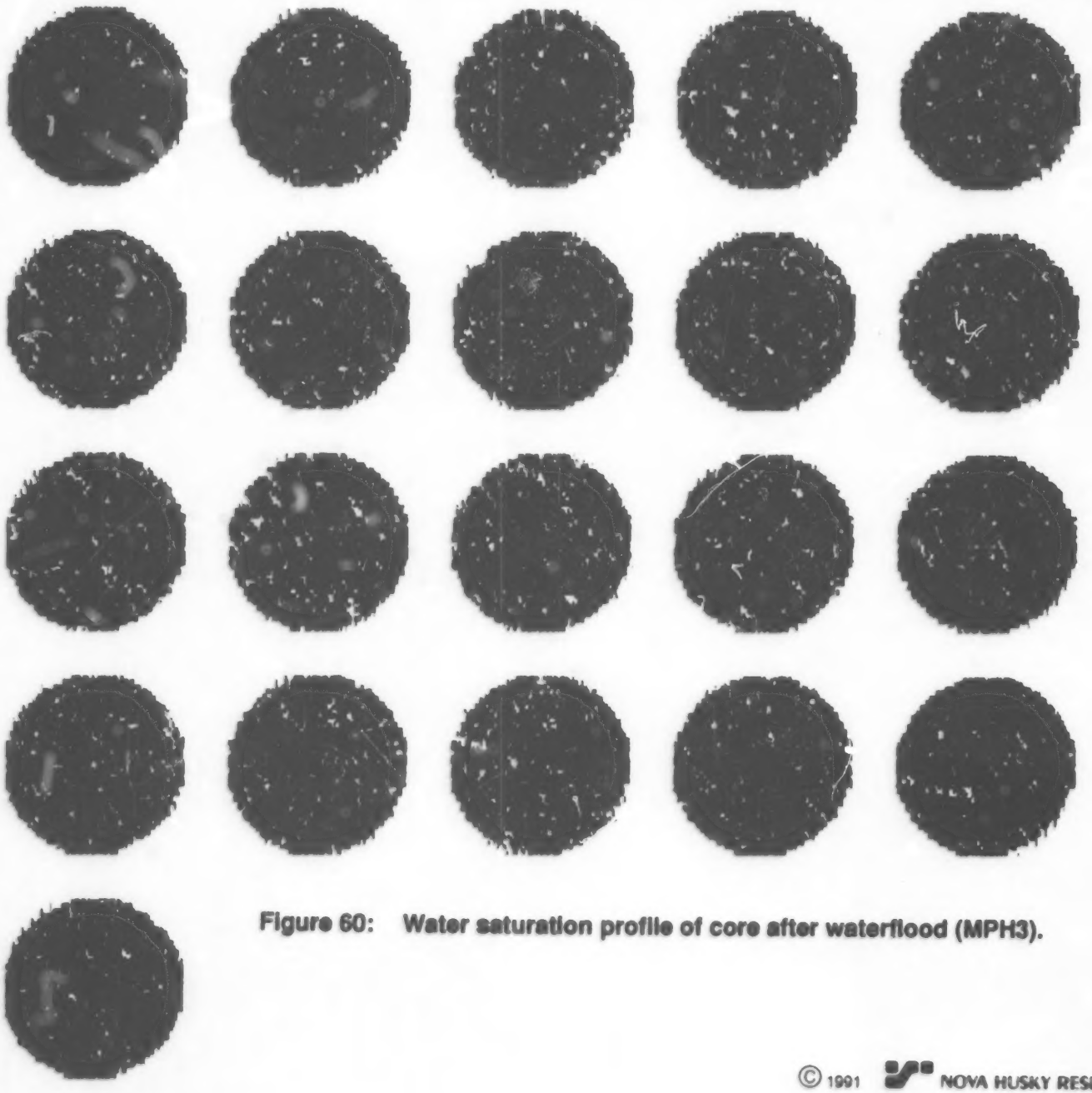

Figure 60: Water saturation profile of core after waterflood (MPH3).

© 1991 NOVA HUSKY RESEARCH CORPORATION

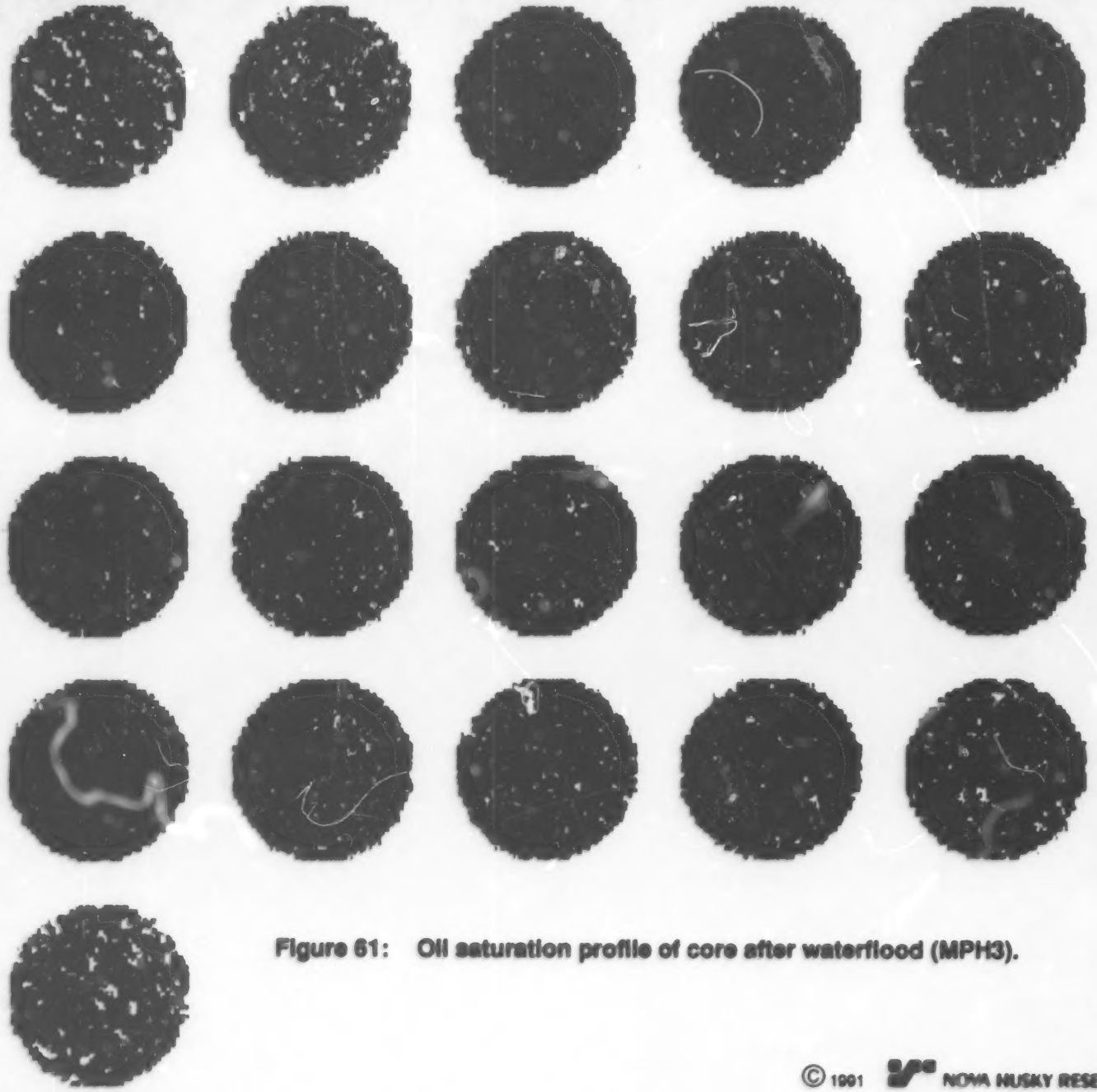

Figure 61: Oil saturation profile of core after waterflood (MPH3).

© 1991 NOVA HUSKY RESEARCH CORPORATION

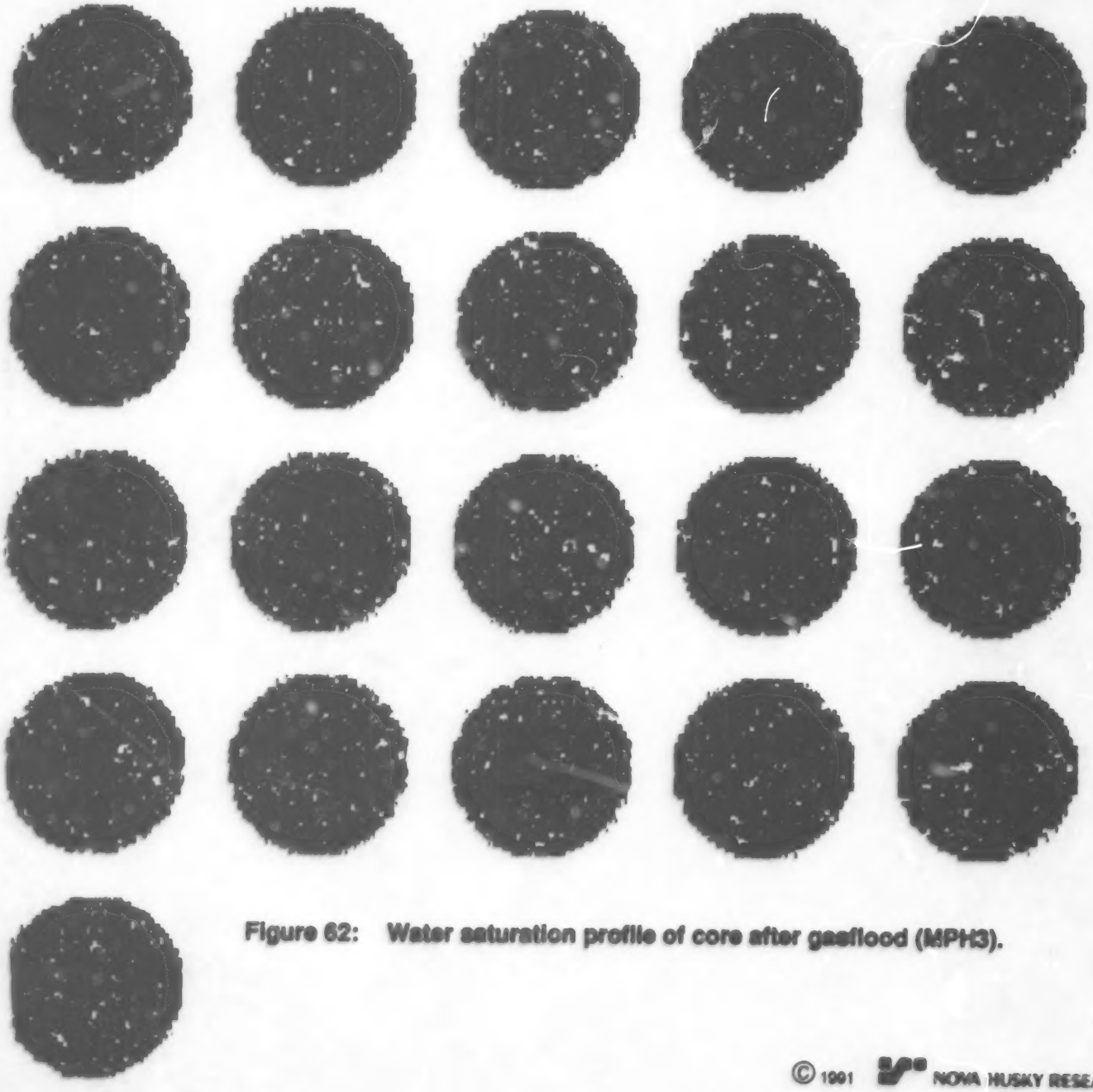

Figure 62: Water saturation profile of core after gasflood (MPH3).

© 1991 NOVA HUSKY RESEARCH CORPORATION

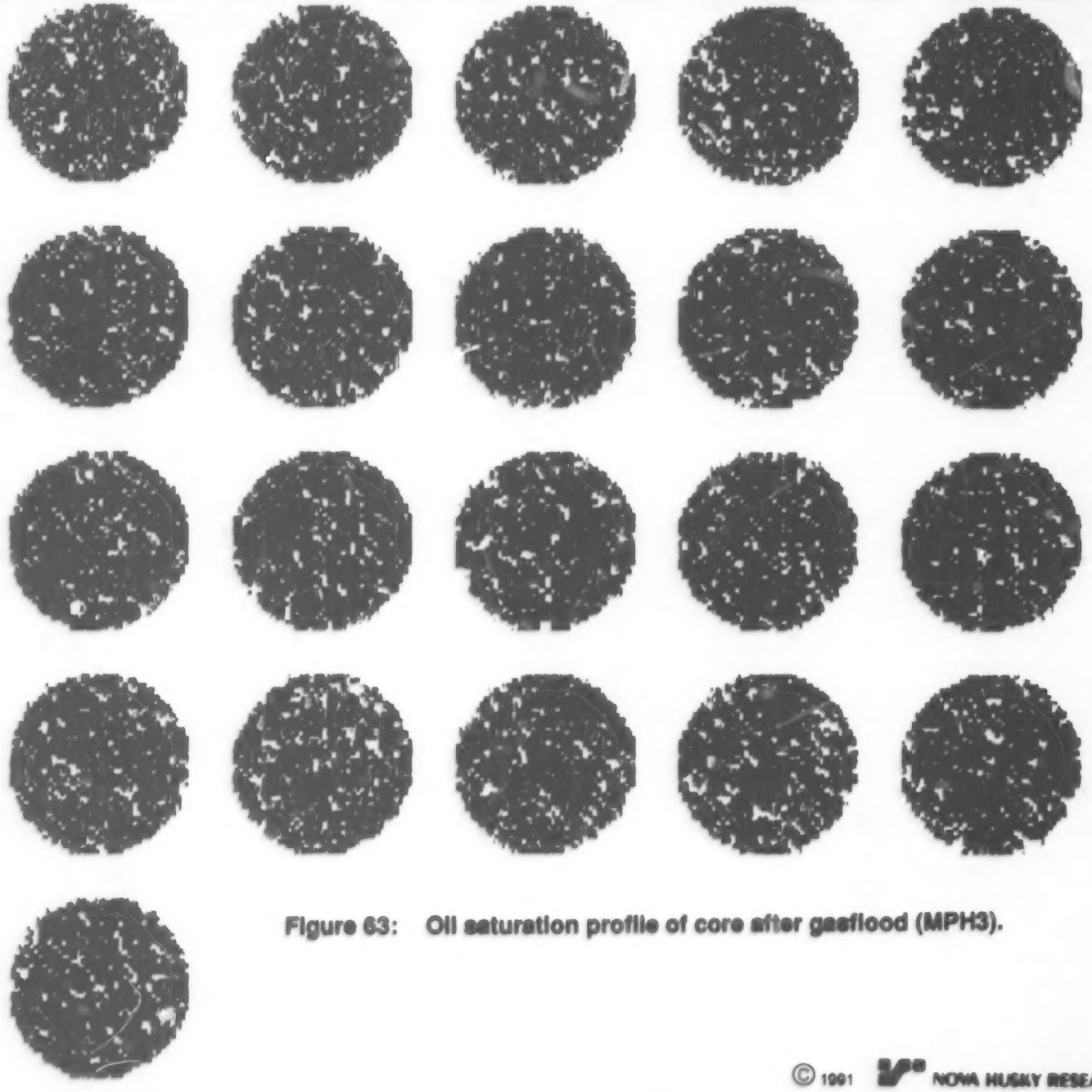

Figure 63: Oil saturation profile of core after gasflood (MPH3).

© 1991 NOVA HUSKY RESEARCH CORPORATION

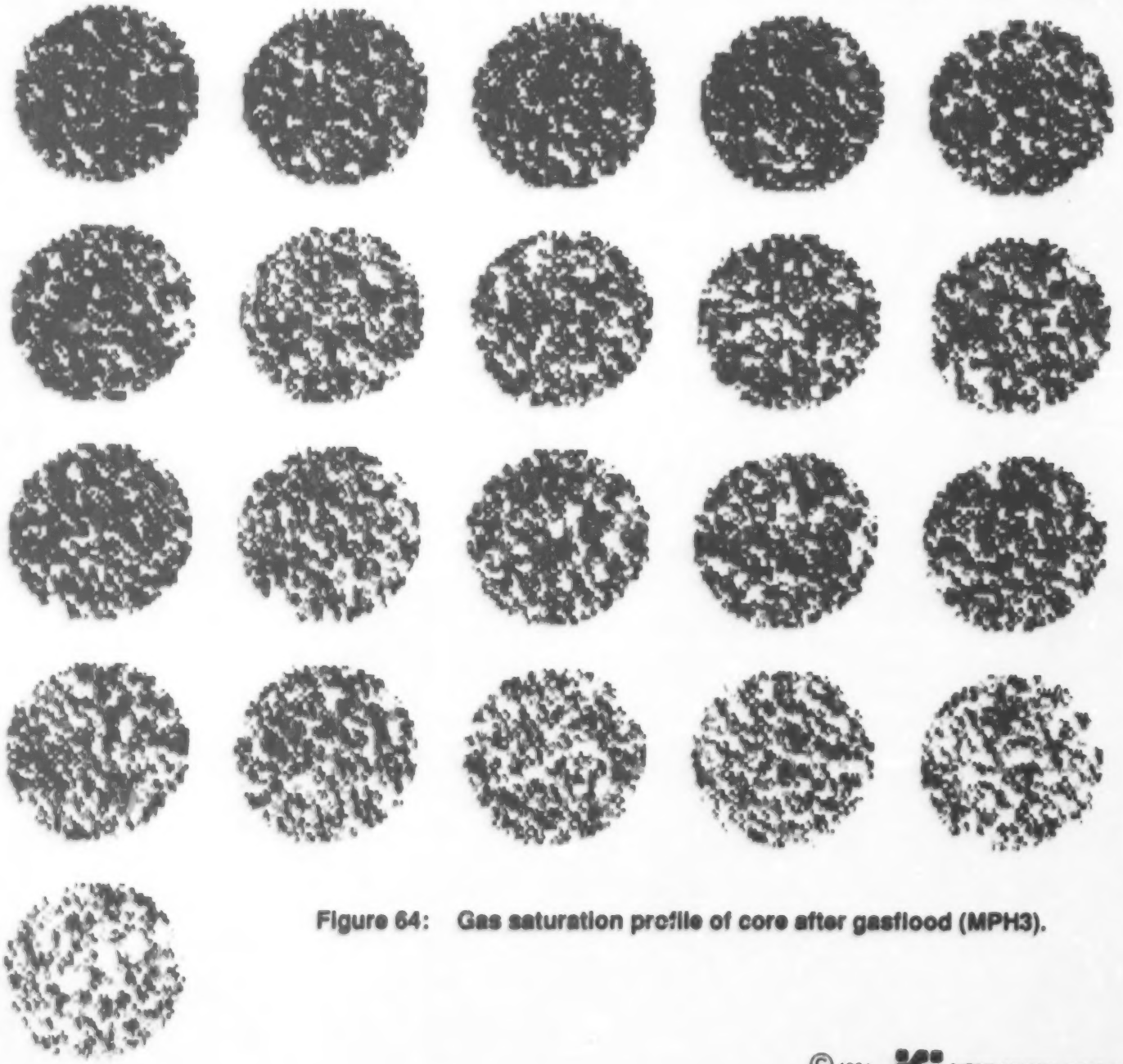

Figure 64: Gas saturation profile of core after gasflood (MPH3).

© 1991 NOVA HUSKY RESEARCH CORPORATION

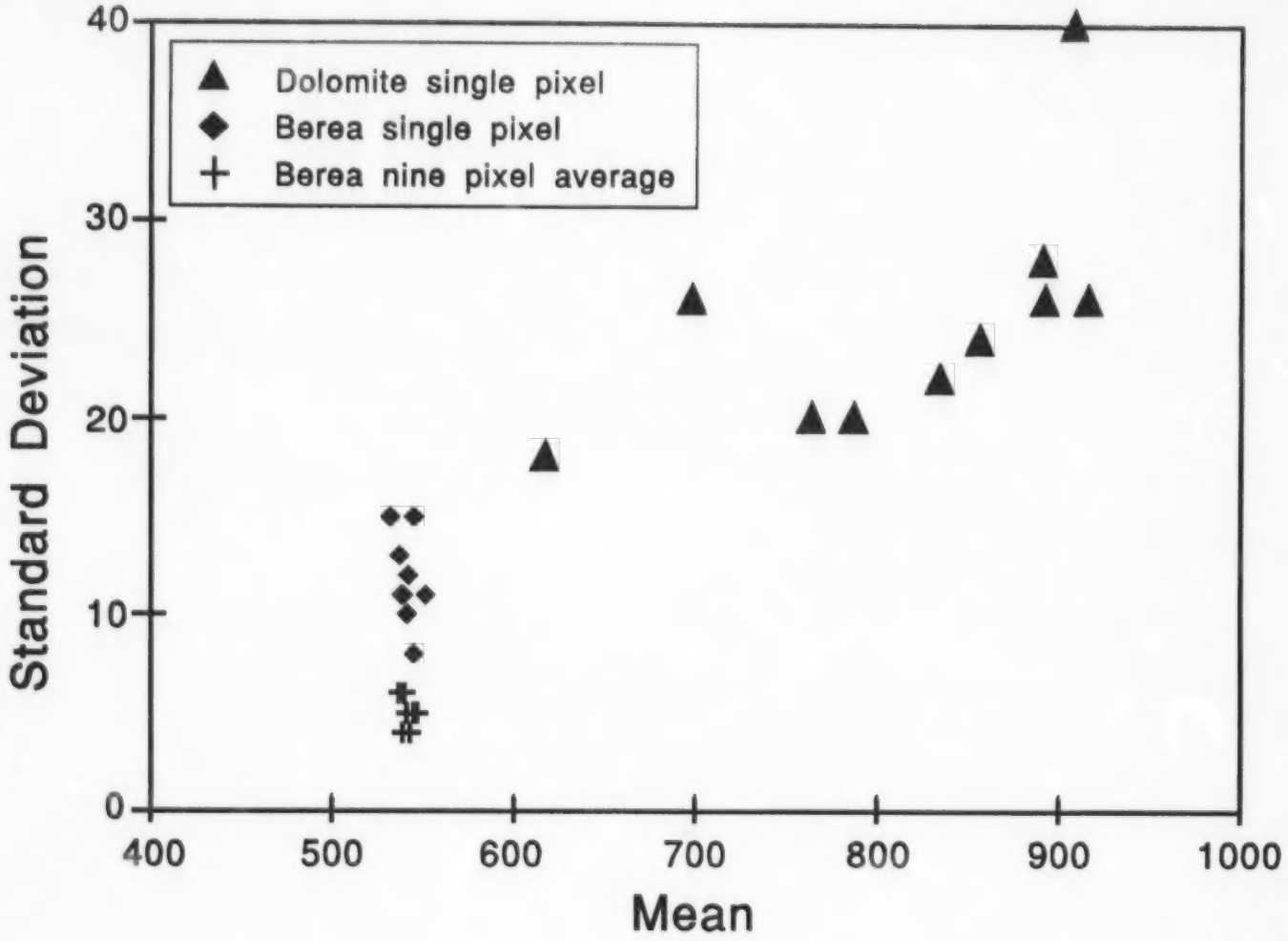

Figure 65: CT number mean and standard deviation for Berea and Rainbow Lake dolomite at 140 kVp.

© 1991 NOVA HUSKY RESEARCH CORPORATION

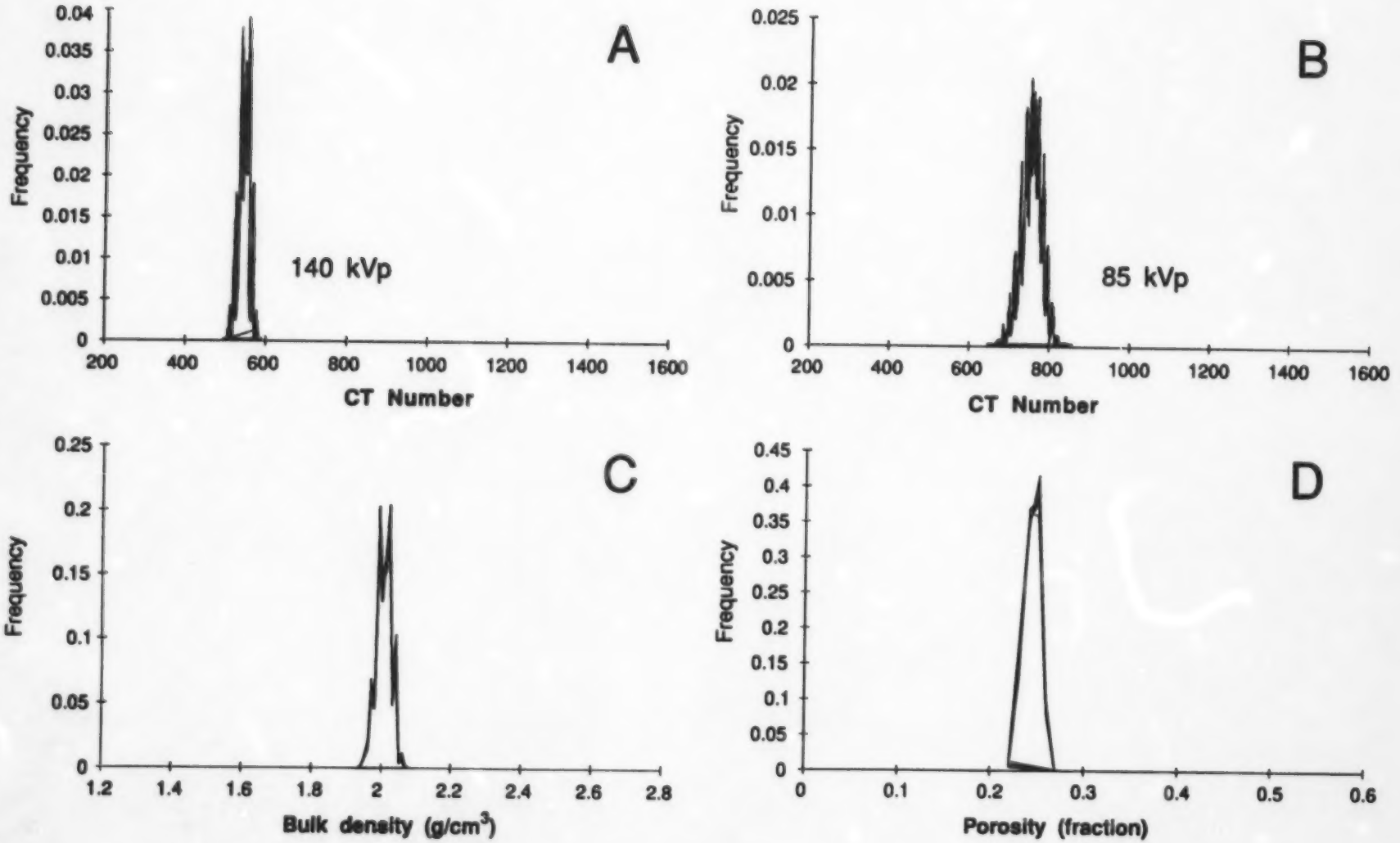

Figure 66: Frequency distributions of a relatively homogeneous medium (Berea).

© 1991 NOVA HUSKY RESEARCH CORPORATION

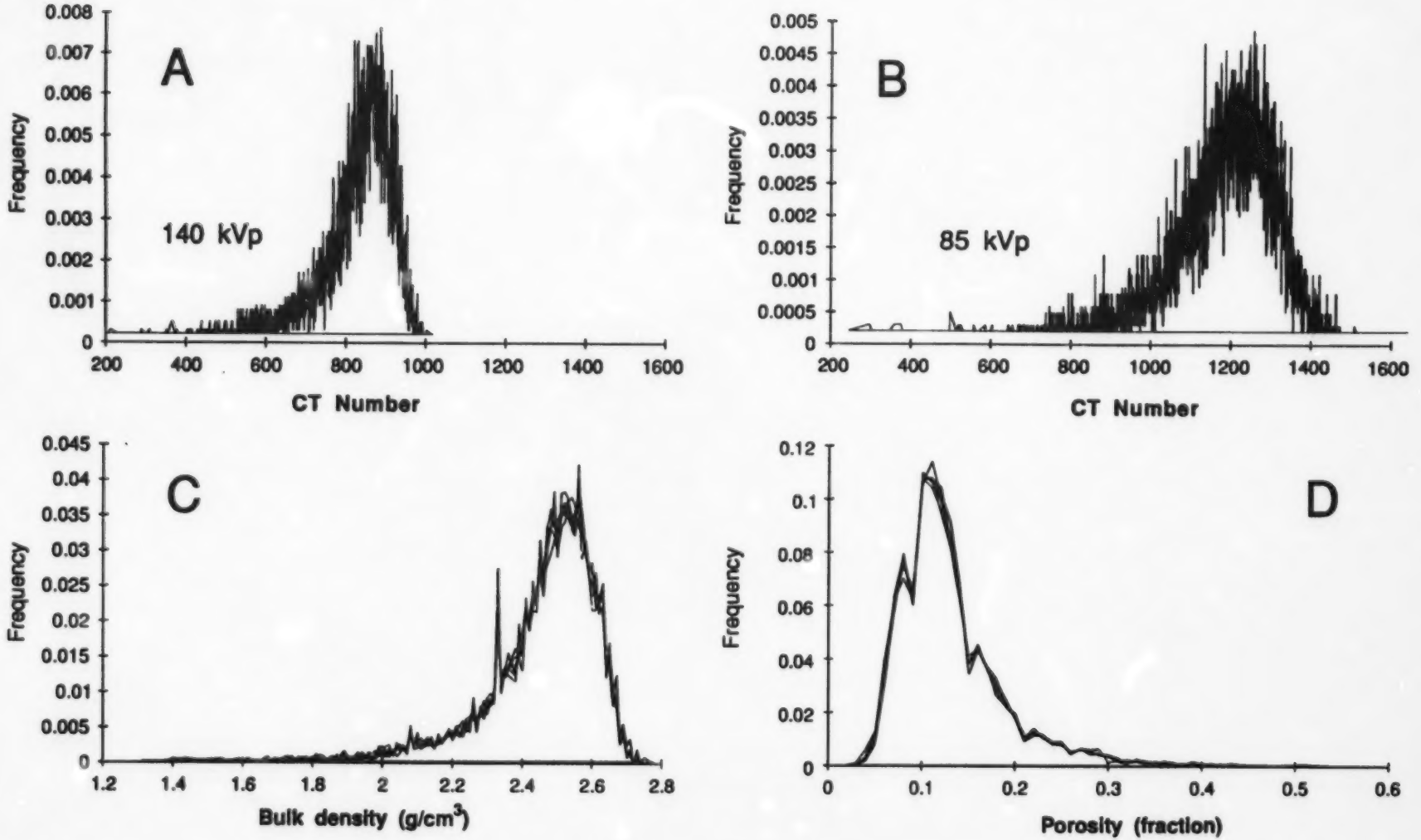

Figure 67: Frequency distributions of a heterogeneous medium (Rainbow dolomite).

© 1991 NOVA HUSKY RESEARCH CORPORATION

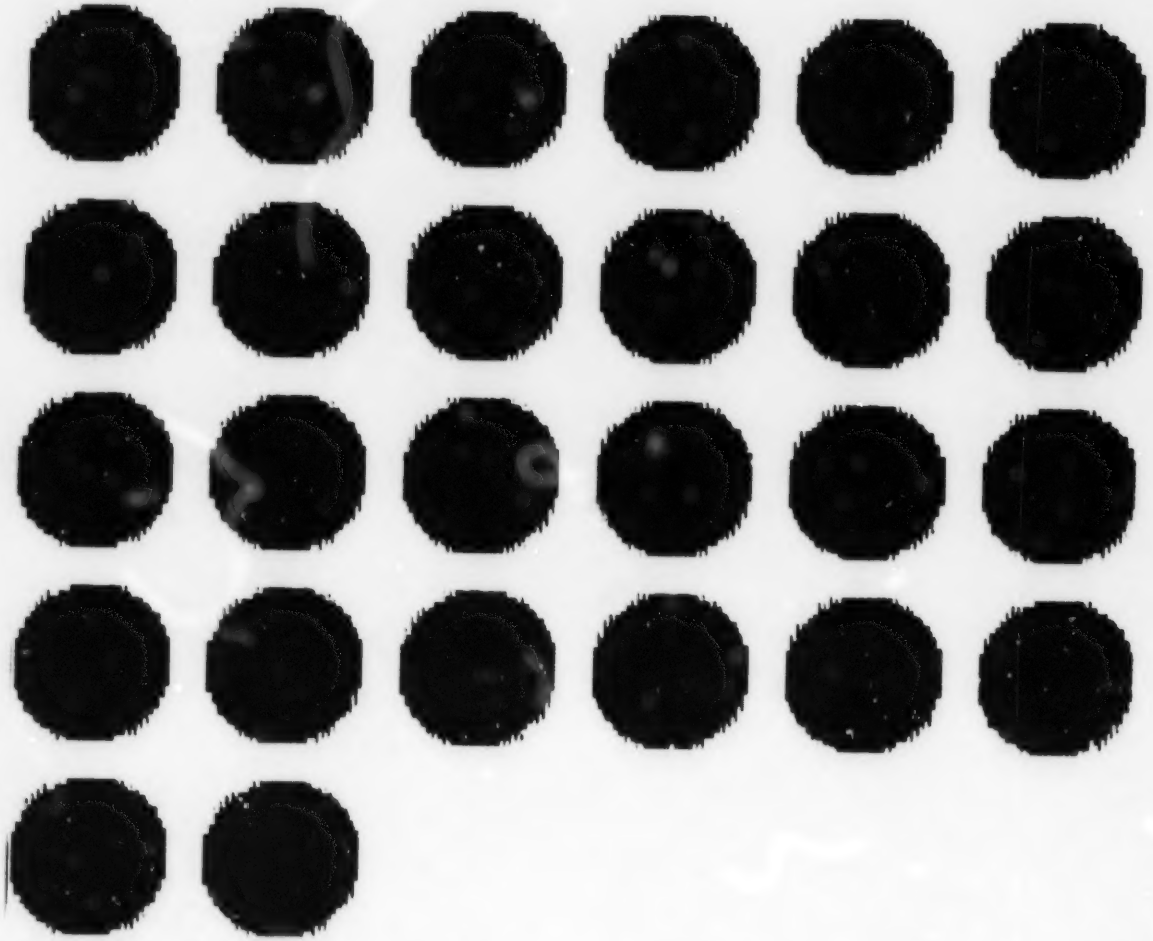

Figure 68: **Bulk density images for slices 1 to 22 prior to plugging, column A.**

© 1991 NOVA HUSKY RESEARCH CORPORATION

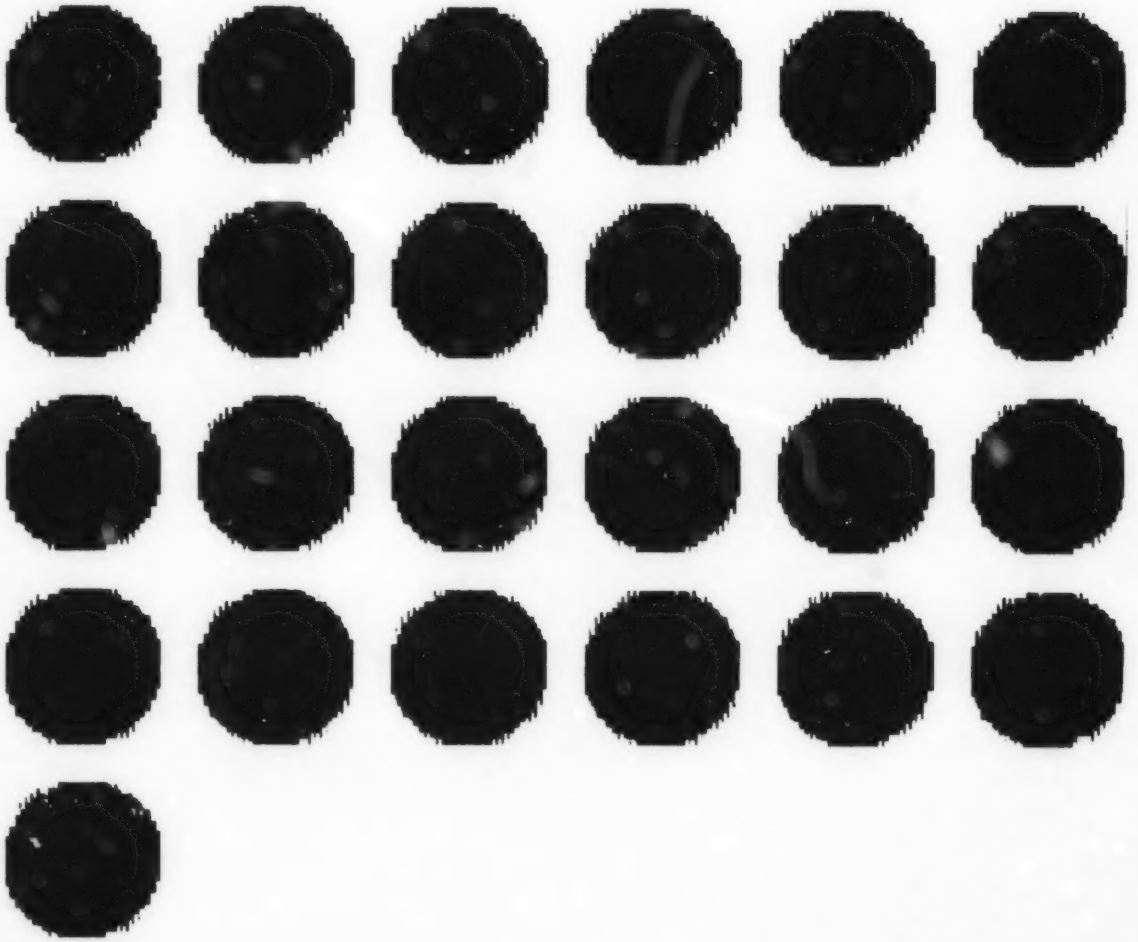

Figure 69: Bulk density images for slices 23 to 44 prior to plugging, column A.

© 1991 NOVA HUSKY RESEARCH CORPORATION

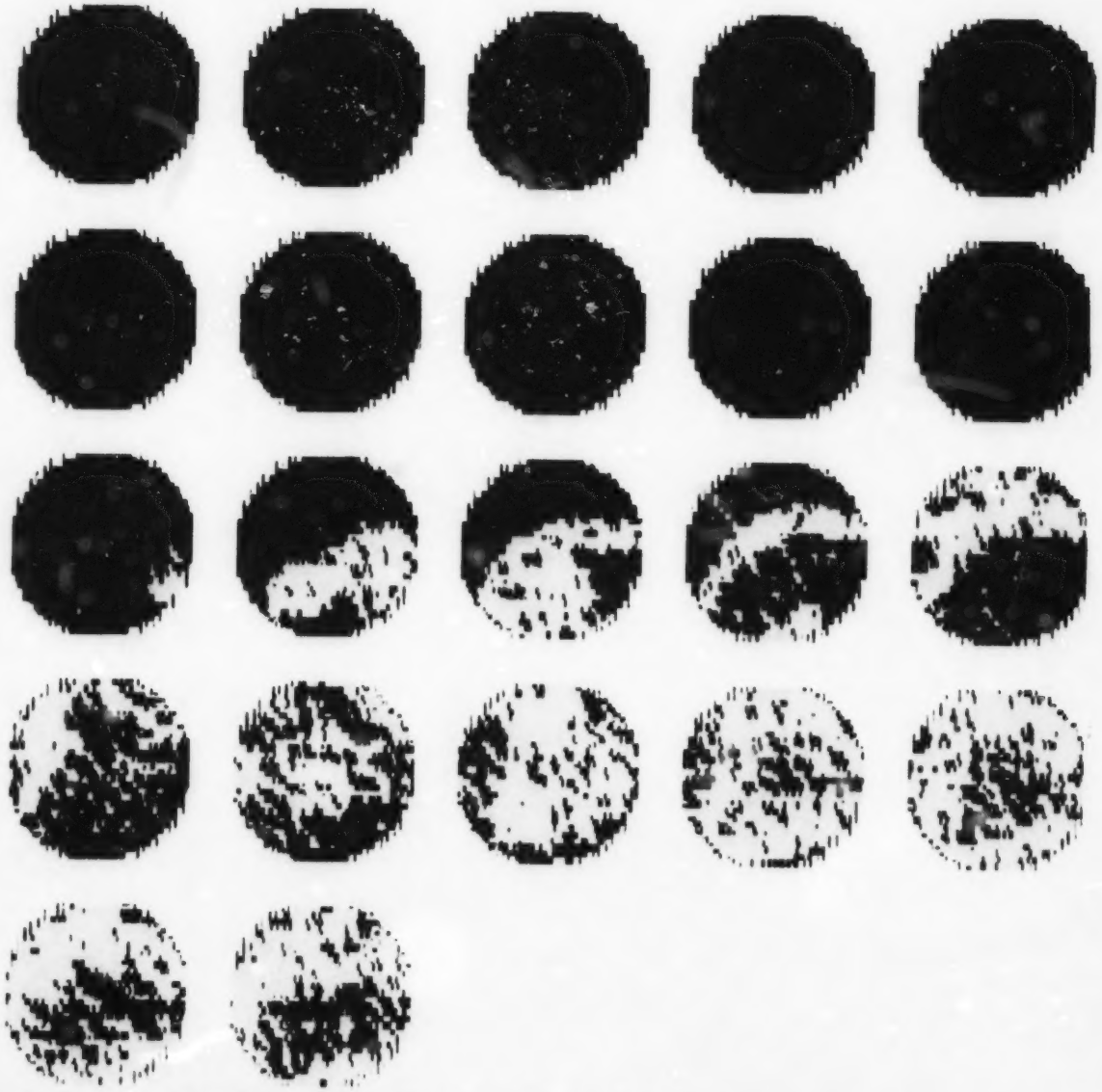

Figure 70: Bulk density images for slices 45 to 70 prior to plugging, column A.

© 1991 NOVA HUSKY RESEARCH CORPORATION

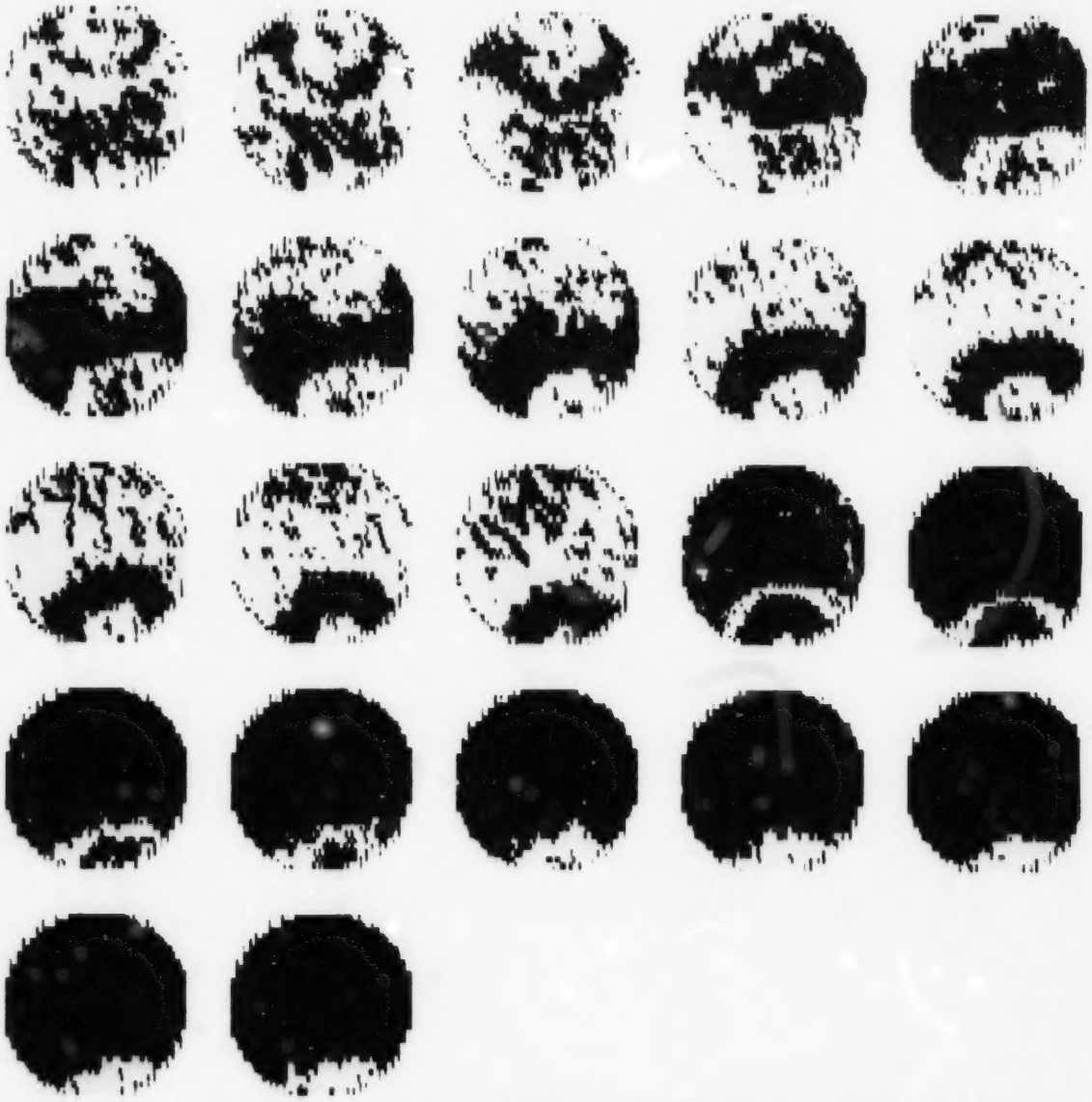

Figure 71: Bulk density images for slices 71 to 95 prior to plugging, column A.

© 1991 NOVA HUSKY RESEARCH CORPORATION

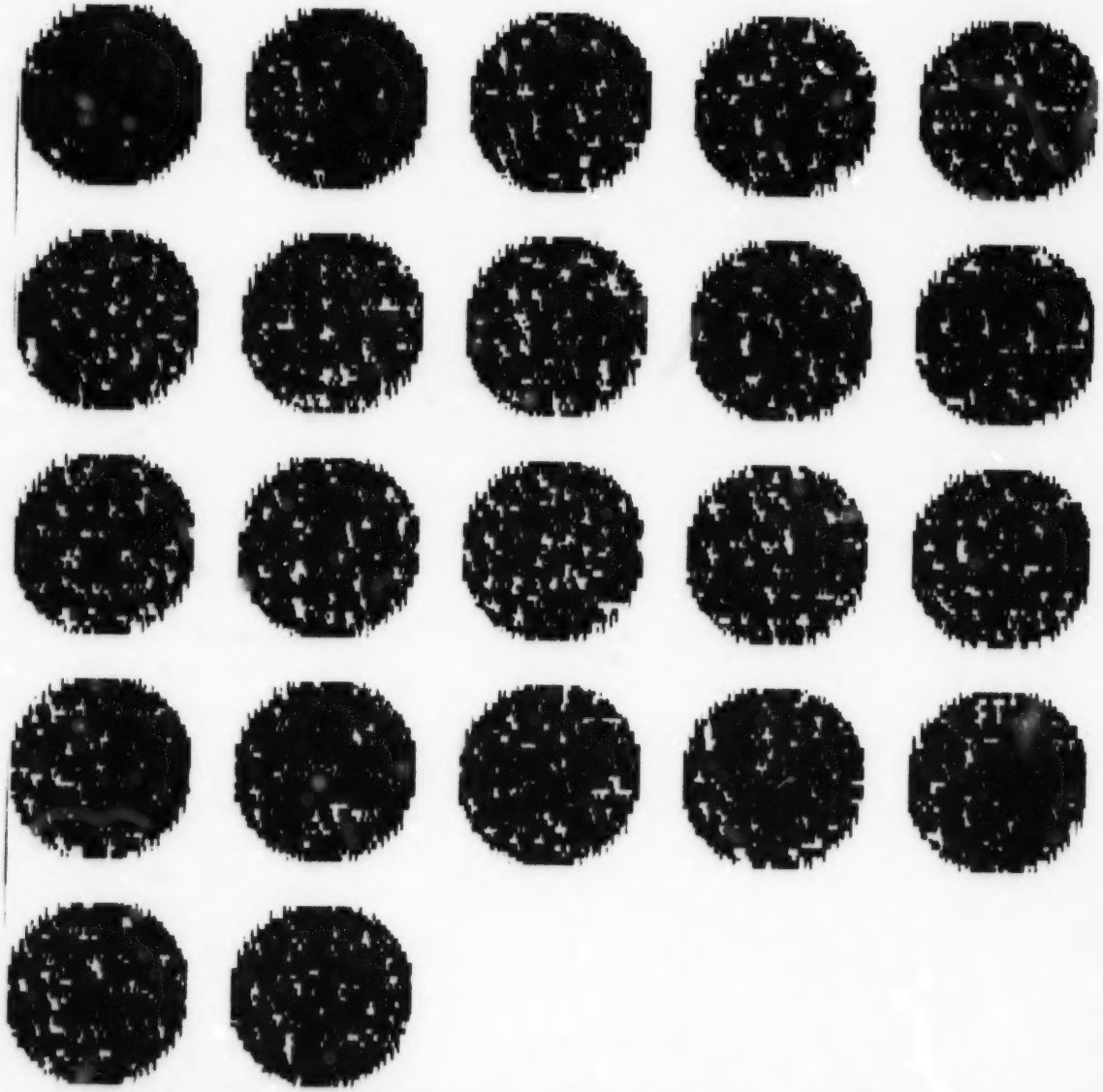

Figure 72: Bulk density images for slices 1 to 22 after plugging, column A.

© 1991 NOVA HUSKY RESEARCH CORPORATION

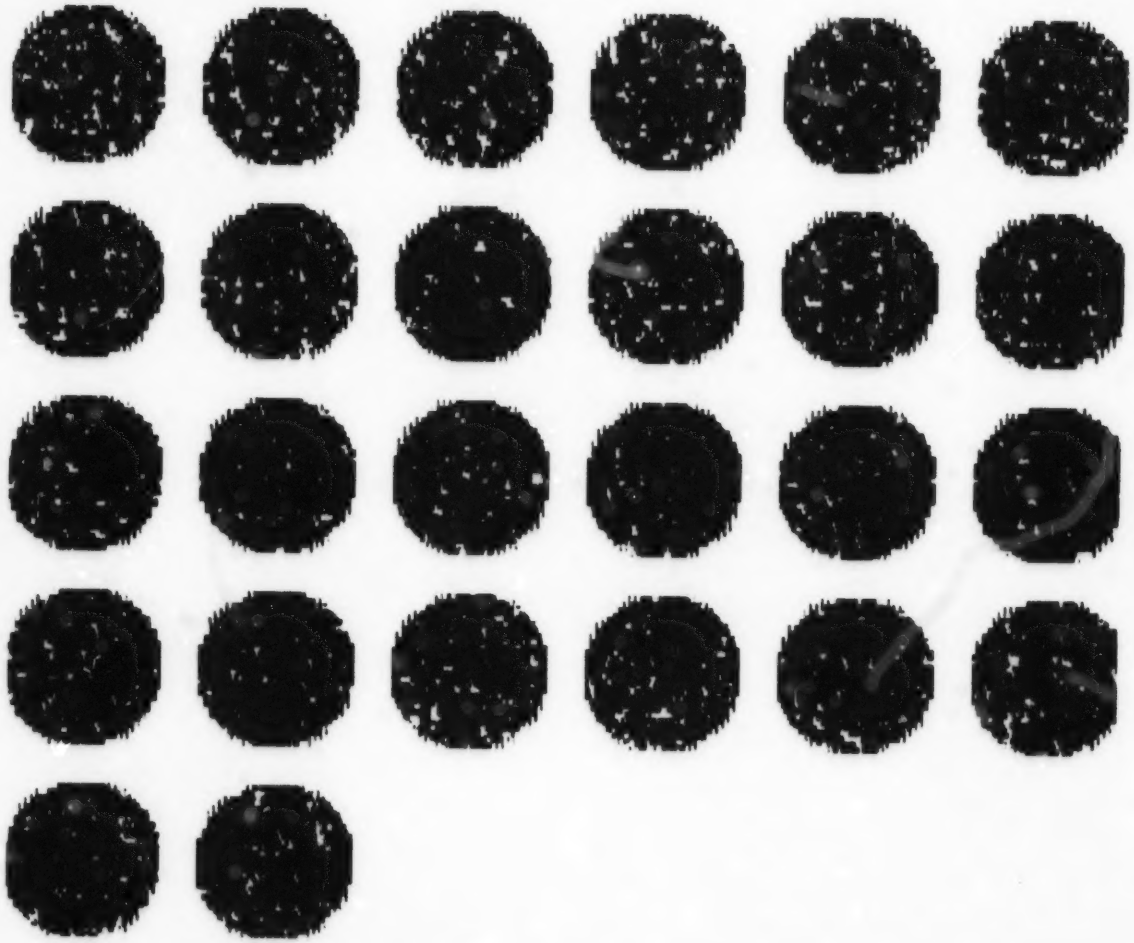

Figure 73: Bulk density images for slices 23 to 44 after plugging, column A.

© 1991 NOVA HUSKY RESEARCH CORPORATION

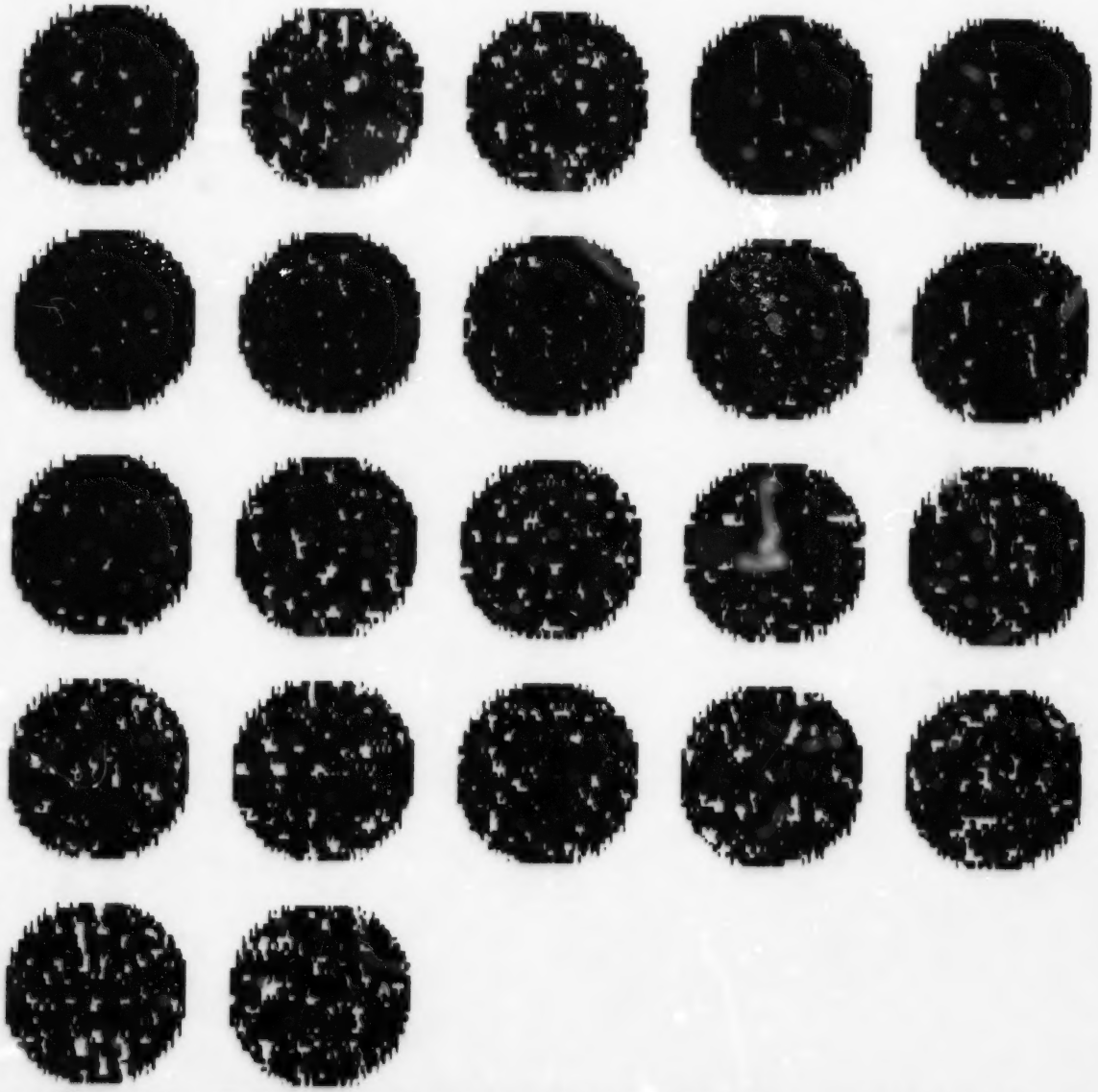

Figure 74: **Bulk density images for slices 1 to 22 prior to plugging, column B.**

© 1991 NOVA HUSKY RESEARCH CORPORATION

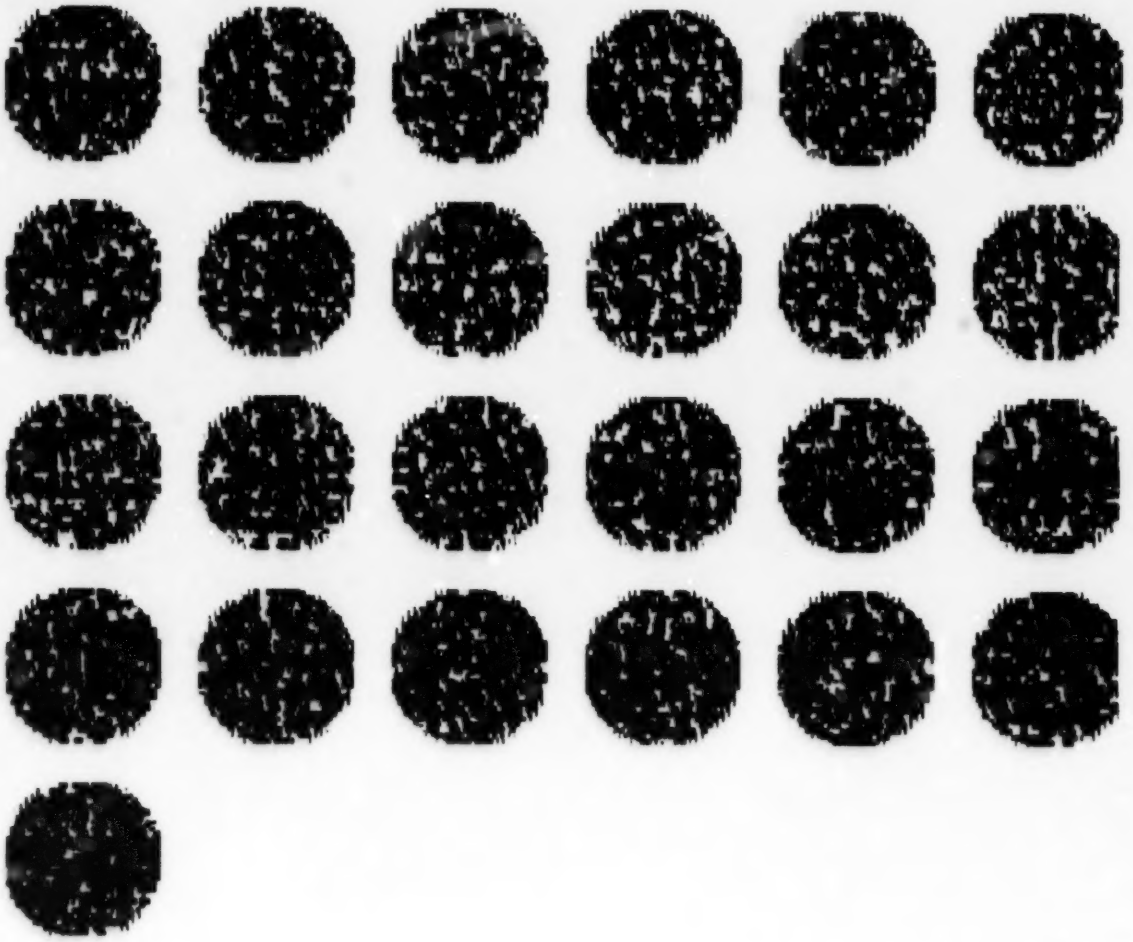

Figure 75: Bulk density images for slices 23 to 44 prior to plugging, column B.

© 1991 NOVA HUSKY RESEARCH CORPORATION

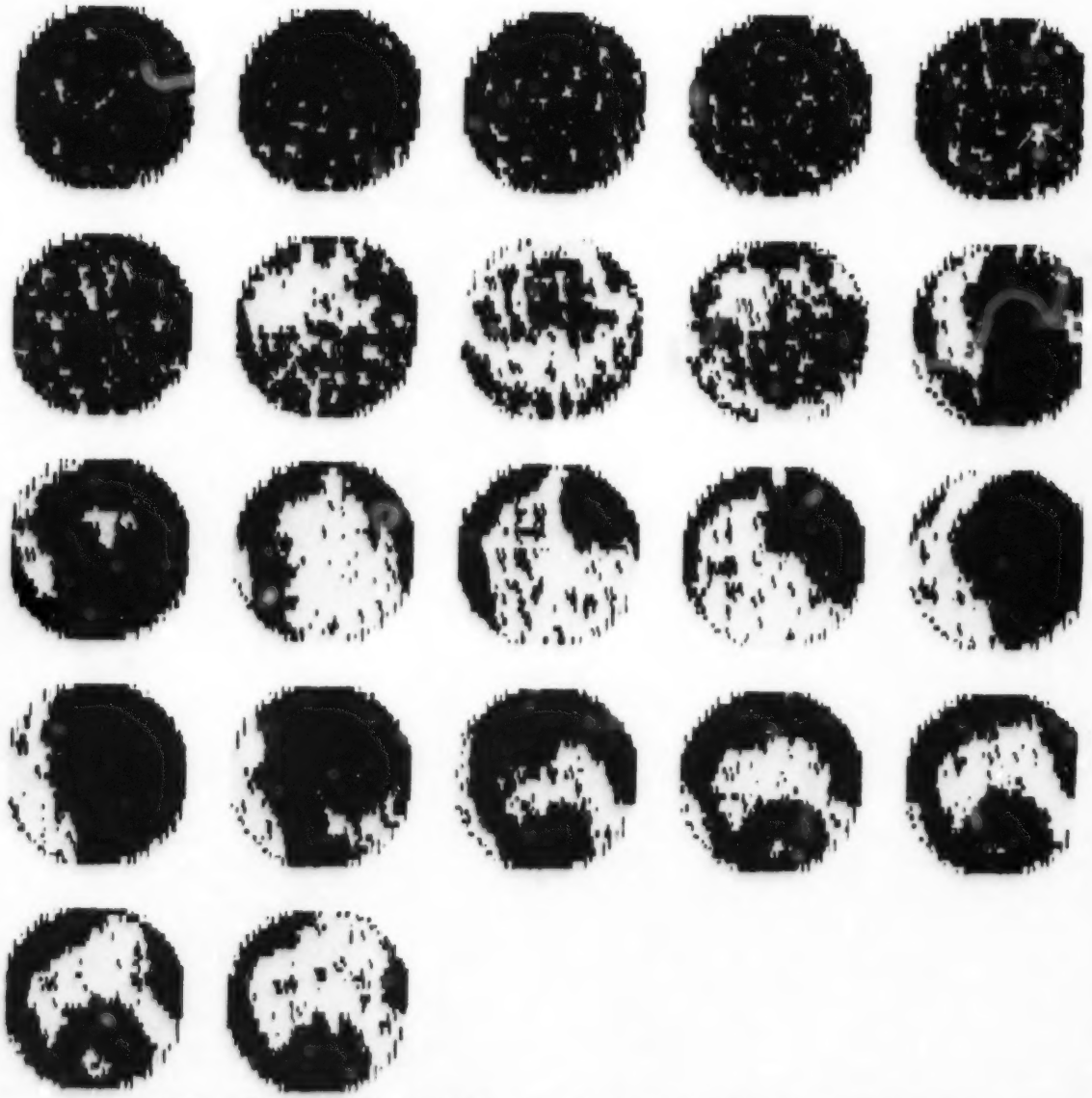

Figure 76: Bulk density images for slices 45 to 70 prior to plugging, column B.

© 1991 NOVA HUSKY RESEARCH CORPORATION

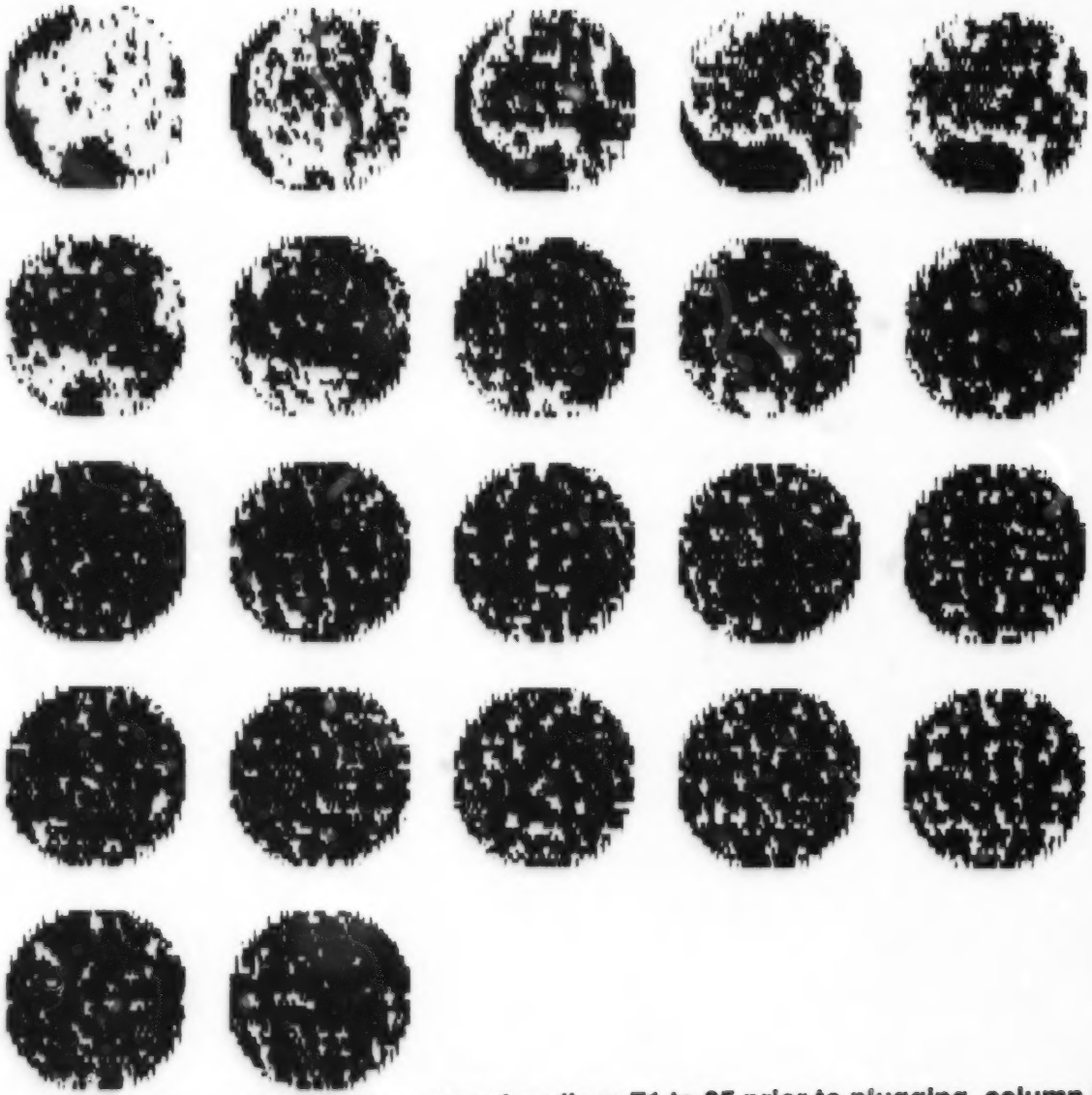

Figure 77: Bulk density images for slices 71 to 95 prior to plugging, column B.

© 1991 NOVA HUSKY RESEARCH CORPORATION

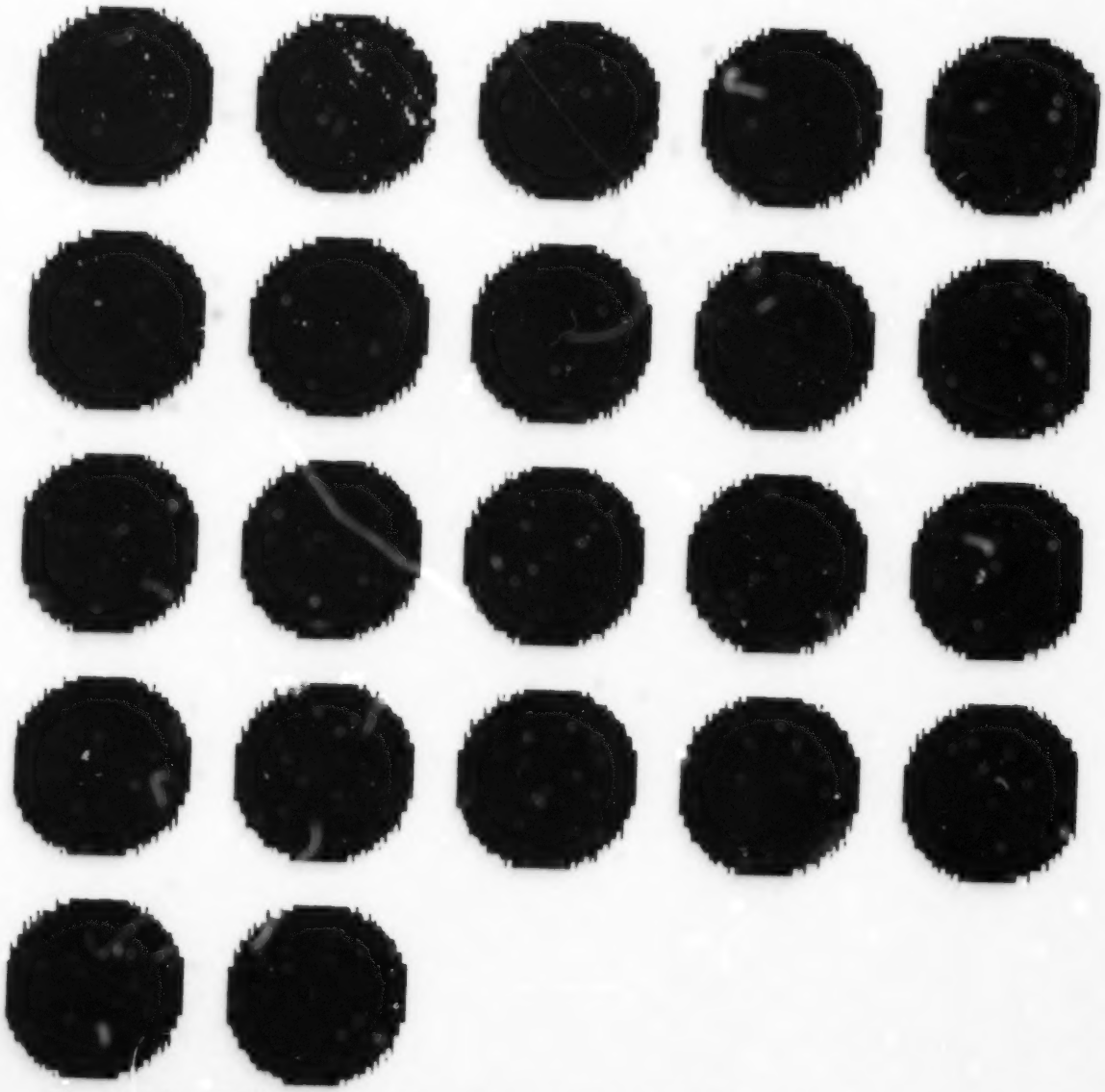

Figure 78: Bulk density images for slices 1 to 22 after plugging, column B.

© 1991 NOVA HUSKY RESEARCH CORPORATION

Figure 79: Bulk density images for slices 23 to 44 after plugging, column B.

© 1991 NOVA HUSKY RESEARCH CORPORATION

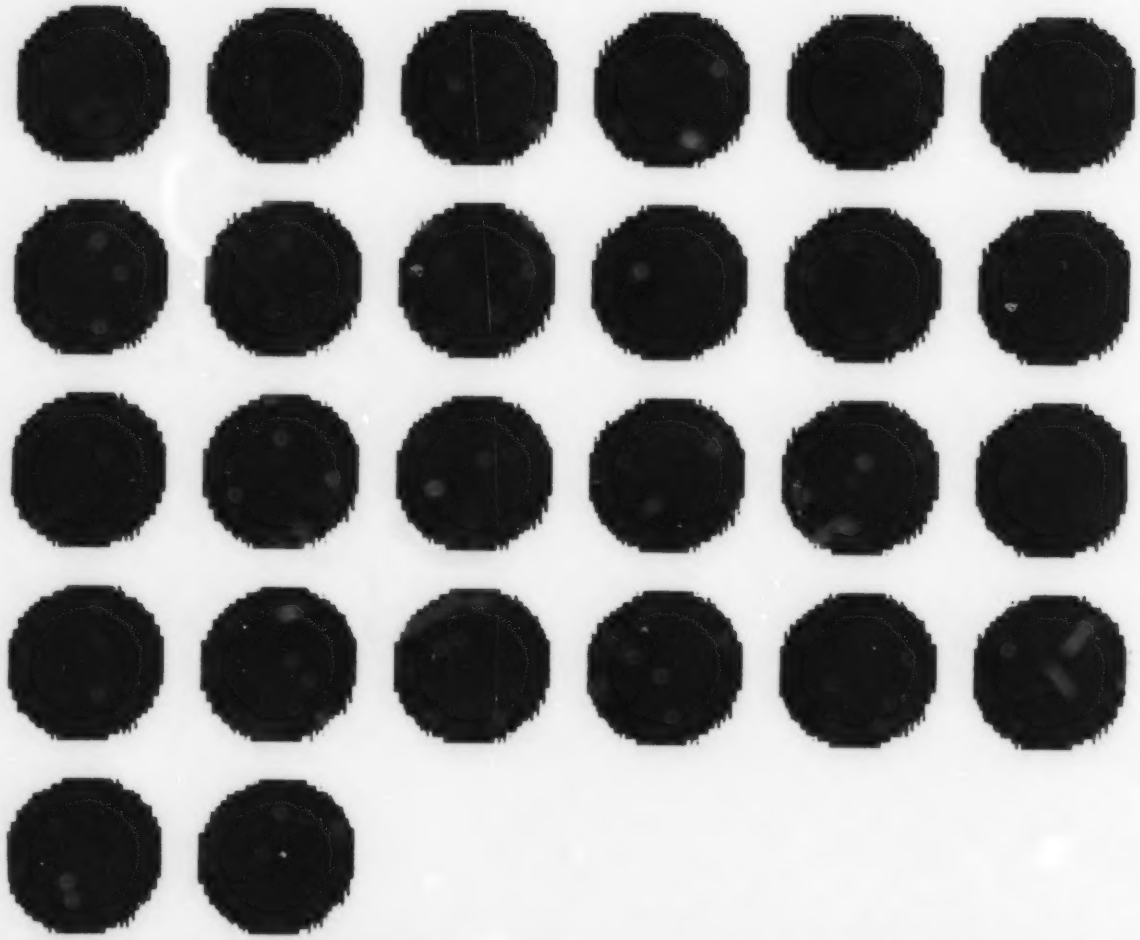

Figure 80: Bulk density images for slices 1 to 22 prior to plugging, column C.

© 1991 NOVA HUSKY RESEARCH CORPORATION

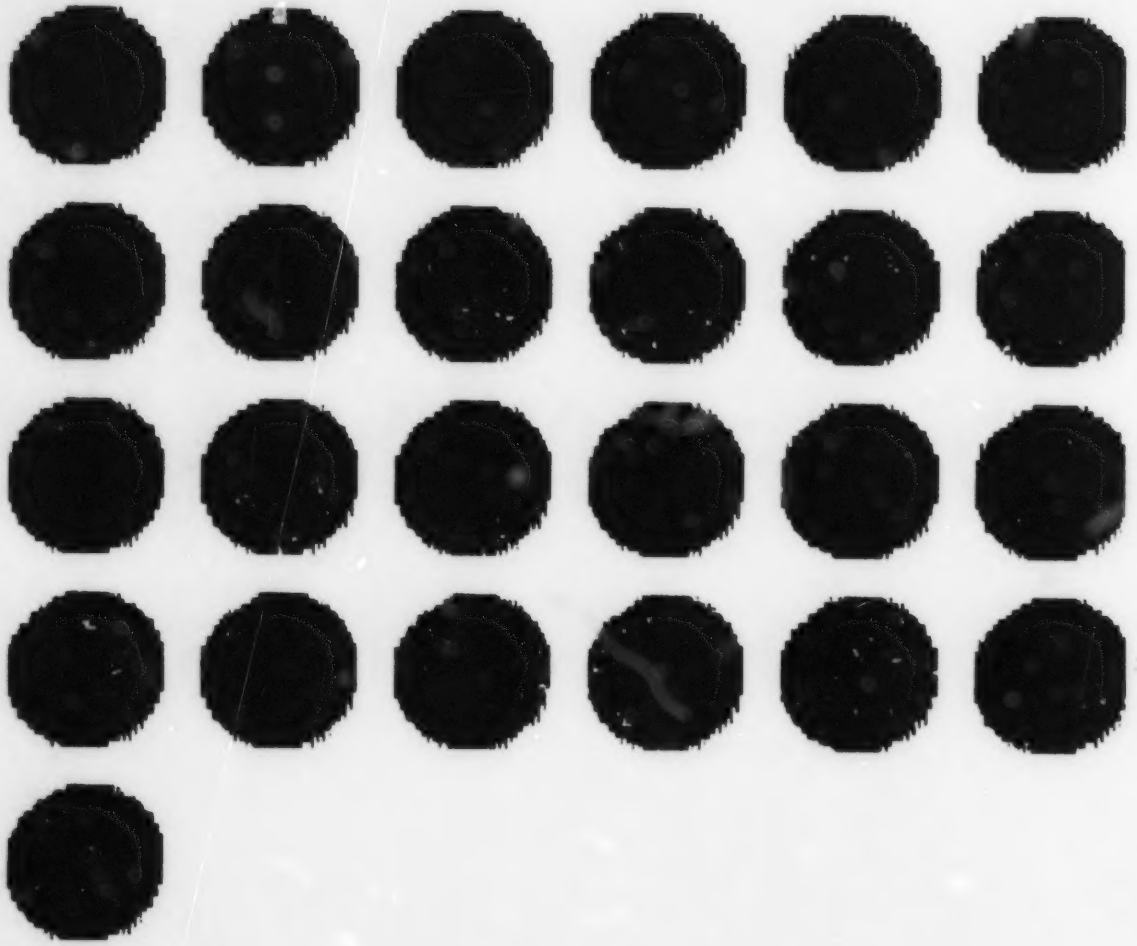

Figure 81: Bulk density images for slices 23 to 44 prior to plugging, column C.

© 1991 NOVA HUSKY RESEARCH CORPORATION

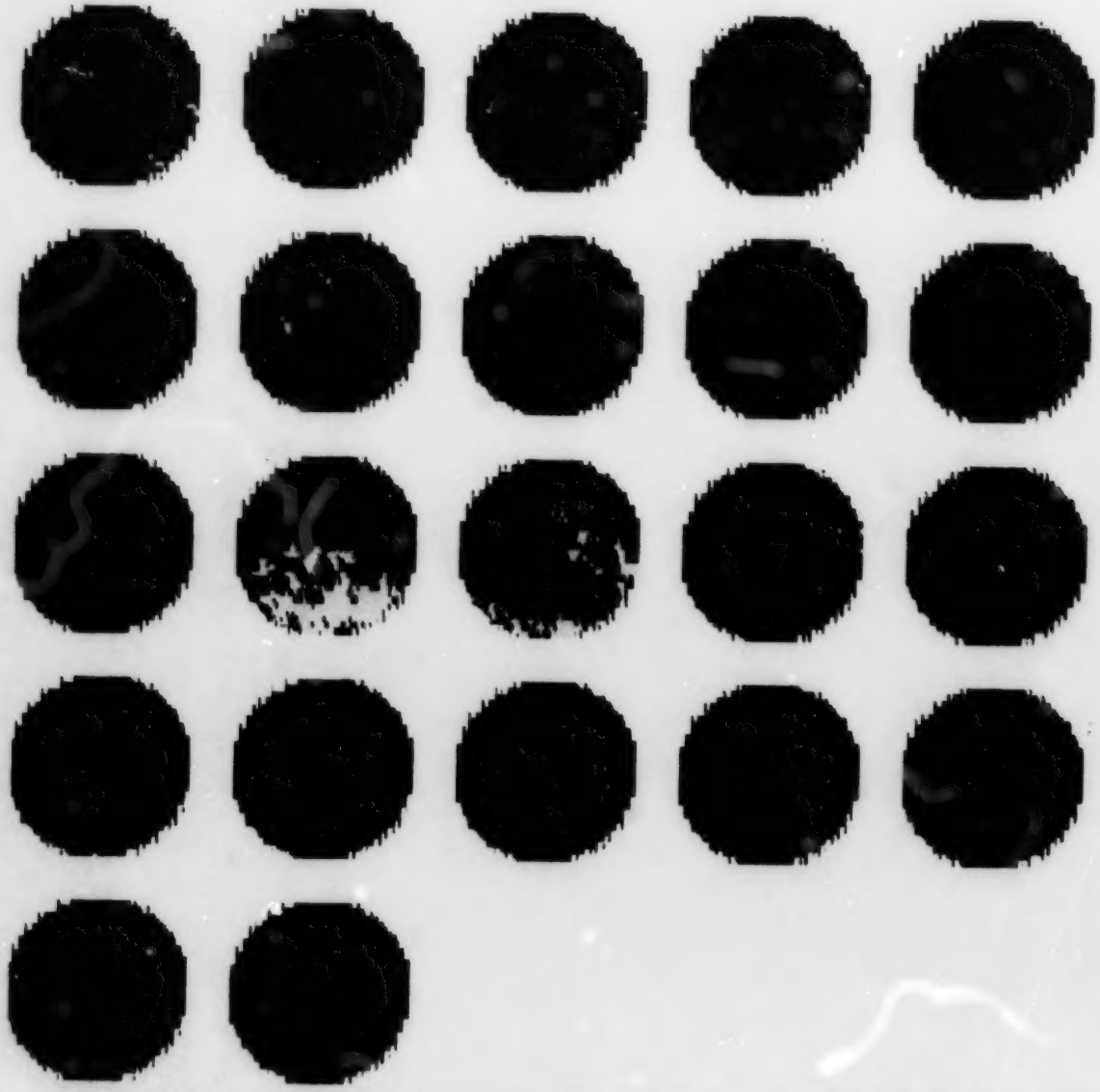

Figure 82: Bulk density images for slices 45 to 70 prior to plugging, column C.

© 1991 NOVA HUSKY RESEARCH CORPORATION

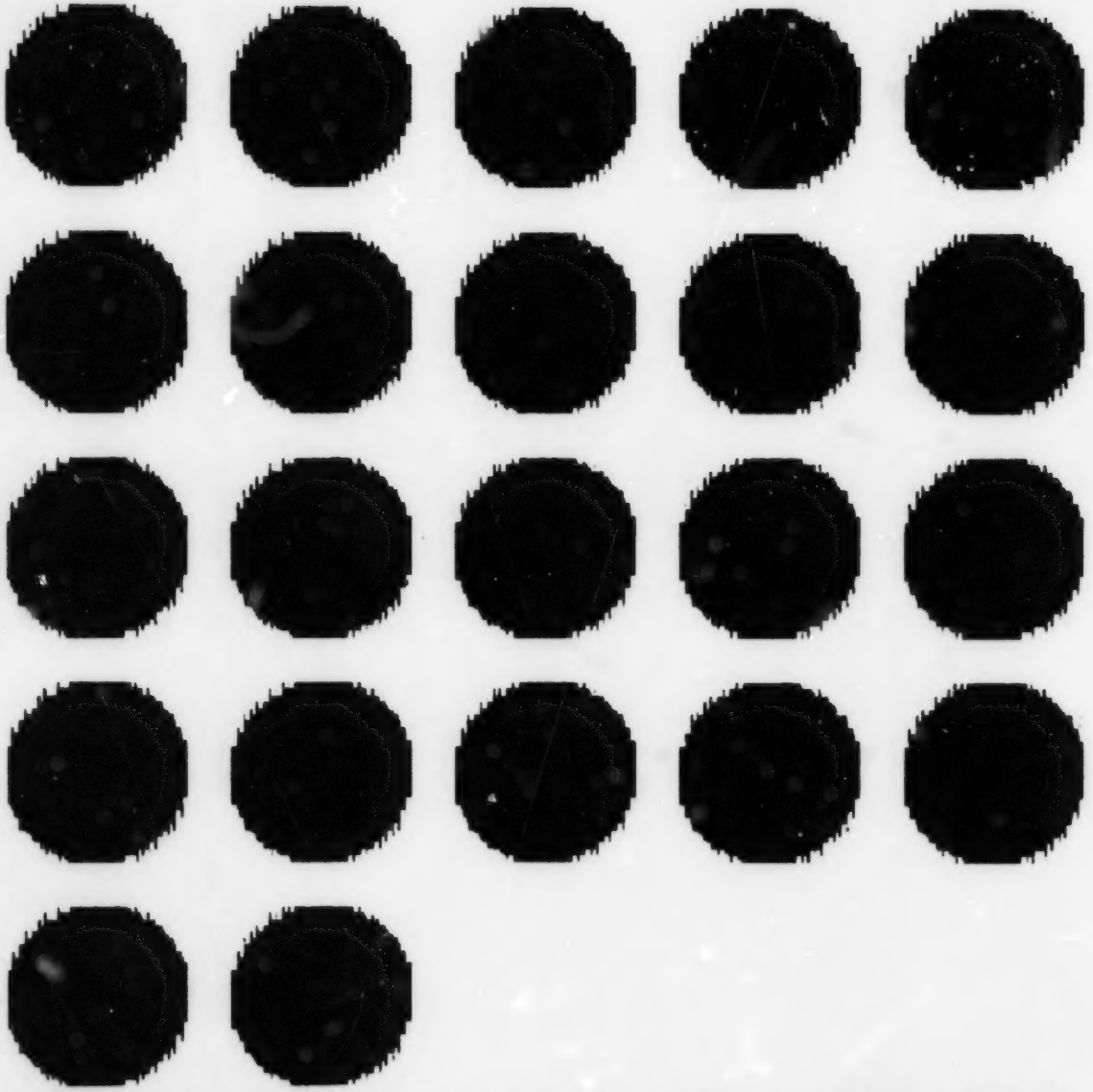

Figure 83: Bulk density images for slices 71 to 95 prior to plugging, column C.

© 1991 NOVA HUSKY RESEARCH CORPORATION

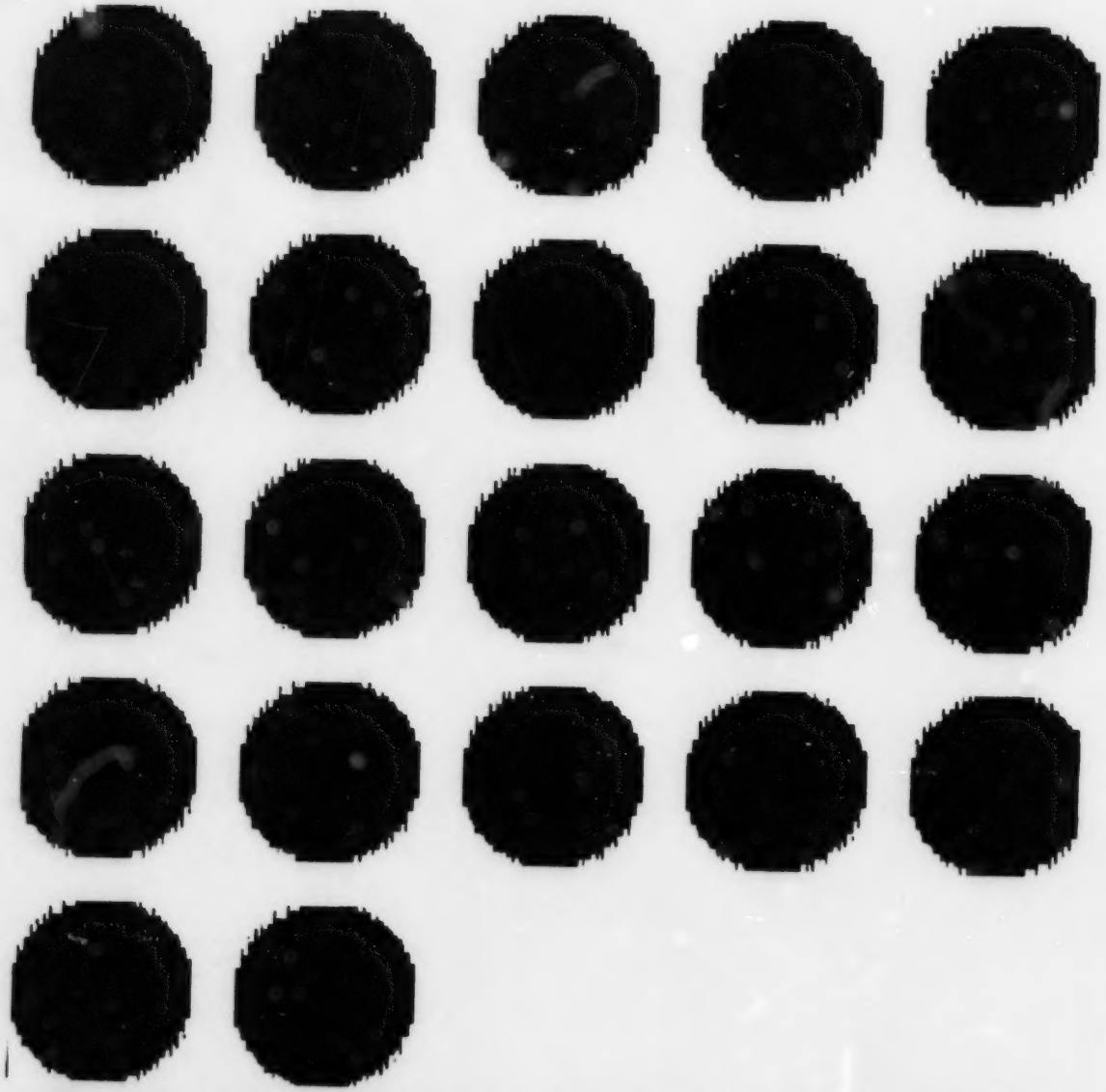

Figure 84: Bulk density images for slices 1 to 22 after plugging, column C.

© 1991 NOVA HUSKY RESEARCH CORPORATION

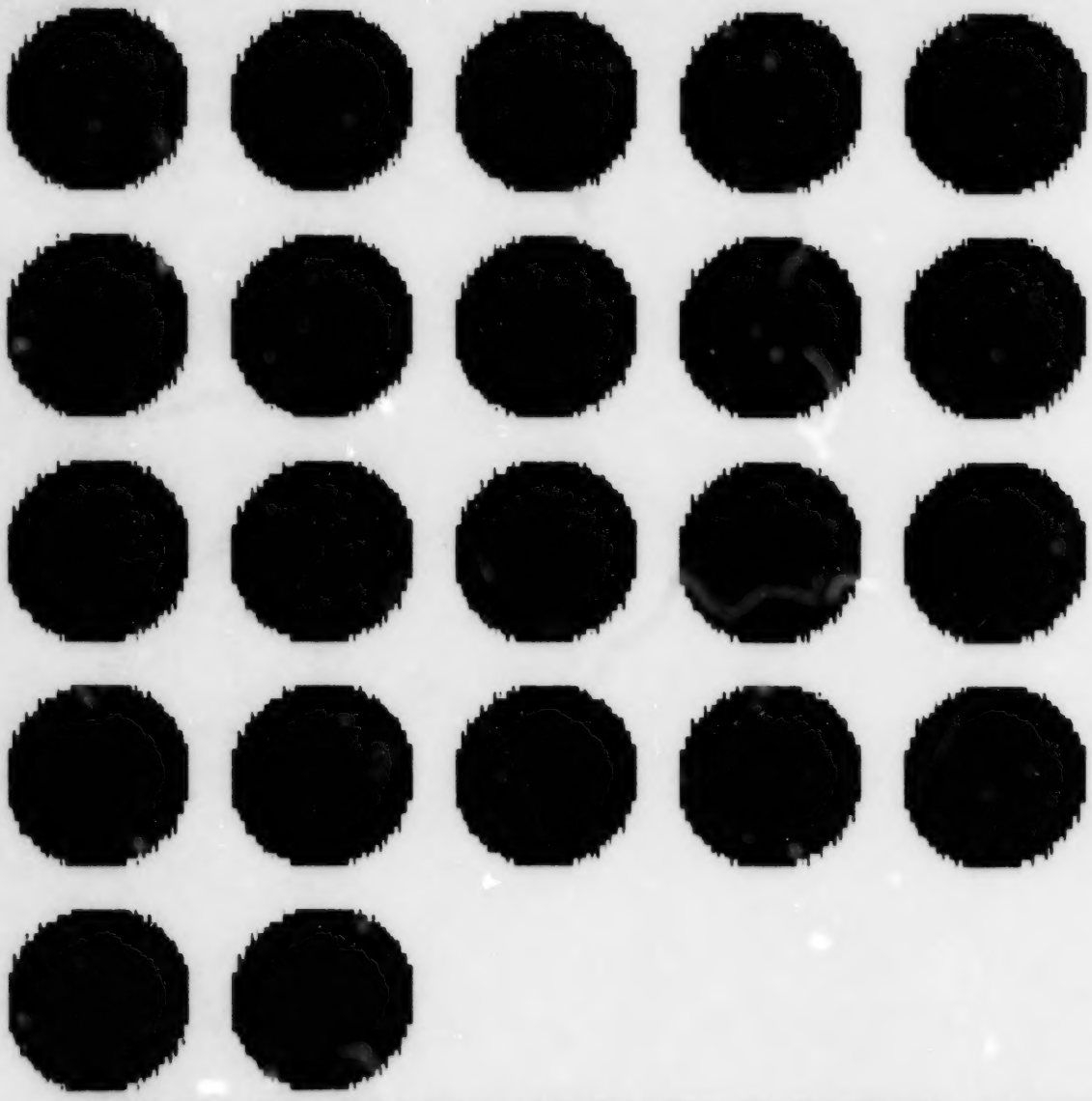

Figure 85: Bulk density images for slices 23 to 44 after plugging, column C.

© 1991 NOVA HUSKY RESEARCH CORPORATION

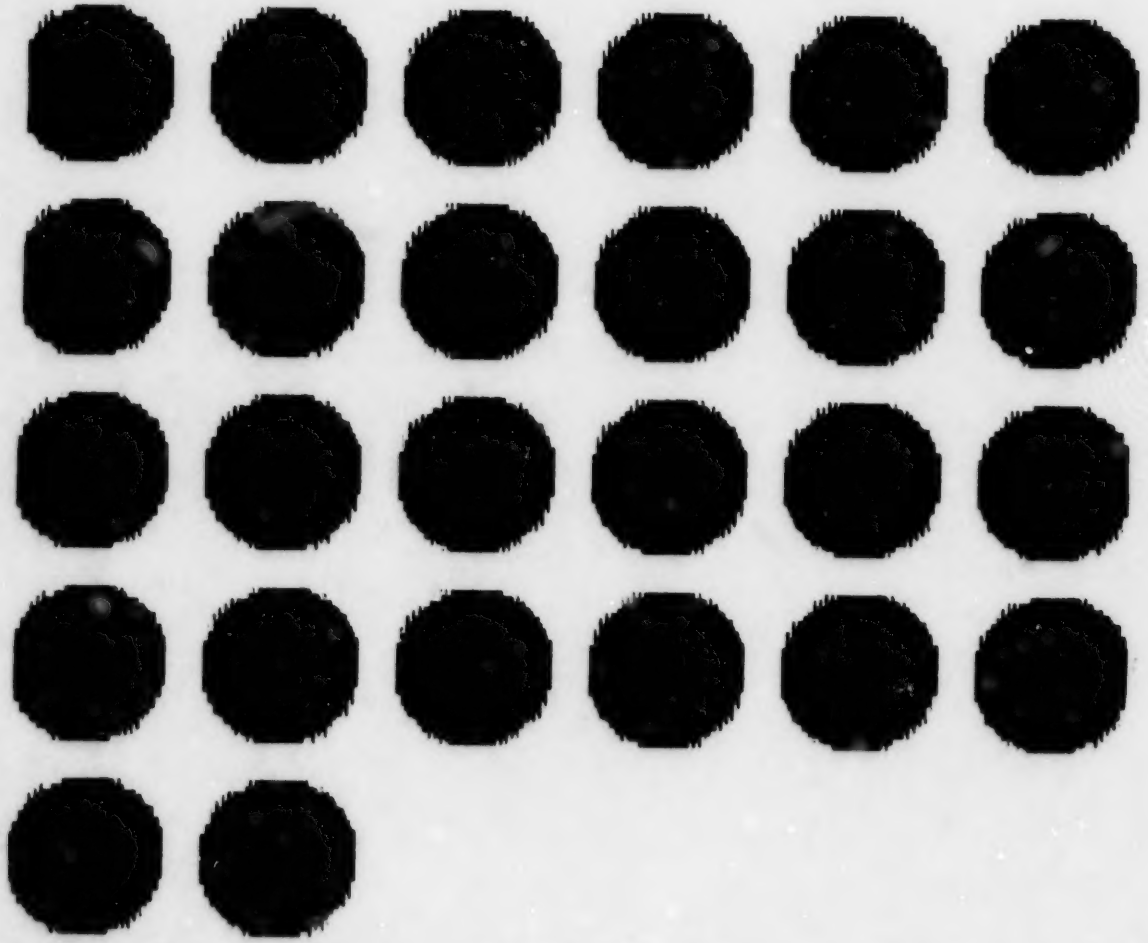

Figure 86: Bulk density images for slices 1 to 22 prior to plugging, column D.

© 1991 NOVA HUSKY RESEARCH CORPORATION

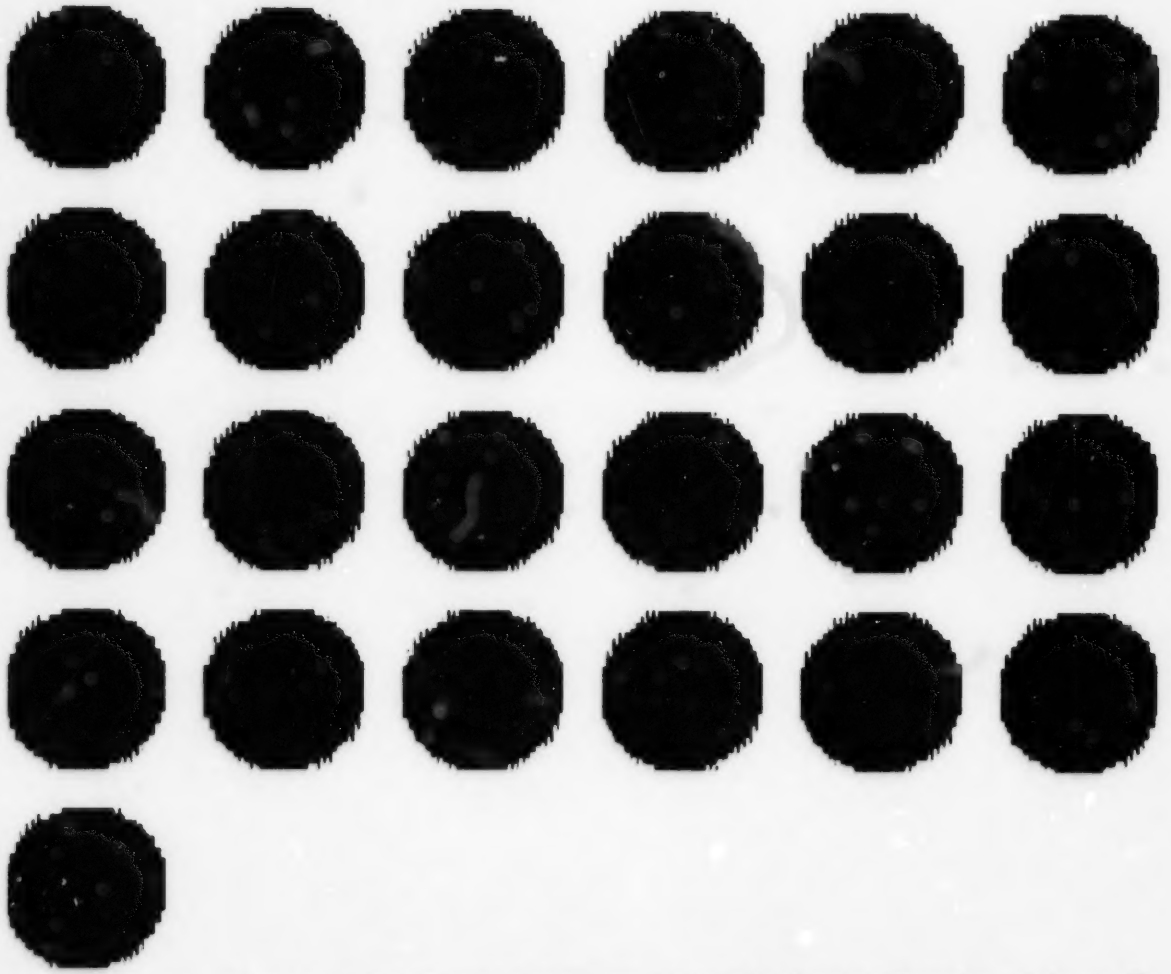

Figure 87: Bulk density images for slices 23 to 44 prior to plugging, column D.

© 1991 NOVA HUSKY RESEARCH CORPORATION

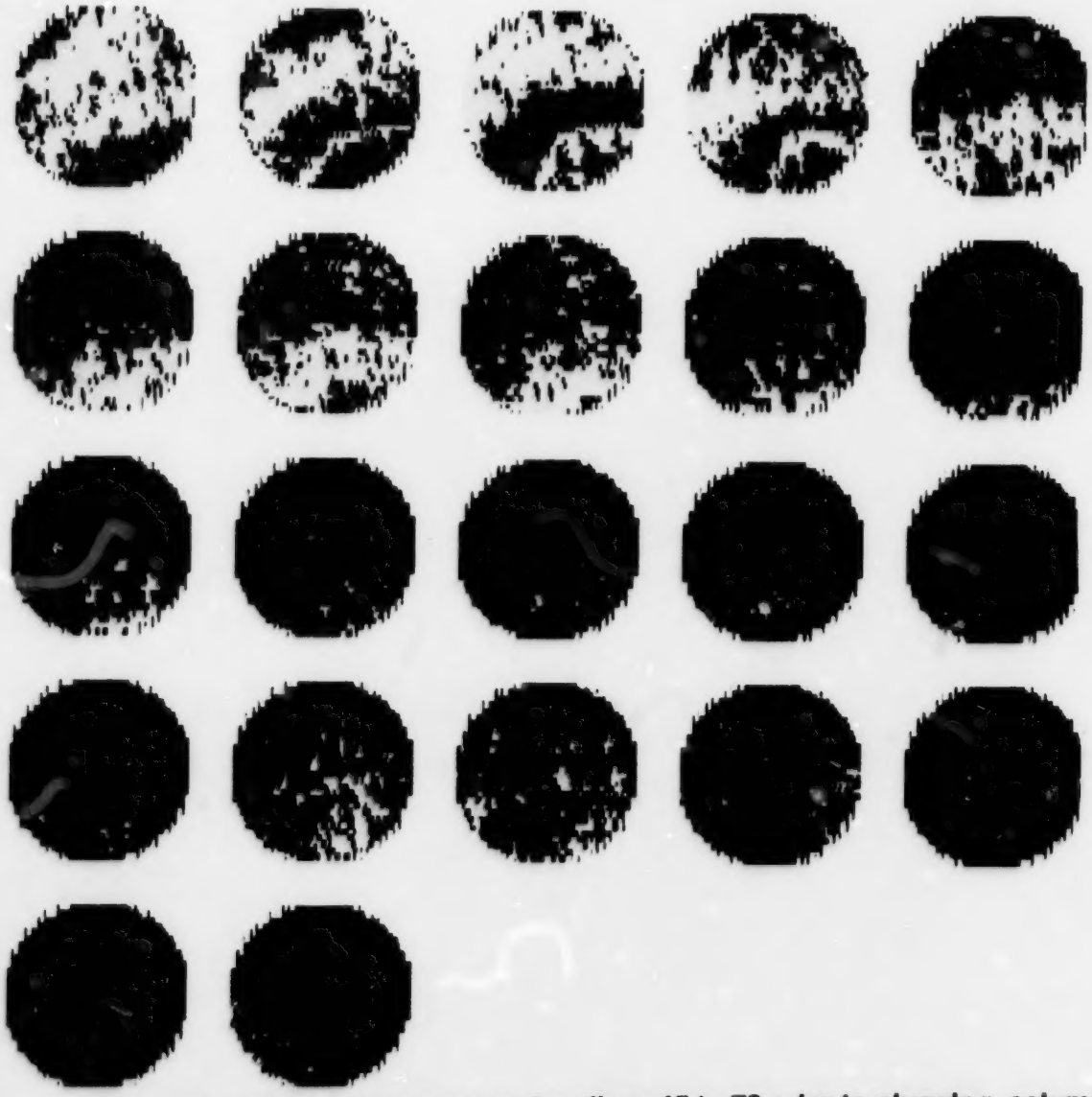

Figure 88: Bulk density images for slices 45 to 70 prior to plugging, column D.

© 1991 NOVA HUSKY RESEARCH CORPORATION

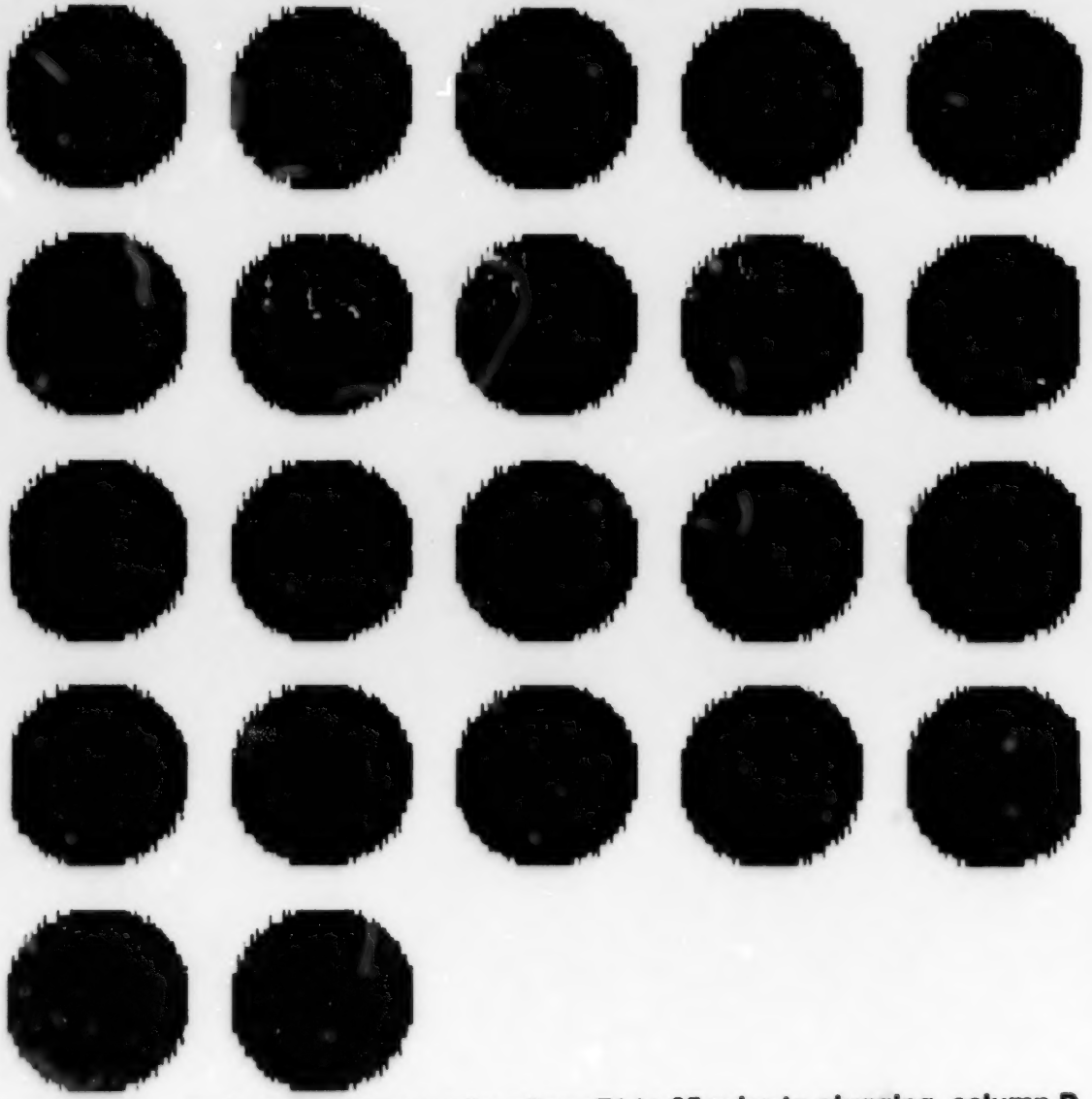

Figure 89: Bulk density images for slices 71 to 95 prior to plugging, column D.

© 1991 NOVA HUSKY RESEARCH CORPORATION

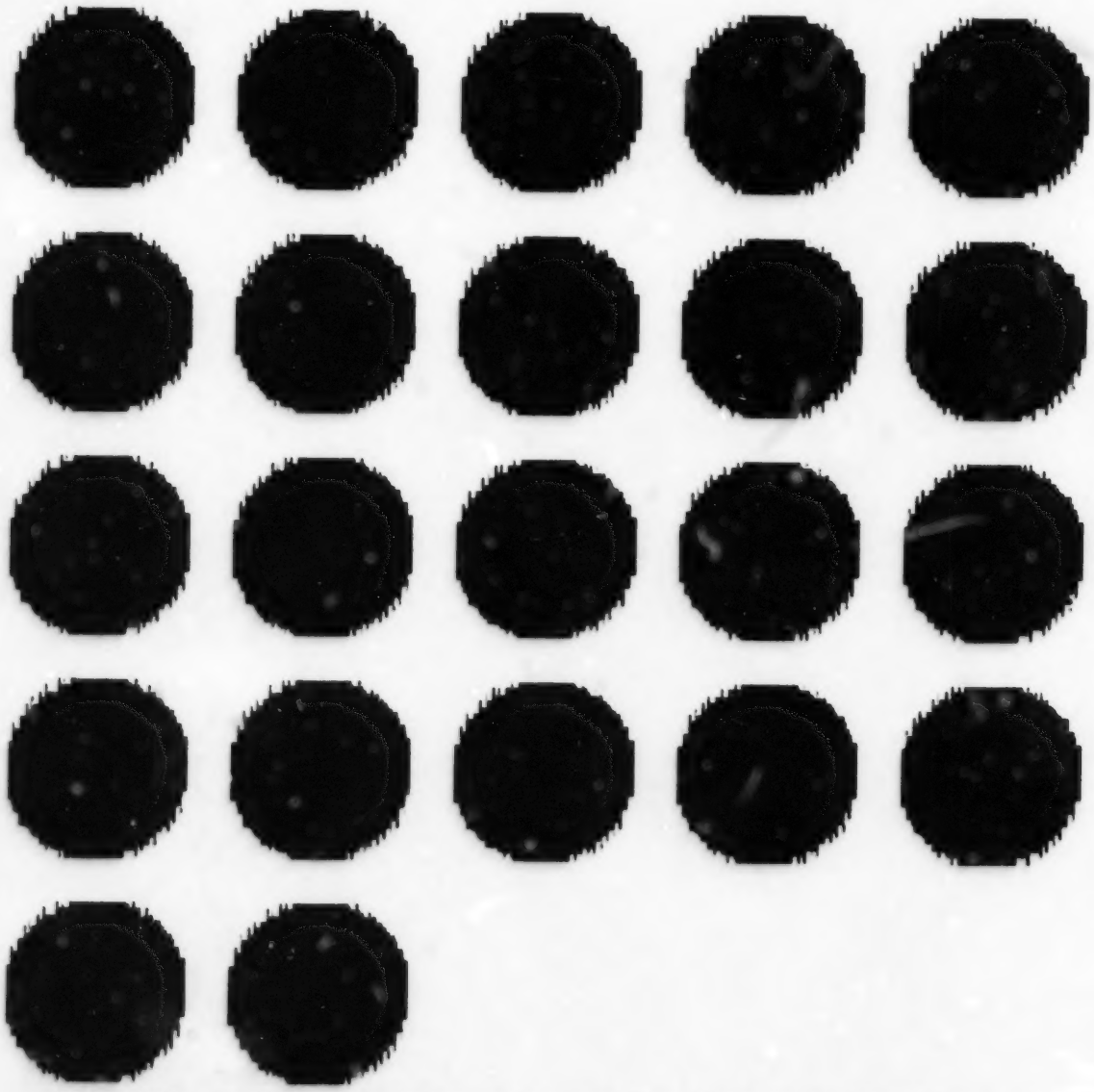

Figure 90: Bulk density images for slices 1 to 22 after plugging, column D.

© 1991 NOVA HUSKY RESEARCH CORPORATION

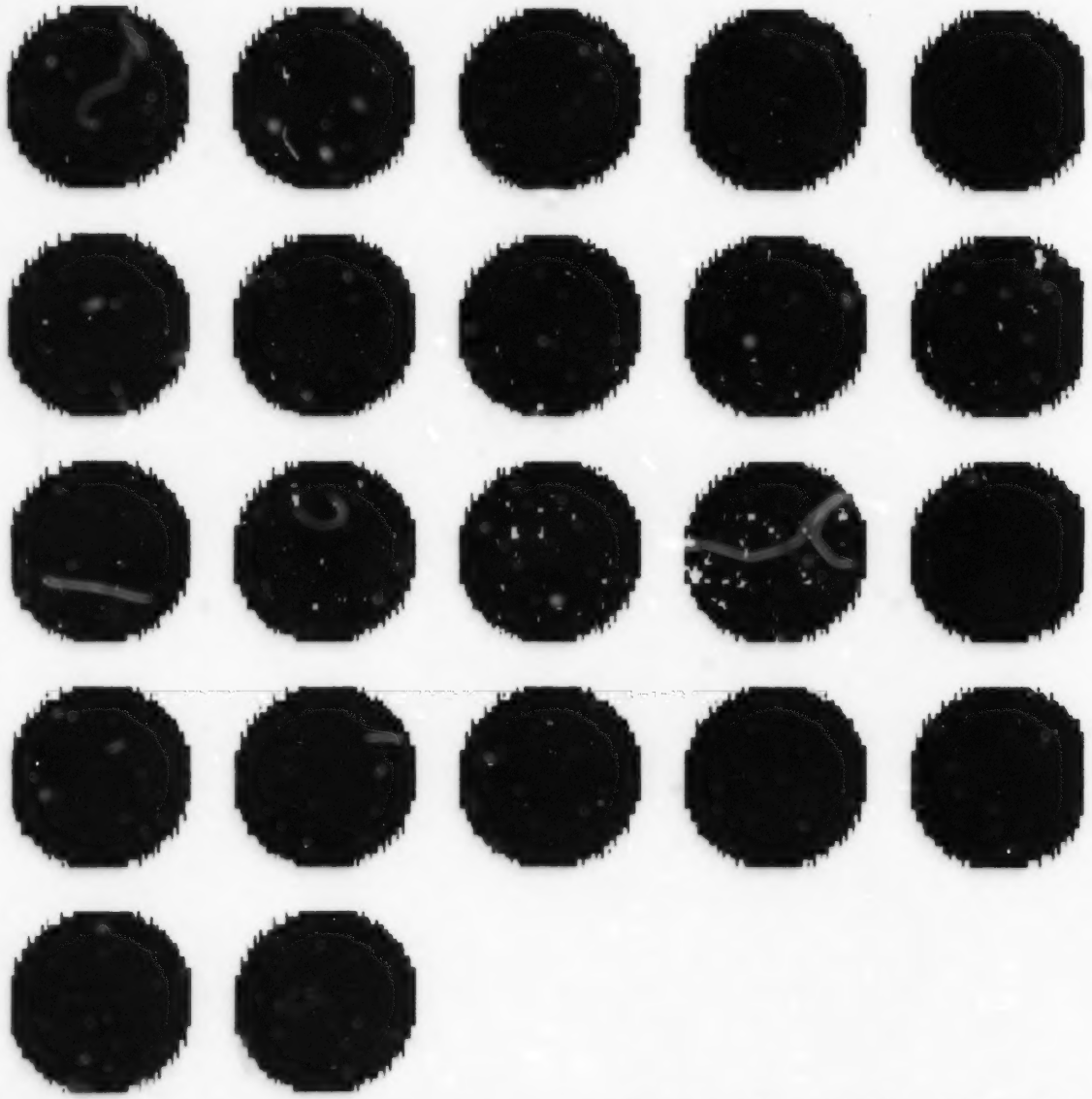

Figure 91: Bulk density images for slices 23 to 44 after plugging, column D.

© 1991 NOVA HUSKY RESEARCH CORPORATION

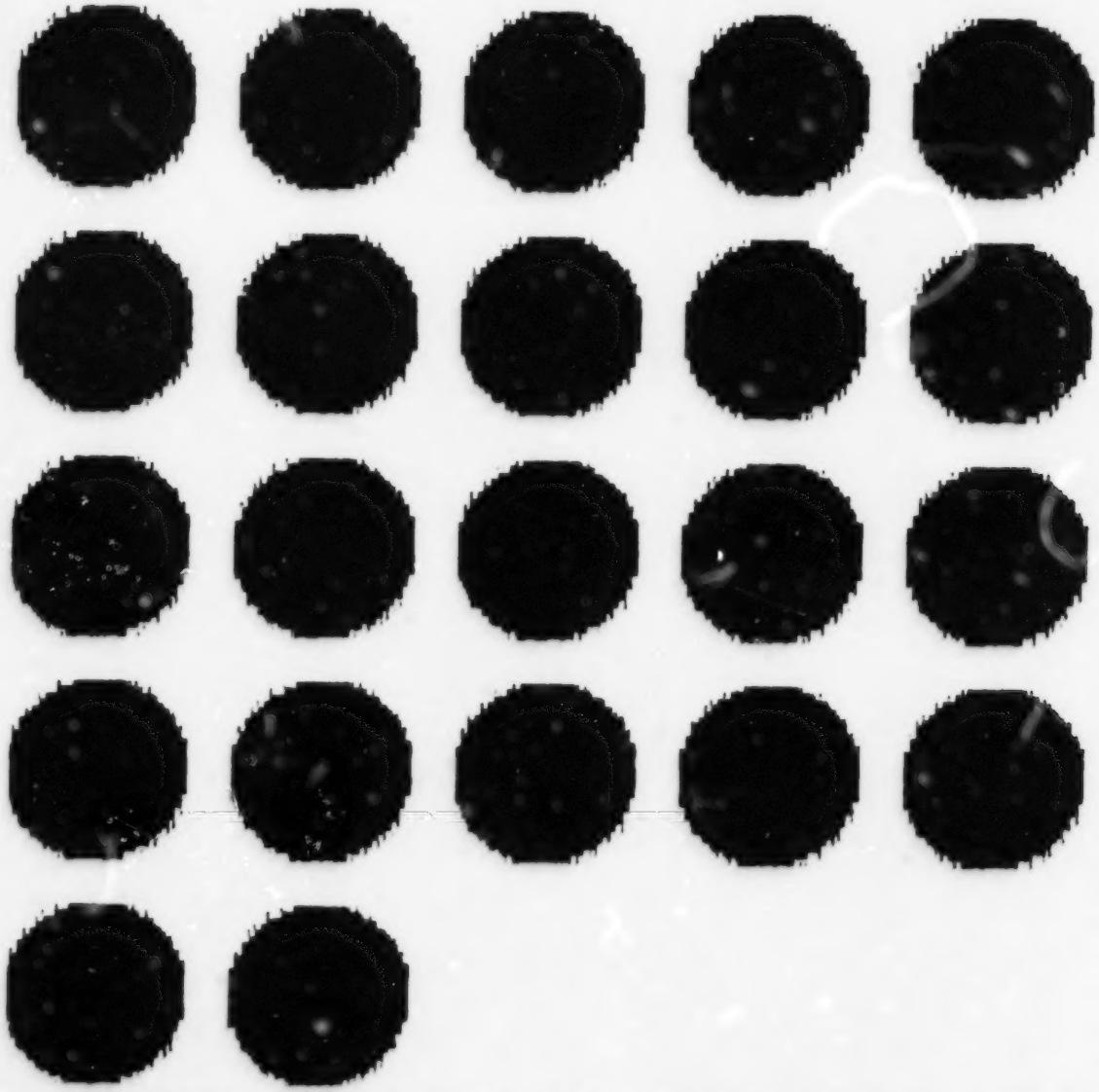

Figure 92: Porosity images for slices 1 to 22 prior to plugging, column A.

© 1991 NOVA HUSKY RESEARCH CORPORATION

Figure 93: Porosity images for slices 23 to 44 prior to plugging, column A.

© 1991 NOVA HUSKY RESEARCH CORPORATION

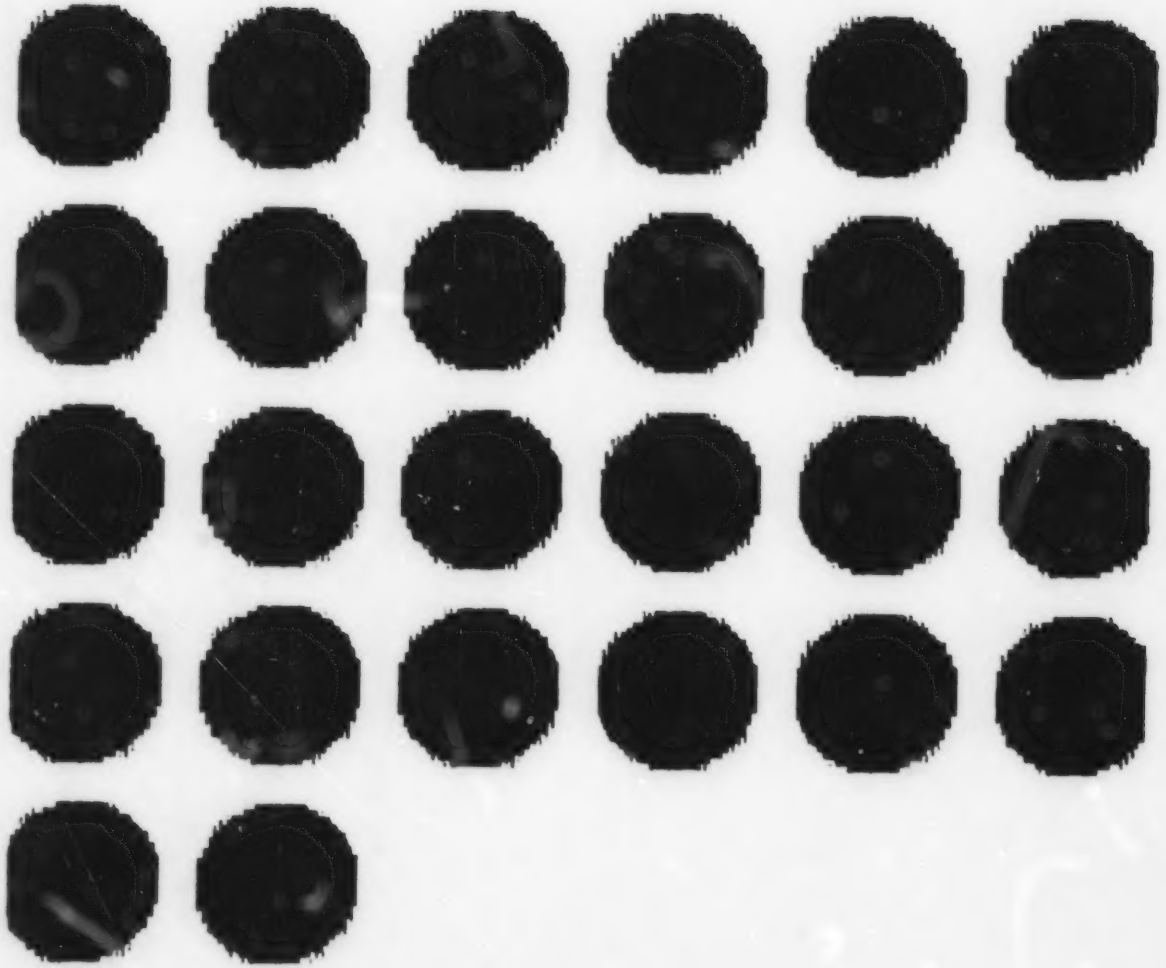

Figure 94: Porosity images for slices 45 to 70 prior to plugging, column A.

© 1991 NOVA HUSKY RESEARCH CORPORATION

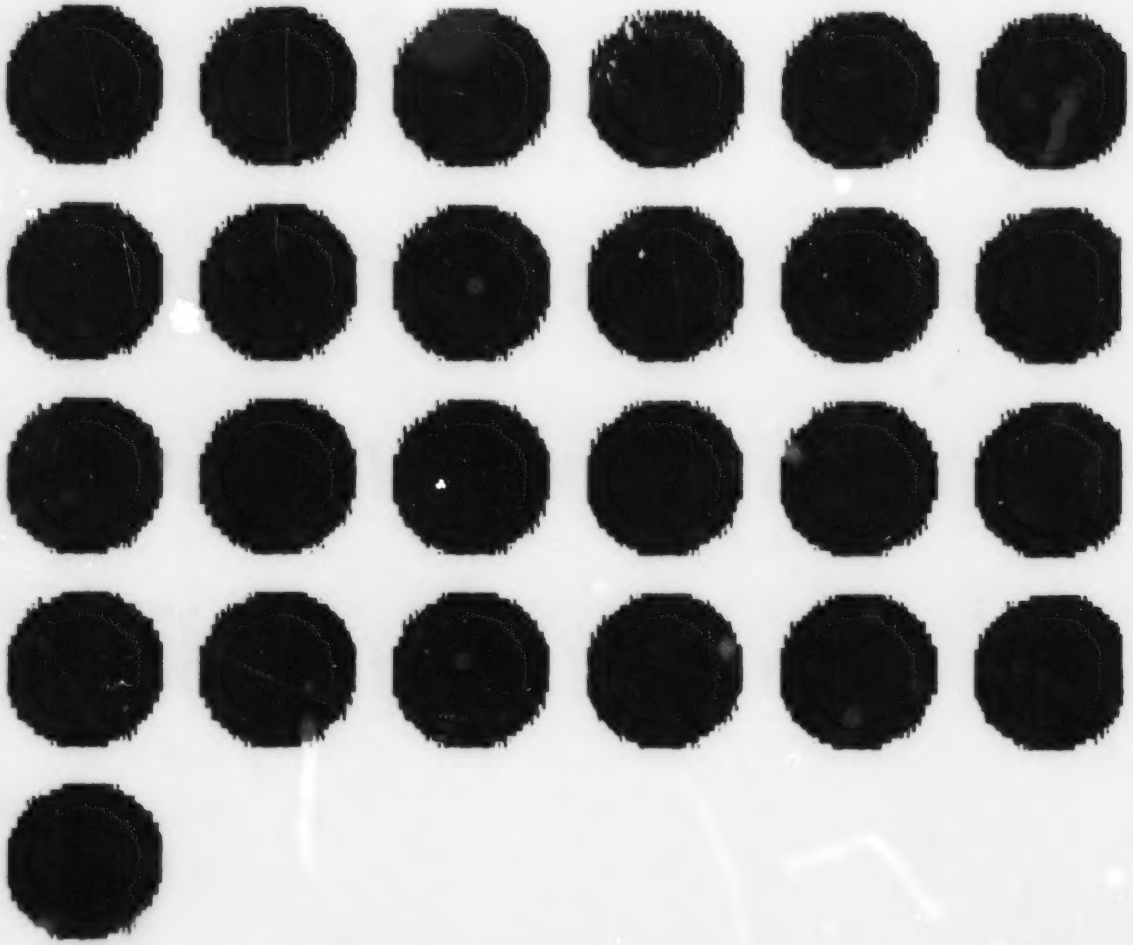

Figure 95: Porosity images for slices 71 to 95 prior to plugging, column A.

© 1991 NOVA HUSKY RESEARCH CORPORATION

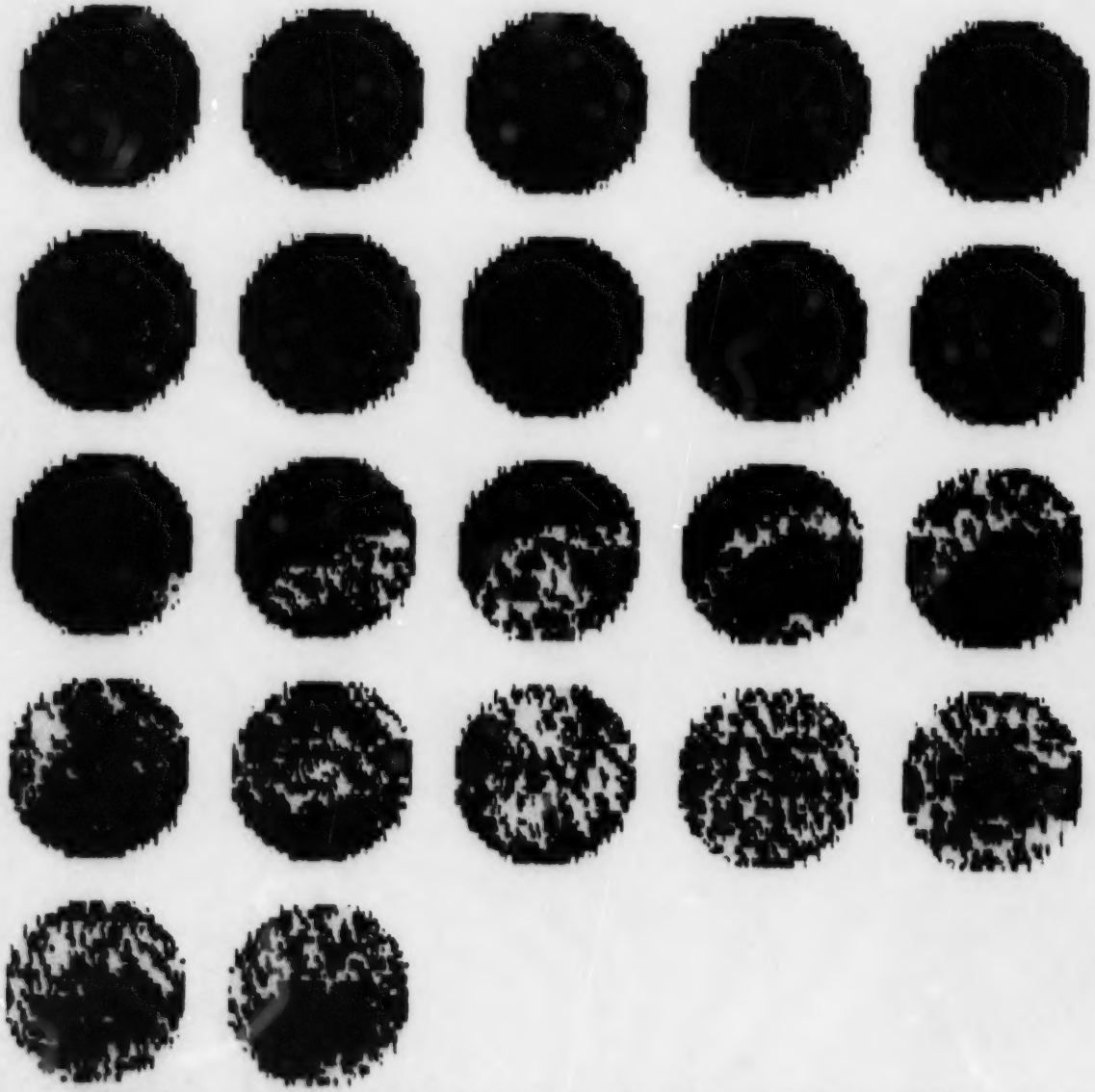

Figure 96: Porosity images for slices 1 to 22 after plugging, column A.

© 1991 NOVA HUSKY RESEARCH CORPORATION

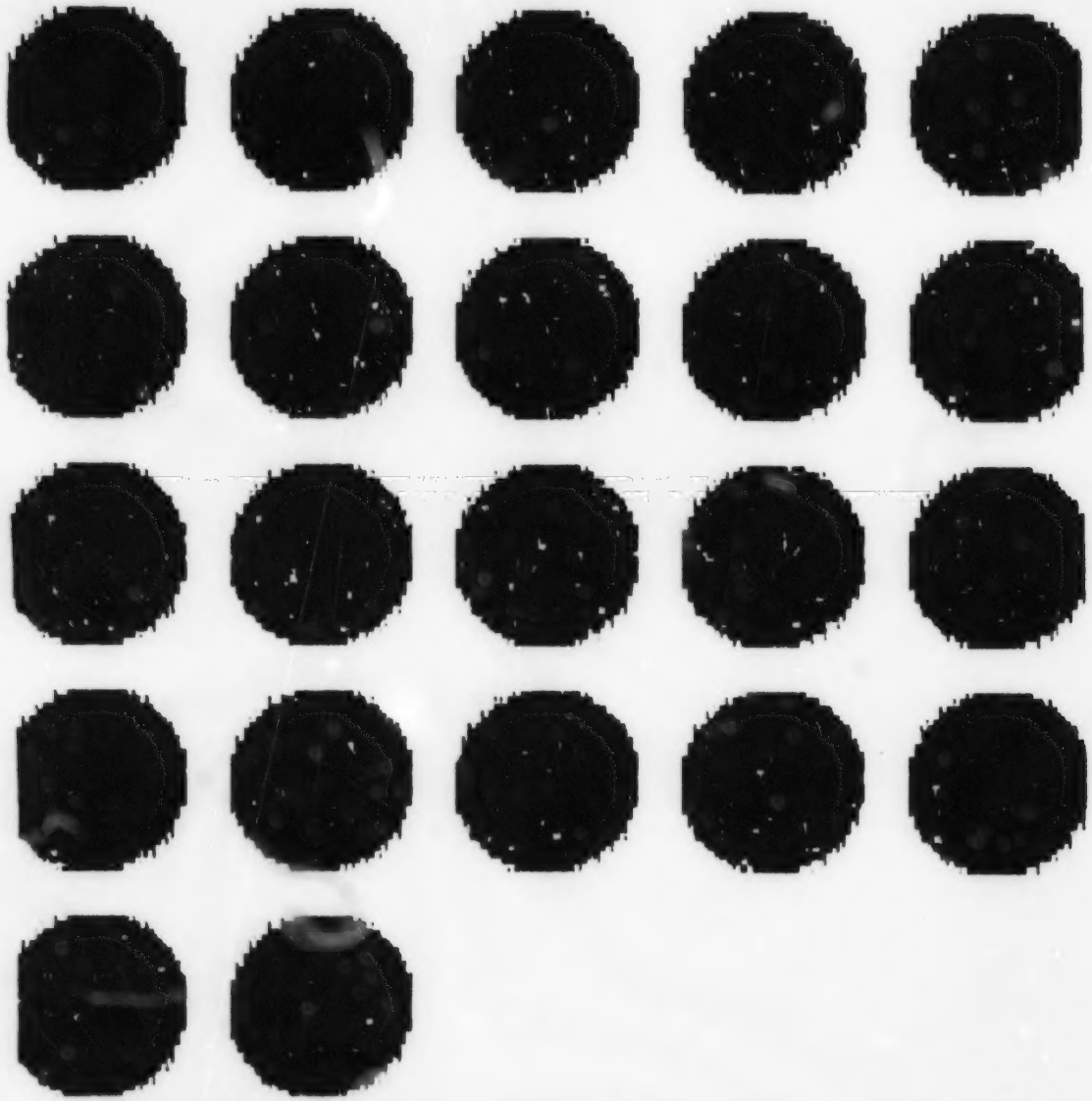

Figure 97: Porosity images for slices 23 to 44 after plugging, column A.

© 1991 NOVA HUSKY RESEARCH CORPORATION

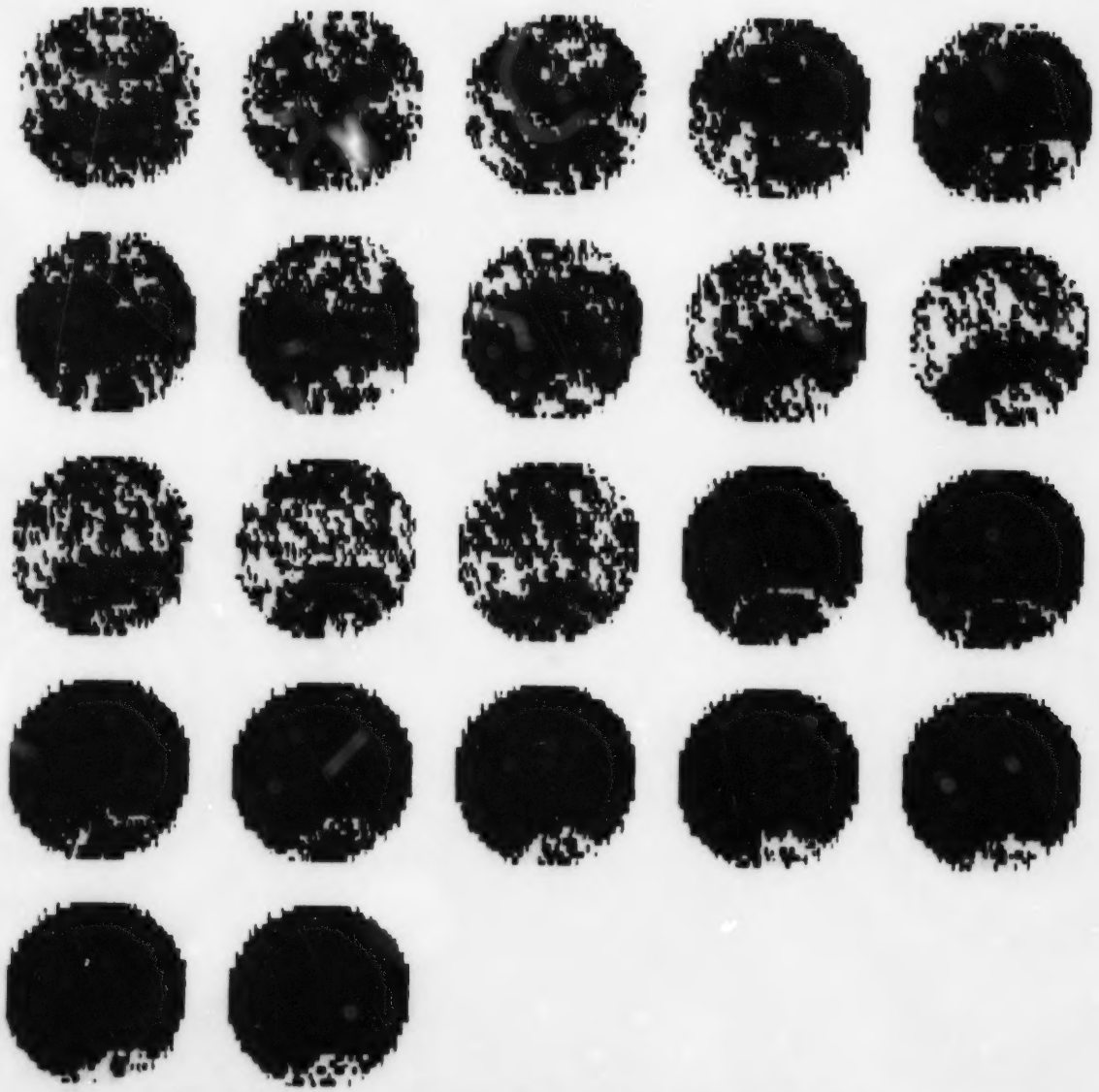

Figure 98: Porosity images for slices 1 to 22 prior to plugging, column B.

© 1991 NOVA HUSKY RESEARCH CORPORATION

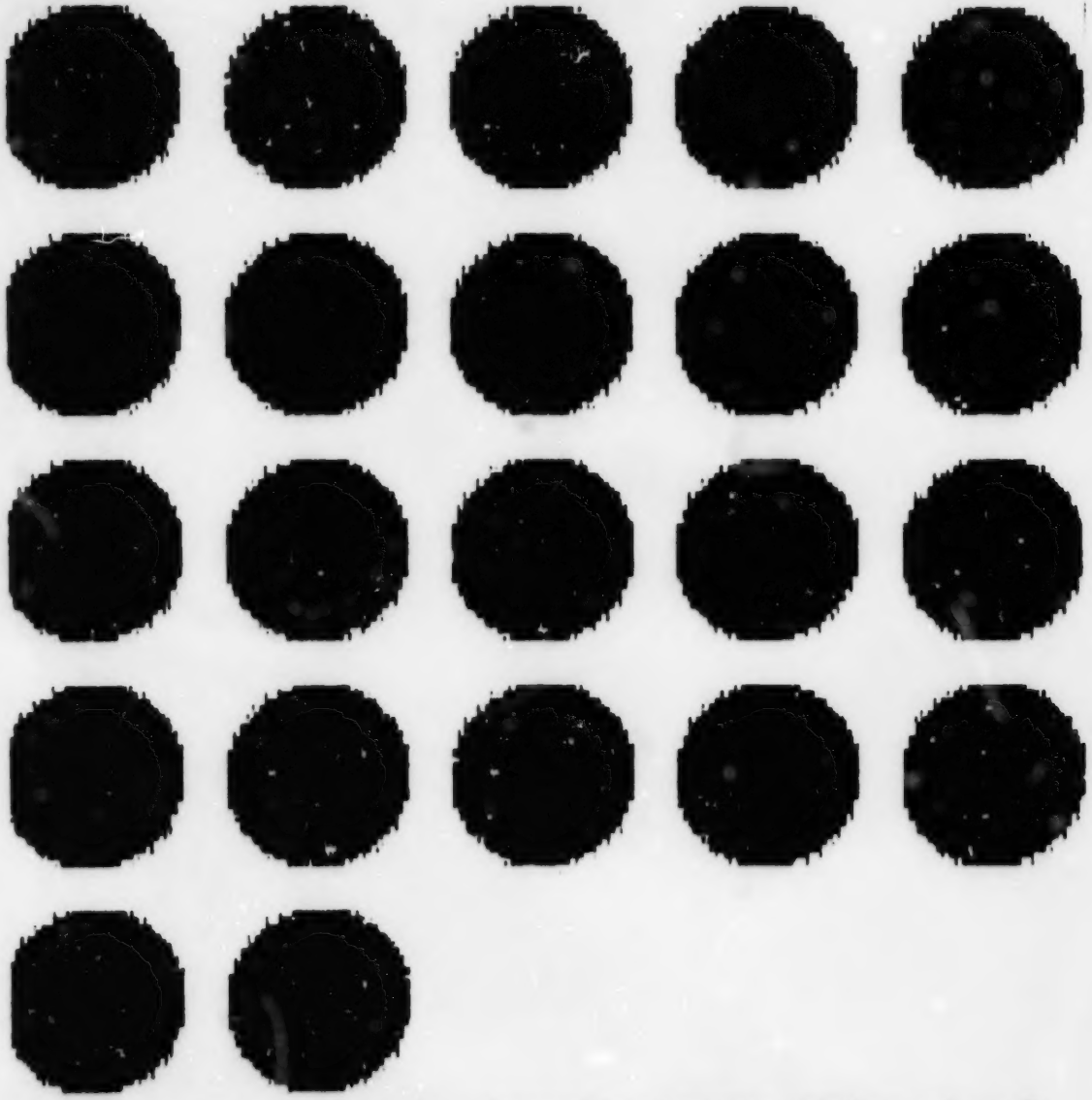

Figure 99: Porosity images for slices 23 to 44 prior to plugging, column B.

© 1991 NOVA HUSKY RESEARCH CORPORATION

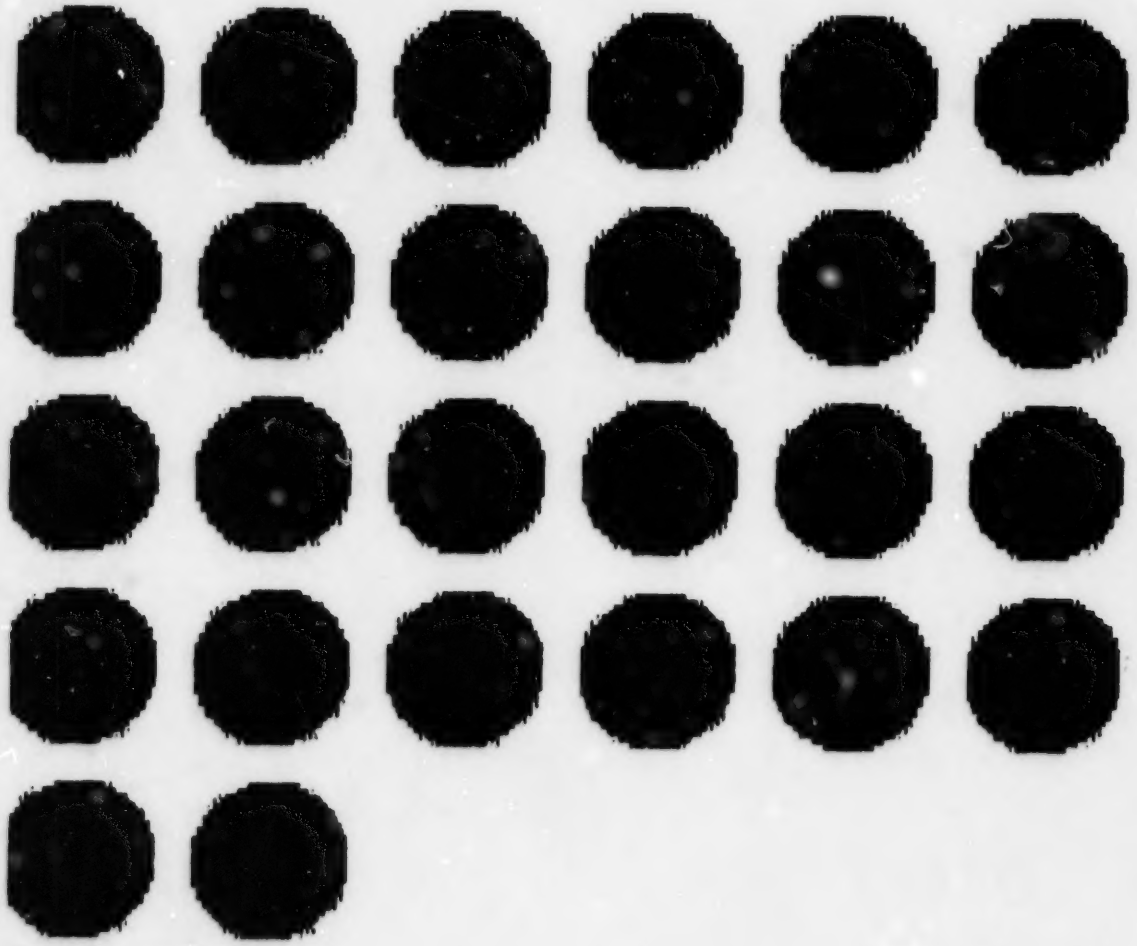

Figure 100: Porosity images for slices 45 to 70 prior to plugging, column B.

© 1991 NOVA HUSKY RESEARCH CORPORATION

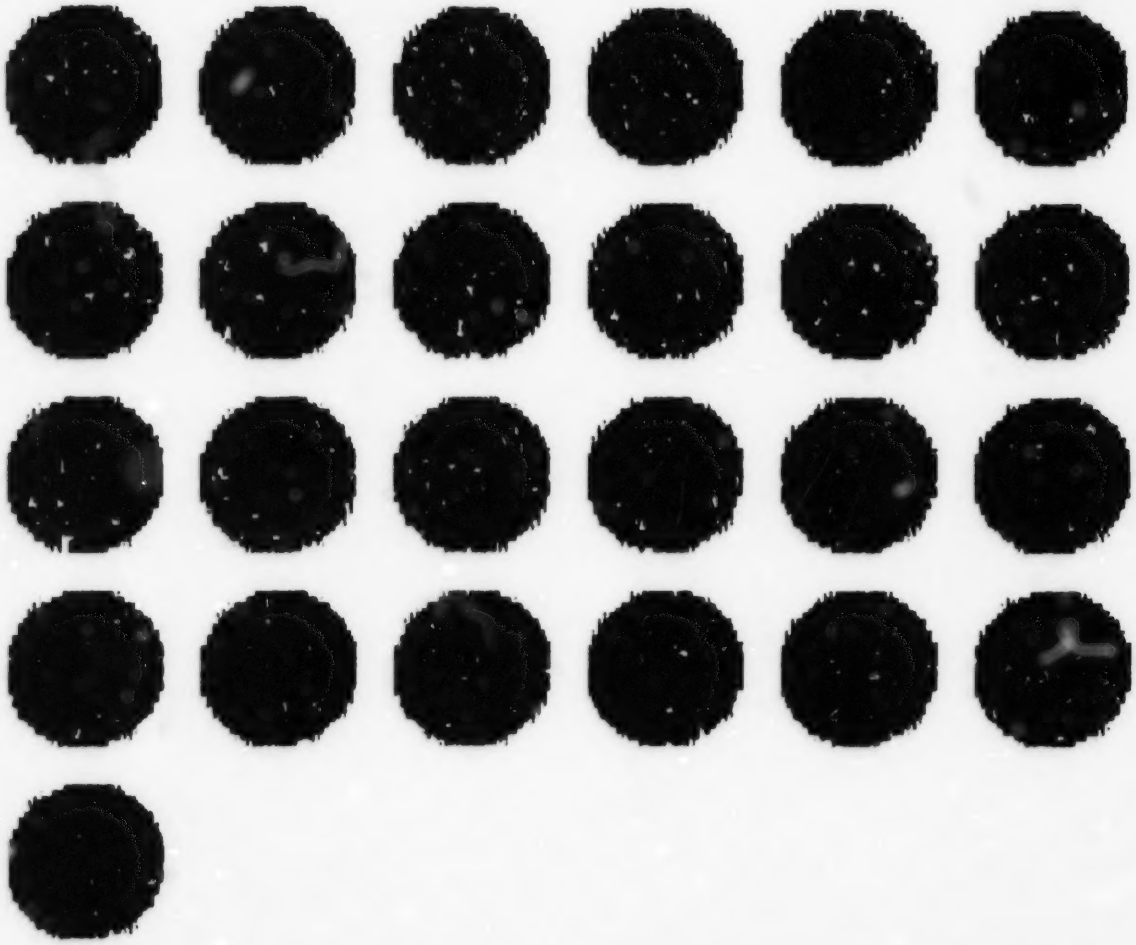

Figure 101: Porosity images for slices 71 to 95 prior to plugging, column B.

© 1991 NOVA HUSKY RESEARCH CORPORATION

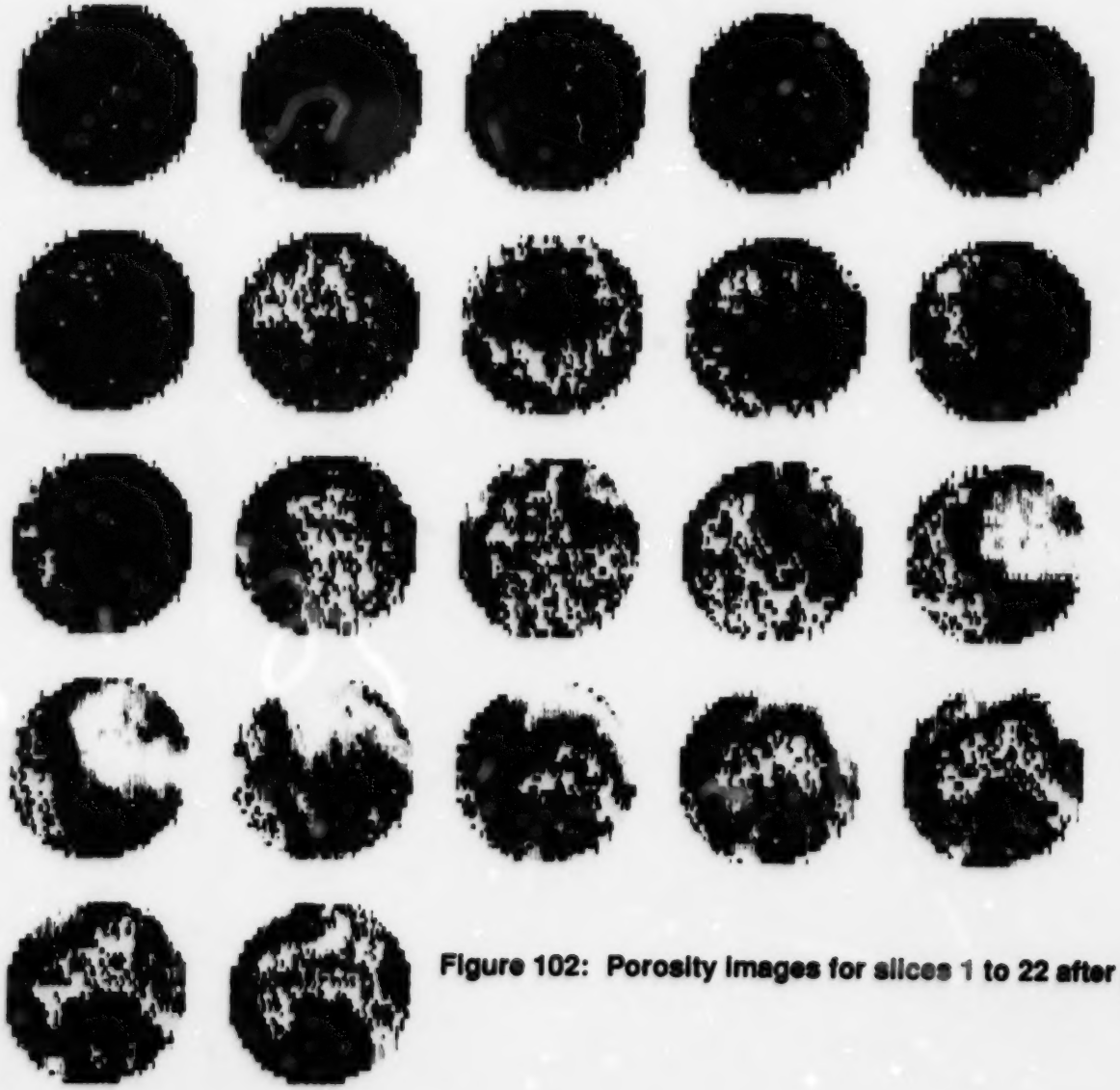

Figure 102: Porosity images for slices 1 to 22 after plugging, column B.

© 1991 NOVA HUSKY RESEARCH CORPORATION

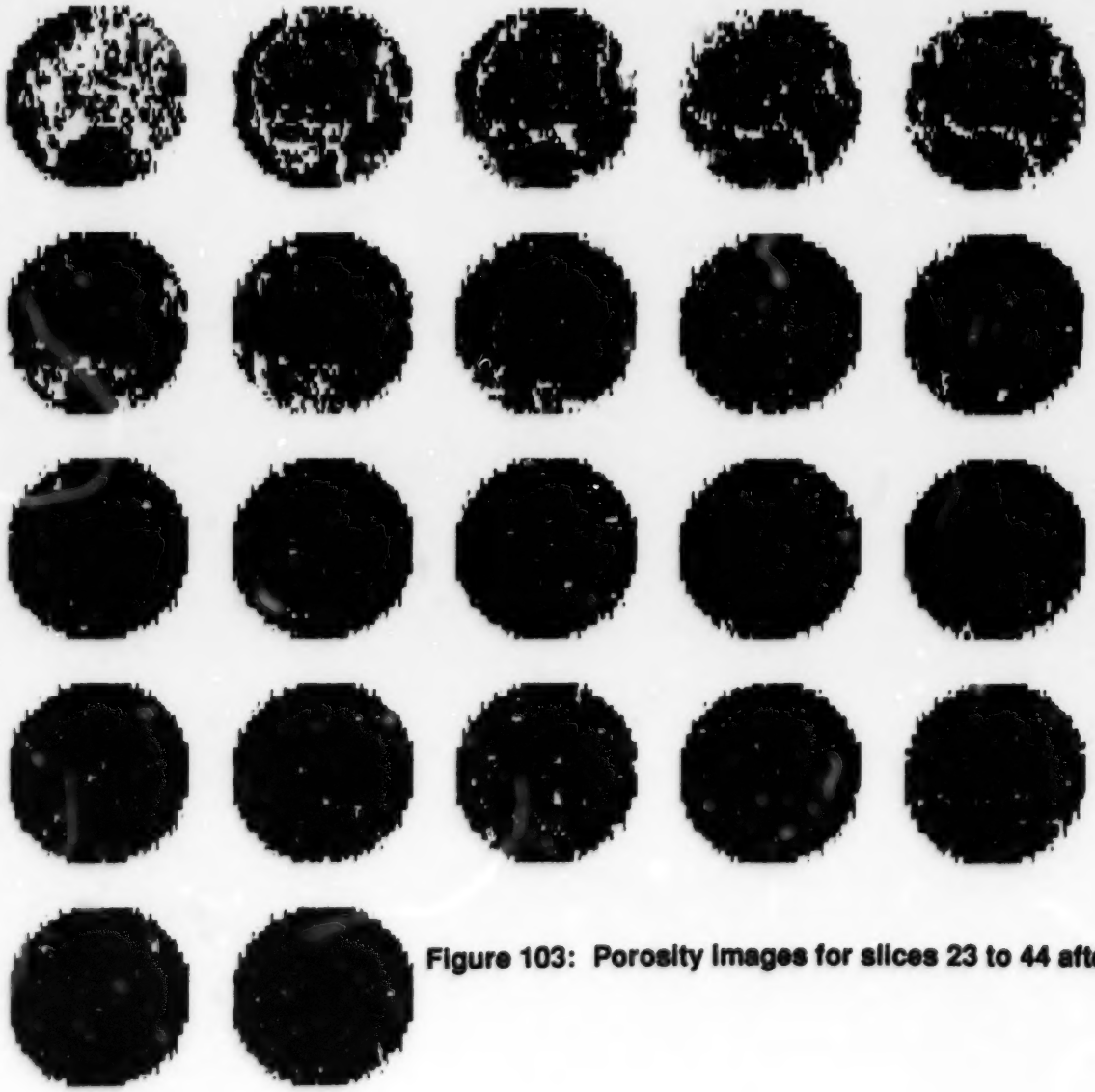

Figure 103: Porosity images for slices 23 to 44 after plugging, column B.

© 1991 NOVA HUSKY RESEARCH CORPORATION

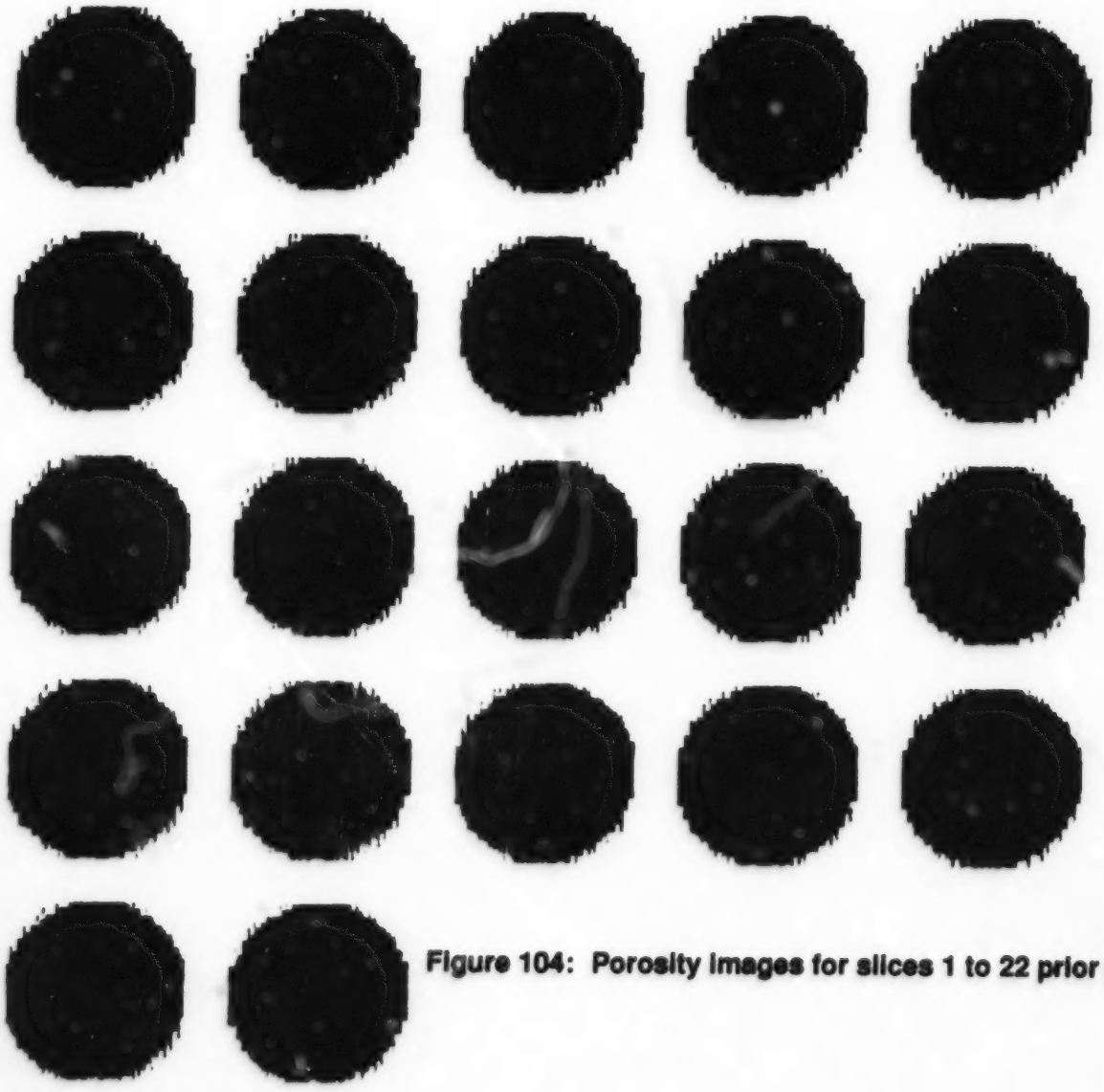

Figure 104: Porosity images for slices 1 to 22 prior to plugging, column C.

© 1991 NOVA HUSKY RESEARCH CORPORATION

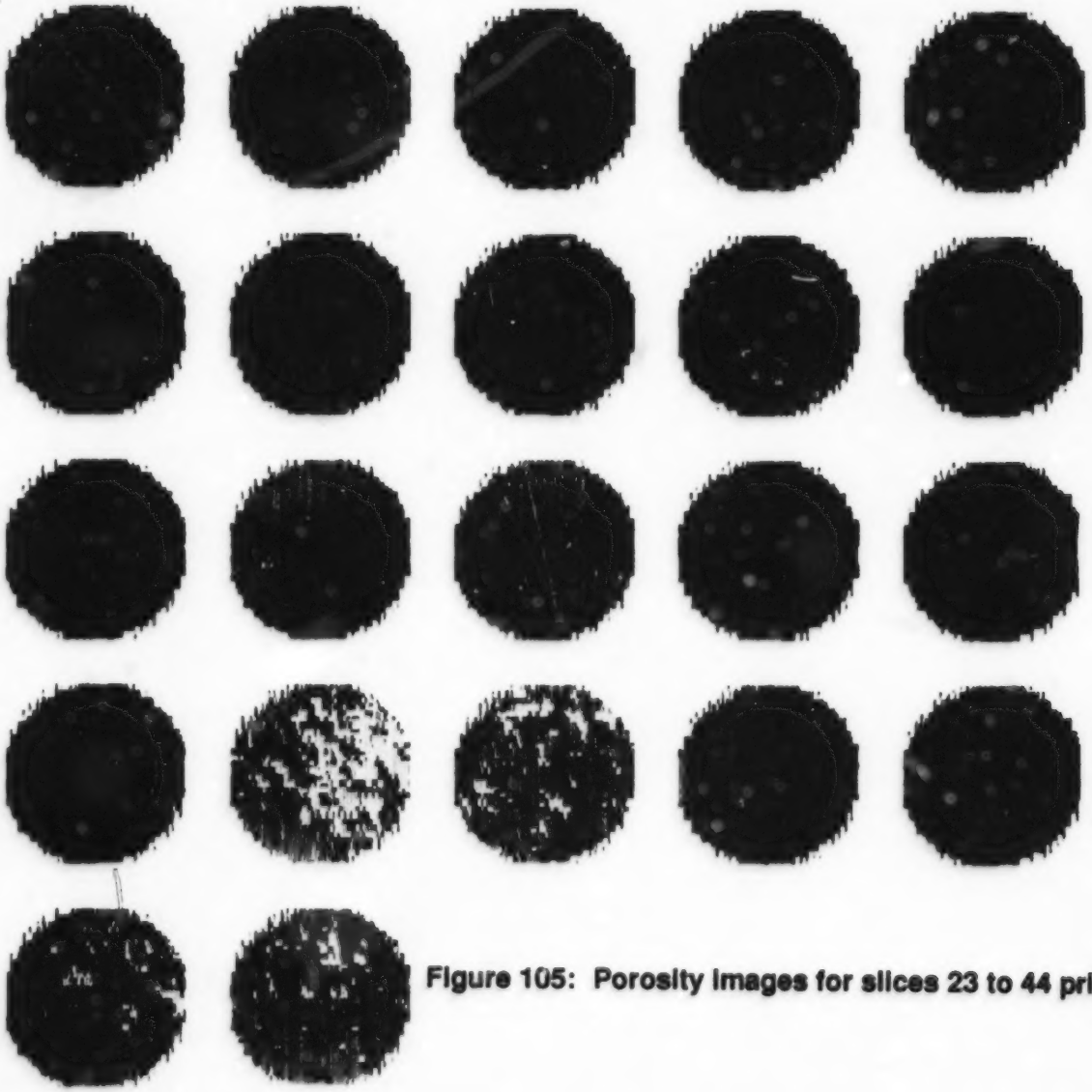

Figure 105: Porosity images for slices 23 to 44 prior to plugging, column C.

© 1991 NOVA HUSKY RESEARCH CORPORATION

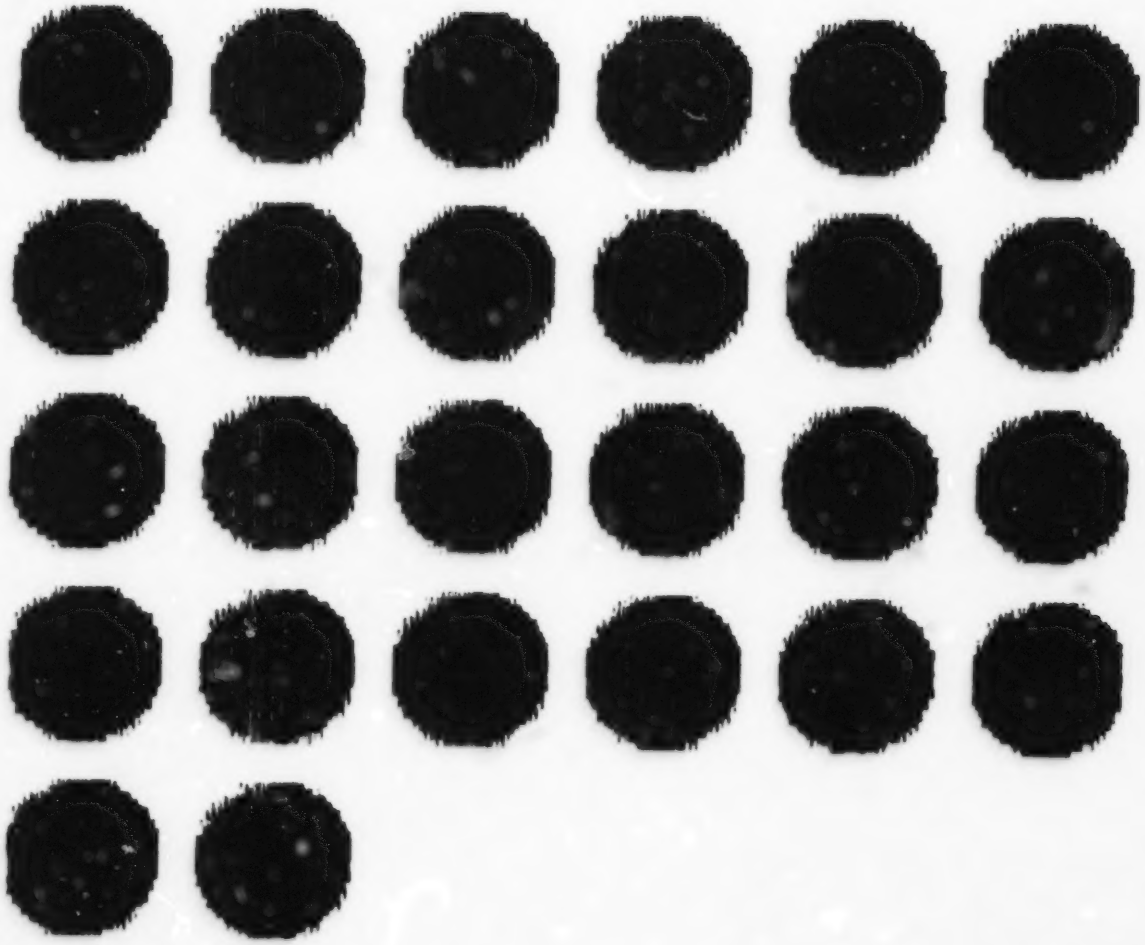

Figure 106: Porosity images for slices 45 to 70 prior to plugging, column C.

© 1991 NOVA HUSKY RESEARCH CORPORATION

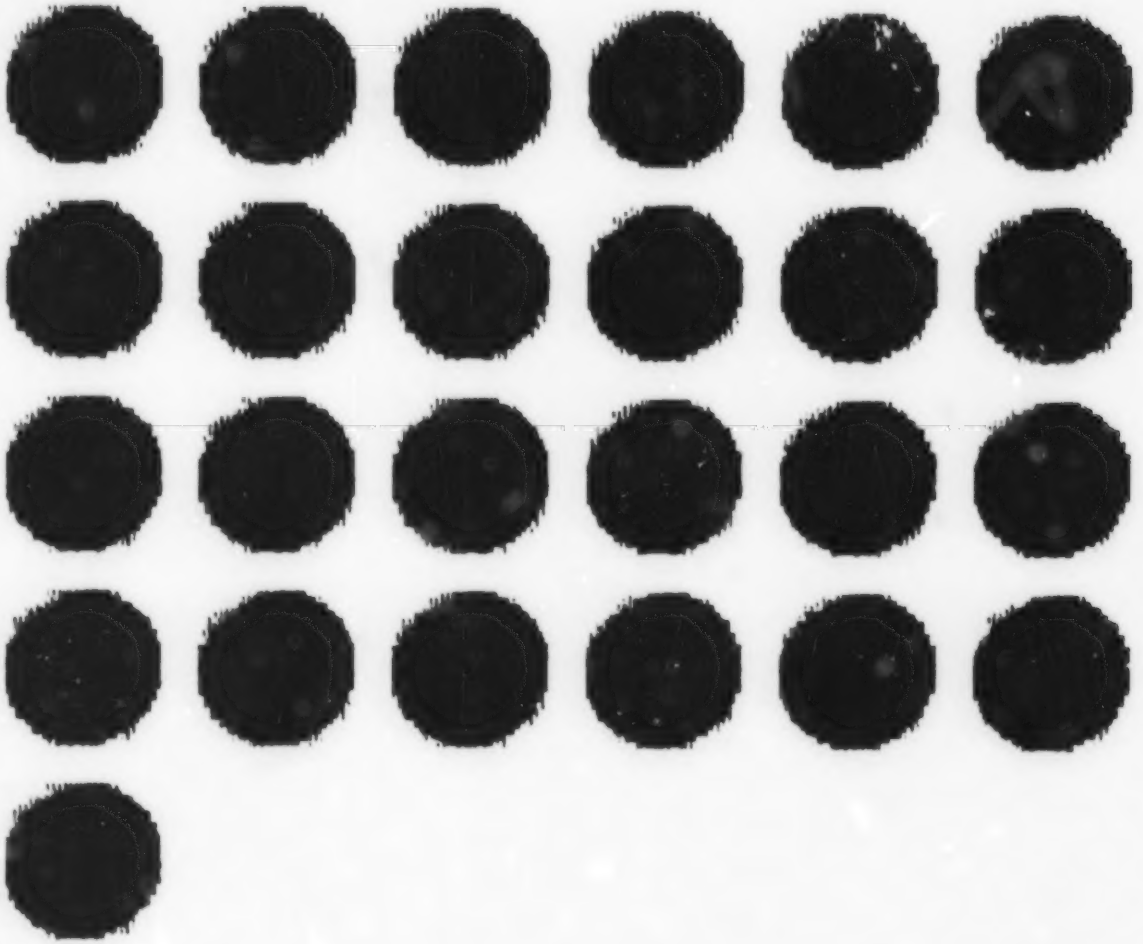

Figure 107: Porosity images for slices 71 to 95 prior to plugging, column C.

© 1991 NOVA HUSKY RESEARCH CORPORATION

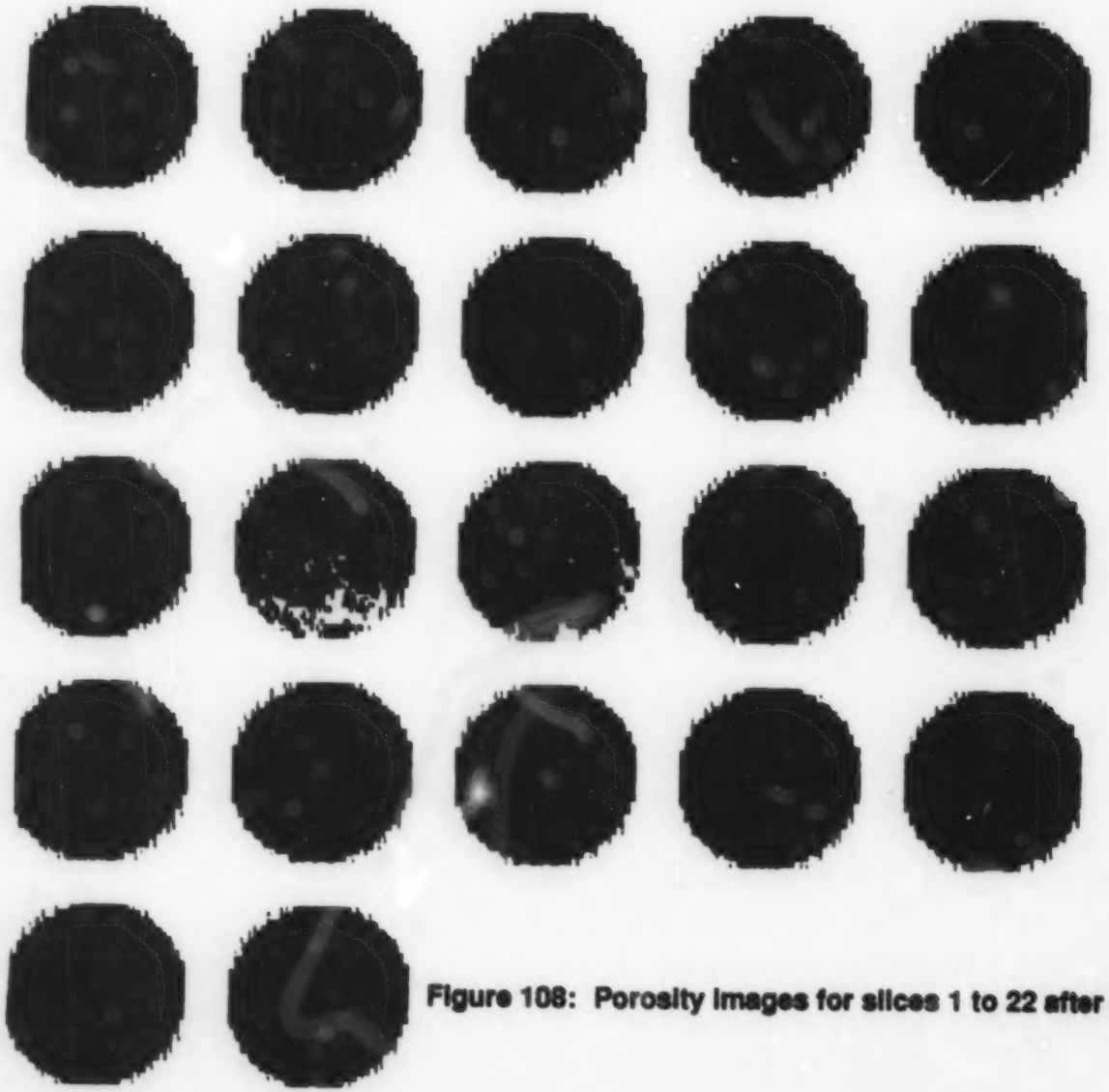

Figure 108: Porosity images for slices 1 to 22 after plugging, column C.

© 1991 NOVA HUSKY RESEARCH CORPORATION

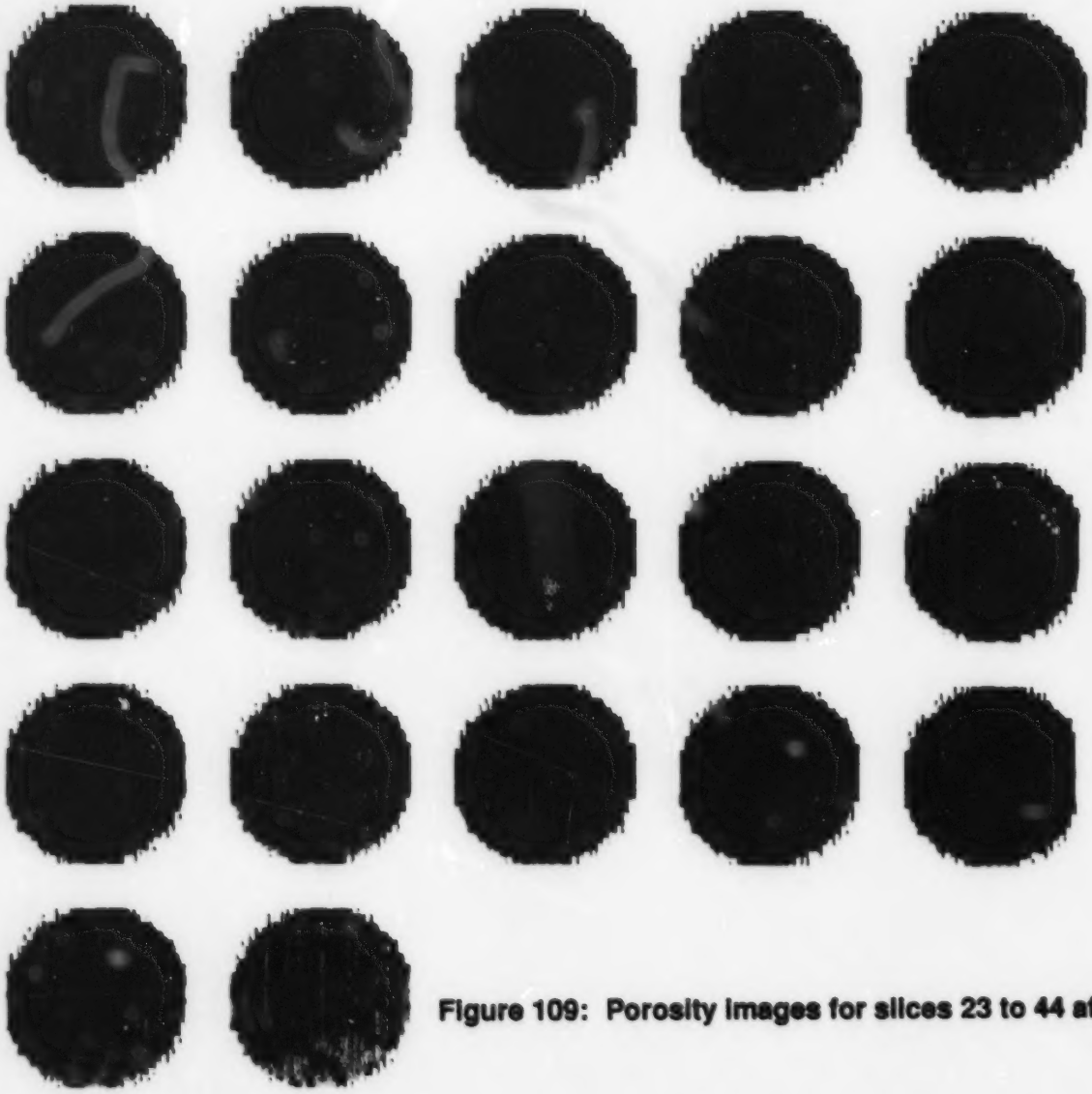

Figure 109: Porosity images for slices 23 to 44 after plugging, column C.

© 1991 NOVA HUSKY RESEARCH CORPORATION

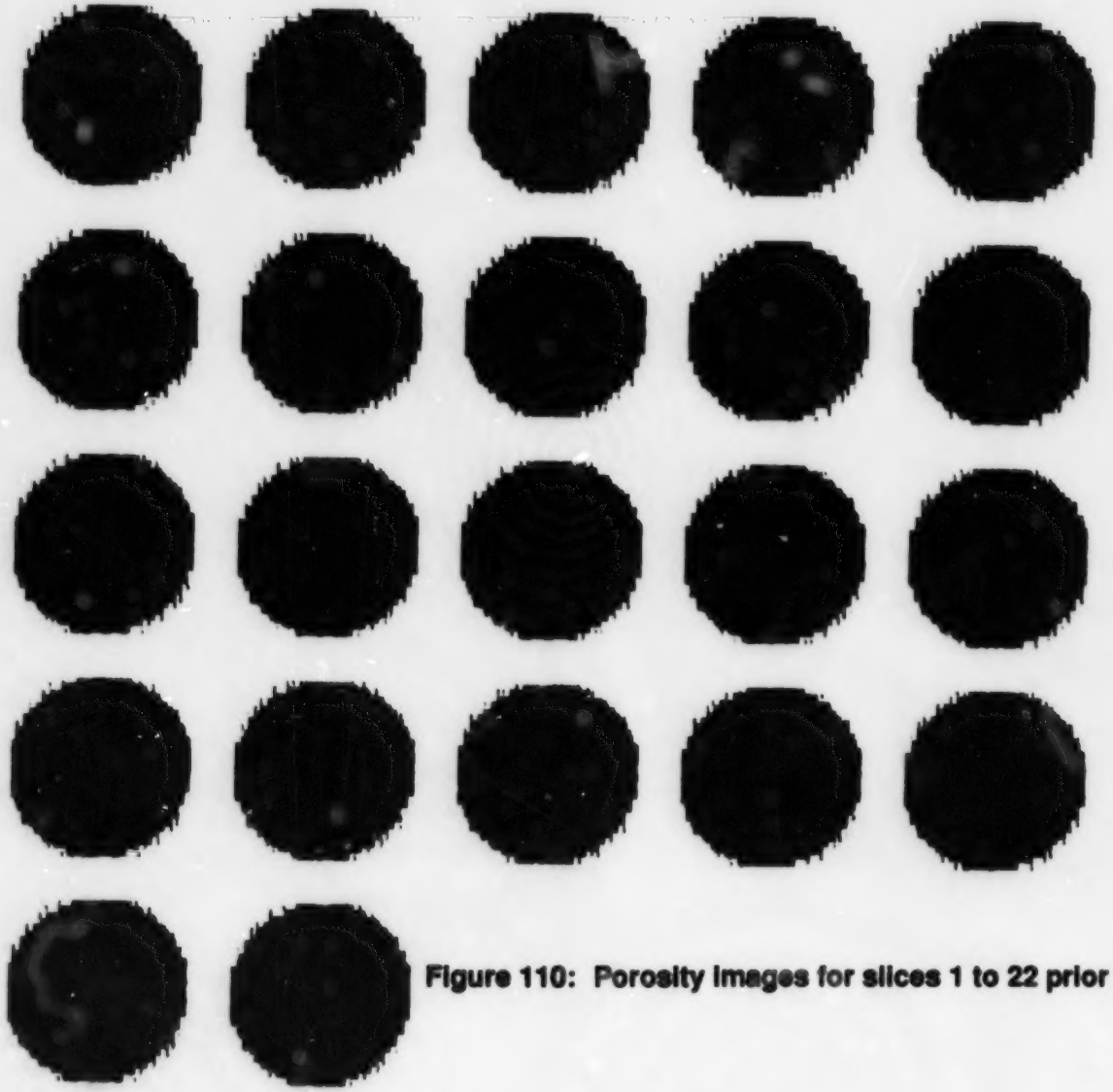

Figure 110: Porosity images for slices 1 to 22 prior to plugging, column D.

© 1991 NOVA HUSKY RESEARCH CORPORATION

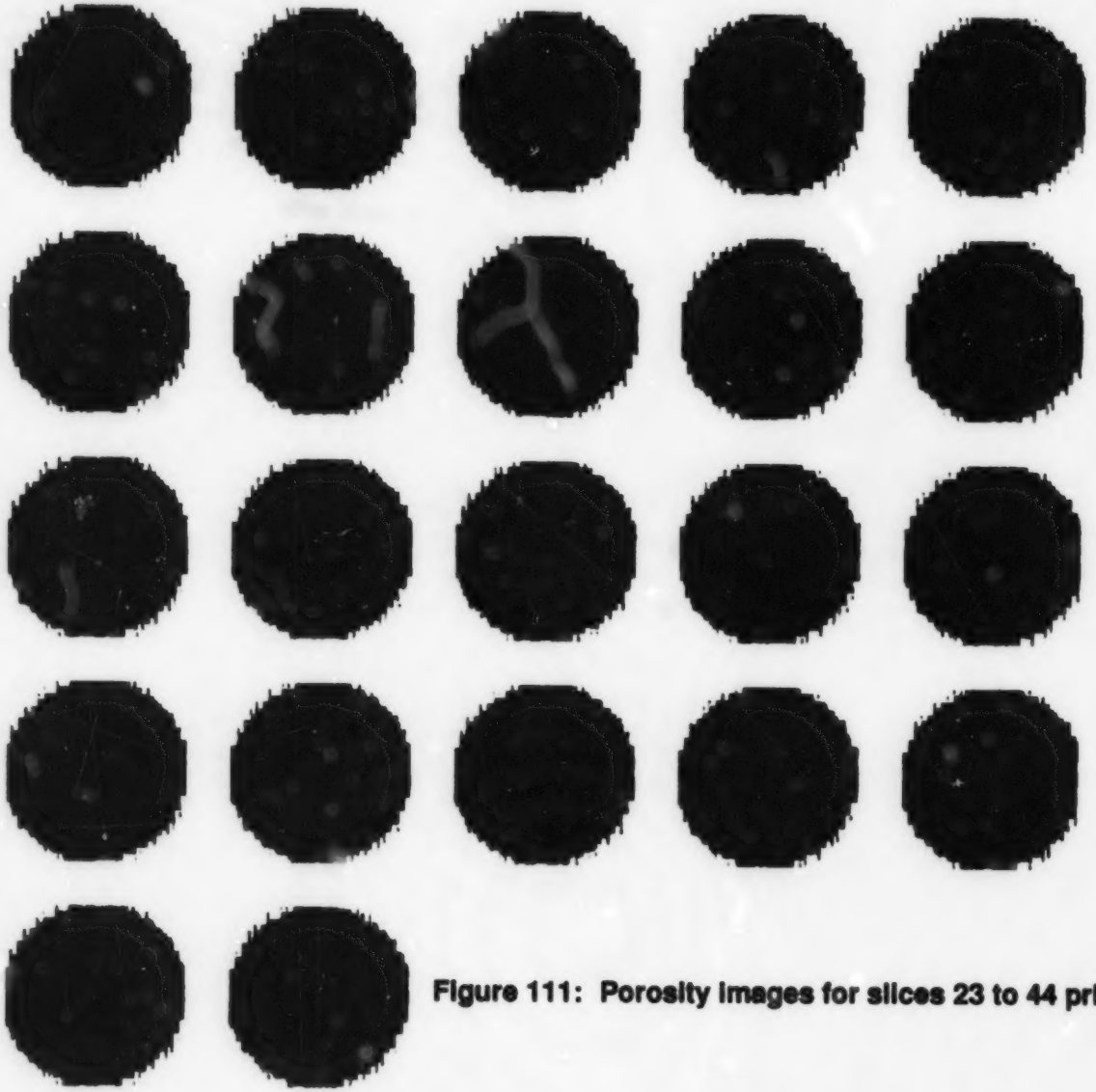

Figure 111: Porosity images for slices 23 to 44 prior to plugging, column D.

© 1991 NOVA HUSKY RESEARCH CORPORATION

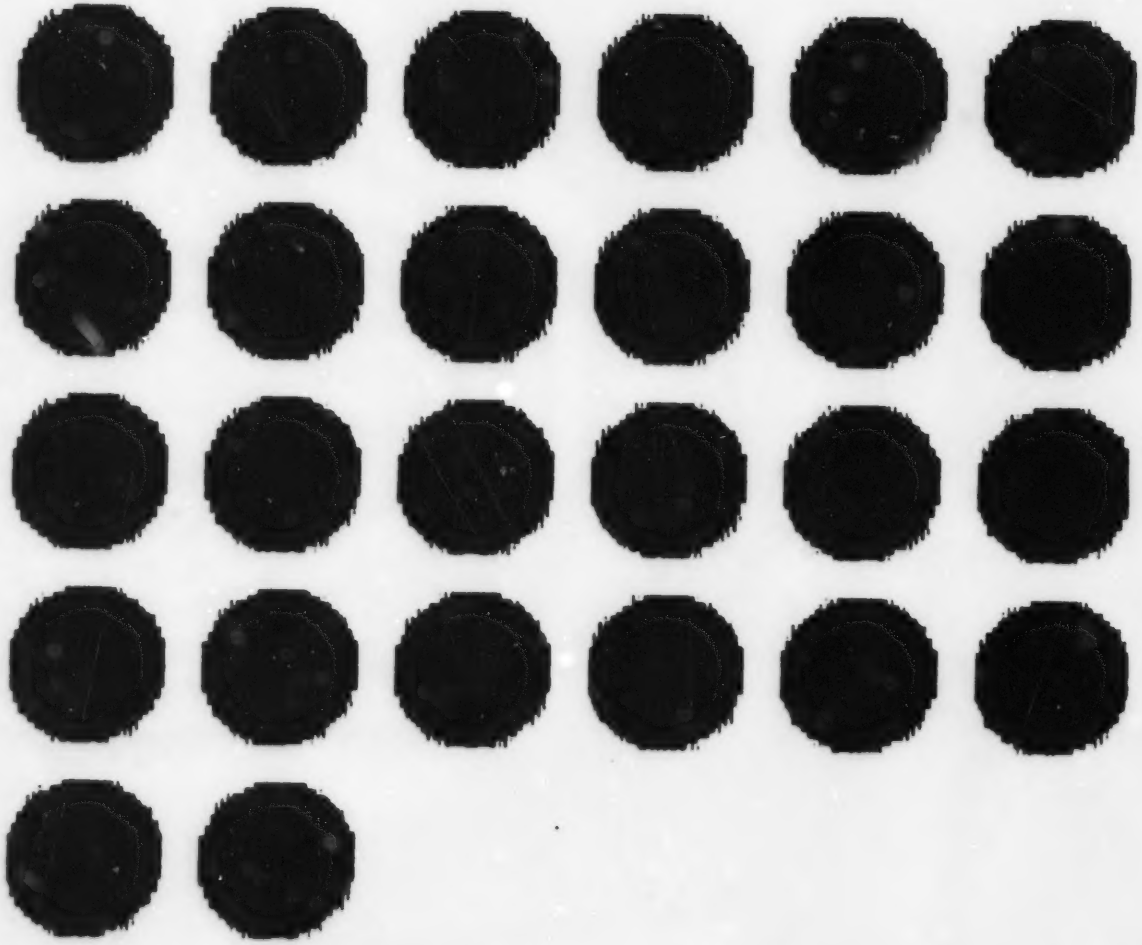

Figure 112: Porosity images for slices 45 to 70 prior to plugging, column D.

© 1991 NOVA HUSKY RESEARCH CORPORATION

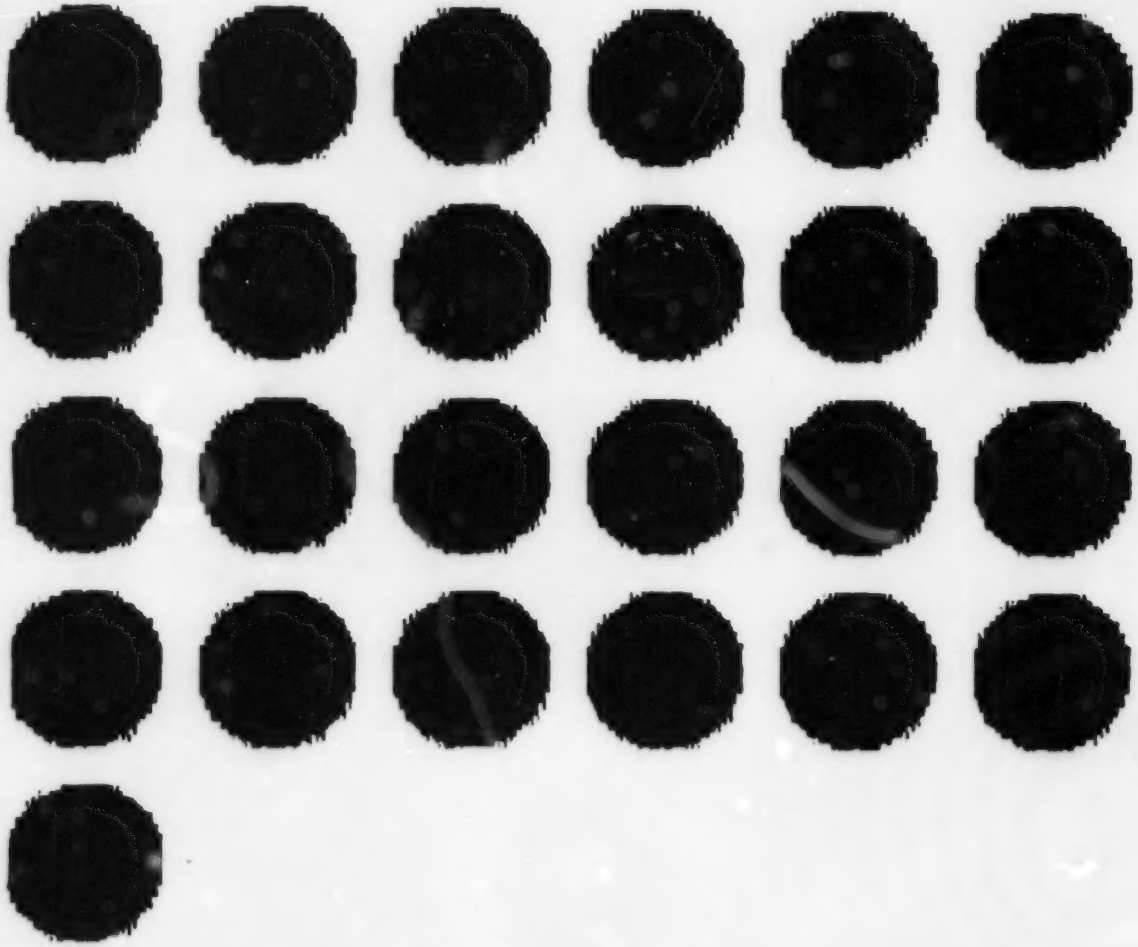

Figure 113: Porosity images for slices 71 to 95 prior to plugging, column D.

© 1991 NOVA HUSKY RESEARCH CORPORATION

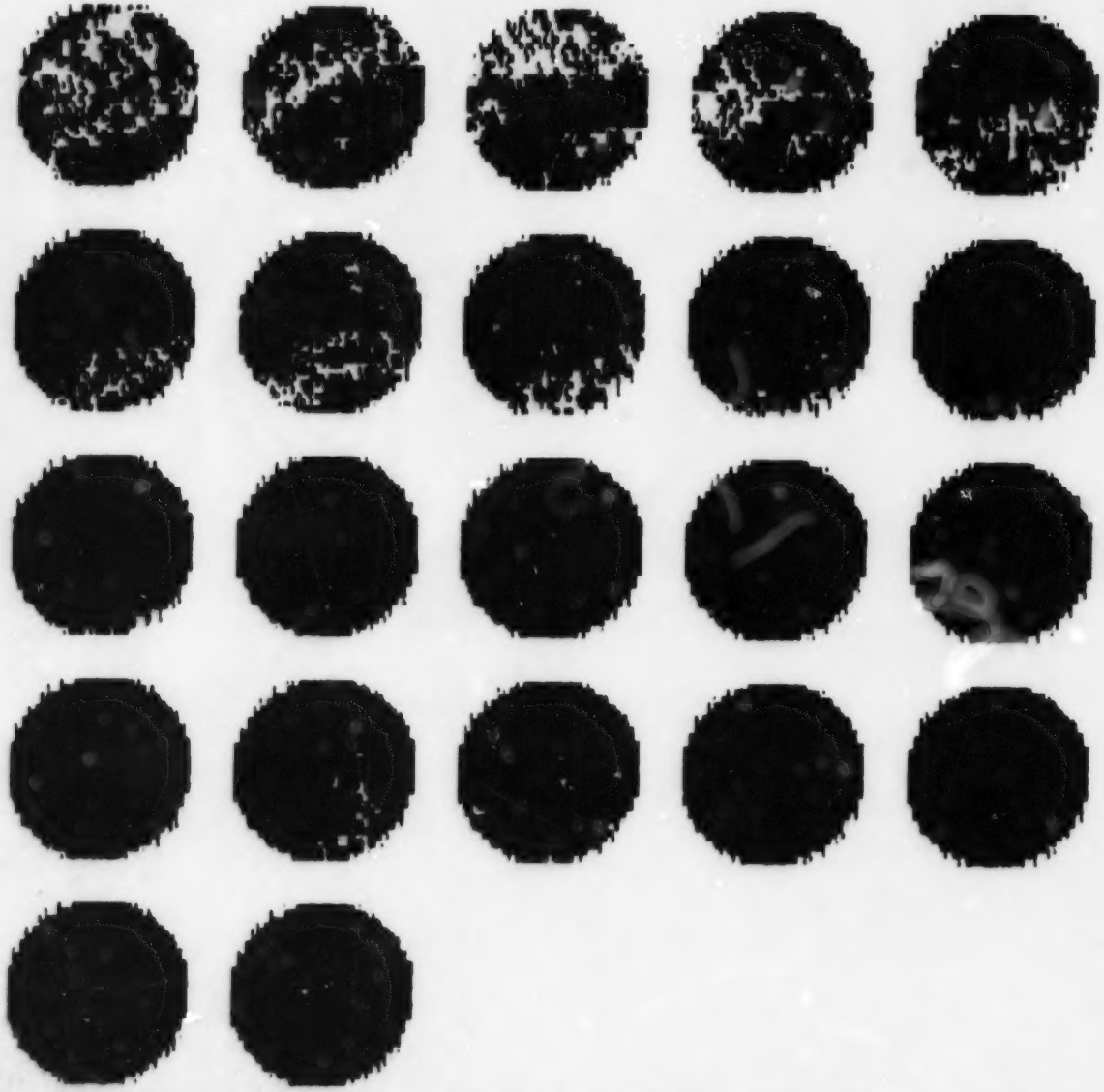

Figure 114: Porosity images for slices 1 to 22 after plugging, column D.

© 1991 NOVA HUSKY RESEARCH CORPORATION

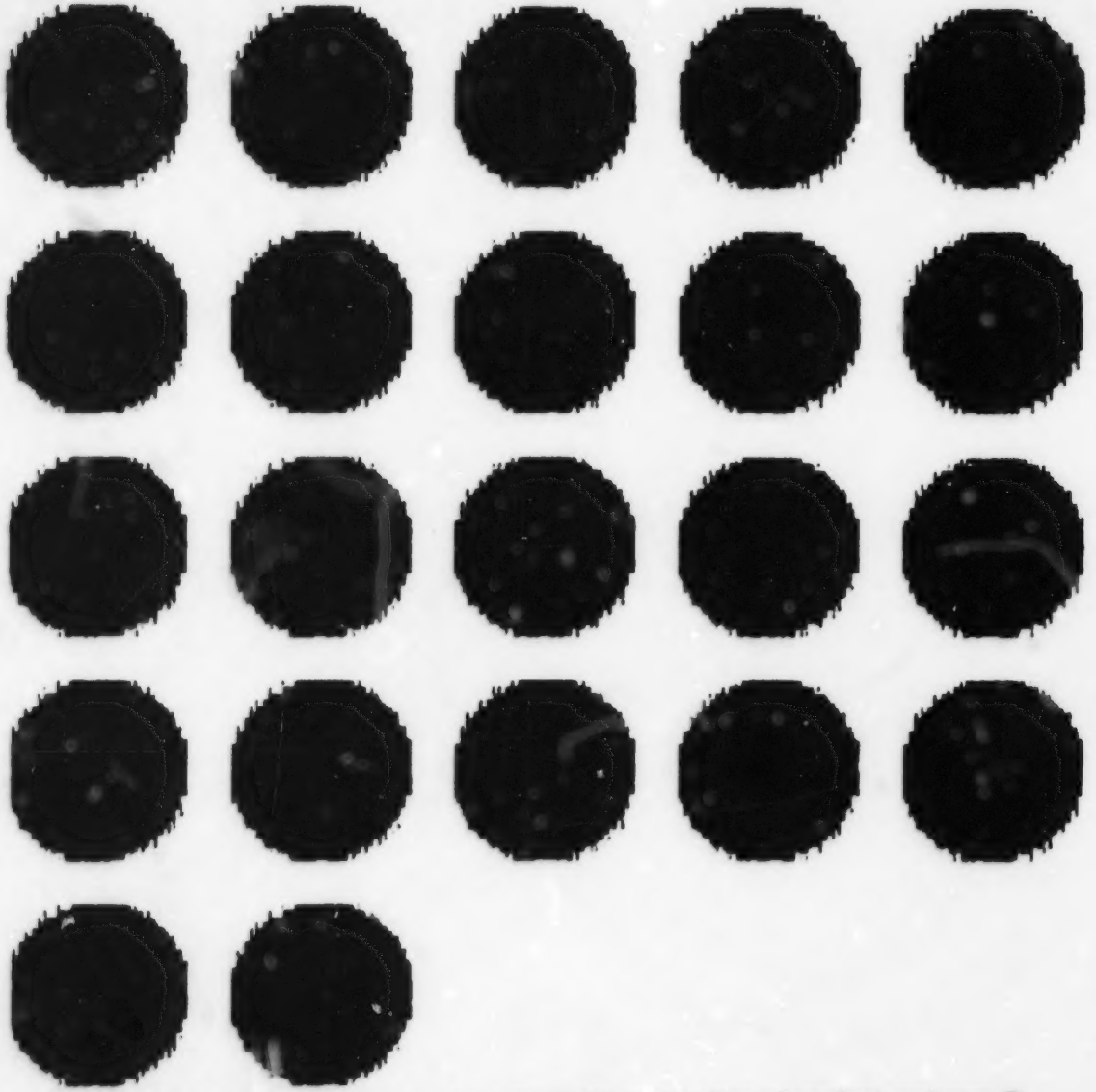

Figure 115: Porosity images for slices 23 to 44 after plugging, column D.

© 1991 NOVA HUSKY RESEARCH CORPORATION

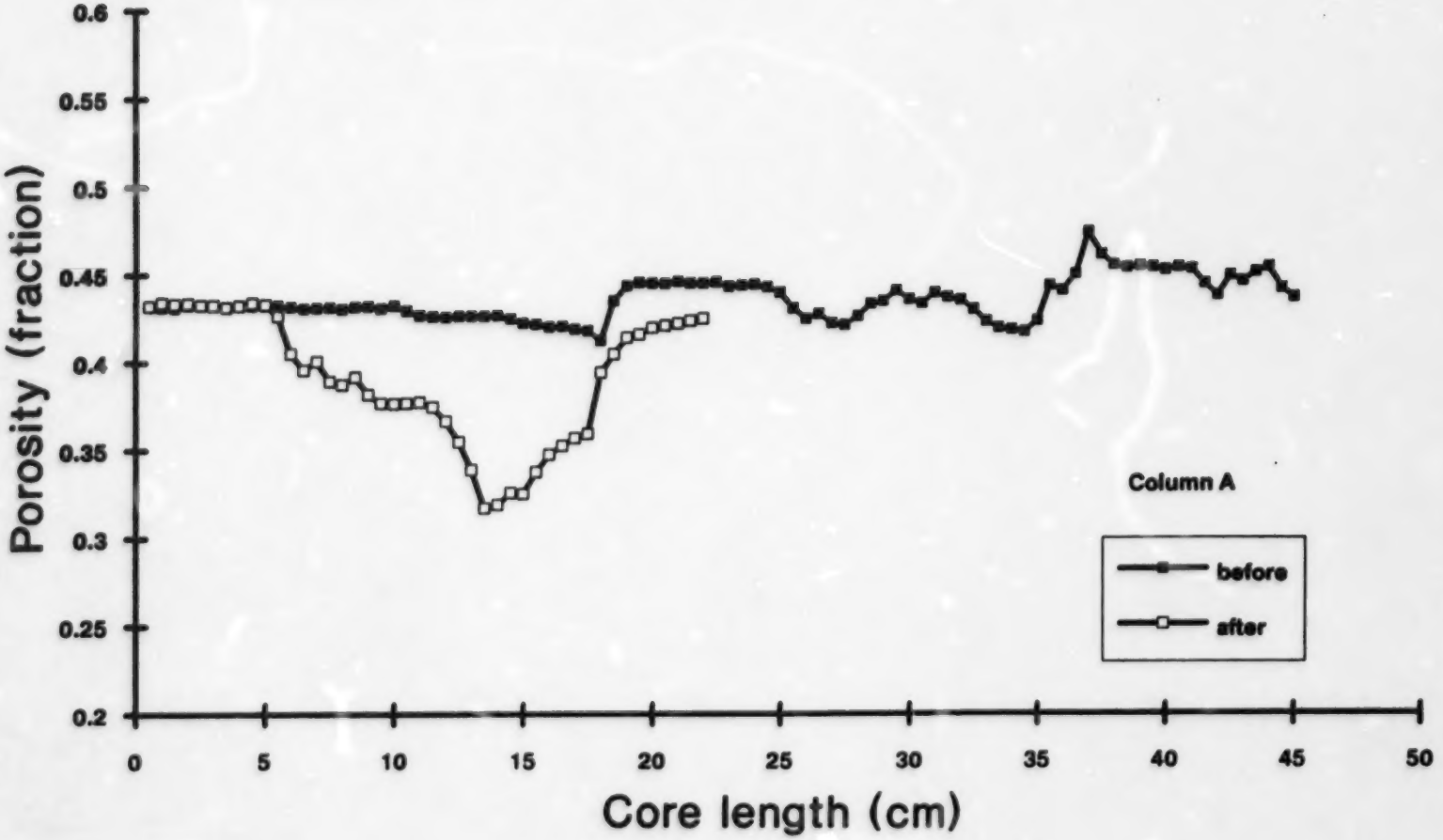

Figure 116: Average slice bulk density prior to and after plugging, Column A.

© 1991 NOVA HUSKY RESEARCH CORPORATION

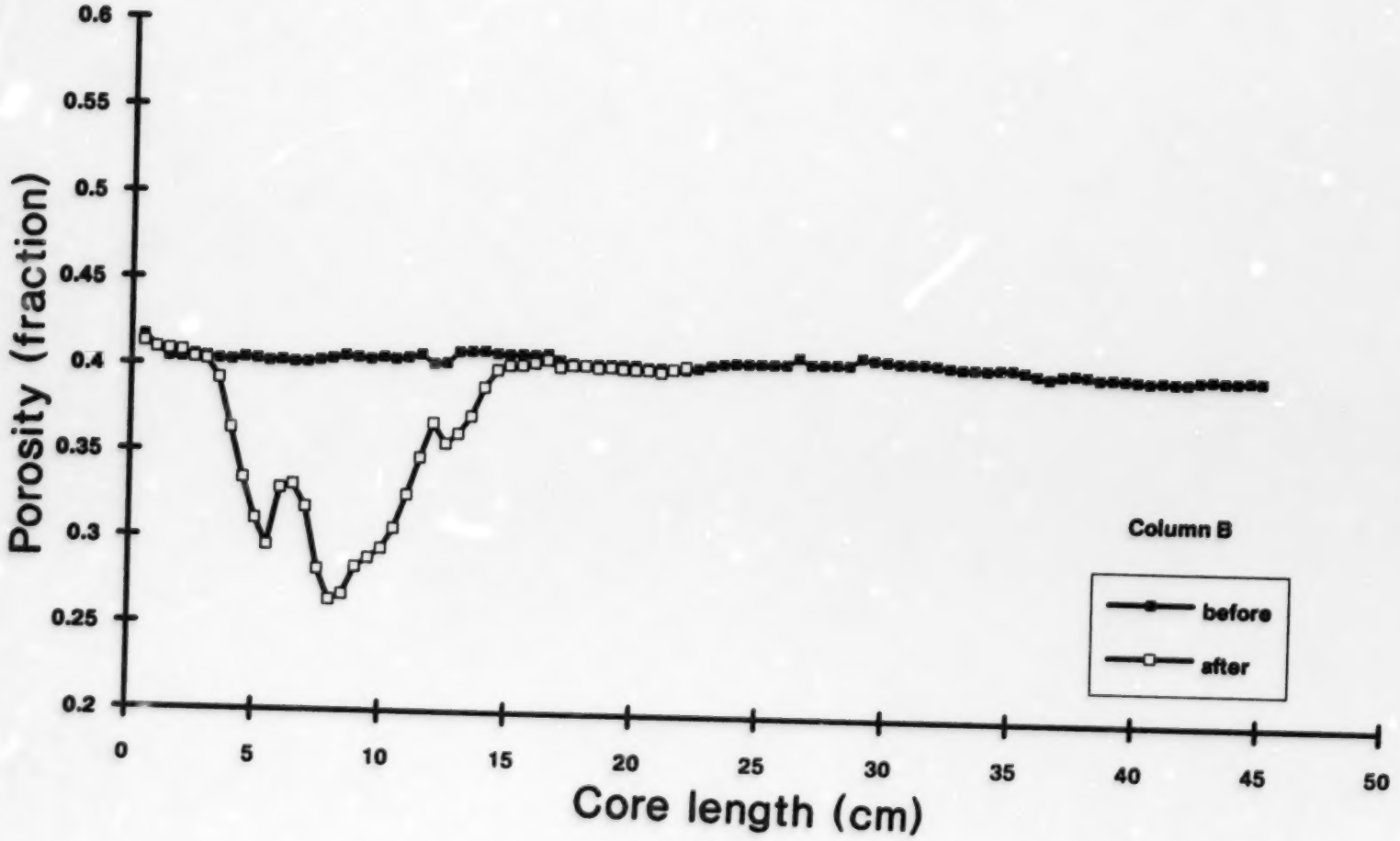

Figure 117: Average slice bulk density prior to and after plugging, Column B.

© 1991 NOVA HUSKY RESEARCH CORPORATION

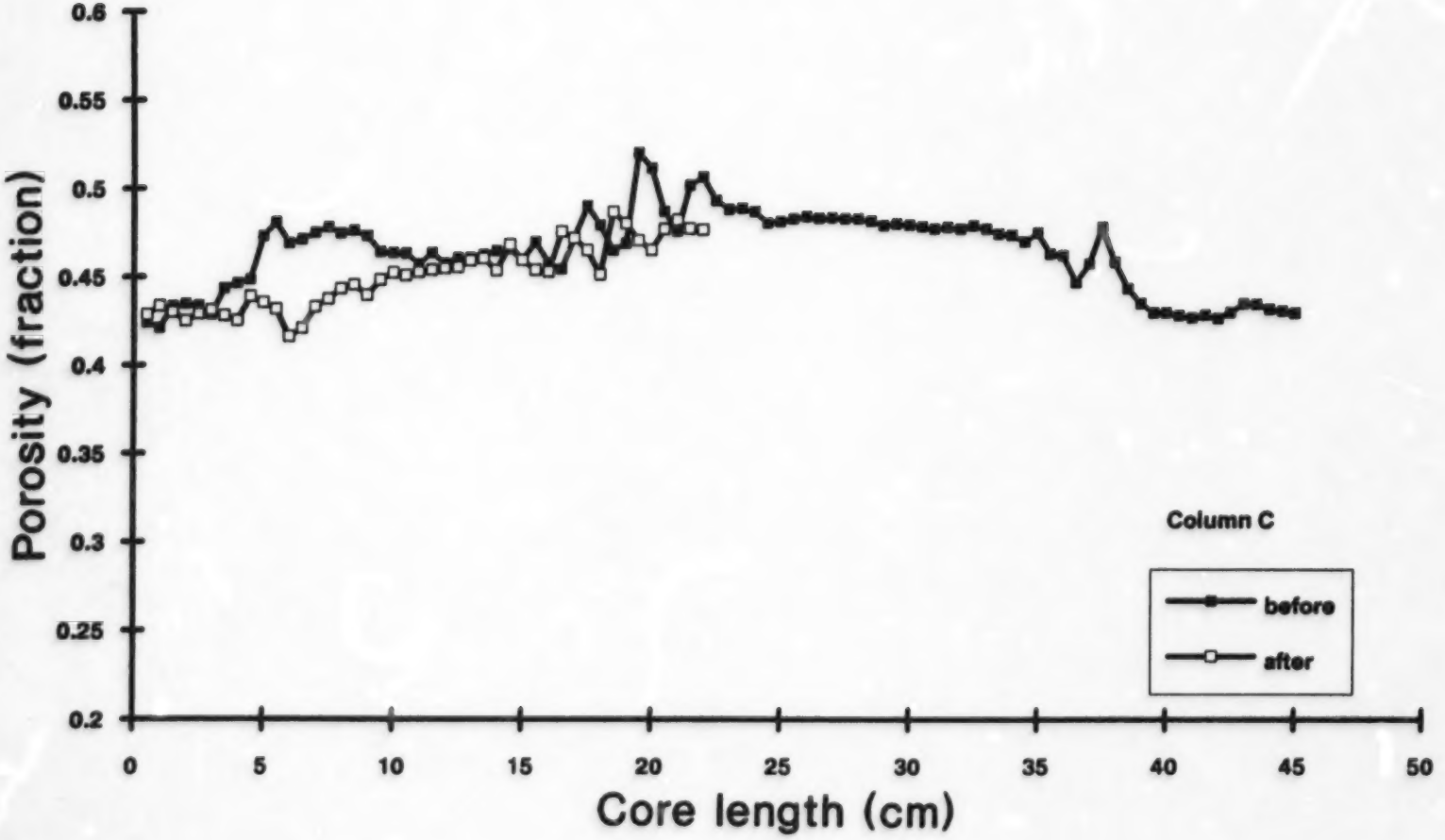

Figure 118: Average slice bulk density prior to and after plugging, Column C.

© 1991 NOVA HUSKY RESEARCH CORPORATION

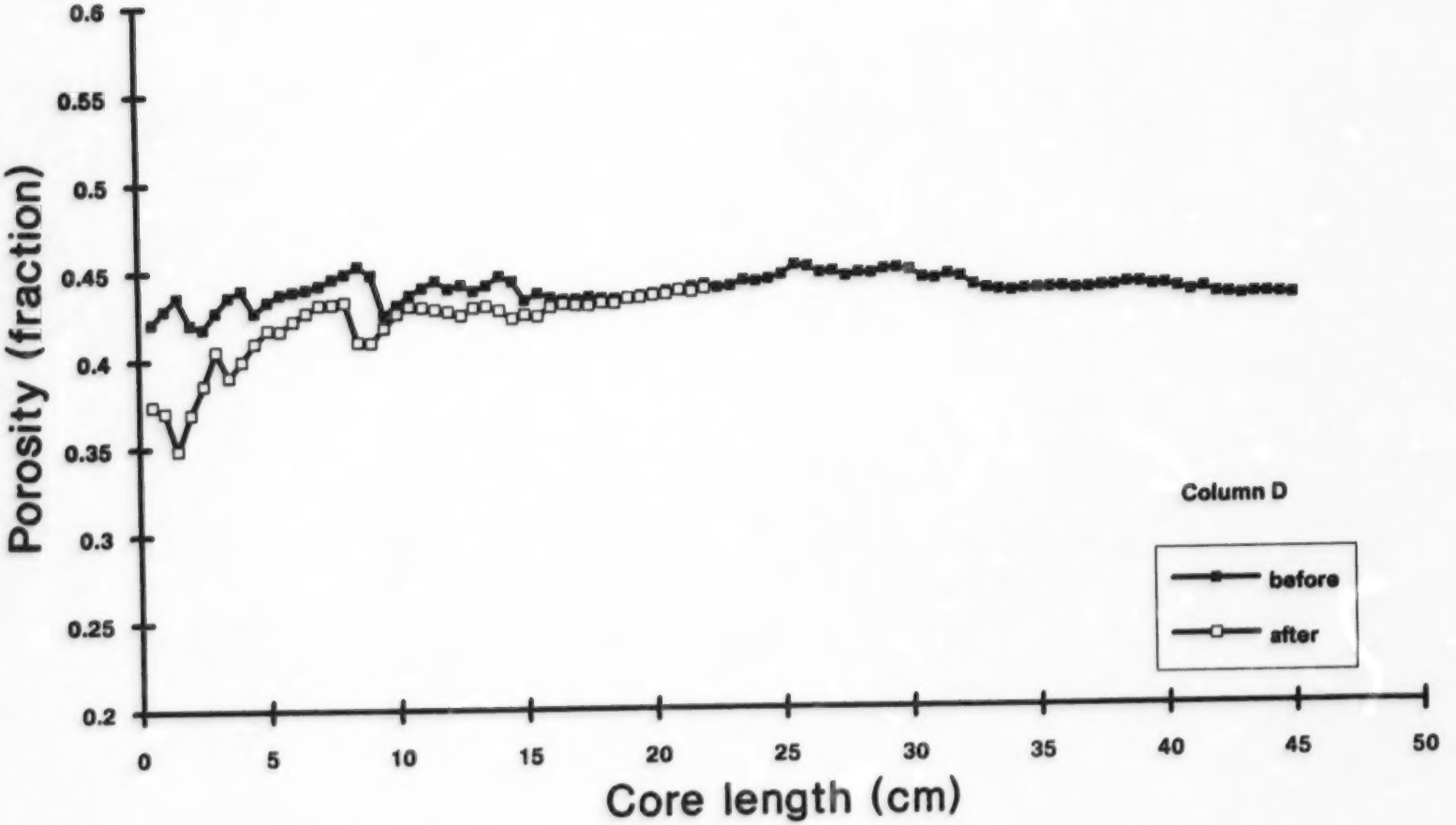

Figure 119: Average slice bulk density prior to and after plugging, Column D.

© 1991 NOVA HUSKY RESEARCH CORPORATION

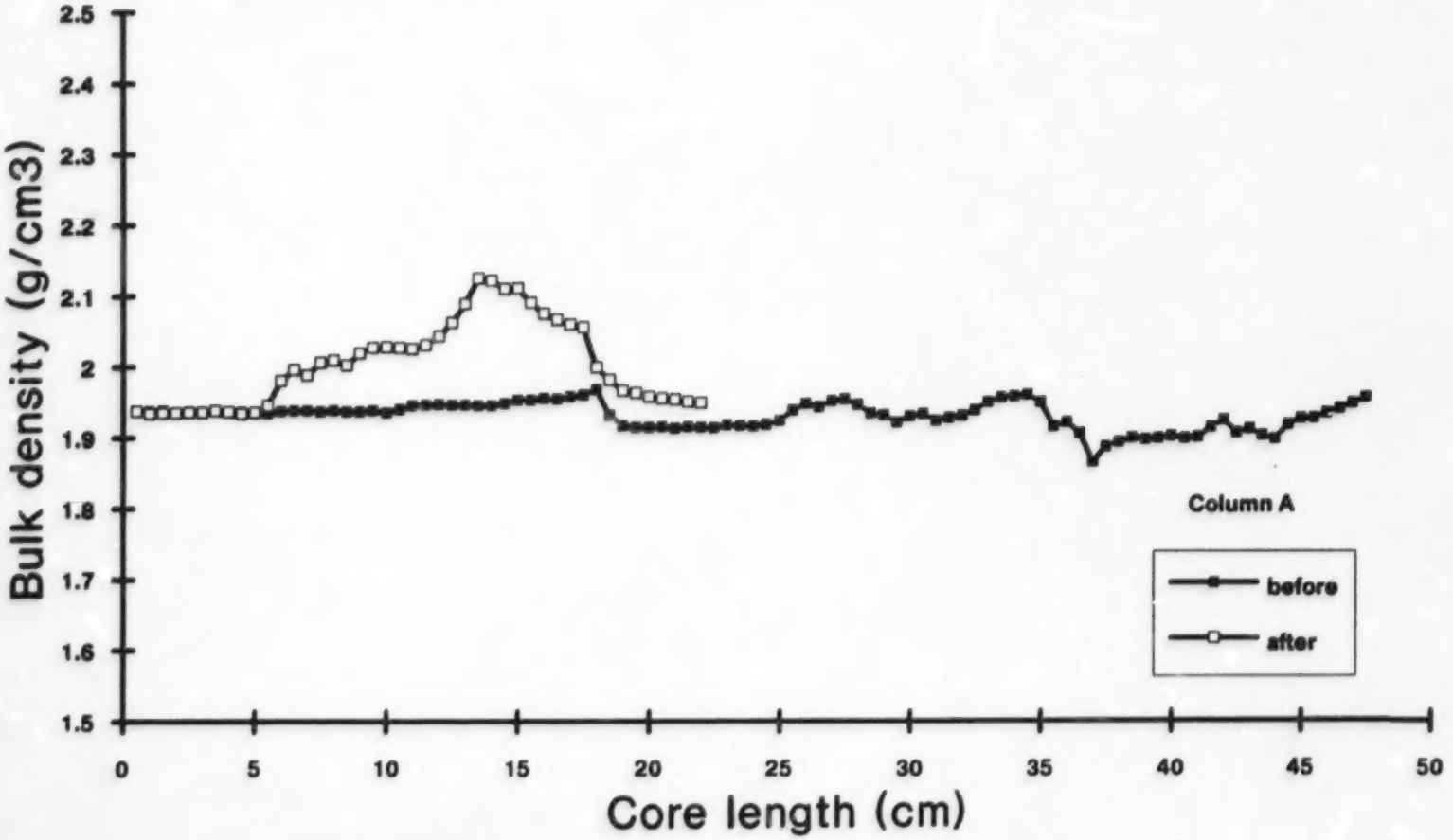

Figure 120: Average slice porosity prior to and after plugging, Column A.

© 1991 NOVA HUSKY RESEARCH CORPORATION

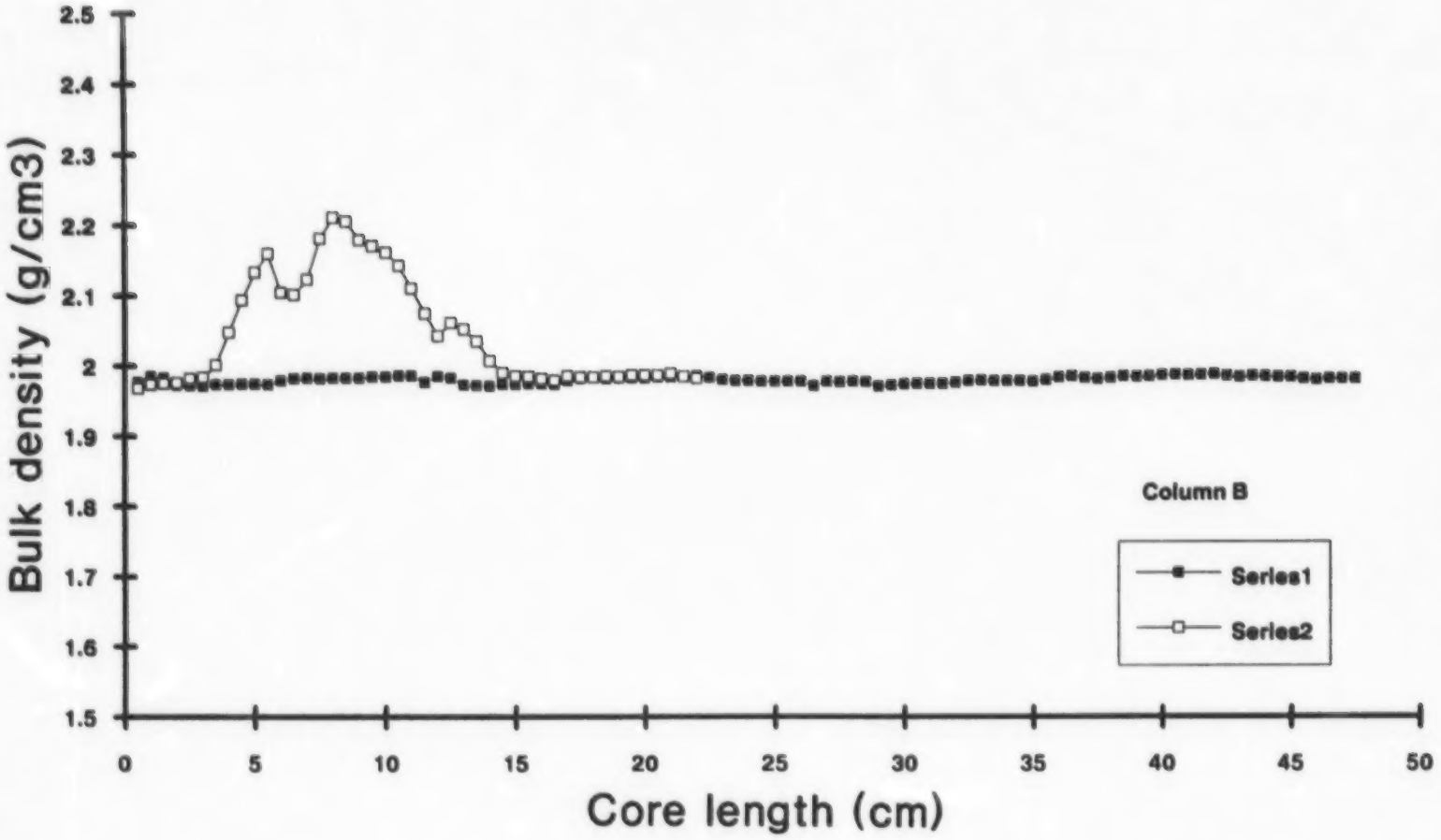

Figure 121: Average slice porosity prior to and after plugging, Column B.

© 1991 NOVA HUSKY RESEARCH CORPORATION

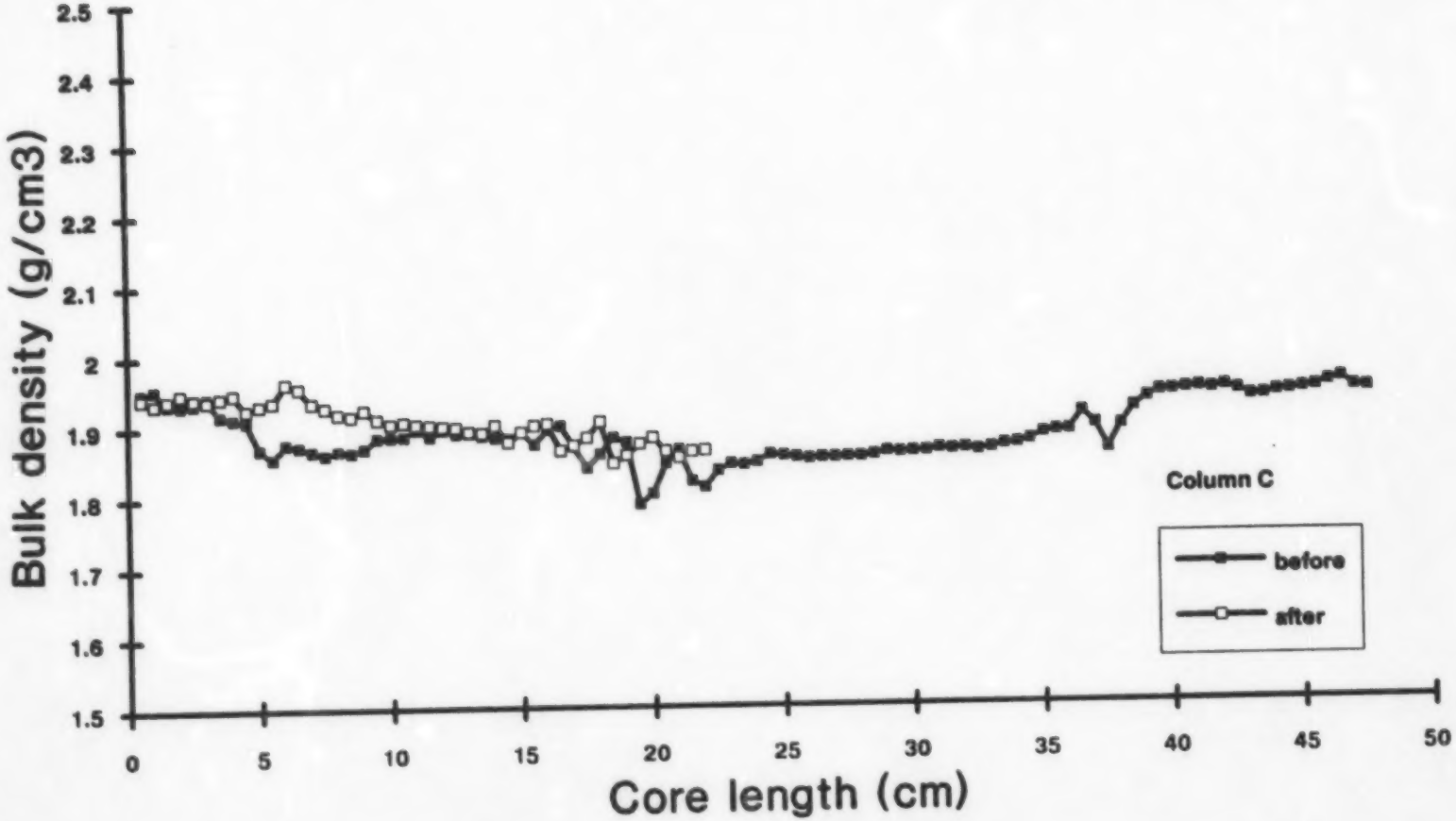

Figure 122: Average slice porosity prior to and after plugging, Column C.

© 1991 NOVA HUSKY RESEARCH CORPORATION

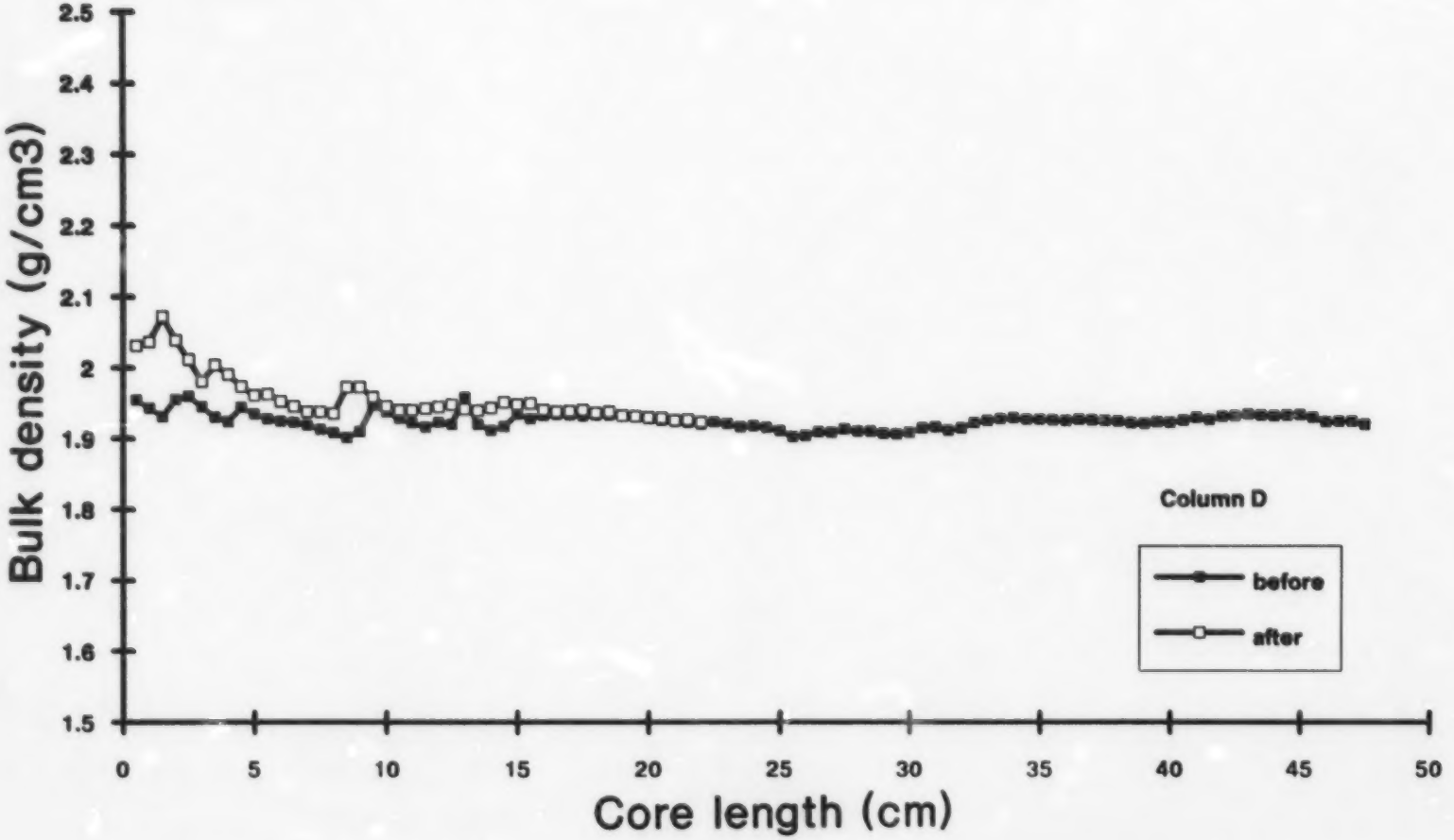

Figure 123: Average slice porosity prior to and after plugging, Column D.

© 1991 NOVA HUSKY RESEARCH CORPORATION

Figure 124: Photographs of the first section (0 - 6 cm) of column A after completion of the experimen
The small solidified section is shown at the left end.

© 1991 NOVA HUSKY RESEARCH CORPORATION

Figure 125: Photographs of the second section (6 - 18 cm) of column A after completion of the experiment. The solidified sections can be shown.

© 1991 NOVA HUSKY RESEARCH CORPORATION

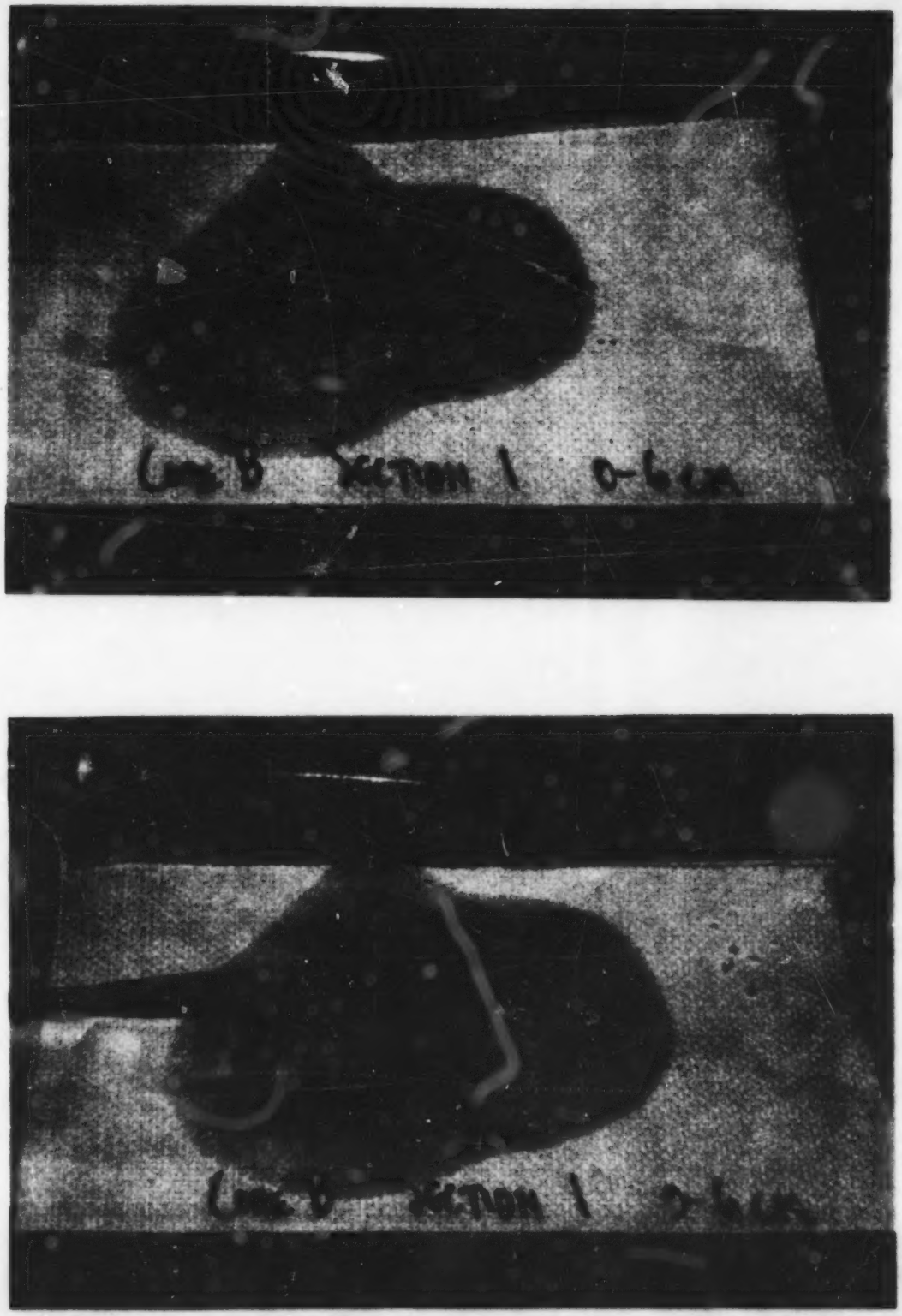

Figure 126: Photographs of the first section (0 - 6 cm) of column B after completion of the experimen
There is no solidified section.

© 1991 NOVA HUSKY RESEARCH CORPORATION

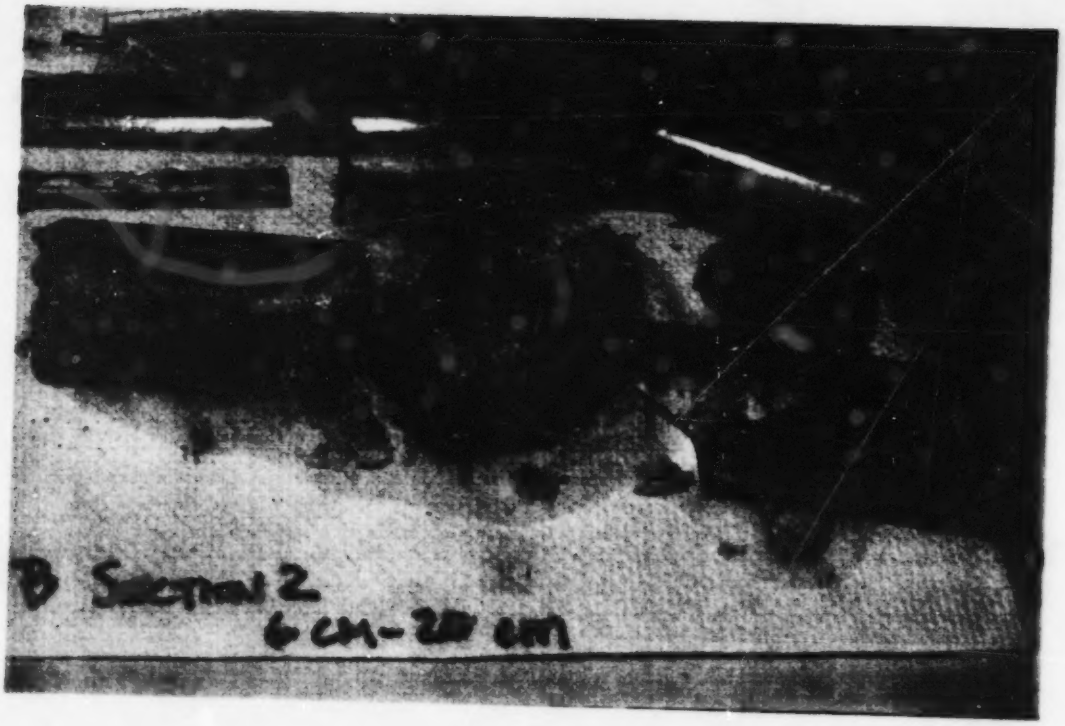

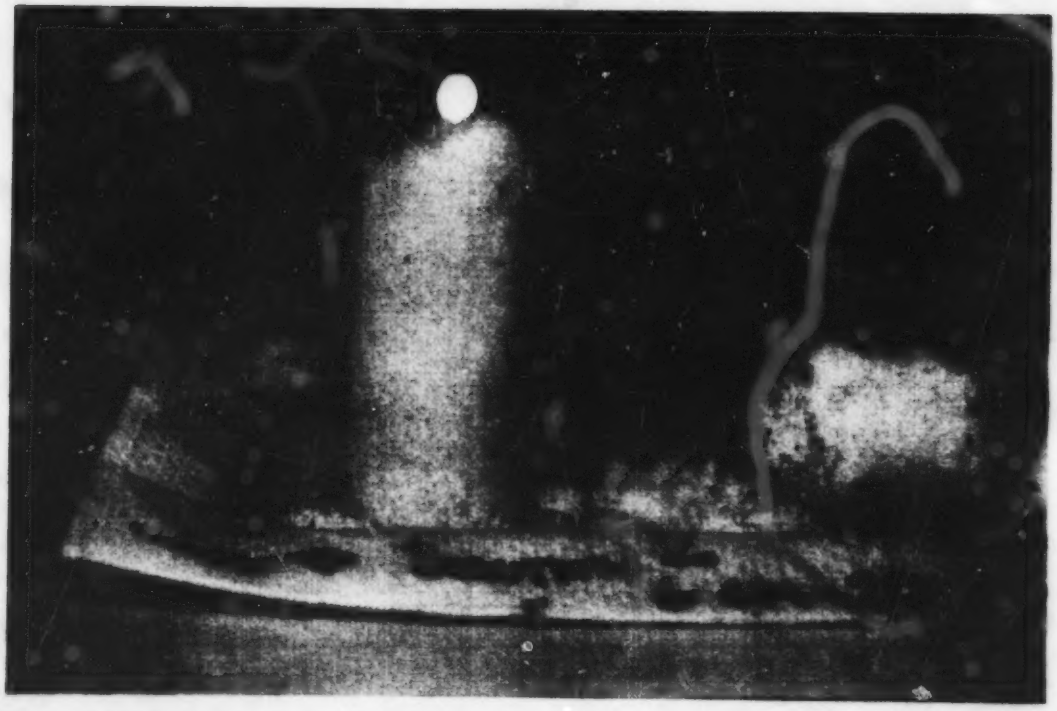

Figure 127: Photographs of the second section (6 - 20 cm) of column B after completion of the experiment. Two solidified sections can be seen.

Figure 128: Photograph of the remaining sections of columns A and B where no plugging has taken place.

© 1991 NOVA HUSKY RESEARCH CORPORATION

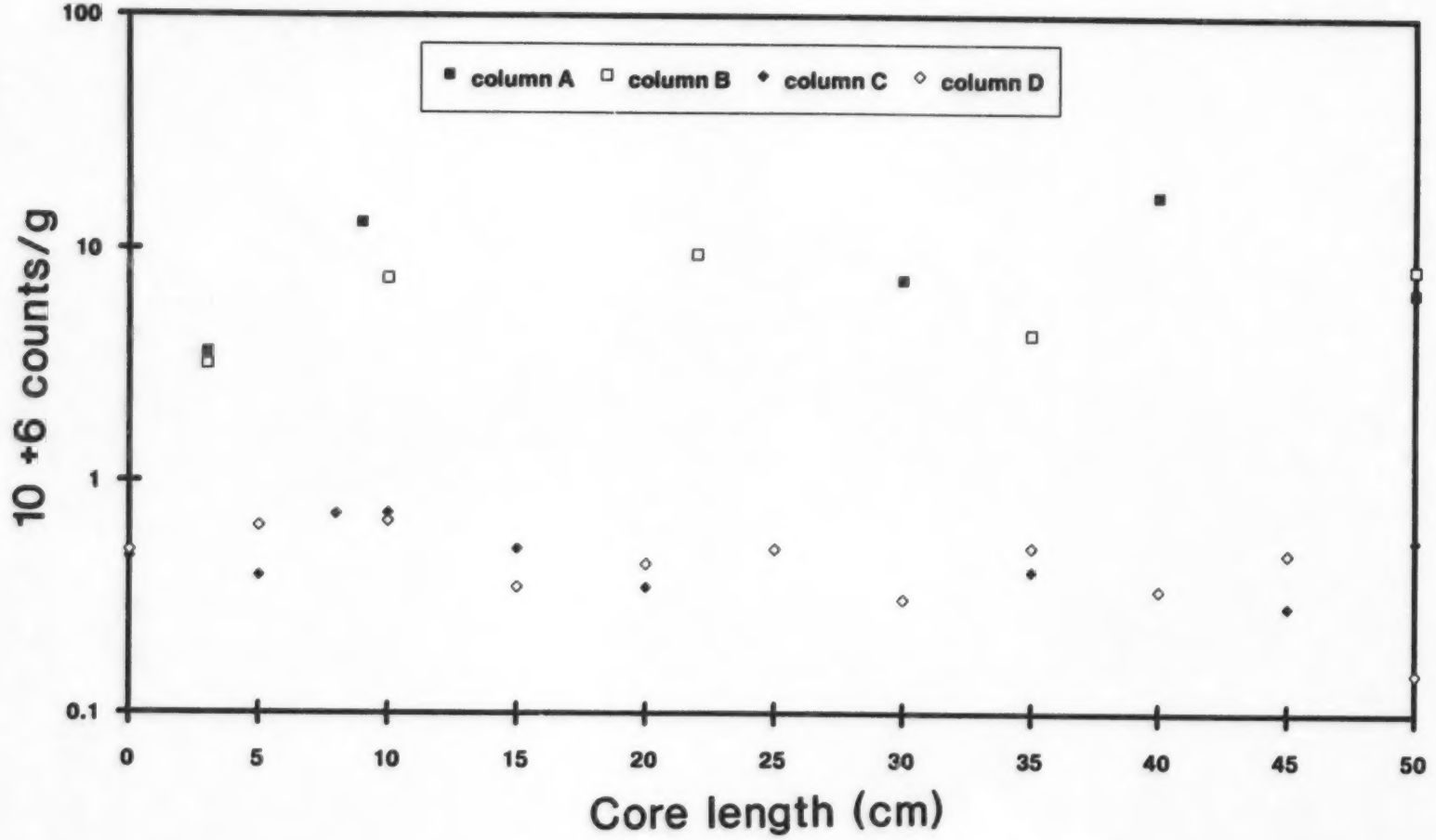

Figure 129: Bacterial Population distributions along the length of the different columns.

© 1991 NOVA HUSKY RESEARCH CORPORATION

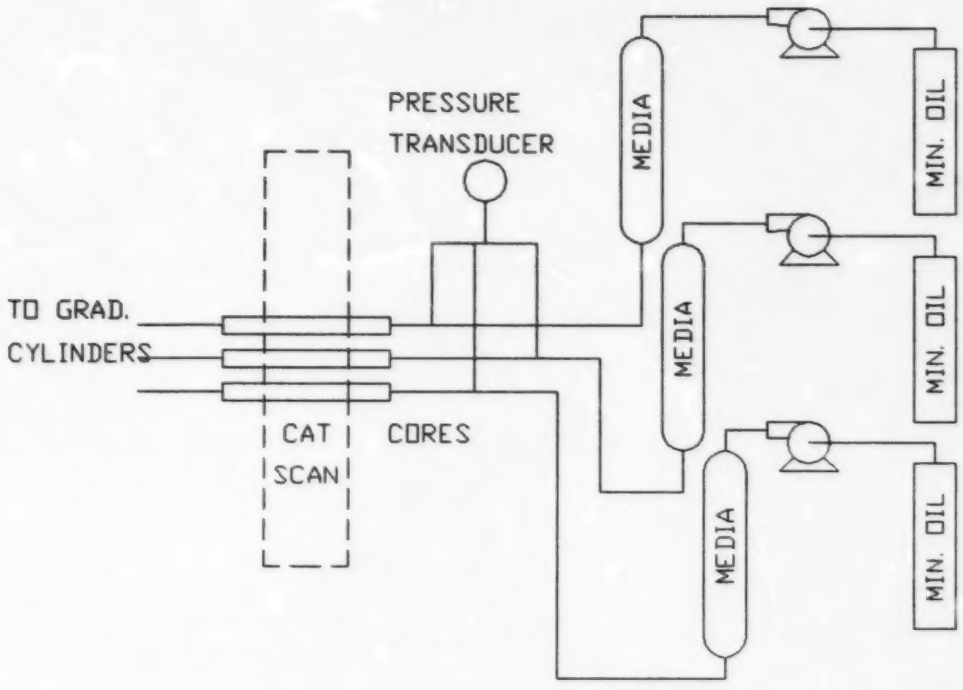

Figure 130: Schematic of the bacterial mineral plugging apparatus.

© 1991 NOVA HUSKY RESEARCH CORPORATION